OBSERVER-BASED NONLINEAR DYNAMIC INVERSION ADAPTIVE CONTROL WITH STATE CONSTRAINTS

A Dissertation

by

DOUGLAS I. FAMULARO

Submitted to the Office of Graduate and Professional Studies of
Texas A&M University
in partial fulfillment of the requirements for the degree of

DOCTOR OF PHILOSOPHY

Chair of Committee,	John Valasek
Committee Members,	Suman Chakravorty
	Aniruddha Datta
	Srinivas Rao Vadali
Head of Department,	Rodney Bowersox

December 2017

Major Subject: Aerospace Engineering

ABSTRACT

Hypersonic vehicle research and development has grown recently in the aerospace industry due to the powerful potential of operating a vehicle that flies at substantially higher speeds than typical aircraft. From a guidance, navigation and control perspective, hypersonic vehicles are particularly interesting due both to inherent vehicle complexities as well as practical concerns that only arise at high Mach numbers. Challenges inherent to the vehicle include nonlinearities, a wide range of operating conditions, high elasticity, high temperatures and parametric uncertainty. Although these challenges have by no means fully been explored in the literature, in the realm of control theory, they are somewhat common. Hypersonic vehicle control is difficult however, because in addition to these more traditional complexities a control designer must also deal with problems very specific to flying at high speeds such as: inlet unstart, overcoming sensing deficiencies at high speeds and creating an implementable digital control framework for a plant with extremely fast dynamics. This dissertation develops three novel theoretical approaches for addressing these challenges through advances in the nonlinear dynamic inversion adaptive control technique.

Although hypersonic vehicle control is the motivation and often the application that the control algorithms in this dissertation are tested on, several of the theoretical developments apply to a general class of nonlinear continuous time systems. First, in order to address the problem of inlet unstart, two state constraint mechanisms which integrate into the nonlinear dynamic inversion adaptive control framework are presented. These state constraining control laws require full state feedback and are capable of restricting the outputs of nonlinear systems containing parameter uncertainty to specific regions of the state-space. The first state constraint mechanism achieves this objective using sliding mode control and the second uses bounding functions to smoothly adjust the control and adaptive laws and drive the states toward the origin when constraints are approached. Stability is proven using Lyapunov analysis and these techniques are demonstrated in

a nonlinear simulation of a hypersonic vehicle.

Second, an observer-based feedback controller is developed that allows for a nonlinear system to track a reference trajectory with bounded errors and without measuring multiple states. Again, the technique used is nonlinear dynamic inversion adaptive control, but because of uncertainty in the system state, it is not assumed that the nonlinear control effectiveness matrix can be canceled perfectly. A nonlinear observer is implemented to estimate the values of the unknown states. This observer allows for the closed-loop stability of the system to be proven through Lyapunov analysis. It is shown that parametric uncertainty can successfully be accounted for using an adaptive mechanism and that all tracking and estimation errors are uniformly ultimately bounded.

Finally, a sampled-data nonlinear dynamic inversion adaptive control architecture is introduced. Despite the prevalence of digital controllers in practice, a nonlinear dynamic inversion adaptive control scheme in a sampled-data setting has not previously been developed. The method presented in this dissertation has the capability of extending the benefits of nonlinear dynamic inversion adaptive control - robust control of nonlinear systems with respect to model uncertainty - to more practical platforms.

DEDICATION

To my parents and to Kim

Constant support, even from a thousand miles away

ACKNOWLEDGMENTS

I would like to acknowledge my advisor, Dr. John Valasek, for his guidance and for giving me the opportunity to be a graduate student. For many professors, it would be quite a risk to hire Ph.D. students that did not major in their current field as undergraduates. Dr. Valasek saw in me a willingness to learn and to work hard despite not being an Aerospace Engineering major and I am very grateful for that. I hope he has gotten as much out of working together as I have.

I would also like to acknowledge Dr. Michael Bolender and Dr. Jonathan Muse of the Air Force Research Laboratory at Wright-Patterson Air Force Base, whom I did research with for three summers. This dissertation could not have been succesfully completed without their guidance and I learned very much from working with them.

Additionally, I would like to acknowledge the professors of the Texas A & M Aerospace Engineering Department that I have interacted with in my time here. In particular Dr. Robert Skelton and my dissertation committee, Dr. Suman Chakravorty, Dr. Aniruddha Datta and Dr. Srinivas Rao Vadali. They have inspired in me a deep interest in control theory and I thank them for that. I would also like to thank the administrative staff of the Aerospace Engineering department, in particular Rose Sauser for all of her help.

Finally, I would like to thank the members of the Vehicle Systems & Control Laboratory and any other graduate students who have been instrumental to my education. Graduate school has been a challenging endeavor, but I enjoyed it and am better for it, and I look forward to the next one.

CONTRIBUTORS AND FUNDING SOURCES

Contributors

This work was supported by a dissertation committee consisting of Professor John Valasek, advisor, Professors Suman Chakravorty and Srinivas Rao Vadali of the Department of Aerospace Engineering and Professor Aniruddha Datta of the Department of Electrical & Computer Engineering.

The simulation results of Section 3.7 were generated in part by Sean Whitney of the Department of Aerospace Engineering. All other work conducted for the dissertation was completed by the student independently.

Funding Sources

This research was funded in part by the Air Force Research Laboratory/Air Vehicles Directorate Summer Researcher Program.

NOMENCLATURE

α	angle-of-attack
β	sideslip angle
γ	flight path angle
$\bar{\delta}_i$	trim condition for control surface δ_i
$\bar{c}$	mean aerodynamic chord length
$\bar{q}$	dynamic pressure
$\begin{bmatrix}\delta_{f,l} & \delta_{f,r} & \delta_{t,l} & \delta_{t,r}\end{bmatrix}$	deflection of left elevon, right elevon, left ruddervator, right ruddervator
$\begin{bmatrix}\delta_a & \delta_e & \delta_r\end{bmatrix}$	deflection of aileron, elevator, rudder
$\begin{bmatrix}\phi & \theta & \psi\end{bmatrix}$	Euler angles
$\begin{bmatrix}F_{T_x} & F_{T_y} & F_{T_z}\end{bmatrix}$	components of thrust force along the body fixed axes
$\begin{bmatrix}I_x & I_y & I_z & I_{xz}\end{bmatrix}$	moment of inertia components about body fixed axes
$\begin{bmatrix}N_{dis} & E_{dis} & h\end{bmatrix}$	vehicle displacment vector
$\begin{bmatrix}p & q & r\end{bmatrix}$	body-axis angular rates
b	span
C_D	aerodynamic drag coefficient
C_L	aerodynamic lift coefficient
C_Y	aerodynamic sideforce coefficient
C_ℓ	roll moment coefficient
C_{ℓ_p}	roll damping coefficient
C_m	pitch moment coefficient

C_{m_q}	pitch damping coefficient
C_n	yaw moment coefficient
C_{n_r}	yaw damping coefficient
D	drag force
F_T	thrust force vector
g	acceleration due to gravity
h_E	engine angular momentum
L	lift force
m	vehicle mass
M_T	moment vector due to thrust
P_{eng}	engine power
S	planform area
V_T	total velocity
x_{cg}	x-coordinate of the center of gravity
Y	side force
NDI	Nonlinear Dynamic Inversion
DOF	Degree-of-Freedom
GHV	Generic Hypersonic Vehicle
PID	Proportional-Integral-Derivative
SMSC	Sliding Mode State Constraint
BFSC	Bounding Function State Constraint
SISO	Single-Input-Single-Output
MIMO	Multi-Input-Multi-Output
UUB	Uniformly Ultimately Bounded

EnKF	Ensemble Kalman Filter
EKF	Extended Kalman Filter
LMM	Linear Multistep Methods
ARMA	Autoregressive Moving Average

TABLE OF CONTENTS

Page

LIST OF FIGURES

FIGURE Page

LIST OF TABLES

TABLE Page

1. INTRODUCTION

1.1 Motivation

Although adaptive control became widely accepted in the early 1980's [1, 2] it today remains an extremely useful control technique for handling systems with varying or unknown parameters as well as a rich field for research. Control theory in general, but specifically adaptive control, has begun to branch off from linear representations of dynamic systems to the handling of nonlinear representations. On the positive side, nonlinear models allow for a designer to avoid techniques such as gain scheduling and to develop concise algorithms capable of controlling a system in any region of the state-space. On the negative side, accurate nonlinear models can be very hard to obtain. Therefore, the ability to handle parametric uncertainty becomes crucial. This has made adaptive control an excellent candidate for overcoming the deficiencies of model inaccuracy in nonlinear control systems [3, 4]. In cases where not only the open-loop dynamics but the control effectiveness of the system is nonlinear as well, nonlinear dynamic inversion (NDI) adaptive control has proven to be a useful technique [5]. In this dissertation, the primary motivation for the investigation of nonlinear dynamic inversion adaptive control techniques, as well as many of the other issues presented, is the control of hypersonic vehicles.

The first complexity of hypersonic vehicle control that serves as motivation for this dissertation is the problem of inlet unstart. Inlet unstart is a phenomenon only seen in supersonic jet inlets. It occurs when air flow through the inlet is altered in such a way that the shock wave system is disrupted and then expelled from the inlet. Often, it occurs suddenly and has a violent effect on the aircraft: a nearly instantaneous large drop in thrust, an increase in drag, and the potential induction of large undesirable moments. Inlet unstart occurs in one of two ways. In a started inlet with a normal shock at the throat of the nozzle, any increase in back pressure will drive the shock forward into the contraction section, where it cannot be stabilized because the shock Mach number

is greater than the throat value. This leads to a dangerous loss of thrust. The second cause of unstart is flow asymmetries that prevent the flow from passing through the throat of the inlet, which are typically caused by the vehicle operating at too steep of an angle-of-attack or sideslip angle [6, 7]. In this dissertation, this second cause is addressed as the following questions are explored:

1. Can state constraint control techniques that restrict what values of angle-of-attack and sideslip angle can be achieved be used to prevent inlet unstart?

2. In the event of an inlet unstart, what measures can be taken to maintain control effectiveness and return the vehicle to a safe region of the state-space?

Two different methods that extend state constraint enforcement to an NDI adaptive control framework will be presented, the first in Section 2 and the second in Section 3. The stability of these techniques is rigorously proven. Furthermore, it is shown that these controllers are capable of restricting the system to its constraint set in the presence of unacceptable command signals or external disturbances.

The second motivational issue of this dissertation is the control of nonlinear systems in instances where the full state vector cannot be measured. In the case of hypersonic vehicle control, an issue often neglected in the literature is the difficultly that exists in attaining full state feedback. The high operating temperature of these vehicles limits which type of sensors can be used and in particular, external vanes used to measure aerodynamic angles are unavailable [8]. Therefore the vehicle's angle-of-attack and sideslip angle, crucial information for successful flight control, cannot be measured directly and instead must be estimated. The inability to measure the complete state vector invalidates the common assumption in dynamic inversion control techniques that the state dependent portions of the control effectiveness matrix can be canceled perfectly. This adds significant complexity to the control design. In order to handle this complication the following questions are addressed:

1. How can the unmeasured states be estimated such that an NDI adaptive control law based on

the estimated values can rigorously be proven to stabilize the system?

2. What assumptions must be made about the control effectiveness matrix to implement an NDI adaptive control law without full state measurements?

The third motivational issue is the fact that sampled-data control laws synthesized in a continuous time framework are vulnerable to the destabilizing effect of sampling if it is not properly accounted for. For sampled-data systems that are nonlinear, the inability to model the system with an exact discrete time representation presents another challenge in achieving stabilization [9]. Therefore, a discussion of nonlinear discretization methods is given and a sampled-data approach to NDI adaptive control is developed that is capable of extending this technique to more practical systems. In reference to hypersonic vehicle control, the following two questions are examined:

1. How does the performance of the sampled-data NDI control law compare with that of a continuous NDI control law implemented with a sampler and a zero-order hold?

2. How slow can the controller sample such that a plant with extremely fast dynamics and parametric uncertainty can still be accurately controlled?

1.2 Literature Review

In this section a literature review on nonlinear hypersonic vehicle control with an emphasis on adaptive control and dynamic inversion control is conducted. Additional references on state constraint mechanisms, output feedback adaptive controllers, and nonlinear sampled-data controllers are reviewed in their corresponding sections of the dissertation as well.

Nonlinear dynamic inversion control is a technique commonly used when nonlinear models of the system are available and the system is affine in control. Given an accurate model, this method allows for stable control over a wide range of operating conditions without the need for linearization and extensive gain scheduling. Since accurate nonlinear models can be difficult to attain, even in continuous time, NDI control is often combined with an adaptive controller in order

to improve robustness with respect to model and parameter uncertainties. Several studies have been done to test the robustness properties of NDI controllers when used on air vehicles and NDI adaptive control has been shown to be effective on highly nonlinear aircraft applications [10, 11]. It has also been extended to fault tolerant frameworks such that the controller can safely adjust to actuator failure [12].

In the following references some variation of NDI control was utilized in the control of hypersonic vehicles. Wang and Stengel [13] looked at controlling a longitudinal model of a hypersonic vehicle using a stochastic nonlinear dynamic inversion technique. A genetic algorithm was implemented to design the structure of the dynamic inversion and Monte Carlo simulation was used to test its performance. Rollins, et al. developed an adaptive dynamic inversion control architecture for controlling a full 6 degree-of-freedom (DOF) hypersonic vehicle model. Full state measurement was assumed and the paper examined vehicle response to inlet unstart [14]. Sigthorsson, et al. developed an output feedback controller for the flexible longitudinal hypersonic vehicle model created in [15] that successfully controls the vehicle despite being unable to measure the flexible modes [16]. Johnson, et. al developed a guidance and control architecture for hypersonic ascent and entry vehicles and applied it to a six degree-of-freedom X-33 simulation. A trajectory generation algorithm and neural network based dynamic inversion controller were developed. Pseudo-control hedging was used as well [17]. Yang, et. al. presented a nonlinear dynamic inversion controller capable of controlling a rigid-body longitudinal model of a hypersonic vehicle. Unknown external disturbances are included in the dynamics of every state and a nonlinear observer is used to handle disturbances and parameter uncertainties [18]. The majority of the NDI controllers described above rely on full state measurement and do not prevent the system from violating important state constraints. This dissertation offers novel approaches that resolve these practical hypersonic vehicle control concerns.

Other adaptive control frameworks capable of handling nonlinear systems have also been used in the control of hypersonic vehicles. Sun, et. al presented a nonlinear controller capable of

controlling the flexible, longitudinal hypersonic vehicle model developed in [15]. Without using dynamic inversion and by taking advantage of aeropropulsive and elevator-to-lift coupling, this paper reduces the control problem to a set of linear algebraic equations. A nonlinear disturbance observer is used to handle parametric uncertainty and an H-infinity controller is included in order to suppress undesired dynamics due to the flexible modes [19]. Serrani and Bolender developed a nonlinear adaptive controller capable of controlling a 6-DOF rigid body model of a hypersonic vehicle. The inner loop uses dynamic inversion adaptive control to ensure that the forward velocity (u) and the angular rates (p, q, r) track their reference trajectories. The outer loop is composed of three robust controllers that generate reference trajectories for the lateral velocity (v), altitude and heading angle. Actuator dynamics are included in the simulation model and dynamic control allocation is used to account for discrepancy between the commanded and actual deflection values [20]. Sun, et. al present a nonlinear back-stepping approach to controlling a rigid-body longitudinal model of a hypersonic vehicle. A nonlinear observer is used for disturbance rejection and to handle parametric uncertainty. Simulation studies show the ability of this controller to track altitude and velocity step commands [21]. Zong, et. al. developed an adaptive controller for a flexible longitudinal model of a hypersonic vehicle. It focuses on the velocity and altitude subsystems and designs a controller capable of tracking reference trajectories in these two states in the presence of actuator dynamics and constraints. In order to account for uncertainty in the dynamics, a neural network is used to approximate the basis functions that are used in the adaptive law. The rigid body modes are proven to be stable via Lyapunov analysis; the flexible body modes are included and evaluated through simulation [22]. Xu presented an adaptive controller capable of controlling a flexible longitudinal model of a hypersonic vehicle. Nonlinear actuator dynamics as well as an input dead-zone are included in the model. The vehicle attitude is controlled using dynamic surface control, which is similar to back-stepping. Parameter uncertainty is handled using a neural network based adaptive controller [23]. Mu, et. al. developed a neural network based control approach to controlling a longitudinal model of a hypersonic vehicle. A

sliding-mode baseline controller is developed and then integrated with an artificial neural network to account for parametric uncertainties and disturbances. The controller is designed for tracking velocity and altitude commands [24]. Balas, et. al. presented a direct adaptive controller designed for a linear longitudinal hypersonic vehicle model but tested in simulation on a nonlinear model. The coupling between the elevator and fuel-equivalence ratio is examined and accounted for in the control design [25]. By using alternative approaches to NDI, the class of systems that these references address can often be restrictive. The general class of nonlinear systems addressed in this dissertation is described in the next section.

1.3 Baseline Tracking NDI Adaptive Controller

The motivational issues described in Section 1.1 are addressed in this dissertation by building upon a previously developed NDI adaptive control framework capable of tracking a reference model. This baseline tracking NDI adaptive controller will be referred to through out the dissertation, often for comparative purposes. For completeness and in order to ensure proper understanding of these comparison cases, the baseline controller is derived and its stability is proven.

In this dissertation, the class of systems of interest is made up of nonlinear, affine-in-control systems with dynamics that can be represented by the equations

$$\dot{x} = f(x) + g(x)\Lambda u \tag{1.1}$$

$$y = Cx \tag{1.2}$$

where $x \in \mathbb{R}^{n_s}$ is the system state, $u \in \mathbb{R}^m$ is the control, the vector $f(x) \in \mathbb{R}^{n_s}$ represents the nonlinear open-loop dynamics of the system which are assumed to be bounded for bounded x, and $g(x)\Lambda \in \mathbb{R}^{n_s \times m}$ represents the control effectiveness of the system. It is assumed that $f(x)$ and the constant matrix $\Lambda \in \mathbb{R}^{m \times m}$ are unknown but that Λ has full rank. The matrix $g(x) \in \mathbb{R}^{n_s \times m}$ is considered known. In the output equation (1.2), $y \in \mathbb{R}^p$ represents the outputs which are desired

to be controlled such that $n_s \geq m \geq p$. The matrix $C \in \mathbb{R}^{p \times n_s}$ is constant, known, and assumed to have full rank. It is also assumed that the product $Cg(x)\Lambda$ has full rank for all x and that full state feedback is available.

The control objective is for the system outputs to track a linear reference model $y_m \in \mathbb{R}^p$ with dynamics defined by

$$\dot{y}_m = A_m y_m + B_m r \tag{1.3}$$

where $r \in \mathbb{R}^p$ is a reference input signal. The matrix $A_m \in \mathbb{R}^{p \times p}$ is Hurwitz, and $B_m \in \mathbb{R}^{p \times p}$. It is assumed that the reference input signal r is continuous and bounded. The system tracking error is defined as

$$e = y_m - y \tag{1.4}$$

1.3.1 Tracking Error Dynamics

In order to prove that the closed-loop system is stable, it will be useful to formulate the system's tracking error dynamics. The first step towards achieving this is taking a derivative of Equation (1.4) with respect to time,

$$\dot{e} = \dot{y}_m - \dot{y}$$

$$\dot{e} = \dot{y}_m - Cf(x) - Cg(x)\Lambda u \tag{1.5}$$

It is assumed that the matrix Λ can be decomposed as

$$\Lambda = I + \delta\Lambda \tag{1.6}$$

where I is the identity matrix and $\delta\Lambda \in \mathbb{R}^{m \times m}$ is characterized by $0 < \delta\Lambda < I$, that is no eigenvalue of $\delta\Lambda$ has a magnitude greater than 1. In order to account for the uncertainty in the matrix Λ, the estimate $\hat{\Lambda}$ is defined as

$$\hat{\Lambda} = I + \delta\hat{\Lambda} \tag{1.7}$$

where $\delta\hat{\Lambda} \in \mathbb{R}^{m\times m}$. The error dynamics are finalized by adding and subtracting $g(x)\hat{\Lambda}u$ to the right hand side of equation (1.5). Defining $\delta\tilde{\Lambda} = \delta\hat{\Lambda} - \delta\Lambda$ leaves

$$\dot{e} = \dot{y}_m - Cf(x) - Cg(x)\hat{\Lambda}u + Cg(x)\delta\tilde{\Lambda}u \tag{1.8}$$

1.3.2 Control Law Development

The baseline tracking NDI adaptive control law is given by

$$u = [Cg(x)\hat{\Lambda}]^{\dagger}\left(\dot{y}_m - C\hat{f}(x) + Ke - \nu\right) \tag{1.9}$$

where the notation $(\cdot)^{\dagger}$ represents the right-handed pseudo-inverse if $m > p$ and the true inverse if $m = p$. The vector $\nu \in \mathbb{R}^p$ is an adaptive signal used to account for parameter uncertainty. The vector $\hat{f}(x) : \mathbb{R}^n \mapsto \mathbb{R}^n$ is an estimated model of the plant dynamics, and $K \in \mathbb{R}^{p\times p}$ is a positive definite error feedback gain matrices such that $K = K^T > 0$. Substituting the control law (1.9) into Equation (1.8) results in

$$\dot{e} = -Cf(x) + C\hat{f}(x) - Ke + \nu + Cg(x)\delta\tilde{\Lambda}u \tag{1.10}$$

It is assumed that the difference $C\hat{f}(x) - Cf(x)$ can be parameterized as

$$C\hat{f}(x) - Cf(x) = W^T b(x) \tag{1.11}$$

where, $W \in \mathbb{R}^{n_w\times p}$ is a matrix of unknown constant weights and $b(x) \in \mathbb{R}^{n_w}$ is a vector of known, potentially nonlinear, basis functions that is assumed to be bounded for all bounded x. In order to account for the uncertainty in the open-loop dynamics $f(x)$, the adaptive signal ν is defined as

$$\nu = \widehat{W}^T b(x) \tag{1.12}$$

where $\widehat{W}$ is an estimate of the unknown weight matrix W and is updated through an adaptive law.

Defining $\widetilde{W} = \widehat{W} - W$, Equation (1.10) can be rewritten as

$$\dot{e} = -\widetilde{W}^T b(x) - Ke + Cg(x)\delta\tilde{\Lambda}u \tag{1.13}$$

1.3.3 Adaptive Law Development

The adaptive laws of the baseline tracking NDI adaptive controller, which are used to update the estimated matrices $\widehat{W}$ and $\delta\hat{\Lambda}$, are given by

$$\dot{\widehat{W}} = \Gamma_W \mathrm{Proj}_M(\widehat{W}, b(x)e^T) \tag{1.14}$$

$$\delta\dot{\hat{\Lambda}} = \Gamma_\Lambda \mathrm{Proj}_M(\delta\hat{\Lambda}, -g(x)^T C^T e u^T) \tag{1.15}$$

where $\Gamma_W \in \mathbb{R}^{n_w \times n_w}$ and $\Gamma_\Lambda \in \mathbb{R}^{m \times m}$ and $\Gamma_i = \Gamma_i^T > 0$ for $i = W, \Lambda$ are adaptive gain matrices. The operator Proj_M represents the matrix projection operator and is defined as

$$\mathrm{Proj}_M(\hat{\Theta}, Y) = [\mathrm{Proj}(\hat{\theta}_1, y_1), ...\mathrm{Proj}(\hat{\theta}_n, y_n)] \tag{1.16}$$

where $\hat{\Theta} \in \mathbb{R}^{a \times b} = [\hat{\theta}_1, \hat{\theta}_2, ...\hat{\theta}_b]$, $Y \in \mathbb{R}^{a \times b} = [y_1, y_2, ...y_b]$, and Proj represents the vector projection operator. In adaptive systems, $\hat{\Theta}$ typically represents a matrix of estimates of some unknown constant parameters $\Theta \in \mathbb{R}^{a \times b}$. The vector projection operator is defined as,

$$\mathrm{Proj}(\hat{\theta}_i, y_i) = \begin{cases} y_i - \frac{\nabla h(\hat{\theta}_i)(\nabla h(\hat{\theta}_i))^T}{\|\nabla h(\hat{\theta}_i)\|^2} y_i h(\hat{\theta}_i), & \text{if } h(\hat{\theta}_i) > 0, \;\; y_i^T \nabla h(\hat{\theta}_i) > 0 \\ \\ y_i, & \text{otherwise} \end{cases} \tag{1.17}$$

where $\hat{\theta}_i \in \mathbb{R}^a$, $y_i \in \mathbb{R}^a$, $h(\hat{\theta}_i) : \mathbb{R}^a \to \mathbb{R}$ is a convex function, and

$$\nabla h(\hat{\theta}_i) = \begin{bmatrix} \partial h(\hat{\theta}_i)/\partial \hat{\theta}_{i,1} & \dots & \partial h(\hat{\theta}_i)/\partial \hat{\theta}_{i,a} \end{bmatrix}^T$$

The projection operator is constructed so that a known maximum bound can be set for each of the vectors, $\hat{\theta}_i$ [26, 27]. For the class of systems of interest in this development, this corresponds to known bounds on the norm of the columns of the unknown parameter matrices, $\widehat{W}$ and $\delta\hat{\Lambda}$. The bounds are selected based on one's knowledge of the uncertainty in the system. If the uncertainty is assumed to be unbounded there may not be enough actuator authority to guarantee that control objectives are met. Therefore, it is assumed that there is some understanding of the uncertainty in the system, and that knowledge is reflected in the controller by bounding the weights through the projection operator. The following lemmas, given in [26], describe important properties of the projection operator that makes it useful in the field of adaptive control.

Lemma 1.3.1. *Let $\hat{\theta}_i \in \mathbb{R}^a$ be the estimate of an unknown constant vector $\theta_i \in \mathbb{R}^a$ which is contained in the convex set Ω_0 defined as $\Omega_0 \triangleq \{\theta \in \mathbb{R}^a | h(\theta) \leq 0\}$ such that $\theta \in \Omega_0$. The following condition holds*

$$\left(\hat{\theta}_i - \theta_i\right)^T \left(\mathrm{Proj}(\hat{\theta}_i, y) - y\right) \leq 0 \tag{1.18}$$

Proof. See Appendix A. □

Remark 1.3.1. Let $\Theta \in \mathbb{R}^{a \times b} = [\theta_1, \theta_2, ...\theta_b]$. Given the definitions of $\hat{\Theta}$ and Y used in (1.16), it is straightforward to show using Lemma 1.3.1 that

$$tr\left((\hat{\Theta} - \Theta)^T(\mathrm{Proj}_M(\hat{\Theta}, Y) - Y)\right) \leq 0 \tag{1.19}$$

where $tr(\cdot)$ is the trace operator.

Lemma 1.3.2. *Given the convex function $h(\theta) : \mathbb{R}^a \to \mathbb{R}$, if an initial value problem, i.e. adaptive*

control algorithm with adaptive law and initial conditions, is defined by

1. $\dot{\hat{\theta}}_i = \text{Proj}(\hat{\theta}_i, y)$

2. $\hat{\theta}_i(t=0) \in \Omega_1 \triangleq \{\theta \in \mathbb{R}^a | h(\theta) \leq 1\}$

then $\hat{\theta}_i \in \Omega_1$ *for all* $t \geq 0$.

Proof. See Appendix A. □

Additionally, it is shown in Appendix B that through the use of the projection operator in the adaptive law for $\delta\hat{\Lambda}$, the total estimate $\hat{\Lambda}$ is guaranteed to be invertible at all times as required by the control law (1.9).

1.3.4 Stability Analysis

Theorem 1. *Consider the nonlinear dynamical system defined in (1.1), the reference model defined in (1.3), the baseline tracking NDI adaptive control law defined in (1.9) and the adaptive laws defined in (1.14) and (1.15). Given a continuous and bounded reference input signal,* r*, the tracking error* $e \to 0$ *as* $t \to \infty$.

Proof. In order to prove the stability of the baseline tracking NDI controller, the following candidate Lyapunov Function is chosen

$$V = \frac{1}{2}\left(e^T e + tr(\widetilde{W}^T \Gamma_W^{-1} \widetilde{W}) + tr(\delta\tilde{\Lambda}\Gamma_\Lambda^{-1}\delta\tilde{\Lambda}^T)\right) \tag{1.20}$$

A derivative of (1.20) is taken with respect to time along the system trajectories

$$\dot{V} = e^T \dot{e} + tr(\widetilde{W}^T \Gamma_W^{-1} \dot{\widehat{W}}) + tr(\delta\tilde{\Lambda}\Gamma_\Lambda^{-1}\delta\dot{\hat{\Lambda}}^T) \tag{1.21}$$

Substituting in the error dynamics, Equation (1.13), and applying the trace identity $a^T b = tr(ba^T)$,

results in

$$\dot{V} = -e^T K e + tr\left(\widetilde{W}^T(\Gamma_W^{-1}\dot{\widehat{W}} - b(x)e^T)\right) + tr\left(\delta\tilde{\Lambda}(\Gamma_\Lambda^{-1}\delta\dot{\hat{\Lambda}}^T + ue^T C g(x))\right) \tag{1.22}$$

Substituting the adaptive laws (1.14) and (1.15) and utilizing Lemma 1.3.1 leaves

$$\dot{V} \leq -e^T K e \leq 0 \tag{1.23}$$

which implies that e, $\widetilde{W}$, and $\delta\tilde{\Lambda}$ are bounded and that $\int_0^\infty e^T K e dt$ exists and is finite. Since the reference signal r is assumed to be continuous and bounded, this implies that y_m, $b(x)$, u, and $\dot{e}$ are bounded as well which implies that e is uniformly continuous in time. Therefore, Barbalat's Lemma [28] implies that $e \to 0$ as $t \to \infty$. □

Remark 1.3.2. A significant limitation of the above approach is that it does not formally address the issue of actuator saturation limits. The projection operator is useful in ensuring that the adaptive signals remain small but the control law given in Equation (1.9) makes it clear that the magnitude of the control signal will still be heavily dependent on the specific system dynamics. Nevertheless, NDI adaptive control is well suited for the control of hypersonic vehicles as a very small change in control surface deflection angle will have a significant influence on the vehicle at large Mach numbers. Additionally, although no theoretical guarantees are made about saturation limits, such limits are included in all simulation studies shown in this dissertation and it is demonstrated that even when achieving complex maneuvers they are not encountered.

1.4 Introduction to the Generic Hypersonic Vehicle Model

The primary dynamical model used in this dissertation is a high fidelity, nonlinear, six degree-of-freedom hypersonic vehicle simulation known as the generic hypersonic vehicle (GHV). The GHV is a Simulink based model of a hypersonic aircraft, developed at the Air Force Research Laboratory for the purpose of testing control algorithms. The aerodynamic and thrust forces and

moments acting on the vehicle are modeled using look-up tables that were generated using shock-expansion methods with a viscous correction. The equations of motion for the generic hypersonic vehicle were derived using a Lagrangian approach by Billamoria and Schmidt [29]. The derivation utilizes an Earth-centered inertial frame with a rotating, spherical Earth. The following simplifying assumptions were made:

1. The vehicle is assumed to be inelastic
2. The vehicle is assumed to have no rotors
3. Terms involving fluid flow were dropped as they are accounted for in aerodynamic and engine lookup table data
4. Wind-related terms are neglected

The state vector for the GHV, $x \in \mathbb{R}^9$, and the total control vector, $\bar{u} \in \mathbb{R}^5$, are given by

$$x = \begin{bmatrix} V_T & \Phi & x_a & x_r \end{bmatrix}^T \tag{1.24}$$

$$\Phi = \begin{bmatrix} \phi & \theta & \psi \end{bmatrix}^T \tag{1.25}$$

$$x_a = \begin{bmatrix} \beta & \alpha \end{bmatrix}^T \tag{1.26}$$

$$x_r = \begin{bmatrix} p & q & r \end{bmatrix}^T \tag{1.27}$$

$$\bar{u} = \begin{bmatrix} \delta_{th} & \delta_{f,r} & \delta_{f,l} & \delta_{t,r} & \delta_{t,l} \end{bmatrix}^T \tag{1.28}$$

In this model, the total velocity, V_T, is controlled using a proportional-integral-derivative (PID) controller with the intention of maintaining airspeed. The input to the controller is the desired total velocity, and the output is the air-fuel equivalence ratio. This equivalence ratio is then translated into a throttle command, δ_{th}. For the work presented in this dissertation, the PID controller is considered separate from the NDI adaptive controller of interest. The throttle control signal will be

manifested implicitly in the thrust force and moment terms of the equations of motion. Therefore, the control vector definition is modified such that the control law development only applies to the control surface deflections

$$u = \begin{bmatrix} \delta_{f,r} & \delta_{f,l} & \delta_{t,r} & \delta_{t,l} \end{bmatrix}^T \tag{1.29}$$

The dynamics of the generic hypersonic vehicle model are given by the following first-order differential equations,

Total Velocity Dynamics:

$$\dot{V}_T = \frac{F_T}{m}\cos(\alpha)\cos(\beta) - \frac{D}{m} + g_1 \tag{1.30}$$

Kinematic Equations:

$$\dot{\Phi} = \begin{bmatrix} 1 & \tan\theta\sin\phi & \tan\theta\cos\phi \\ 0 & \cos\phi & -\sin\phi \\ 0 & \sin\phi\sec\theta & \cos\phi\sec\theta \end{bmatrix} x_r \tag{1.31}$$

Aerodynamic Angle Dynamics:

$$\begin{aligned} \dot{x}_a = &\begin{bmatrix} \frac{1}{mV_T}((Y + F_{T_y})\cos\beta + mg_2 - (F_{T_x}\cos\alpha - F_{T_z}\sin\alpha)\sin\beta) \\ \frac{1}{mV_T\cos\beta}(-L + mg_3 - F_{T_x}\sin\alpha + F_{T_z}\cos\alpha) \end{bmatrix} \\ &+ \begin{bmatrix} \sin\alpha & 0 & -\cos\alpha \\ -\tan\beta\cos\alpha & 1 & -\tan\beta\sin\alpha \end{bmatrix} x_r \end{aligned} \tag{1.32}$$

Moment Equations:

$$\dot{x}_r = \begin{bmatrix} I_x & 0 & -I_{xz} \\ 0 & I_y & 0 \\ -I_{xz} & 0 & I_z \end{bmatrix}^{-1} \left(- \begin{bmatrix} -I_{xz}pq + (I_z - I_y)qr \\ (I_x - I_z)pr + I_{xz}(p^2 - r^2) \\ I_{xz}qr + (I_y - I_x)pq \end{bmatrix} + M_T + \bar{q}S \begin{bmatrix} bC_\ell \\ \bar{c}C_m \\ bC_n \end{bmatrix} \right) \tag{1.33}$$

where

$$g_1 = g\left(-\cos(\alpha)\cos(\beta)\sin(\theta) + \sin(\beta)sin(\phi)\cos(\theta) + \sin(\alpha)\cos(\beta)\cos(\phi)\cos(\theta)\right) \tag{1.34}$$

$$g_2 = g(\cos(\alpha)\sin(\beta)\sin(\theta) + \cos(\beta)\sin(\phi)\cos(\theta) - sin(\alpha)\sin(\beta)\cos(\phi)\cos(\theta)) \tag{1.35}$$

$$g_3 = g(\sin(\alpha)\sin(\theta) + \cos(\alpha)\cos(\phi)\cos(\theta)) \tag{1.36}$$

and where the following decompositions can be formed,

$$L = C_L \bar{q} S \tag{1.37}$$

$$D = C_D \bar{q} S \tag{1.38}$$

$$Y = C_Y \bar{q} S \tag{1.39}$$

$$\begin{bmatrix} bC_\ell \\ \bar{c}C_m \\ bC_n \end{bmatrix} = \begin{bmatrix} b\big(C'_\ell(\alpha,\beta) + \frac{b}{2V_T}(C_{\ell_p}p)\big) \\ \bar{c}\left(C'_m(\alpha,\beta) + \frac{\bar{c}}{2V_T}C_{m_q}q + \bar{C}_{m,\delta}\right) \\ b\big(C'_n(\alpha,\beta) + \frac{b}{2V_T}(C_{n_r}r)\big) \end{bmatrix} + Hu \tag{1.40}$$

The vehicle moment's dependence on angle-of-attack and sideslip angle is described by the polynomials $C'_\ell(\alpha,\beta)$, $C'_m(\alpha,\beta)$ and $C'_n(\alpha,\beta)$. The constant $\bar{C}_{m,\delta}$ represents the effect of the control surface deflections on the total pitch moment at the trim condition and is given by,

$$\bar{C}_{m,\delta} = \frac{\partial C_m}{\partial \delta_{f,r}}(\delta_{f,r} = \bar{\delta}_{f,r}) + \frac{\partial C_m}{\partial \delta_{f,l}}(\delta_{f,l} = \bar{\delta}_{f,l}) + \frac{\partial C_m}{\partial \delta_{t,r}}(\delta_{t,r} = \bar{\delta}_{t,r}) + \frac{\partial C_m}{\partial \delta_{t,l}}(\delta_{t,l} = \bar{\delta}_{t,l}) \tag{1.41}$$

and the control effectiveness term $H \in \mathbb{R}^{3\times 4}$ is given by

$$H = \begin{bmatrix} b\frac{\partial C_\ell}{\partial \delta_{f,r}} & b\frac{\partial C_\ell}{\partial \delta_{f,l}} & b\frac{\partial C_\ell}{\partial \delta_{t,r}} & b\frac{\partial C_\ell}{\partial \delta_{t,l}} \\ \bar{c}\frac{\partial C_m}{\partial \delta_{f,r}} & \bar{c}\frac{\partial C_m}{\partial \delta_{f,l}} & \bar{c}\frac{\partial C_m}{\partial \delta_{t,r}} & \bar{c}\frac{\partial C_m}{\partial \delta_{t,l}} \\ b\frac{\partial C_n}{\partial \delta_{f,r}} & b\frac{\partial C_n}{\partial \delta_{f,l}} & b\frac{\partial C_n}{\partial \delta_{t,r}} & b\frac{\partial C_n}{\partial \delta_{t,1}} \end{bmatrix} \tag{1.42}$$

For the sake of brevity, these dynamics are rewritten in vector form as

$$\dot{x} = f(x) + g(x)u \tag{1.43}$$

$$\begin{bmatrix} \dot{V}_T \\ \dot{\Phi} \\ \dot{x}_a \\ \dot{x}_r \end{bmatrix} = \begin{bmatrix} f_{VT}(x) \\ f_{\Phi}(x) \\ f_a(x) \\ f_r(x) \end{bmatrix} + \begin{bmatrix} 0 \\ 0 \\ 0 \\ g_r(x) \end{bmatrix} u \tag{1.44}$$

where,

$$g_r(x) = \begin{bmatrix} I_x & 0 & -I_{xz} \\ 0 & I_y & 0 \\ -I_{xz} & 0 & I_z \end{bmatrix}^{-1} (\bar{q}SH) \tag{1.45}$$

1.4.1 Simulation Example

A simulation example is shown to demonstrate the effectiveness of the baseline tracking NDI adaptive control law. In this example, the control objective was to track an angle-of-attack and sideslip angle trajectory. In order to achieve this objective, the system dynamics were broken down into a subsystem of position-level dynamics and a subsystem of velocity-level dynamics.

The position-level subsystem has dynamics of the form

$$\dot{x}_p = \begin{bmatrix} \dot{\phi} \\ \dot{\theta} \\ \dot{\psi} \\ \dot{\alpha} \\ \dot{\beta} \end{bmatrix} = f_p(x) + g_p(x)\Lambda_p \begin{bmatrix} p_d \\ q_d \\ r_d \end{bmatrix} \tag{1.46}$$

$$y_p = \begin{bmatrix} \alpha & \beta \end{bmatrix}^T \tag{1.47}$$

and the velocity-level subsystem has dynamics of the form

$$\dot{x}_v = \begin{bmatrix} \dot{p} \\ \dot{q} \\ \dot{r} \end{bmatrix} = f_v(x) + g_v(x)\Lambda_v \begin{bmatrix} \delta_{f,r} \\ \delta_{f,l} \\ \delta_{t,r} \\ \delta_{t,l} \end{bmatrix} \tag{1.48}$$

$$y_v = \begin{bmatrix} p & q & r \end{bmatrix}^T \tag{1.49}$$

where, using the notation of Equation (1.44)

$$f_p(x) = \begin{bmatrix} 0 \\ 0 \\ 0 \\ \frac{1}{mV_T}((Y + F_{T_y})\cos\beta + mg_2 - (F_{T_x}\cos\alpha - F_{T_z}\sin\alpha)\sin\beta) \\ \frac{1}{mV_T\cos\beta}(-L + mg_3 - F_{T_x}\sin\alpha + F_{T_z}\cos\alpha) \end{bmatrix} \tag{1.50}$$

$$g_p(x) = \begin{bmatrix} 1 & \tan\theta\sin\phi & \tan\theta\cos\phi \\ 0 & \cos\phi & -\sin\phi \\ 0 & \sin\phi\sec\theta & \cos\phi\sec\theta \\ \sin\alpha & 0 & -\cos\alpha \\ -\tan\beta\cos\alpha & 1 & -\tan\beta\sin\alpha \end{bmatrix} \tag{1.51}$$

$$f_v(x) = f_r(x) \tag{1.52}$$

$$g_v(x) = g_r(x) \tag{1.53}$$

Due to the fact that $g_p(x)$ is made up of known trigonometric functions, it is assumed that $\Lambda_p = I_3$ is known perfectly. Although Λ_v is equal to the identity matrix, the initial estimate $\hat{\Lambda}_v(t = t_0)$ was set to

$$\hat{\Lambda}_v(t = t_0) = \begin{bmatrix} 1.1 & 0 & 0 & 0 \\ 0 & 1.1 & 0 & 0 \\ 0 & 0 & 1.1 & 0 \\ 0 & 0 & 0 & 1.1 \end{bmatrix} \tag{1.54}$$

The weight estimate matrices were initialized as $\widehat{W}_p(t = 0) = \widehat{W}_v(t = 0) = 0$.

Note that for the position-level subsystem, the control vector is made up of the desired body-axis angular rates and for the velocity-level subsystem, the control vector is made up of the control surface complement of the GHV, two elevons and two ruddervators. The desired angular rates are calculated using (1.9) and the position-level subsystem dynamics and are then fed into the velocity-level subsystem which tries to track them by once again using (1.9), as shown in Figure 1.1. To make the simulation more realistic, second-order actuator dynamics with damping ratio $\zeta = 0.7$ and natural frequency $\omega_n = 25Hz$ were included and position and rate limits were placed on the

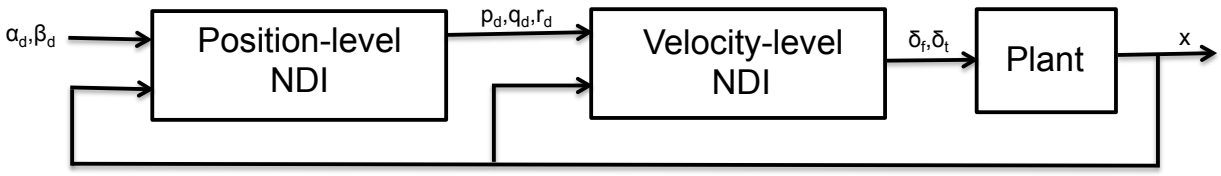

Figure 1.1: Breakdown of the position-level and velocity-level subsystems of the GHV.

actuators of $30\,\mathrm{deg}$ and $100\,\mathrm{deg}/s$, respectively. In addition, a time delay of $0.01s$ was included in the simulation. The initial flight condition was a velocity of Mach 6 and altitude of $80,000ft$.

1.4.2 Results

Using the baseline NDI adaptive controller, the generic hypersonic vehicle was commanded to track a $4\,\mathrm{deg}$ angle-of-attack doublet followed by a $2\,\mathrm{deg}$ sideslip angle doublet. Time histories of the aerodynamic angles, total velocity, and control surface deflections are shown in Figure 1.2 demonstrating successful completion of the control objective. The Euler angle and body-axis angular rate trajectories are shown in Figure 1.3 and the evolution of the adaptive parameters $\widehat{W}$ and $\hat{\Lambda}$ are shown in Figure 1.4.

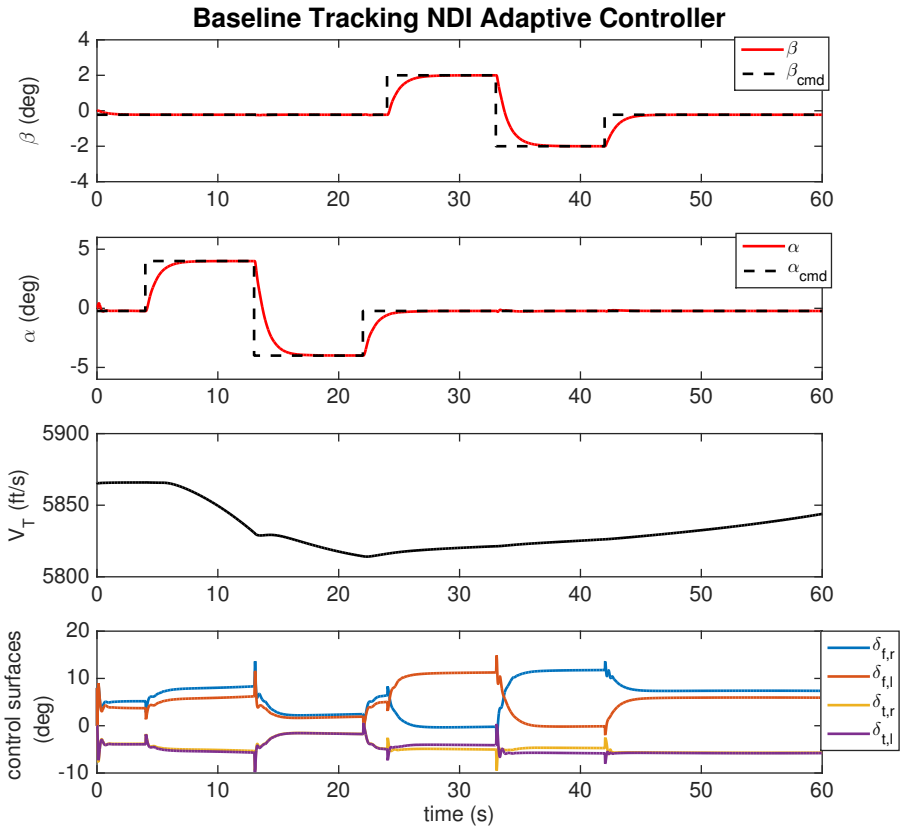

Figure 1.2: Baseline Tracking NDI Controller. Time histories of sideslip angle, angle-of-attack, total velocity and the control surface deflections.

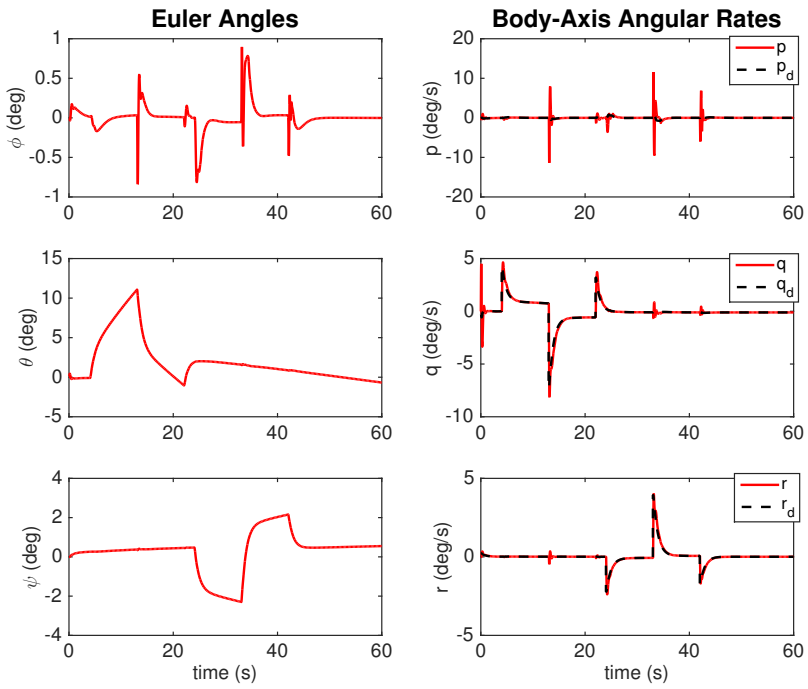

Figure 1.3: Baseline Tracking NDI Controller. Time histories of Euler angles and body-axis angular rates.

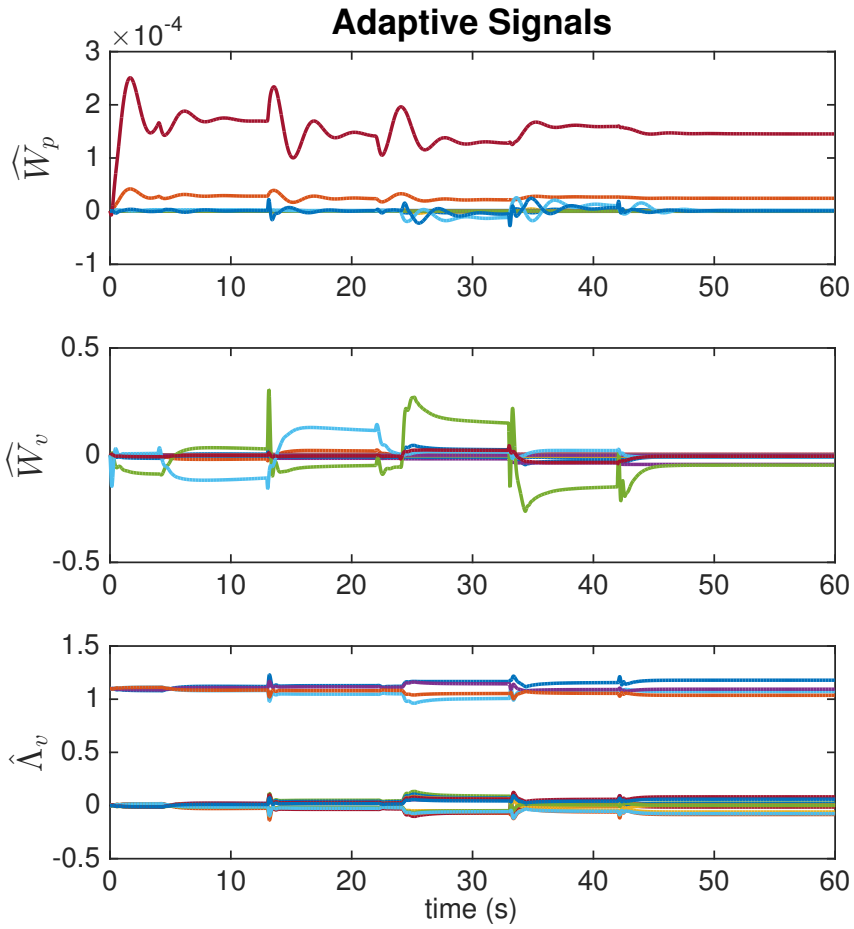

Figure 1.4: Baseline Tracking NDI Controller. Time histories of the adaptive signals.

2. NONLINEAR DYNAMIC INVERSION ADAPTIVE CONTROL WITH STATE CONSTRAINTS USING SLIDING MODE CONTROL*

2.1 Introduction

There are many situations in control systems theory, and particularly in flight control, where it is useful (if not imperative) to restrict which regions of the state-space the system can access. This has led to the integration of state constraint techniques with existing control architectures. When looking at aircraft control, this safety region is often referred to as the *flight envelope*. State constraining augmentation systems have been shown to be capable of preventing pilots from commanding an aircraft to enter the stall region by limiting angle-of-attack [30] and have also been used to limit the amount of g-force that can be applied to a vehicle [31]. In addition, it has been shown that supersonic and hypersonic vehicles are susceptible to a phenomenon known as inlet unstart if the vehicle flies at medium or large values of angle-of-attack or sideslip angle [32]. Inlet unstart can be defined as a disruption of the airflow through the inlet which can lead to a loss of thrust as well as the induction of large undesirable moments and departure from controlled flight. State constraint control techniques that can restrict the values of angle-of-attack and sideslip angle that can be achieved could potentially be used to prevent inlet unstart. Although the state constraint methods developed in this dissertation are motivated by the problem of inlet unstart, they are applicable to a general class of nonlinear systems.

Enforcing state constraints has been developed in the fields of linear control theory [33], optimal control [34–36], model-predictive control [37], and adaptive control [38–41]. In this section, a sliding mode controller is presented which was motivated by the work done in [38] and [39].

*Part of this Section is reprinted with permission from "Enforcing State Constraints on a Model of a Hypersonic Vehicle" by Douglas Famularo, John Valasek, Jonathan A. Muse and Michael A. Bolender in AIAA Guidance, Navigation and Control Conference (San Diego, California), January 2016.

In [38], an adaptive controller is developed which uses a neural approximation to handle unknown nonlinearities. As the state exits a certain region of the state-space, these approximations become poor and the controller uses a modulation function containing the saturation function in order to change modes, restrict the system states, and maintain stability. In [39] a state limiting adaptive controller that also uses a modulation function with the saturation function to change modes is developed and shown to enforce state constraints on uncertain systems with dynamics representing the decoupled fast responses of aircraft. The saturation-based modulation function concept allows for such sliding mode controllers to smoothly transition between “tracking mode" and “state constraining mode". The method presented in this section takes advantage of this technique in order to achieve smooth transitions, however its implementation in an NDI framework leads to significant changes in the overall development. Unlike the two papers previously discussed, the modulation function defined here depends primarily on the reference trajectory that the system is being commanded to follow. This allows for the controller to differentiate between commanded trajectories that are safe and those which exceed some constraint. A slight modification is made in the modulation function definition such that state constraints are still enforced in the presence of disturbances. The development of this approach is an expansion of the concept first presented in [42].

The control objective is to stabilize the system tracking error while maintaining that the system outputs remain in a predefined constraint set. Through the use of a modulation function, the control and adaptive laws alter their behavior as an output approaches a particular region of the state-space and it is proven through Lyapunov analysis that such alterations restrict the output from exceeding its constraint. Furthermore, if the system is given a reference command that is well within the safe region of the state-space, the controller presented in this section reduces to the tracking controller described in Section 1.3. Following the derivation of the controller and the stability analysis, the sliding mode state constraint (SMSC) controller is implemented in the GHV simulation and it is shown that it is capable of restricting what values of angle-of-attack and sideslip angle the vehicle can achieve.

2.2 Problem Statement

Consider the class of systems described in Section 1 that is composed of nonlinear, affine-in-control systems with dynamics that can be represented by the equations

$$\dot{x} = f(x) + g(x)\Lambda u \tag{2.1}$$

$$y = Cx \tag{2.2}$$

where $x \in \mathbb{R}^{n_s}$ is the system state, $u \in \mathbb{R}^m$ is the control, the vector $f(x) \in \mathbb{R}^{n_s}$ represents the nonlinear open-loop dynamics of the system which are assumed to be bounded for bounded x, and $g(x)\Lambda \in \mathbb{R}^{n_s \times m}$ represents the control effectiveness of the system. It is assumed that $f(x)$ and the constant matrix $\Lambda \in \mathbb{R}^{m \times m}$ are unknown but that Λ has full rank. The matrix $g(x) \in \mathbb{R}^{n_s \times m}$ is considered known. In the output equation (2.2), $y \in \mathbb{R}^p$ represents the outputs which are desired to be controlled and/or constrained such that $n_s \geq m \geq p$. The matrix $C \in \mathbb{R}^{p \times n_s}$ is constant, known, and assumed to have full rank. In order to utilize a dynamic inversion control law, the scope is limited to systems where the product $Cg(x)\Lambda$ has full rank for all x.

For the state constraint controller presented in this section it is assumed that full state feedback is available. The control objective is to stabilize the system tracking error while maintaining that $y \in \mathbb{Y}$ where $\mathbb{Y}$ is a predefined constraint set for the outputs of interest. The system tracking error is defined as

$$e = y_m - y \tag{2.3}$$

where y_m represents a reference model signal for the system outputs. It is assumed that the system outputs are selected such that if the tracking error is bounded it can be concluded that the full state vector x is bounded as well. The desired reference model dynamics are given by

$$\dot{y}_m = A_m y_m + B_m r \tag{2.4}$$

where $y_m \in \mathbb{R}^p$ and $r \in \mathbb{R}^p$ is a reference input signal. The matrix $A_m \in \mathbb{R}^{p\times p}$ is Hurwitz, and $B_m \in \mathbb{R}^{p\times p}$. It is assumed that the reference input signal r is continuous and bounded such that there exists a known constant C_m where

$$\|y_m\| \leq C_m \quad \|\dot{y}_m\| \leq C_m \tag{2.5}$$

Note that the constant C_m does not restrict the reference model to remain within the predefined constraint set, i.e. y_m may be in the set $\mathbb{Y}$ but it need not be. Given the definitions and derivation of Section 1.3.1 the error dynamics can be expressed as

$$\dot{e} = \dot{y}_m - Cf(x) - Cg(x)\hat{\Lambda}u + Cg(x)\delta\tilde{\Lambda}u \tag{2.6}$$

2.3 Control Law Development

In this section the SMSC controller is introduced and it is shown that either the system's tracking error e or threshold error e_{th} is uniformly ultimately bounded for all $t > 0$. The threshold error is defined as

$$e_{th} = y_{th} - y \tag{2.7}$$

where

$$y_{th,i} = \begin{cases} y_{max,i} + \delta_i & \text{if } |y_{max,i} - y_i| < |y_{min,i} - y_i| \\ y_{min,i} - \delta_i & \text{if } |y_{min,i} - y_i| < |y_{max,i} - y_i| \end{cases} \tag{2.8}$$

The definition (2.8) describes how the pre-defined parameters $y_{max,i} + \delta_i$ and $y_{min,i} - \delta_i$ form the $p-$dimensional hypercube $\mathbb{Y}$, inside of which it is desired that the outputs remain. The variables $\delta_i > 0$ are tuning parameters that define the size of the transitional space in which the controller slides from "tracking mode" to "state-constraining mode". Therefore, a smaller hypercube, $\mathbb{Y}-\Delta\mathbb{Y}$ is defined with boundaries defined by the parameters $y_{max,i}$ and $y_{min,i}$. A two-dimensional generic example of such hypercubes is shown in Figure 2.1. Note that the parameters that define $\mathbb{Y}$ and

$\mathbb{Y} - \Delta\mathbb{Y}$ need not be symmetric. The mechanism used for sliding between the different control

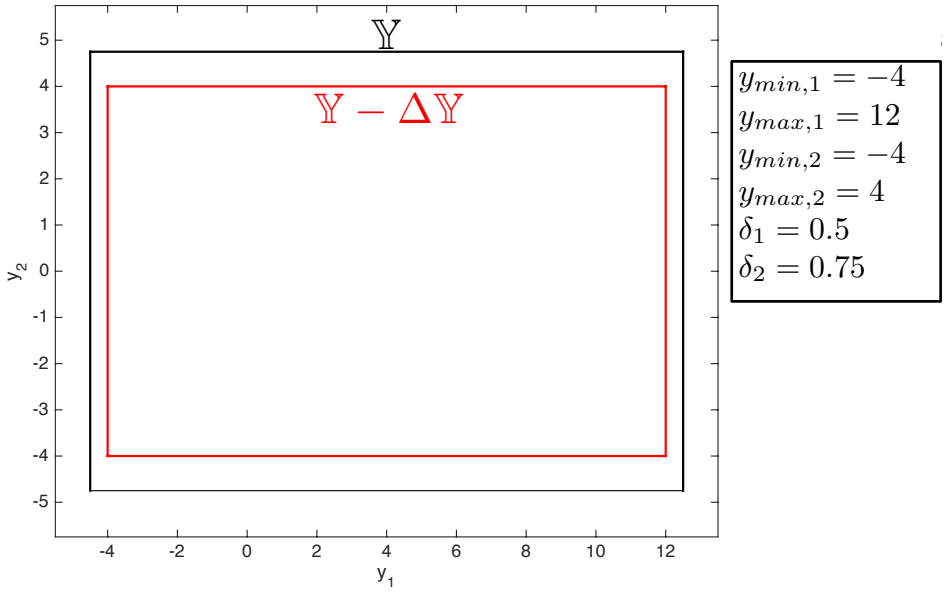

Figure 2.1: Two dimensional example of the hypercube that defines the output constraint set for two generic outputs, y_1 and y_2.

modes is known as a modulation function and is defined as

$$m_i(y_{m,i}) = \begin{cases} 1 & \text{if } y_{m,i} < y_{min,i} - \delta_i \text{ or } y_i < y_{min,i} - \delta_i \\ (-y_{m,i} + y_{min,i})/\delta_i & \text{if } y_{min,i} - \delta_i \leq y_{m,i} < y_{min,i} \text{ and } y_{min,i} - \delta_i < y_i < y_{max,i} + \delta_i \\ 0 & \text{if } y_{min,i} \leq y_{m,i} < y_{max,i} \text{ and } y_{min,i} - \delta_i < y_i < y_{max,i} + \delta_i \\ (y_{m,i} - y_{max,i})/\delta_i & \text{if } y_{max,i} \leq y_{m,i} < y_{max,i} + \delta_i \text{ and } y_{min,i} - \delta_i < y_i < y_{max,i} + \delta_i \\ 1 & \text{if } y_{max,i} + \delta_i \leq y_{m,i} \text{ or } y_{max,i} + \delta_i \leq y_i \end{cases} \tag{2.9}$$

The modulation function's dependency on the reference model is useful because it allows for the controller to differentiate between commanded trajectories that are safe, and those which exceed

some constraint. The additional dependency on the true outputs, i.e. $m_i = 1$ if $y_i < y_{min,i} - \delta_i$ or $y_i > y_{max,i} + \delta_i$ is included as a safety measure to handle disturbances. With this added precaution, the SMSC controller is capable of enforcing state constraints both when an unacceptably large command is given and in the presence of disturbances. Both will be demonstrated in simulation. Equation (2.9) is but one of many possible modulation function options for achieving the control objective. Here, the transition from 0 to 1 and from 1 to 0 occurs linearly. This transition however, can take place in a multitude of ways as long as $m_i(y_{m,i})$ remains piecewise differentiable [39].

In order to ensure that the tracking error dynamics given in Equation (2.6) remain stable, the SMSC control law is given by

$$u = [Cg(x)\hat{\Lambda}]^{\dagger} \left(\dot{y}_m - C\hat{f}(x) + (I - M)(K_1 e - \nu) + M(K_2 e_{th} - \nu_{SC}) \right) \tag{2.10}$$

where the notation $(\cdot)^{\dagger}$ represents the right-handed pseudo-inverse if $m > p$ and the true inverse if $m = p$. The matrix $M \in \mathbb{R}^{n \times n}$ in the control law is a diagonal matrix of the form

$$M = \begin{bmatrix} m_1(y_{m,1}) & 0 & \dots & 0 \\ 0 & m_2(y_{m,2}) & \dots & 0 \\ \vdots & \vdots & \ddots & \vdots \\ 0 & 0 & \dots & m_p(y_{m,p}) \end{bmatrix} \tag{2.11}$$

The vector $\nu \in \mathbb{R}^p$ is an adaptive signal used to account for parameter uncertainty and $\nu_{SC} \in \mathbb{R}^p$ is a state constraint signal. The vector $\hat{f}(x) : \mathbb{R}^n \mapsto \mathbb{R}^n$ is an estimated model of the plant dynamics, and $K_i \in \mathbb{R}^{p \times p}$ for $i = 1, 2$ are diagonal error feedback gain matrices such that $K_i = K_i^T > 0$.

Substituting the SMSC control law, Equation (2.10), into the tracking error dynamics, Equation (2.6), results in

$$\dot{e} = -Cf(x) + C\hat{f}(x) - (I - M)(K_1 e - \nu) - M(K_2 e_{th} - \nu_{SC}) + Cg(x)\delta\tilde{\Lambda}u \tag{2.12}$$

As shown in Section 1, it is assumed that the difference $C\hat{f}(x) - Cf(x)$ can be parameterized as

$$C\hat{f}(x) - Cf(x) = W^T b(x) \tag{2.13}$$

where $W \in \mathbb{R}^{n_w \times p}$ is a matrix of unknown constant weights and $b(x) \in \mathbb{R}^{n_w}$ is a vector of known, potentially nonlinear, basis functions that is assumed to be bounded for all bounded x. In order to account for the uncertainty in the open-loop dynamics $f(x)$, the adaptive signal ν is defined as

$$\nu = \widehat{W}^T b(x) \tag{2.14}$$

where $\widehat{W}$ is an estimate of the unknown weight matrix W and is updated through an adaptive law. This allows for Equation (2.12) to be rewritten as

$$\dot{e} = -\widetilde{W}^T b(x) - (I - M)K_1 e - M(K_2 e_{th} - \nu_{SC} + \nu) + Cg(x)\delta\tilde{\Lambda}u$$

where $\widetilde{W} = \widehat{W} - W$. The adaptive laws which are used to update the estimated matrices $\widehat{W}$ and $\delta\hat{\Lambda}$ are given by

$$\dot{\widehat{W}} = \Gamma_W \mathrm{Proj}_M(\widehat{W}, b(x)[e^T(I - M) + e_{th}^T M]) \tag{2.15}$$

$$\delta\dot{\hat{\Lambda}} = \Gamma_\Lambda \mathrm{Proj}_M(\delta\hat{\Lambda}, -g(x)^T C^T[(I - M)e + Me_{th}]u^T) \tag{2.16}$$

where $\Gamma_W \in \mathbb{R}^{n_w \times n_w}$ and $\Gamma_\Lambda \in \mathbb{R}^{m \times m}$ and $\Gamma_i = \Gamma_i^T > 0$ for $i = W, \Lambda$ are adaptive gain matrices. The state constraint signal ν_{SC} is defined as

$$\nu_{SC} = \nu + K_{SC} sat(e_{th}/\epsilon_{th}) + b_{SC}$$

where $K_{SC} \in \mathbb{R}^{p \times p}$ is a time-varying gain matrix defined as

$$K_{SC,ij} = \begin{cases} -m_i^* \left| \dot{y}_{m,i} + (1 - m_i(y_{m,i})) K_{1,ii} e_i \right| & \text{if } i = j \\ 0 & \text{otherwise} \end{cases} \tag{2.17}$$

$$m_i^* = \begin{cases} \frac{1}{m_i(y_{m,i})} & \text{if } m_i(y_{m,i}) \geq \epsilon_m \\ 0 & \text{otherwise} \end{cases}$$

and where ϵ_m is a tuning parameter that ensures m_i^* does not grow very large. The matrix K_{SC} acts upon a vector that utilizes the saturation function and is defined as

$$sat(e_{th}/\epsilon_{th}) = \begin{bmatrix} sat(e_{th,1}/\epsilon_{th,1}) & sat(e_{th,2}/\epsilon_{th,2}) & \dots & sat(e_{th,p}/\epsilon_{th,p}) \end{bmatrix}^T \tag{2.18}$$

$$sat(e_{th,i}/\epsilon_{th,i}) = \begin{cases} \frac{e_{th,i}}{\epsilon_{th,i}} & \text{if } |\frac{e_{th,i}}{\epsilon_{th,i}}| < 1 \\ sign(e_{th,i}) & \text{otherwise} \end{cases} \tag{2.19}$$

The saturation function is used to smoothen the transition from “tracking mode" to “state-constraining mode" and helps to prevent chattering in the control signal. The variables $\epsilon_{th,i} > 0$ are tuning parameters which moderate the behavior of the saturation functions and $b_{SC} \in \mathbb{R}^p$ is a vector to be defined. With the control law now completely defined, the tracking error dynamics can be finalized as

$$\dot{e} = -\widetilde{W}^T b(x) - (I - M)K_1 e - M(K_2 e_{th} - K_{SC} sat(e_{th}/\epsilon_{th}) - b_{SC}) + Cg(x)\delta\tilde{\Lambda}u \tag{2.20}$$

2.4 Stability Analysis

Theorem 2. *Consider the nonlinear dynamical system defined in (2.1), the reference model defined in (2.4), the SMSC control law defined in (2.10) and the adaptive laws defined in (2.15) and (2.16).*

Given a continuous and bounded reference input signal, r, and assuming finite initial conditions, either the tracking error e or the threshold error e_{th} is bounded for all $t > 0$, which implies that the control signal is bounded as well. Furthermore, if the steady-state value of the reference model $y_{m,ss} \in \mathbb{Y} - \Delta\mathbb{Y}$ then e is asymptotically stable and if $y_{m,ss} \notin \mathbb{Y}$ then e_{th} is asymptotically stable.

Proof. To prove the stability of the SMSC controller the following candidate Lyapunov function is chosen

$$V = \frac{1}{2}\left(e^T(I-M)e + e_{th}^T M e_{th} + tr(\widetilde{W}^T\Gamma_W^{-1}\widetilde{W}) + tr(\delta\tilde{\Lambda}\Gamma_\Lambda^{-1}\delta\tilde{\Lambda}^T)\right) \tag{2.21}$$

A derivative of (2.21) is taken with respect to time along the system trajectories. Note that $\dot{M} = M'\dot{y}_m$ where $M' \in \mathbb{R}^{n\times n}$ is a diagonal matrix with $m_i'(y_{m,i}) = dm_i/dy_{m,i}$ along the diagonal. Also note that when $m_i \neq 0$, $\dot{e}_{th,i} = -\dot{y}_i$. The derivative is given by

$$\dot{V} = e^T(I-M)\dot{e} - \frac{1}{2}e^T M'\dot{Y}_m e - e_{th}^T M\dot{y} + \frac{1}{2}e_{th}^T M'\dot{Y}_m e_{th} + tr(\widetilde{W}^T\Gamma_W^{-1}\dot{\widehat{W}}) + tr(\delta\tilde{\Lambda}^T\Gamma_\Lambda^{-1}\delta\dot{\hat{\Lambda}}^T) \tag{2.22}$$

where $\dot{Y}_m \in \mathbb{R}^{p\times p}$ is a diagonal matrix with the vector $\dot{y}_m$ along the diagonal. Substituting in the error dynamics given by Equation (2.20) and deriving a new expression for the output dynamics using $\dot{y} = \dot{y}_m - \dot{e}$, Equation (2.22) can be rewritten as

$$\begin{aligned}\dot{V} =& e^T(I-M)\left(-\widetilde{W}^T b(x) - (I-M)K_1 e - M(K_2 e_{th} - K_{SC}sat(e_{th}/\epsilon_{th}) - b_{SC}) + Cg(x)\delta\tilde{\Lambda}u\right)\\ &- e_{th}^T M\left(\dot{y_m} + \widetilde{W}^T b(x) + (I-M)K_1 e + M(K_2 e_{th} - K_{SC}sat(e_{th}/\epsilon_{th}) - b_{SC}) - Cg(x)\delta\tilde{\Lambda}u\right)\\ &- \frac{1}{2}e^T M'\dot{Y}_m e + \frac{1}{2}e_{th}^T M'\dot{Y}_m e_{th} + tr(\widetilde{W}^T\Gamma_W^{-1}\dot{\widehat{W}}) + tr(\delta\tilde{\Lambda}^T\Gamma_\Lambda^{-1}\delta\dot{\hat{\Lambda}}^T)\end{aligned} \tag{2.23}$$

Applying the trace identity $a^T b = tr(ba^T)$, results in

$$\begin{aligned}\dot{V} =& e^T(I-M)\left(-(I-M)K_1 e - M(K_2 e_{th} - K_{SC} sat(e_{th}/\epsilon_{th}) - b_{SC})\right) - \frac{1}{2}e^T M' \dot{Y}_m e \\ & - e_{th}^T M\left(\dot{y_m} + (I-M)K_1 e + M(K_2 e_{th} - K_{SC} sat(e_{th}/\epsilon_{th}) - b_{SC})\right) + \frac{1}{2}e_{th}^T M' \dot{Y}_m e_{th} \\ & + tr\left(\widetilde{W}^T(\Gamma_W^{-1}\dot{\widehat{W}} - b(x)[e^T(I-M) + e_{th}^T M])\right) + tr\left(\delta\tilde{\Lambda}^T(\Gamma_\Lambda^{-1}\delta\dot{\hat{\Lambda}}^T + u[e^T(I-M) + e_{th}^T M]Cg(x))\right)\end{aligned} \tag{2.24}$$

Substituting the adaptive laws (2.15) and (2.16) and utilizing the properties of the projection operator leaves

$$\begin{aligned}\dot{V} \leq& e^T(I-M)\left(-(I-M)K_1 e - M(K_2 e_{th} - K_{SC} sat(e_{th}/\epsilon_{th}) - b_{SC})\right) - \frac{1}{2}e^T M' \dot{Y}_m e \\ & - e_{th}^T M\left(\dot{y}_m + (I-M)K_1 e + M(K_2 e_{th} - K_{SC} sat(e_{th}/\epsilon_{th}) - b_{SC})\right) + \frac{1}{2}e_{th}^T M' \dot{Y}_m e_{th}\end{aligned} \tag{2.25}$$

In order to complete the proof, the system is analyzed across three cases: $M = 0$, $M = I$, and $0 < M < I$. These cases correspond to very specific scenarios where all of the reference states are either inside their independent constraint sets, i.e. $y_m \in \mathbb{Y} - \Delta\mathbb{Y}$, outside their independent constraint sets, i.e. $y_m \notin \mathbb{Y}$, or transitioning between the two sets. In general, at any given time $m_i(y_{m,i})$ may equal zero for some i and have a non-zero value for others. However due to the fact that M, K_1, K_2, M' and $\dot{Y}_m$ are diagonal, the analysis shown here can be performed almost identically on an output-by-output basis and therefore analysis of the three cases mentioned above is sufficient.

Case 1: $M = 0$

If $M = 0$ then $M' = 0$ as well and the Lyapunov function derivative (2.25) simplifies to

$$\dot{V} \leq -e^T K_1 e \leq 0 \tag{2.26}$$

which implies that, assuming finite initial values, e, e_{th}, $\widetilde{W}$ and $\delta\tilde{\Lambda}$ are bounded whenever $M = 0$. Furthermore, if $M = 0$ in steady-state, the inequality (2.26) implies that e_{ss}, $e_{th,ss}$, $\widetilde{W}_{ss}$ and $\delta\tilde{\Lambda}_{ss}$ are bounded and that $\int_0^\infty e_{ss}^T K e_{ss} dt$ exists and is finite. The subscript "ss" signifies the steady-state value. Since the reference signal r is assumed to be continuous and bounded this implies that u_{ss} and $\dot{e}_{ss}$ are bounded as well, which implies that e_{ss} is uniformly continuous in time. Therefore, Barbalat's Lemma implies that if $M = 0$ as $t \to \infty$, then $e \to 0$ as $t \to \infty$.

Case 2: $M = I$

If instead $M = I$ it once again implies that $M' = 0$ and the Lyapunov function derivative (2.25) can be rewritten as

$$\dot{V} \leq -e_{th}^T K_2 e_{th} - e_{th}^T(\dot{y}_m - K_{SC} sat(e_{th}/\epsilon_{th}) - b_{SC}) \tag{2.27}$$

It will be shown that $b_{SC} = 0$ if $M = I$. Consider the scenario where $sat(e_{th,i}/\epsilon_{th,i}) = sign(e_{th,i}/\epsilon_{th,i})$. The inequality (2.27) can then be rearranged as

$$\dot{V} \leq -e_{th}^T K_2 e_{th} - |e_{th}^T| \left(\dot{Y}_m sign(e_{th}) + |\dot{y}_m|\right) \leq 0 \tag{2.28}$$

where for any vector $v \in \mathbb{R}^v$, the absolute value notation $|v|$ signifies $\begin{bmatrix} |v_1| & |v_2| & \dots & |v_v| \end{bmatrix}^T$ and

$$sign(e_{th}) = \begin{bmatrix} sign(e_{th,1}) & sign(e_{th,2}) & \dots & sign(e_{th,p}) \end{bmatrix}^T$$

This implies that whenever $M = I$ the threshold error e_{th} is driven to a set where

$$|e_{th,i}| \leq \epsilon_{th,i} \ \ \forall i \tag{2.29}$$

at which point $|sat(e_{th,i}/\epsilon_{th,i})| < 1$ for all i. This also implies that $\widetilde{W}$ and $\delta\tilde{\Lambda}$ are bounded when-

ever $M = I$. Furthermore, if $M = I$ in steady-state then the inequality (2.28) reduces to

$$\dot{V} \leq -e_{th}^T K_2 e_{th} \leq 0 \tag{2.30}$$

which implies that e_{ss}, $e_{th,ss}$, $\widetilde{W}_{ss}$ and $\delta\tilde{\Lambda}_{ss}$ are bounded. Using a similar argument to the one made above and invoking Barbalat's Lemma, the expression (2.30) implies that if $M = I$ as $t \to \infty$ then $e_{th} \to 0$ as $t \to \infty$.

Case 3: $0 < M < I$

Finally, we examine the case where $0 < M < I$, that is, when the controller is transitioning between "tracking mode" and "state-constraining mode". Once again we begin by considering the scenario where $sat(e_{th,i}/\epsilon_{th,i}) = sign(e_{th,i}/\epsilon_{th,i})$. The Lyapunov function derivative (2.25) can be rewritten as

$$\begin{aligned}\dot{V} \leq & e^T(I-M)\left(-(I-M)K_1 e - M(K_2 e_{th} - K_{SC} sign(e_{th}) - b_{SC})\right) - \frac{1}{2}e^T M' \dot{Y}_m e + \frac{1}{2}e_{th}^T M' \dot{Y}_m e_{th} \\ & - |e_{th}^T| M\left(Sign(e_{th})\left(\dot{y}_m + (I-M)K_1 e +\right) - MK_{SC}\right) - e_{th}^T M^2 (K_2 e_{th} - b_{SC})\end{aligned} \tag{2.31}$$

where $Sign(e_{th})$ is a diagonal matrix with the vector $sign(e_{th})$ along the diagonal. It was shown above that when the modulation function $m_i(y_{m,i})$ is equal to zero, the tracking error e is tightly bounded. Therefore, we assume that whenever $0 < m_i(y_{m,i}) \leq \epsilon_m$,

$$|e_{th,i}| m_i(y_{m,i}) \leq \epsilon_m \delta_i \tag{2.32}$$

In addition, we assume that when $0 < m_i(y_{m,i}) \leq \epsilon_m$,

$$m_i^2(y_{m,i}) \approxeq m_i(y_{m,i})(1 - m_i(y_{m,i})) \approxeq 0$$

Therefore, if $0 < m_i(y_{m,i}) \leq \epsilon_m$ for all i, the Lyapunov function derivative reduces to

$$\dot{V} \leq -e^T(I-M)^2K_1e - \frac{1}{2}e^TM'\dot{Y}_me + \frac{1}{2}e_{th}^TM'\dot{Y}_me_{th} - e_{th}^TM\dot{y}_m \tag{2.33}$$

which can be rewritten as

$$\dot{V} \leq -e^T(I-M)^2K_1e + \frac{1}{2}(y_{th}-y_m)^TM'\dot{Y}_m(y_{th}-y_m) - e_{th}^TM\dot{y}_m \tag{2.34}$$

Note that whenever $0 < M < I$, the difference $y_{th,i} - y_{m,i}$ is by definition bounded by

$$|y_{th,i} - y_{m,i}| \leq \delta_i \tag{2.35}$$

Therefore, due to the inequalities (2.5) and (2.32) the following inequality holds

$$\dot{V} \leq -e^T(I-M)^2K_1e + p\left(\frac{1}{2}+\epsilon_m\right)\delta_{max}C_m \tag{2.36}$$

where

$$\delta_{max} = \max_i \delta_i$$

This implies that whenever $0 < M < \epsilon_m I$ the tracking error e is driven to a set where

$$|e_i|^2 \leq \frac{\left(\frac{1}{2}+\epsilon_m\right)\delta_i C_m}{(1-\epsilon_m)^2K_{1,ii}} \tag{2.37}$$

If instead, $\epsilon_m < m_i(y_{m,i}) < 1$ for all i, then by substituting in the definition of K_{SC} given in

Equation (2.17) the Lyapunov function derivative becomes

$$\begin{aligned}\dot{V} \leq & -e^T(I-M)^2K_1e + e^T(I-M)\left(-M(K_2e_{th} - K_{SC}sign(e_{th}) - b_{SC})\right) - \frac{1}{2}e^TM'\dot{Y}_me \\ & \frac{1}{2}e_{th}^TM'\dot{Y}_me_{th} - e_{th}^TM^2(K_2e_{th} - b_{SC})\end{aligned} \tag{2.38}$$

This can be rearranged as,

$$\dot{V} \leq -e^T(I-M)^2K_1e - e_{th}^TM^2K_2e_{th} + \frac{1}{2}(y_{th}-y_m)^TM'\dot{Y}_m(y_{th}-y_m) + \sum_{i=1}^{i=p}\gamma_i + \sum_{i=1}^{i=p}\eta_ib_{SC,i} \tag{2.39}$$

where

$$\gamma_i = e_i(1-m_i(y_{m,i}))\Big(-m_i(y_{m,i})(K_{2,ii}e_{th,i} - K_{SC,ii}sign(e_{th,i}))\Big) \tag{2.40}$$

$$\eta_i = e_{th,i}m_i^2(y_{m,i}) + e_im_i(y_{m,i})(1-m_i(y_{m,i})) \tag{2.41}$$

To account for the terms γ_i which may be greater than zero, the vector b_{SC} is defined as

$$b_{SC,i} = \begin{cases} -\frac{\gamma_i}{\eta_i} & \text{if } \epsilon_m < m_i(y_{m,i}) < 1 \text{ and } \gamma_i > 0 \\ 0 & \text{otherwise} \end{cases} \tag{2.42}$$

which implies that if $\epsilon_m I < M < I$,

$$\dot{V} \leq -e^T(I-M)^2K_1e - e_{th}^TM^2K_2e_{th} + \frac{1}{2}p\delta_{max}C_m \tag{2.43}$$

The inequalities (2.36) and (2.43) imply that whenever $0 < M < I$, either the tracking error e is

bounded according to (2.37) or the threshold error e_{th} is bounded according to

$$|e_{th,i}|^2 \leq \frac{\frac{1}{2}\delta_i C_m}{\epsilon_m^2 K_{2,ii}} \tag{2.44}$$

To handle the situation when $|sat(e_{th,i}/\epsilon_{th,i})| < 1$ the tuning parameter $\epsilon_{th,i}$ is set to be less than or equal to the right hand side of (2.44) for all i. This implies that $\widetilde{W}$ and $\delta\tilde{\Lambda}$ are bounded as well.

It has now been shown that assuming finite initial values the tracking error or threshold error remain bounded regardless of the value that M takes. This implies that the chosen outputs y are bounded for all $t > 0$ which was assumed above to imply that the full state vector x is bounded. The state being bounded implies that all signals in the control law (2.10) are bounded as well. It was also shown that if $M = 0$ in steady-state then e is asymptotically stable and if $M = I$ in steady-state then e_{th} is asymptotically stable. Finally, recall that these conclusions can be drawn on an output-by-output basis such that if M contains both zero and non-zero entries along the diagonal, the stability analysis still holds. This concludes the proof. □

2.5 Generic Hypersonic Vehicle Simulation

The SMSC controller developed above was implemented and tested in the nonlinear Generic Hypersonic Vehicle simulation. The motivation for this simulation study was the issue of inlet unstart; a sudden breakdown of the shock system in an inlet which can lead to departure from controlled flight in supersonic and hypersonic air vehicles. Although inlet unstart is still a topic of current research, one known cause for the phenomenon is that it can occur when the vehicle flies at medium to large values of angle-of-attack or sideslip angle. Therefore, the state constraint mechanism developed in this section was used to restrict what values of angle-of-attack and sideslip angle the GHV could achieve and prevent inlet unstart from occurring.

In order to achieve the control objective of restricting position-level states, the system dynamics were broken down into a subsystem of position-level dynamics and a subsystem of velocity-level

dynamics. The position-level subsystem has dynamics of the form

$$\dot{x}_p = \begin{bmatrix} \dot{\phi} \\ \dot{\theta} \\ \dot{\psi} \\ \dot{\alpha} \\ \dot{\beta} \end{bmatrix} = f_p(x) + g_p(x)\Lambda_p \begin{bmatrix} p_d \\ q_d \\ r_d \end{bmatrix} \tag{2.45}$$

$$y_p = \begin{bmatrix} \alpha & \beta \end{bmatrix}^T \tag{2.46}$$

where the dynamics $f_p(x)$ and $g_p(x)$ are defined in Section 1. Note that for this subsystem the control vector is made up of the desired body-axis angular rates. This control signal is calculated using the SMSC controller defined in Section 2.3 and taking into account the constraints on angle-of-attack and sideslip angle. The velocity-level subsystem has dynamics of the form

$$\dot{x}_v = \begin{bmatrix} \dot{p} \\ \dot{q} \\ \dot{r} \end{bmatrix} = f_v(x) + g_v(x)\Lambda_v \begin{bmatrix} \delta_{f,r} \\ \delta_{f,l} \\ \delta_{t,r} \\ \delta_{t,l} \end{bmatrix} \tag{2.47}$$

$$y_v = \begin{bmatrix} p & q & r \end{bmatrix}^T \tag{2.48}$$

where again the dynamics $f_v(x)$ and $g_v(x)$ are given in Section 1. For this subsystem the control vector is made up of the control surfaces of the GHV, two elevons ($\delta_{f,i}$) and two ruddervators ($\delta_{t,i}$). Since there are no constraints on the velocity-level outputs this control signal is calculated using the tracking NDI control law derived in Section 1.3. This is equivalent to setting $m_i(y_{m,i}) = 0$ for all $t \geq 0$, $i = p, q, r$.

Parametric uncertainty was assumed in the moments of inertia of the vehicle as well as the lift,

drag, sideforce and various moment coefficients which are contained in the functions $f_p(x)$ and $f_v(x)$. Except for the moment of inertia parameters, the initial estimate of the various aerodynamic coefficients differed by at least 20% of the truth value. Given the notation used in Section 1 to describe the parametric uncertainty in the GHV simulation, this is equivalent to $|\hat{C}_X| \leq |0.8C_X|$ or $|\hat{C}_X| \geq |1.2C_X| \; \forall X$. The basis functions used in the adaptive laws are denoted as $b_p(x)$ and $b_v(x)$ for the position-level and velocity-level subsystem respectively and are given by

$$b_p(x) = \begin{bmatrix} \frac{\bar{q}}{V_T \cos\beta} & \frac{\bar{q}}{V_T \cos\beta}\alpha & \frac{\bar{q}}{V_T \cos\beta}\alpha^2 & \frac{\bar{q}}{V_T} & \frac{\bar{q}}{V_T}\beta \end{bmatrix}^T \tag{2.49}$$

$$b_v(x) = \begin{bmatrix} M_T^T & \bar{q} & \frac{\bar{q}}{V_T}x_v^T & pq & qr & pr & p^2 - r^2 & \bar{q}y_p^T & \bar{q}y_p^{(2)T} & \bar{q}y_p^{(3)T} \end{bmatrix}^T \tag{2.50}$$

$$y_p^{(i)} = \begin{bmatrix} \alpha^i & \beta^i \end{bmatrix}^T \quad i = 2, 3 \tag{2.51}$$

In order to make the simulation more realistic, second-order actuator dynamics with damping ratio $\zeta = 0.7$ and natural frequency $\omega_n = 25Hz$ were included and position and rate limits were placed on the actuators of $30\,\mathrm{deg}$ and $100\,\mathrm{deg}/s$, respectively. In addition, a time delay of $0.01s$ was included in the simulation. The initial flight condition was a velocity of Mach 6 and altitude of $80,000ft$. The constraints placed on the vehicle's angle-of-attack and sideslip angle were selected based on wind tunnel testing of a 10.5-inch HIFiRE 6 model at the Department of Aeronautics, U.S. Air Force Academy [32]. From their experiments, the recorded values at which an inlet unstart will occur are $14.5\,\mathrm{deg}$ and $-5.7\,\mathrm{deg}$ for angle-of-attack and $\pm 5.4\,\mathrm{deg}$ for sideslip angle. Therefore, in order to include a safety buffer the output threshold values were set as

$$\begin{bmatrix} \alpha_{max} & \alpha_{min} & \delta_\alpha & \beta_{max} & \beta_{min} & \delta_\beta \end{bmatrix} = \begin{bmatrix} 13 & -4 & 0.5 & 4 & -4 & 0.5 \end{bmatrix} \mathrm{deg} \tag{2.52}$$

Note that in general these constraint parameters may vary greatly with varying vehicle and inlet geometries.

The following gain and controller parameters were kept constant through out all presented

simulation trials. For the velocity-level subsystem, the reference model was defined as

$$\dot{y}_{m,v} = -10y_{m,v} + 10 \begin{bmatrix} p_d \\ q_d \\ r_d \end{bmatrix} \tag{2.53}$$

The feedback gain $K_{1,v}$ using the notation used for the SMSC controller or K_v using the notation used for in the tracking controller of Section 1 were set as

$$K_{1,v} = K_v = \begin{bmatrix} 7.5 & 0 & 0 \\ 0 & 7.5 & 0 \\ 0 & 0 & 7.5 \end{bmatrix} \tag{2.54}$$

Note that because no constraints were set for the velocity-level subsystem, there is no need to define the matrix $K_{2,v}$. The adaptive gains were set as $\Gamma_{\Lambda,v} = (1e-5)I_4$ and

$$\Gamma_{W,v} = \begin{bmatrix} (1e-5)I_7 & 0 \\ 0 & (1e-3)I_{10} \end{bmatrix} \tag{2.55}$$

where I_N represents the $N \times N$ identity matrix. Although $\Lambda_v = I_4$ the initial estimate $\hat{\Lambda}_v(t=0)$ was set to $1.1I_4$. The weight estimate matrix was initialized as $\widehat{W}_v(t=0) = 0$. For the position-level subsystem, the reference model was defined as

$$\dot{y}_{m,p} = -y_{m,p} + \begin{bmatrix} \alpha_{cmd} \\ \beta_{cmd} \end{bmatrix} \tag{2.56}$$

The feedback gains were iteratively tuned and set to

$$K_{1,p} = K_{2,p} = \begin{bmatrix} 1 & 0 \\ 0 & 4 \end{bmatrix} \tag{2.57}$$

Because $g_p(x)$ is made up of known trigonometric functions, it is assumed that $\Lambda_p = I_3$ is known perfectly. The adaptive gain matrix was set as $\Gamma_{W,p} = (1e-4)I_5$ and the weight estimate matrix was initialized as $\widehat{W}_p(t=0) = 0$. The remaining controller parameters were set as $\epsilon_{th,\alpha} = \epsilon_{th,\beta} = 0.05\,\text{deg}$ and $\epsilon_m = 0.2$.

2.5.1 Results: Commanding an Unacceptable Reference Trajectory

Two test cases were examined in order to demonstrate the effectiveness of the SMSC controller when dealing with unacceptably large reference trajectory commands. In the first test case $6\,\text{deg}$ doublets were commanded and in the second test case $10\,\text{deg}$ doublets were commanded. Note that according to (2.52), these commands violate the constraints α_{min}, β_{min} and β_{max} but not α_{max}. The purpose of choosing such commands was to demonstrate the controllers' ability to handle both symmetric and asymmetric constraint sets.

Each test case was also examined using the tracking controller which had no state constraint mechanism. No inlet unstart model was included in the simulation when generating the results in this section and therefore adverse effects are not seen when α and β exceed their constraints in these comparative cases. They are useful however for studying how the control signal and velocity-level states are affected by the use of the SMSC controller.

Test Case 1: 6 degree Doublet Command

Figures 2.2 and 2.4 show the time histories for the position-level outputs α and β, as well as the control surface deflections and total velocity. The Euler angle and velocity-level outputs are shown in Figures 2.3 and 2.5. The results shown in Figure 2.3 indicate that the SMSC controller induced

a larger pitch rate than the tracking controller in achieving the angle-of-attack based control objective. Otherwise, when commanding a $6\,\mathrm{deg}$ doublet in angle-of-attack the signals are fairly similar across both controllers. Greater variation is seen across controllers in Figures 2.4 and 2.5 where sideslip angle is being commanded. In successfully restricting β, the control surface deflections vary significantly from those of the tracking control law. In addition, the SMSC control law led to a much larger roll rate command and therefore larger roll angle (although well within the acceptable range for hypersonic air vehicles) when compared to the tracking controller. In both examples that were investigated in Test Case 1, the control objective was achieved.

Test Case 2: 10 degree Doublet Command

The second test case contained two more challenging examples as $10\,\mathrm{deg}$ doublets were commanded despite the constraint set given in (2.52) remaining constant. The time histories are separated as they were for Test Case 1: Sideslip angle, angle-of-attack, the control surface deflections and total velocity are shown in Figures 2.6 and 2.8 while Euler angle and velocity-level outputs are shown in Figures 2.7 and 2.9. In this test case some chattering is seen in the signals generated using SMSC control law, in particular when sideslip angle was commanded. Therefore, when commanding the system to enter a region of the state-space that significantly violates the constraint set extra care must be taken if utilizing the SMSC controller. Nevertheless, in both examples shown, the SMSC controller achieves the control objective despite the large command signal without violating actuator limitations.

Note that in Figure 2.8, the tracking control law led to a large drop in airspeed while the vehicle is flying at a large sideslip angle. In actuality, flying at such a sideslip angle would lead to an inlet unstart in most hypersonic vehicles. By constraining what values of sideslip angle the vehicle can achieve, not only can inlet unstart be prevented but the vehicle is able to maintain airspeed. Also note that as in Case 1, Figure 2.9 indicates that the SMSC controller led to a larger roll rate and roll angle than the tracking controller.

2.5.2 Results: Disturbance Rejection

In order to successfully prevent inlet unstart, a state constraint mechanism must be able to restrict the system outputs not only when a large trajectory is commanded, but also in the presence of disturbances. The SMSC controller can successfully reject disturbances due to the modulation function's additional dependency on the true outputs, i.e. $m_i = 1$ if $y_i < y_{min,i} - \delta_i$ or $y_i > y_{max,i} + \delta_i$. In order to demonstrate this capability, $5\,\mathrm{deg}$ doublet trajectories were commanded in both sideslip angle and angle-of-attack. During the angle-of-attack trajectory simulation, show in Figure 2.10, a $1250lbf$ disturbance force lasting one second was applied to the vehicle at $t = 17sec$ in the positive z (down) direction. During the sideslip angle trajectory simulation, show in Figure 2.11, a $2000lbf$ disturbance force lasting one second was applied to the vehicle at $t = 20sec$ in the negative y direction. The disturbance forces were implemented as exogenous forces acting on the center of mass of the vehicle in the Simulink block containing the true plant dynamics. No information about the disturbance force timing or magnitude was provided to the controller. In both cases, the vehicle was restricted from entering a region of the state-space within which inlet unstart would occur. When the same disturbance was applied to the vehicle using the tracking controller, a constraint violation occurred in both examples at the moment in time indicated in the Figures. This demonstrates the SMSC controller's capability to enforce state constraints not only when large command signals are applied but also in the presence of disturbances.

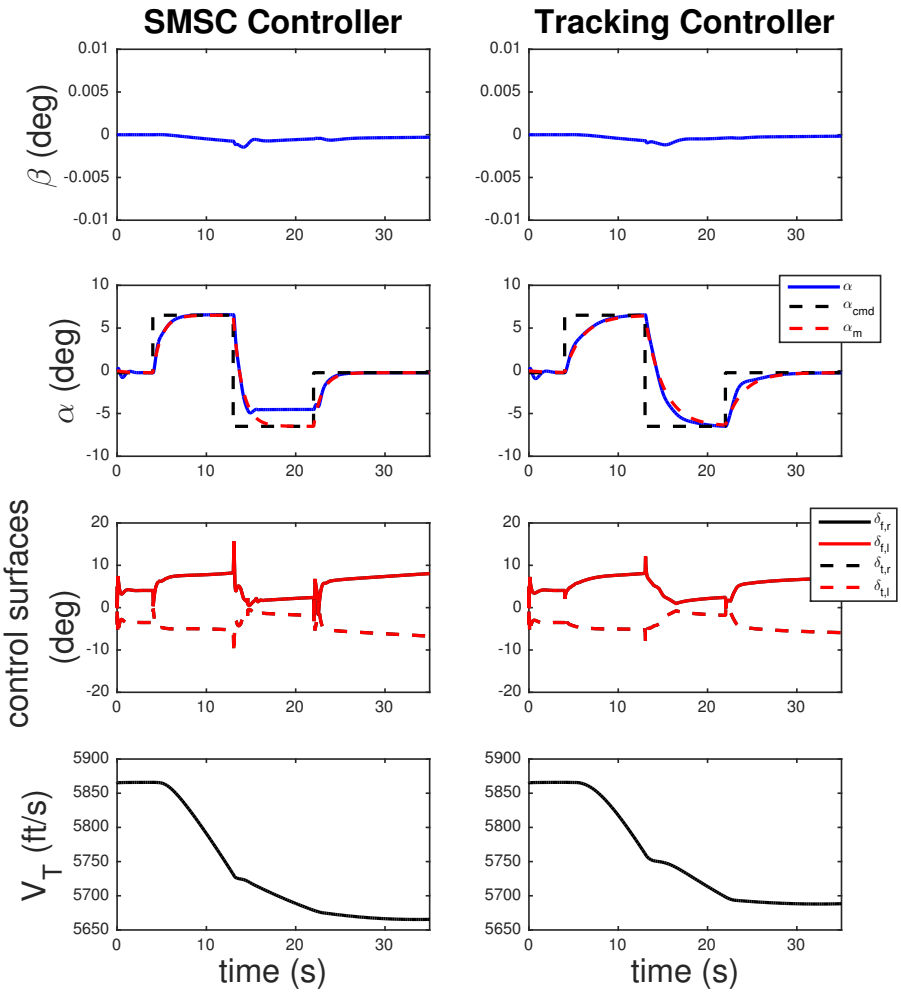

Figure 2.2: Response to 6 degree doublet command in angle-of-attack. Time histories are shown of sideslip angle, angle-of-attack, the control surface deflections and total velocity.

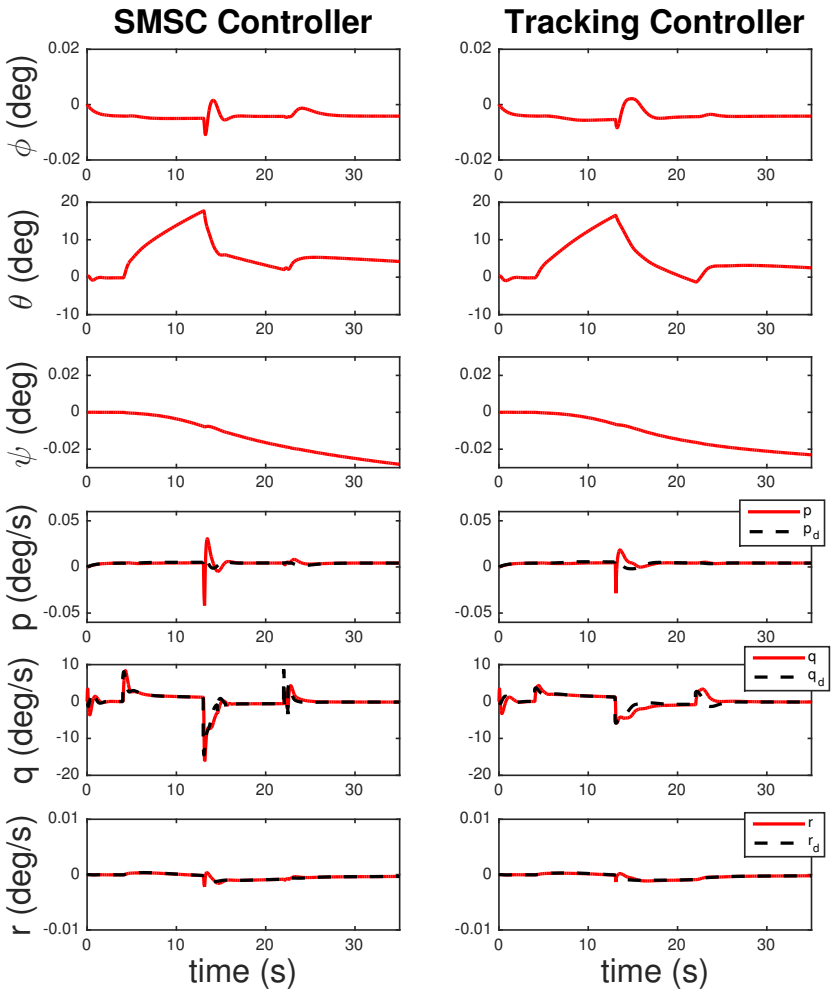

Figure 2.3: Response to 6 degree doublet command in angle-of-attack. Time histories are shown of the vehicle's Euler angles and body-fixed angular rates.

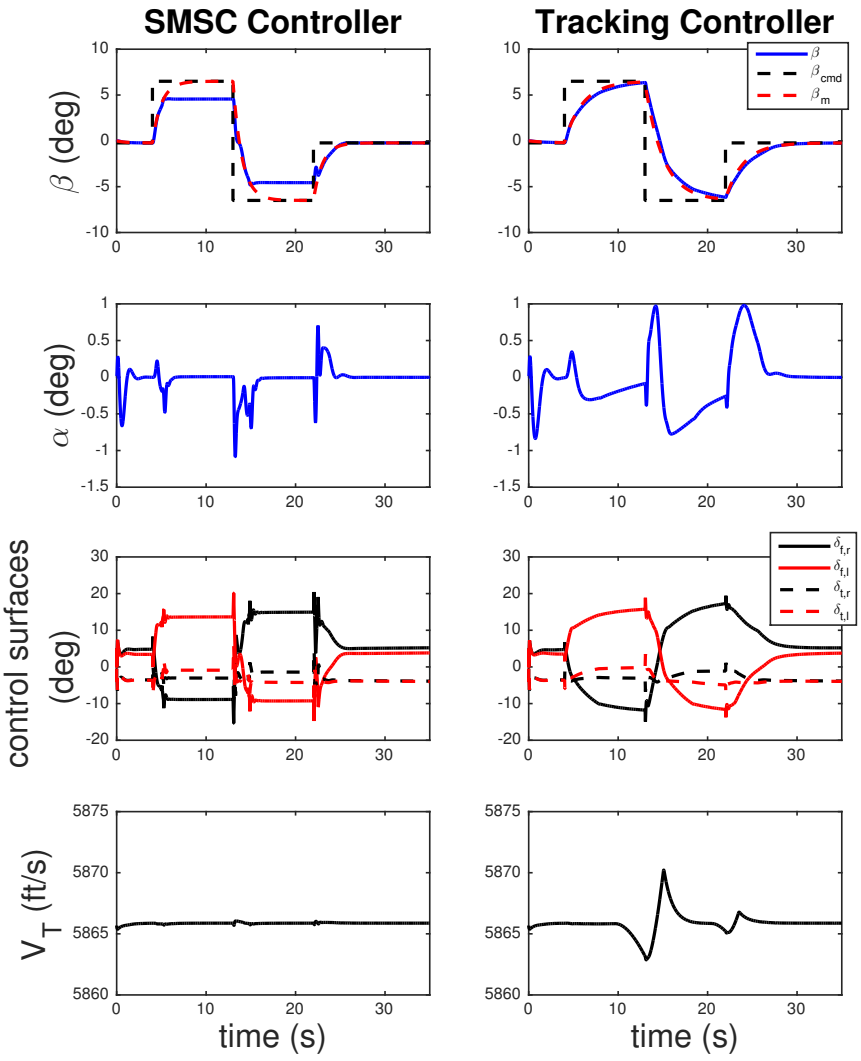

Figure 2.4: Response to 6 degree doublet command in sideslip angle. Time histories are shown of sideslip angle, angle-of-attack, the control surface deflections and total velocity.

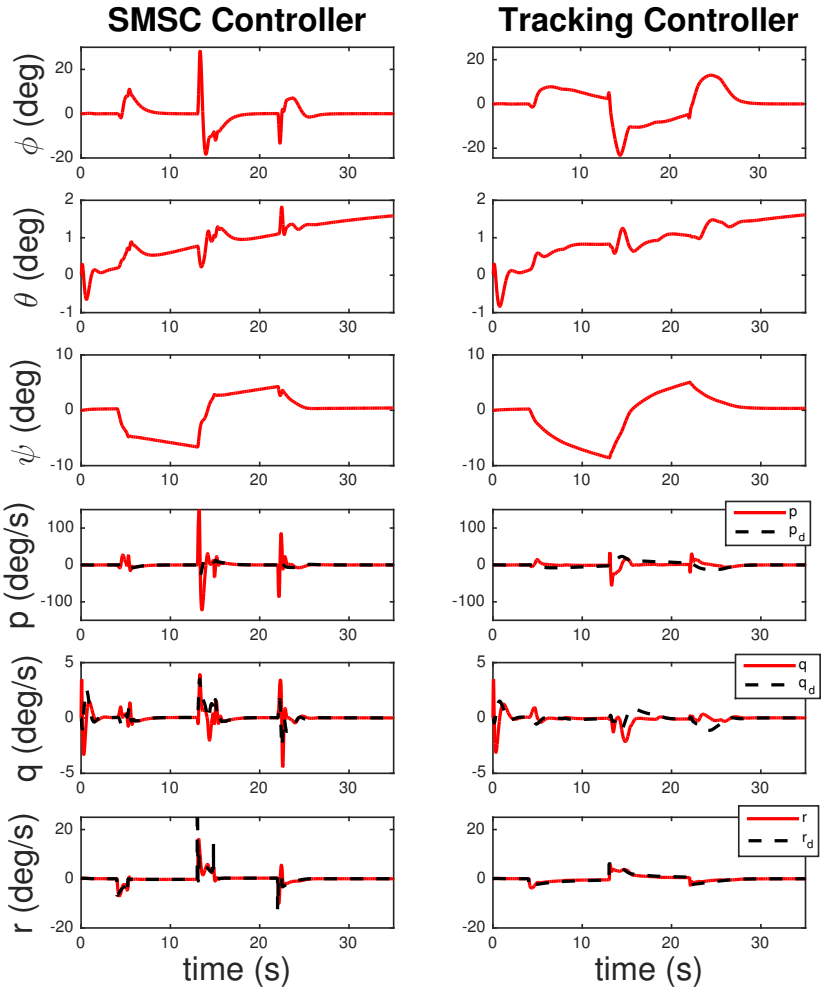

Figure 2.5: Response to 6 degree doublet command in sideslip angle. Time histories are shown of the vehicle's Euler angles and body-fixed angular rates.

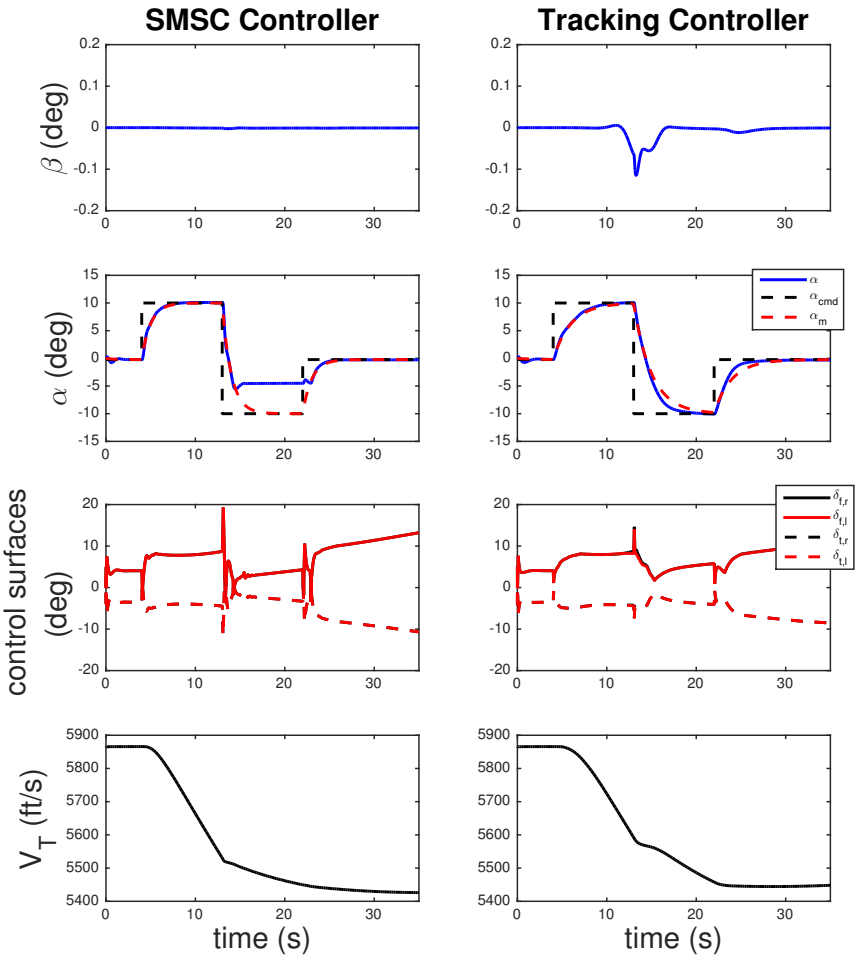

Figure 2.6: Response to 10 degree doublet command in angle-of-attack. Time histories are shown of sideslip angle, angle-of-attack, the control surface deflections and total velocity.

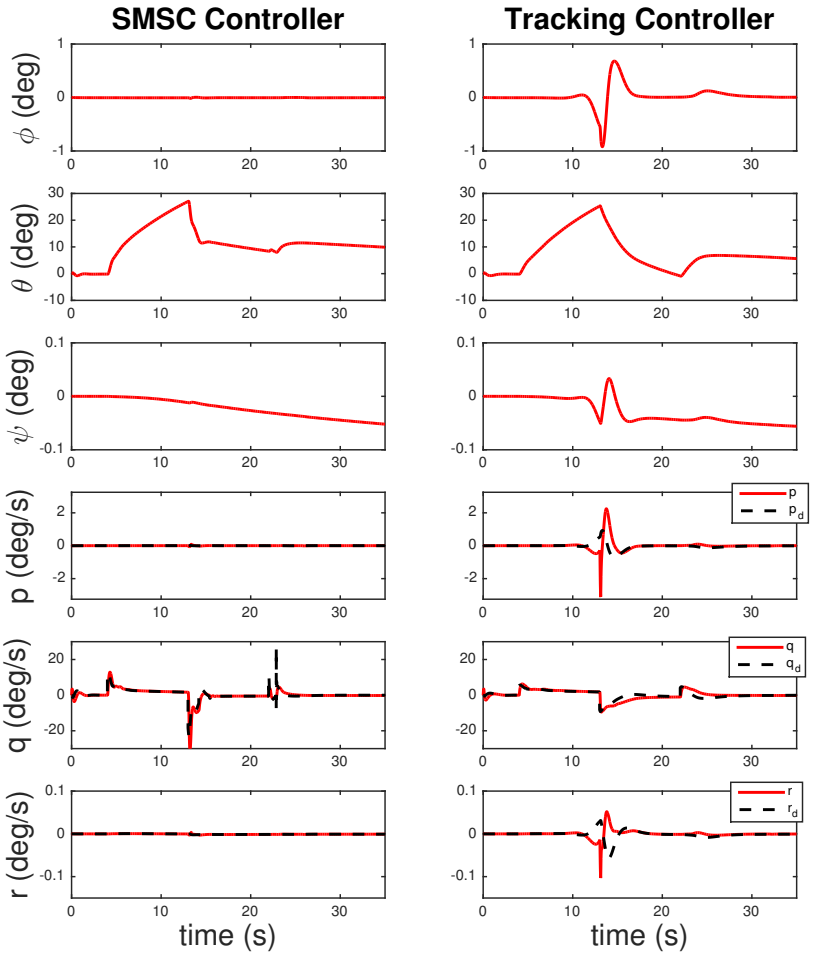

Figure 2.7: Response to 10 degree doublet command in angle-of-attack. Time histories are shown of the vehicle's Euler angles and body-fixed angular rates.

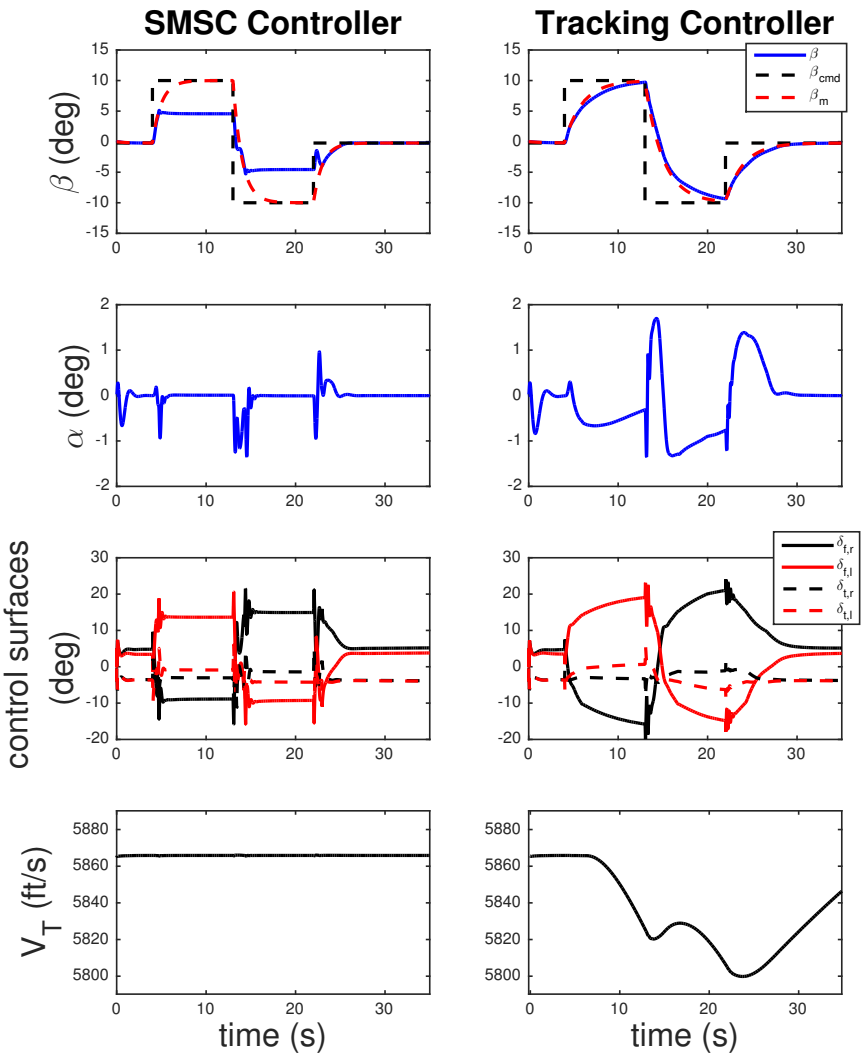

Figure 2.8: Response to 10 degree doublet command in sideslip angle. Time histories are shown of sideslip angle, angle-of-attack, the control surface deflections and total velocity.

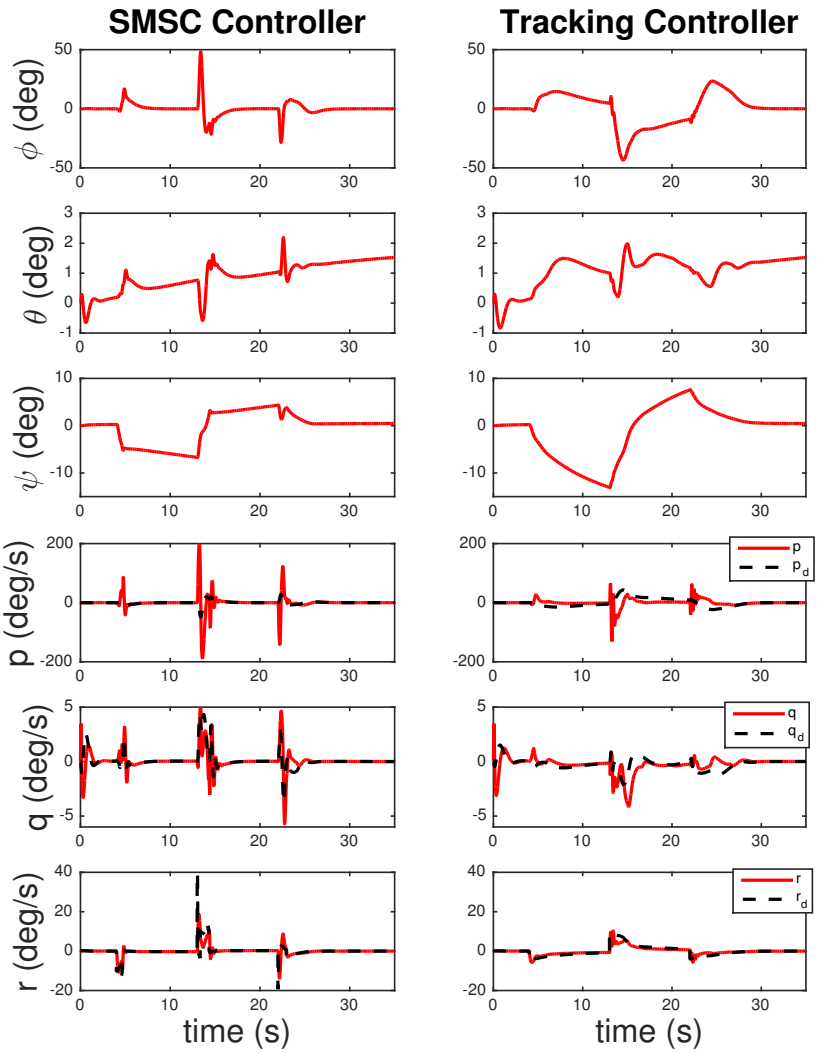

Figure 2.9: Response to 10 degree doublet command in sideslip angle. Time histories are shown of the vehicle's Euler angles and body-fixed angular rates.

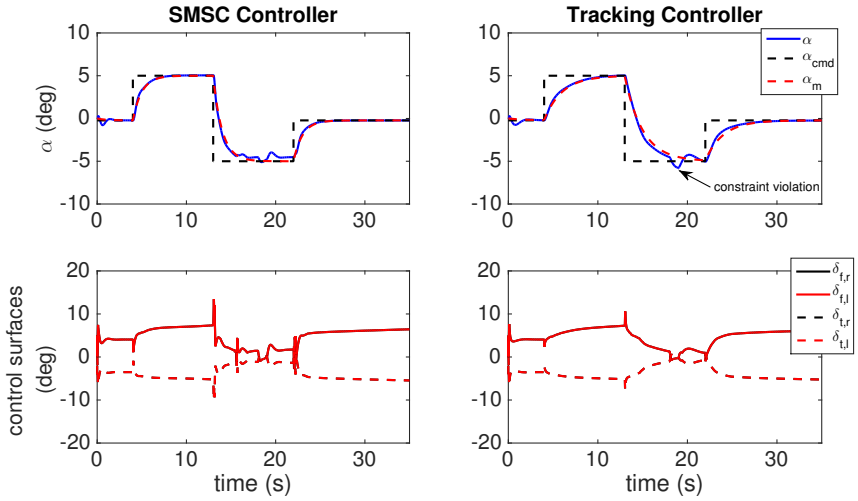

Figure 2.10: Longitudinal Disturbance Rejection Example. Time histories are shown of angle-of-attack and the control surface deflections.

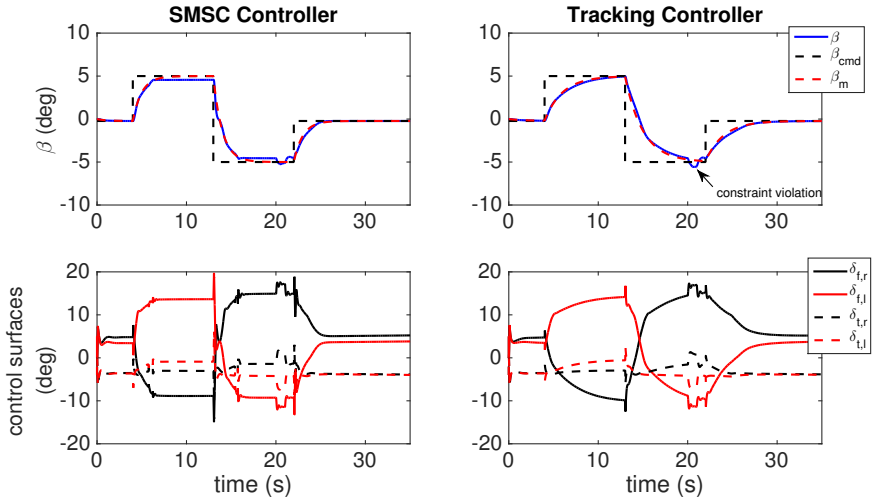

Figure 2.11: Lateral/Directional Disturbance Rejection Example. Time histories are shown of sideslip angle and the control surface deflections.

3. NONLINEAR DYNAMIC INVERSION ADAPTIVE CONTROL WITH STATE CONSTRAINTS USING BOUNDING FUNCTIONS

3.1 Introduction

In this section the second technique capable of enforcing state constraints in a nonlinear dynamic inversion adaptive control framework is presented in order to address the research issues described in Section 2. Specifically, when developing and implementing new control algorithms the need to restrict dynamical systems within certain regions of the state-space is an important consideration. In the case of hypersonic vehicles, for example, state constraint enforcement can prevent inlet unstart from occurring. In integrating such mechanisms with an NDI adaptive control algorithm, the control techniques presented in this section and the previous one allow for successful state constraint enforcement when dealing with nonlinear systems with models containing significant parametric uncertainty.

The method developed in this section enforces state constraints using a bounding function technique first developed in [40] for linear systems with unknown nonlinear disturbances. The bounding functions used in this technique allow for significant flexibility in designing how the controller transitions between “tracking mode" and “state constraining mode". Such flexibility allows for this technique to potentially lessen chattering in the control signal to an even greater extent than the sliding mode controllers of Section 2. It also allows for the use of more complex constraint sets, which will be discussed below. Other instances of using state-dependent functions in the control law that become prevalent as the state approaches a constraint bound have been developed in [43] and [44]. In these papers, Barrier Lyapunov functions are analyzed to ensure that these additional functions in the control law will remain less than infinity. In [43], this method is used to directly enforce state constraints in nonlinear systems in strict feedback form. In [44], a neural network adaptive controller is introduced for a class of uncertain nonlinear systems. The Barrier Lyapunov

function method is used to ensure that the system states remain within a constraint set, and therefore ensures that the neural network approximation of the unknown nonlinear dynamics remains valid. Alternatively, the state-dependent functions used in the presented method are bounded by definition and the control algorithm applies to a wider class of nonlinear affine-in-control systems - no specific feedback structure is required. Because the bounding functions depend on the states themselves, this technique is capable of enforcing state constraints both when an unacceptably large command is given and in the presence of disturbances.

As in Section 2, the control objective is to stabilize the system tracking error while maintaining that the system outputs remain in a predefined constraint set. Stability of the bounding function state constraint (BFSC) controller is proven with three theorems that are based on Lyapunov analysis. The first theorem proves that, through use of the BFSC control technique, the system states and the tracking error are bounded for a bounded input signal. Through the second theorem, it is proven that if the steady-state value of the reference model is within the constraint set, perfect tracking will occur. As with the SMSC controller, at times when no state constraints are in danger of being exceeded the controller developed in this section reduces to the tracking controller described in Section 1.3. The final theorem once again examines the system regardless of where the steady-state value of the reference model lies and produces a conservative, analytical bound for the system output and tracking error. Following the derivation of the controller and the stability analysis, the BFSC controller is implemented in the GHV simulation and it is shown that it is capable of restricting the values of angle-of-attack and sideslip angle the vehicle can achieve.

Due to its ability to significantly lessen chattering in the control signal while enforcing state constraints, the BFSC controller was also tested in an inlet unstart recovery feasibility study. A simplified inlet unstart model, which will be described in detail in this section, was included in the GHV simulation. This testing is referred to as a feasibility study because the included model lacks some of the significant aerodynamic effects of inlet unstart. This is primarily due to the fact that inlet unstart is still a current research topic and actual aerodynamic data is difficult to obtain

for export control reasons. Nevertheless, it was demonstrated that using this simplistic model the BFSC controller could not only be used to prevent inlet unstart but also to perform important maneuvers necessary to recover from one as well.

3.2 Problem Statement

Consider the nonlinear, affine-in-control class of systems with dynamics that can be represented by the equations

$$\dot{x} = f(x) + g(x)\Lambda u \tag{3.1}$$

$$y = Cx \tag{3.2}$$

where $x \in \mathbb{R}^{n_s}$ is the system state, $u \in \mathbb{R}^m$ is the control, the vector $f(x) \in \mathbb{R}^{n_s}$ represents the nonlinear open-loop dynamics of the system which are assumed to be bounded for bounded x, and $g(x)\Lambda \in \mathbb{R}^{n_s \times m}$ represents the control effectiveness of the system. It is assumed that $f(x)$ and the constant matrix $\Lambda \in \mathbb{R}^{m \times m}$ are unknown but that Λ has full rank. The matrix $g(x) \in \mathbb{R}^{n_s \times m}$ is considered known. In the output equation (3.2), $y \in \mathbb{R}^p$ represents the outputs which are desired to be controlled and/or constrained such that $n_s \geq m \geq p$. The matrix $C \in \mathbb{R}^{p \times n_s}$ is constant, known, and assumed to have full rank. In order to utilize a dynamic inversion control law, we limit the scope to systems where the product $Cg(x)\Lambda$ has full rank for all x.

For the state constraint controller presented in this section it is assumed that full state feedback is available. As in Section 2, the control objective is to stabilize the system tracking error while maintaining that y remains within a predefined constraint set. The system tracking error is defined as

$$e = y_m - y \tag{3.3}$$

where y_m represents a reference model signal for the system outputs. It is assumed that the system outputs are selected such that if the tracking error is bounded it can be concluded that the full state

vector x is bounded as well. The desired reference model dynamics are given by

$$\dot{y}_m = A_m y_m + B_m r \tag{3.4}$$

where $y_m \in \mathbb{R}^p$ and $r \in \mathbb{R}^p$ is a reference input signal. The matrix $A_m \in \mathbb{R}^{p\times p}$ is Hurwitz, and $B_m \in \mathbb{R}^{p\times p}$. It is assumed that the reference input signal r is continuous and bounded such that there exists a known constant C_m where

$$\|y_m\| \leq C_m \quad \|\dot{y}_m\| \leq C_m \tag{3.5}$$

Note that the constant C_m does not restrict the reference model to remain within the predefined constraint set. With the definitions and derivation of Section 1.3.1 the error dynamics can be expressed as

$$\dot{e} = \dot{y}_m - Cf(x) - Cg(x)\hat{\Lambda}u + Cg(x)\delta\tilde{\Lambda}u \tag{3.6}$$

3.3 Bounding Functions

The bounding function state constraint controller utilizes specifically designed functions which activate when an output approaches a predefined constraint value, and smoothly adjust the control and adaptive laws accordingly. The general definition for a bounding function $f_b(\cdot)$ is given below.

Definition 3.3.1. *$f_b : \mathbb{R} \mapsto \mathbb{R}$ is a bounding function if it is continuously differentiable and satisfies the following properties:*

- $f_b(a) = 0, \quad \forall a \leq \bar{b}$
- $f_b(a) > 0, \quad \forall a > \bar{b}$
- $f_b(a) \to \infty, \;\; a \to \infty$
- *$f_b'(a)$ is locally Lipschitz and monotonically increasing.*

- $f_b^{'}(a) = 0, \quad \forall a \leq \bar{b}$
- $f_b^{'}(a) > 0, \quad \forall a > \bar{b}$

where a is a scalar dependent variable, $f_b^{'}(a)$ is the derivative of $f_b(a)$ with respect to a, and $\bar{b}$ is a designer chosen constraint.

For each output which is desired to be controlled and/or constrained, a bounding function is constructed which corresponds to that output's predefined threshold values and is denoted as $f_{b,i}(y_i^2)$. The control objective can theoretically be achieved with any bounding function that satisfies the above definition. Although alternative methods are available, one specific process for constructing bounding functions that produce the desired behavior is presented.

3.3.1 A Method for Constructing Bounding Functions

The proposed bounding function is given by

$$f_{b,i}(y_i^2) = \begin{cases} f_{b,i}^{min}(y_i^2) & \text{if } y_{th,i} = y_{min,i} - \delta_i \\ \\ f_{b,i}^{max}(y_i^2) & \text{if } y_{th,i} = y_{max,i} + \delta_i \end{cases} \tag{3.7}$$

where $y_{th,i}$ is again defined by (2.8). To allow for more flexibility in the design and for asymmetric constraint sets, a separate bounding function is used to handle the maximum output bound and the minimum output bound. Both of these functions are constructed as

$$f_{b,i}^j(y_i^2) = \begin{cases} 0 & \text{if } y_i^2 \leq y_{j,i}^2 \\ f_{t,i}^j(y_i^2) & \text{if } y_{j,i}^2 < y_i^2 \leq y_{th,i}^2 \\ \exp(\rho_i^j y_i^2) - \phi_{0,i}^j & \text{if } y_i^2 > y_{th,i}^2 \end{cases} \tag{3.8}$$

for $j = \{min, max\}$. The polynomial $f^j_{t,i}(y_i^2)$ is chosen to transitionally activate the bounding function when the output is between the predetermined regions $y_{j,i}$ and $y_{th,i}$. The parameter δ_i is chosen based on how quickly one desires the bounding function to transition from 0 to an exponential function, and the parameter $\rho_i^j > 0$ affects the growth rate of the bounding function.

The transition polynomial takes the form

$$f^j_{t,i}(y_i^2) = \phi^j_{1,i}(y_i^2)^4 + \phi^j_{2,i}(y_i^2)^3 + \phi^j_{3,i}(y_i^2)^2 + \phi^j_{4,i}(y_i^2) + \phi^j_{5,i} \tag{3.9}$$

The constants $\phi^j_{0,i}, \phi^j_{1,i}...\phi^j_{5,i}$ are solved for by looking at the desired boundary conditions for the bounding function. These boundary conditions are

$$f^j_{b,i}(y^2_{j,i}) = f'^j_{b,i}(y^2_{j,i}) = f''^j_{b,i}(y^2_{j,i}) = 0 \tag{3.10}$$

$$f^j_{b,i}(y^2_{th,i}) = \exp(\rho_i^j y_i^2) - \phi^j_{0,i} \tag{3.11}$$

$$f'_{b,i}(y^2_{th,i}) = \rho_i^j \exp(\rho_i y_i^2) \tag{3.12}$$

$$f''_{b,i}(y^2_{th,i}) = (\rho_i^j)^2 \exp(\rho_i^j y_i^2) \tag{3.13}$$

where the prime symbol in Equations (3.10)−(3.13) represents differentiation with respect to y_i^2. By taking two derivatives of the general form of the transitional function $f^j_{t,i}(y_i^2)$,

$$f'^j_{t,i}(y_i^2) = 4\phi_{1,i}(y_i^2)^3 + 3\phi_{2,i}(y_i^2)^2 + 2\phi_{3,i}(y_i^2) + \phi_{4,i} \tag{3.14}$$

$$f''^j_{t,i}(y_i^2) = 12\phi_{1,i}(y_i^2)^2 + 6\phi_{2,i}(y_i^2) + 2\phi_{3,i} \tag{3.15}$$

and applying the six given boundary conditions, Equations (3.10)−(3.13), one is left with six linear equations which can be used to solve for the six $\phi_{j,i}$'s as long as $\delta_i \neq 0$. Note that because the bounding functions depend on the true outputs y_i, this technique is capable of enforcing state constraints when both an unacceptably large command is given, and in the presence of disturbances.

Unlike the SMSC controller this technique does not specifically recognize which command signals are outside of the constraint set. Instead, the controller alters its behavior if, in tracking the reference signal, the true output gets too close to a constraint boundary.

More complicated constraint sets are easily applicable with this bounding function construction technique. In addition to including both a maximum and minimum bound, this could include more sophisticated structures where the desired bounds are determined based on the current operating condition of the system. In this scenario, a bounding function with the same behavior but different coefficients would be needed to handle the other constraint boundaries. One way to deal with this is to calculate the bounding function value that gets implemented in the control law in real time based on which constraint, maximum or minimum for example, is most in danger of being exceeded such as in the definition (3.7). Because the function construction process described in this section is nothing more than a set of six linear equations, calculating the bounding functions in real time is computationally inexpensive.

3.4 Control Law Development

The control law for the BFSC controller is given by

$$u = [Cg(x)\hat{\Lambda}]^{\dagger}\left(\dot{y}_m - C\hat{f}(x) + Ke + \nu - F'_*(y)[\dot{y}_m + Ky_m]\right) \tag{3.16}$$

where $K \in \mathbb{R}^{p\times p}$ is a diagonal error feedback gain matrix such that $K = K^T > 0$, the vector $\nu \in \mathbb{R}^p$ is an adaptive signal used to account for parameter uncertainty, and the matrix $F'_*(y) \in \mathbb{R}^{p\times p}$ is defined as

$$F'_*(y) = \begin{bmatrix} \frac{f'_{b,1}(y_1^2)}{1+f'_{b,1}(y_1^2)} & 0 & \dots & 0 \\ 0 & \frac{f'_{b,2}(y_2^2)}{1+f'_{b,2}(y_2^2)} & \dots & 0 \\ \vdots & \vdots & \ddots & \vdots \\ 0 & 0 & \dots & \frac{f'_{b,n}(y_n^2)}{1+f'_{b,n}(y_n^2)} \end{bmatrix} \tag{3.17}$$

Once again, it is assumed that $C\hat{f}(x) - Cf(x)$ can be parameterized as in (2.13) and the adaptive signal ν is defined as in (2.14). Therefore, substituting the BFSC control law (3.16) into the system error dynamics given in (3.6) results in

$$\dot{e} = -Ke + F'_*(y)[\dot{y}_m + Ky_m] - \widetilde{W}^T b(x) + g(x)\delta\tilde{\Lambda}u \tag{3.18}$$

The adaptive laws used to update the estimated matrices $\widehat{W}$ and $\delta\hat{\Lambda}$ are given by

$$\dot{\widehat{W}} = \Gamma_W \mathrm{Proj}_M\Big(\widehat{W}, b(x)\left(e^T - y^T F'(y)\right)\Big) \tag{3.19}$$

$$\delta\dot{\hat{\Lambda}} = \Gamma_\Lambda \mathrm{Proj}_M\Big(\delta\hat{\Lambda}, g(x)^T C^T\left(-eu^T + F'(y)yu^T\right)\Big) \tag{3.20}$$

where $\Gamma_W \in \mathbb{R}^{n_w \times n_w}$ and $\Gamma_\Lambda \in \mathbb{R}^{m\times m}$ and $\Gamma_i = \Gamma_i^T > 0$ for $i = W, \Lambda$ are adaptive gain matrices and the matrix $F'(y)$ is defined as

$$F'(y) = \begin{bmatrix} f'_{b,1}(y_1^2) & 0 & \dots & 0 \\ 0 & f'_{b,2}(y_2^2) & \dots & 0 \\ \vdots & \vdots & \ddots & \vdots \\ 0 & 0 & \dots & f'_{b,n}(y_n^2) \end{bmatrix} \tag{3.21}$$

3.5 Stability Analysis

In this section it is shown that using the BFSC control architecture defined above, the system outputs and the tracking error are bounded for a bounded input signal. The size of this bound will depend on, among other things, the steady-state value of the reference model. This is a direct result of the state constraint mechanism. If the steady-state value of the reference model is outside of a predetermined constraint set, perfect tracking is not desired. Instead, the system should remain at the boundary of its constraint set.

Three theorems are presented in order to prove the stability of the system. Theorem 3 states

that the closed-loop signals will be bounded regardless of if the steady-state value of the reference model is within or without the constraint set. Theorem 4 states that *if* the steady-state value of the reference model is within the constraint set, the tracking error will be asymptotically stable. Finally, Theorem 5 analyzes the system regardless of where the steady-state value of the reference model lies and a conservative, analytical bound for the system output and tracking error is produced.

Theorem 3. *Consider the nonlinear dynamical system given in Equation (3.1), the reference model defined in Equation (3.4), the control law defined in Equation (3.16), and the adaptive laws defined in Equations (3.19) and (3.20). Suppose that the reference input signal, r, is bounded, then the tracking error, e, and the system outputs, y, are bounded.*

Proof. In order to prove the stability of the BFSC controller, the following candidate Lyapunov function is chosen

$$V = \frac{1}{2}\left(e^T e + tr(\widetilde{W}^T \Gamma_W^{-1} \widetilde{W}) + tr(\delta\tilde{\Lambda}\Gamma_\Lambda^{-1}\delta\tilde{\Lambda}^T) + \sum_{i=1}^{n} f_{b,i}(y_i^2)\right) \tag{3.22}$$

The derivative of (3.22) is taken with respect to time along the system trajectories, resulting in

$$\dot{V} = e^T \dot{e} + tr(\widetilde{W}^T \Gamma_W^{-1} \dot{\widehat{W}}) + tr(\delta\tilde{\Lambda}\Gamma_\Lambda^{-1}\delta\dot{\hat{\Lambda}}^T) + \sum_{i=1}^{n} y_i f'_{b,i}(y_i^2)\dot{y}_i \tag{3.23}$$

Using the matrix $F'(y)$, defined above, the summation can be rewritten as,

$$\dot{V} = e^T \dot{e} + tr(\widetilde{W}^T \Gamma_W^{-1} \dot{\widehat{W}}) + tr(\delta\tilde{\Lambda}\Gamma_\Lambda^{-1}\delta\dot{\hat{\Lambda}}^T) + y^T F'(y)\dot{y} \tag{3.24}$$

Substituting in the error dynamics from Equation (3.18) and calculating the output dynamics using

$\dot{y} = \dot{y}_m - e$ leads to

$$\begin{aligned}\dot{V} =& e^T\left(-Ke + F_*'(y)[\dot{y}_m + Ky_m]\right) - e^T\widetilde{W}^T b(x) + e^T Cg(x)\delta\tilde{\Lambda}u \\ &+ y^T F'(y)\left(\dot{y}_m + Ke - F_*'(y)[\dot{y}_m + Ky_m]\right) + y^T F'(y)\widetilde{W}^T b(x) \\ &- y^T F'(y)Cg(x)\delta\tilde{\Lambda}u + tr(\widetilde{W}^T\Gamma_W^{-1}\dot{\widehat{W}}) + tr(\delta\tilde{\Lambda}\Gamma_\Lambda^{-1}\delta\dot{\hat{\Lambda}}^T)\end{aligned} \tag{3.25}$$

Applying the trace identity $a^T b = tr(ba^T)$, Equation (3.25) is rewritten

$$\begin{aligned}\dot{V} =& e^T\left(-Ke + F_*'(y)[\dot{y}_m + Ky_m]\right) + tr(\widetilde{W}^T(\Gamma_W^{-1}\dot{\widehat{W}} - b(x)e^T + \beta(x)y^T F'(y))) \\ &+ y^T F'(y)\left(\dot{y}_m + Ke - F_*'(y)[\dot{y}_m + Ky_m]\right) + tr(\delta\tilde{\Lambda}(\Gamma_\Lambda^{-1}\delta\dot{\hat{\Lambda}}^T + ue^T Cg(x) - uy^T F'(y)Cg(x)))\end{aligned} \tag{3.26}$$

The adaptive laws, given in Equations (3.19) and (3.20), ensure that the second and fourth terms in Equation (3.26) will be less than or equal to zero. Therefore, the following inequality holds

$$\dot{V} \leq e^T\left(-Ke + F_*'(y)[\dot{y}_m + Ky_m]\right) + y^T F'(y)\left(\dot{y}_m + Ke - F_*'(y)[\dot{y}_m + Ky_m]\right) \tag{3.27}$$

By utilizing the definition of the tracking error, $e = y_m - y$, the inequality (3.27) can be rearranged as

$$\begin{aligned}\dot{V} \leq& -e^T Ke - y^T F'(y)Ky + e^T\left(F_*'(y) - F'(y) + F_*'(y)F'(y)\right)[\dot{y}_m + Ky_m] \\ &+ y_m^T\left(F'(y) - F'(y)F_*'(y)\right)[\dot{y}_m + Ky_m]\end{aligned} \tag{3.28}$$

By definition of the matrices $F'(y)$ and $F_*'(y)$, it can be shown that

$$F_*'(y) - F'(y) + F_*'(y)F'(y) = 0$$

$$F'(y) - F'(y)F_*'(y) = F_*'(y)$$

Therefore, (3.28) can be simplified to

$$\dot{V} \leq -e^T K e - y^T F'(y) K y + y_m^T F_*'(y)[\dot{y}_m + K y_m] \tag{3.29}$$

Let y_{mss} be the steady-state value of the reference model. The following is equivalent to (3.29),

$$\begin{aligned} \dot{V} \leq & - e^T K e - y^T F'(y) K y + y_{mss}^T F_*'(y) K y_{mss} + y_m^T F_*'(y) \dot{y}_m + y_m^T F_*'(y) K y_m \\ & - y_{mss}^T F_*'(y) K y_{mss} \end{aligned} \tag{3.30}$$

Recall that since $F'(y)$ is a positive semi-definite diagonal matrix and K is a positive definite diagonal matrix, their product will also be a positive semi-definite matrix. Therefore, if

$$y^T F'(y) K y \geq y_{mss}^T F_*'(y) K y_{mss} + \left\| y_m^T F_*'(y) \dot{y}_m + y_m^T F_*'(y) K y_m - y_{mss}^T F_*'(y) K y_{mss} \right\|_2 \tag{3.31}$$

then $\dot{V} \leq 0$. Since y_m and $\dot{y}_m$ are bounded given a bounded input signal and $F_*'(y)$ is bounded by definition, this implies that y is bounded and therefore e is also bounded, as intended. □

The following theorem demonstrates that if the steady-state value of the reference model does not violate any state constraint, perfect tracking will occur as $t \to \infty$. As with the SMSC control law, a similar analysis could be performed to show that the same conclusion can be drawn on an output-by-output basis. In other words, perfect tracking is ensured for any individual output whose steady-state reference signal value does not violate its individual constraint.

Theorem 4. *Suppose all of the conditions in Theorem 3 are met. Let $r_{ss} \in \mathbb{R}^m$ and $y_{mss} = -A_m^{-1} B_m r_{ss}$, where r_{ss} is the steady-state value of the reference input signal and y_{mss} is the steady-state value of the reference model. If $\exists\, \alpha^*, \beta^* \in \mathbb{R}^+$ such that*

$$\left\| r(t) - r_{ss} \right\|_2 \leq \alpha^* \exp(-\beta^* t), \quad t \in [0, \infty) \tag{3.32}$$

and if the condition $y_i^2 < (\lambda_{max}(K)/\lambda_{min}(K))\, y_{i,mss}^2$ *implies that* $f'_{b,i}(y_i^2) = 0$*, then* $e \to 0$ *as* $t \to \infty$.

Proof. Since $\exists\, \alpha^*, \beta^* \in \mathbb{R}$ such that $\|r(t) - r_{ss}\|_2 \leq \alpha^* \exp(-\beta^* t)$ at all times and the reference dynamics in Equation (2.4) are stable, it can be shown that $\exists\, \alpha_0, \beta_0 \in \mathbb{R}^+$ such that

$$\|y_m^T F'_*(y)\dot{y}_m + y_m^T F'_*(y) K y_m - y_{mss}^T F'_*(y) K y_{mss}\|_2 \leq \alpha_0 \exp(-\beta_0 t), \quad t \in [0, \infty) \tag{3.33}$$

The expression for the Lyapunov function derivative given by the inequality (3.30) can now be rewritten as

$$\dot{V} \leq -e^T K e - y^T F'(y) K y + y_{mss}^T F'_*(x) K y_{mss} + \alpha_0 \exp(-\beta_0 t) \tag{3.34}$$

Evaluating the second and third terms of the inequality (3.34), the following relationship can be established

$$-y^T F'(x) K x + y_{mss}^T F'_*(x) K y_{mss} \leq -\lambda_{min}(K) \sum_{i=1}^{n} f'_{b,i}(y_i^2) y_i^2 + \lambda_{max}(K) \sum_{i=1}^{n} f'_{b,i}(y_i^2) y_{i,mss}^2 \tag{3.35}$$

Due to the condition given in the theorem statement that $y_i^2 < (\lambda_{max}(K)/\lambda_{min}(K))\, y_{i,mss}^2$ implies that $f'_{b,i}(x_i^2) = 0$, the second and third terms in the inequality (3.34) always combine to be less than or equal to zero. Therefore, the Lyapunov function derivative can be reduced to

$$\dot{V} \leq -e^T K e + \alpha_0 \exp(-\beta_0 t) \tag{3.36}$$

It follows that,

$$V = V_0 + \int_0^t \dot{V}\, d\tau \tag{3.37}$$

where $V_0 = V(t=0)$. Utilizing the inequality (3.36) leaves,

$$V \leq V_0 + \int_0^t \left(-e^T K e + \alpha_0 \exp(-\beta_0 t)\right)\, d\tau \tag{3.38}$$

which, upon integration, results in

$$V \leq V_0 - \int_0^t e^T K e\, d\tau + \frac{\alpha_0}{\beta_0}\left(1 - \exp(-\beta_0 t)\right) \tag{3.39}$$

Because $V \geq 0$, the following inequality holds

$$0 \leq V \leq V_0 - \int_0^t e^T K e\, d\tau + \frac{\alpha_0}{\beta_0}\left(1 - \exp(-\beta_0 t)\right) \tag{3.40}$$

$$0 \leq \int_0^t e^T K e\, d\tau \leq V_0 + \frac{\alpha_0}{\beta_0}\left(1 - \exp(-\beta_0 t)\right) \tag{3.41}$$

for all $t \geq 0$. This implies that $\int_0^\infty e^T K e\, dt$ exists and is finite. Because y and e are bounded, u and $\dot{e}$ are bounded for all $t \geq 0$ which implies that e is uniformly continuous in time. Therefore, Barbalat's Lemma implies that $e \to 0$ as $t \to \infty$ as intended. □

The final theorem of the section places an analytical upper bound on the system outputs regardless of the steady-state value of the reference model. In this theorem, it will be shown that altering the bounding functions, $f_{b,i}(y_i^2)$, can tighten the bounds on the outputs, y_i. This insight can be used to improve constraint enforcement performance.

Theorem 5. *Suppose all of the conditions in Theorem 3 are met. Also, suppose that the projection operator bounds are chosen such that the unknown ideal weights satisfy* $\|W\|_F \leq \|\widehat{W}\|_{F,max}$ *and* $\|\delta\Lambda\|_F \leq \|\delta\hat{\Lambda}\|_{F,max}$*, where* $\|\widehat{(\cdot)}\|_{F,max}$ *is the maximum allowable Frobenius norm of* $\widehat{W}$ *and* $\delta\hat{\Lambda}$ *respectively. If, at the initial time,* $e = 0$ *and* $y_{min,i} < y_i < y_{max,i}$*, then each of the bounding functions* $f_{b,i}(y_i^2)$ *implemented in the control and adaptive laws, Equations (3.16),(3.19), and (3.20), are bounded for all* $t \geq 0$ *by*

$$f_{b,i}(y_i^2) \leq \frac{1}{2}\left(\frac{4}{\lambda_{min}(\Gamma_W)}\|\widehat{W}\|_{F,max}^2 + \frac{4}{\lambda_{min}(\Gamma_\Lambda)}\|\delta\hat{\Lambda}\|_{F,max}^2 + \phi^T F'(\phi)\phi + \sum_{i=1}^{n} \underset{y_i^2 \leq \phi_i}{max}[f_{b,i}(y_i^2)]\right) \tag{3.42}$$

where $\phi \in \mathbb{R}^p$ is defined such that

$$\lambda_{min}(K)\phi^T F'(\phi)\phi = |y_m^T \dot{y}_m + \lambda_{max}(K) y_m^T y_m|_{max} \tag{3.43}$$

and where $|\cdot|_{max}$ is the maximum value of the argument for all $t \geq 0$. Since, by definition, $f_{b,i}(y_i^2) \to \infty$ as $y_i^2 \to \infty$, the bound (3.42) implies an upper bound on the system outputs.

Proof. Consider the inequality (3.29) which describes a relationship regarding the derivative of the Lyapunov Function used in Theorems 3 and 4,

$$\dot{V} \leq -e^T K e - y^T F'(y) K y + y_m^T F_*'(y)[\dot{y}_m + K y_m] \tag{3.44}$$

Because K is a diagonal positive definite matrix, the following inequality also holds:

$$\dot{V} \leq -\lambda_{min}(K)(e^T e + y^T F'(y) y) + y_m^T F_*'(x)\dot{y}_m + \lambda_{max}(K) y_m^T F_*'(y) y_m \tag{3.45}$$

Next, conditions are derived that ensure $\dot{V}$ is less than or equal to zero. First, if

$$\lambda_{min}(K) y^T F'(y) y \geq |y_m^T F_*'(y)\dot{y}_m + \lambda_{max}(K) y_m^T F_*'(y) y_m|_{max} \tag{3.46}$$

then $\dot{V} \leq 0$. Considering the definition of ϕ given in Equation (3.43), $y_i \geq \phi_i$ for all i implies that $\dot{V} \leq 0$. Using this definition, it can also be seen that if

$$e^T e \geq \phi^T F'(\phi)\phi \tag{3.47}$$

then also, $\dot{V} \leq 0$. The projection operator ensures that the adaptive weights are bounded by

$$\|\widetilde{W}\|_F \leq \|\widetilde{W}\|_{F,max} \quad \text{and} \quad \|\delta\tilde{\Lambda}\|_F \leq \|\delta\tilde{\Lambda}\|_{F,max} \tag{3.48}$$

which implies that $\dot{V} \leq 0$ outside of the compact set Ω, where

$$\Omega(e, y, \widetilde{W}, \delta\tilde{\Lambda}) = \left\{(e, y, \widetilde{W}, \delta\tilde{\Lambda}) : \|e\|_2 \leq \sqrt{\phi^T F'(\phi)\phi}\right\}$$
$$\bigcap\{(e, y, \widetilde{W}, \delta\tilde{\Lambda}) : y_i \leq \phi_i, \text{ for all i}\}$$
$$\bigcap\{(e, y, \widetilde{W}, \delta\tilde{\Lambda}) : \|\widetilde{W}\|_F \leq \|\widetilde{W}\|_{F,max}\}$$
$$\bigcap\{(e, y, \widetilde{W}, \delta\tilde{\Lambda}) : \|\delta\tilde{\Lambda}\|_F \leq \|\delta\tilde{\Lambda}\|_{F,max}\}$$

Because $\dot{V} \leq 0$ outside of the compact set Ω, V cannot grow outside of this set. Therefore, V has the following upper bound

$$V \leq \underset{(e,x,\widetilde{W},\delta\tilde{\Lambda})\in\Omega}{max} V$$

for all $t \geq 0$ which, given the definition of the Lyapunov function in Equation (3.22), can be rewritten as

$$V \leq \underset{(e,x,\widetilde{W},\delta\tilde{\Lambda})\in\Omega}{max} \left(\frac{1}{2}\left(e^T e + tr(\widetilde{W}^T\Gamma_W^{-1}\widetilde{W}) + tr(\delta\tilde{\Lambda}^T\Gamma_\Lambda^{-1}\delta\tilde{\Lambda}) + \sum_{i=1}^{n} f_{b,i}(y_i^2)\right)\right) \tag{3.49}$$

This implies that

$$V \leq \frac{1}{2}\left(\frac{\|\widetilde{W}\|_{F,max}^2}{\lambda_{min}(\Gamma_W)} + \frac{\|\delta\tilde{\Lambda}\|_{F,max}^2}{\lambda_{min}(\Gamma_\Lambda)} + \phi^T F'(\phi)\phi + \sum_{i=1}^{n} \underset{y_i^2\leq\phi_i}{max}[f_{b,i}(y_i^2)]\right) \tag{3.50}$$

Note that for both $\widetilde{W}$ and $\delta\tilde{\Lambda}$, the triangle inequality can be invoked such that

$$\|\widetilde{(\cdot)}\|_F = \|\widehat{(\cdot)} - (\cdot)\|_F \leq \|\widehat{(\cdot)}\|_F + \|(\cdot)\|_F \leq 2\|\widehat{(\cdot)}\|_{F,max}$$

Therefore,

$$V \leq \frac{1}{2}\left(\frac{4}{\lambda_{min}(\Gamma_W)}\|\widehat{W}\|_{F,max}^2 + \frac{4}{\lambda_{min}(\Gamma_\Lambda)}\|\delta\hat{\Lambda}\|_{F,max}^2 + \phi^T F'(\phi)\phi + \sum_{i=1}^{n} \underset{y_i^2 \leq \phi_i}{max}[f_{b,i}(y_i^2)]\right) \tag{3.51}$$

Since the Lyapunov function, Equation (3.22), implies that $f_{b,i}(y_i^2) \leq V$, it can be stated that

$$f_{b,i}(y_i^2) \leq \frac{1}{2}\left(\frac{4}{\lambda_{min}(\Gamma_W)}\|\widehat{W}\|_{F,max}^2 + \frac{4}{\lambda_{min}(\Gamma_\Lambda)}\|\delta\hat{\Lambda}\|_{F,max}^2 + \phi^T F'(\phi)\phi + \sum_{i=1}^{n} \underset{y_i^2 \leq \phi_i}{max}[f_{b,i}(y_i^2)]\right) \tag{3.52}$$

for all i, as intended. □

Remark 3.5.1. Because a finite bound for the bounding functions has been established, a bound for the outputs, y_i, is also established in the form of the vector ϕ. It can be seen from Equation (3.43) that the size of this bound depends on the derivative of the respective bounding function, $f_{b,i}(y_i^2)$. The faster the bounding function grows after $y_i^2 \geq y_{j,i}^2$ for $j = \{min, max\}$, the tighter the state will be bound to its constraint. The parameters $\rho_i^j > 0$, defined in Equation (3.8), directly affect the growth rate of the bounding function and therefore can be used to tighten the constraint. As ρ_i^j increases, the bound on the state y_i tightens.

3.6 Generic Hypersonic Vehicle Simulation

The BFSC controller developed above was implemented and tested in the nonlinear Generic Hypersonic Vehicle simulation. The results presented in this section were developed by putting the BFSC controller through the same litany of tests that the SMSC controller was put through in Section 2. In Section 3.7, results will be presented which were developed after augmenting the GHV simulation with a simplified inlet unstart model and testing the BFSC controller's ability to both prevent and help with the recovery from an inlet unstart.

As was done in Section 2, the system dynamics were broken down into a subsystem of position-

level dynamics and a subsystem of velocity-level dynamics as follows

$$\dot{x}_p = \begin{bmatrix} \dot{\phi} \\ \dot{\theta} \\ \dot{\psi} \\ \dot{\alpha} \\ \dot{\beta} \end{bmatrix} = f_p(x) + g_p(x)\Lambda_p \begin{bmatrix} p_d \\ q_d \\ r_d \end{bmatrix} \tag{3.53}$$

$$y_p = \begin{bmatrix} \alpha & \beta \end{bmatrix}^T \tag{3.54}$$

$$\dot{x}_v = \begin{bmatrix} \dot{p} \\ \dot{q} \\ \dot{r} \end{bmatrix} = f_v(x) + g_v(x)\Lambda_v \begin{bmatrix} \delta_{f,r} \\ \delta_{f,l} \\ \delta_{t,r} \\ \delta_{t,l} \end{bmatrix} \tag{3.55}$$

$$y_v = \begin{bmatrix} p & q & r \end{bmatrix}^T \tag{3.56}$$

In all of the results presented in this section the following simulation parameters were kept identical to those presented in Section 2:

- Reference model dynamics
- Parametric uncertainty in the dynamical model
- Basis functions used in the adaptive laws
- Adaptive gain matrices
- Initial values for the adaptive parameters
- Actuator dynamics and saturation limits
- Time delay

The initial flight condition was a velocity of Mach 6 and altitude of $80,000ft$. The predefined constraint set on angle-of-attack and sideslip angle in order to prevent inlet unstart was again chosen according to [32]. To reiterate, this corresponds to an inlet unstart occurring at $14.5\,\mathrm{deg}$ and $-5.7\,\mathrm{deg}$ for angle-of-attack and $\pm 5.4\,\mathrm{deg}$ for sideslip angle. The output threshold limits used in the construction of the bounding functions are given by

$$\begin{bmatrix} \alpha_{max} & \alpha_{min} & \delta_{\alpha} & \beta_{max} & \beta_{min} & \delta_{\beta} \end{bmatrix} = \begin{bmatrix} 13 & -4 & 0.5 & 4 & -4 & 0.5 \end{bmatrix} \mathrm{deg} \tag{3.57}$$

The following gain and controller parameters were kept constant through out all presented simulation trials. For the velocity-level subsystem, the feedback gain K_v was set as

$$K_v = \begin{bmatrix} 7.5 & 0 & 0 \\ 0 & 7.5 & 0 \\ 0 & 0 & 7.5 \end{bmatrix}$$

For the position-level subsystem, the feedback gain K_p was set as

$$K_p = \begin{bmatrix} 1 & 0 \\ 0 & 2 \end{bmatrix}$$

The parameters required for the BFSC controller were set as $\rho_{\alpha}^{min} = \rho_{\alpha}^{max} = 2$ and $\rho_{\beta}^{min} = \rho_{\beta}^{max} = 3$.

3.6.1 Results: Commanding an Unacceptable Reference Trajectory

The same two test cases used for the SMSC controller in Section 2 were examined in order to demonstrate the effectiveness of the BFSC controller when dealing with unacceptably large reference trajectory commands. In the first test case $6\,\mathrm{deg}$ doublets were commanded and in the second test case $10\,\mathrm{deg}$ doublets were commanded.

Each test case presented was also examined using the tracking controller which had no state constraint mechanism. While producing the results presented in this section, no inlet unstart model was included in the simulation and therefore, adverse effects are not seen when α and β exceed their constraints in these comparative cases.

Test Case 1: 6 degree Doublet Command

In the first test case, $6\,\mathrm{deg}$ doublets were commanded in both angle-of-attack and sideslip angle. Figures 3.1 and 3.3 show the time histories for the position-level outputs α and β, as well as the control surface deflections and total velocity. The Euler angle and velocity-level outputs are shown in Figures 3.2 and 3.4. As with the SMSC controller, the BFSC controller had little trouble when restricting angle-of-attack in response to a $6\,\mathrm{deg}$ doublet command. In commanding sideslip angle, as shown in Figures 3.3 and 3.4, the BFSC controller showed improvement in performance when compared with the SMSC controller. There is less chattering in the control surface deflections and the large induced roll rate is not seen. In fact a larger roll rate and roll angle were required by the tracking controller than by the state constraining controller. In both examples that were explored in Test Case 1, the control objective was achieved.

Test Case 2: 10 degree Doublet Command

The second test case contained two more challenging examples as $10\,\mathrm{deg}$ doublets were commanded despite the constraint set given in (3.57) remaining constant. The time histories are separated as they were for Test Case 1: Sideslip angle, angle-of-attack, the control surface deflections and total velocity are shown in Figures 3.5 and 3.7 while Euler angle and velocity-level outputs are shown in Figures 3.6 and 3.8. In this test case the BFSC controller's ability to lessen chattering in the control signal when compared with sliding mode techniques is clear. By constructing the bounding functions according to the method given in Section 3.3.1, and by tuning the transition polynomials $f_{t,i}(y_i^2)$, the change from "tracking mode" to "state constraint" mode occurs smoothly.

In Figure 3.8 it can be seen that the large roll rate is again avoided by restricting the outputs through the BFSC control technique. In both examples shown, the control objective is achieved despite the $10\,\mathrm{deg}$ command signal.

3.6.2 Results: Disturbance Rejection

As with the SMSC control law, in order to validate the BFSC controller as a successful state constraint technique it must be shown that it can reject disturbances in addition to handling unacceptable input commands. In order to demonstrate this capability, $5\,\mathrm{deg}$ doublet trajectories were commanded in both sideslip angle and angle-of-attack. During the angle-of-attack trajectory simulation, show in Figure 3.9, a $1250lbf$ disturbance force lasting one second was applied to the vehicle at $t = 17sec$ in the positive z (down) direction. During the sideslip angle trajectory simulation, show in Figure 3.10, a $2000lbf$ disturbance force lasting one second was applied to the vehicle at $t = 20sec$ in the negative y direction. In both cases, the vehicle was restricted from entering a region of the state-space within which inlet unstart would occur. When the same disturbance was applied to the vehicle using the tracking controller, a constraint violation occurred in both examples at the moment in time indicated in the Figures. Again, an improvement is seen in the results generated using the BFSC control law when compared with the SMSC controller. Although both controllers successfully rejected the disturbance without inducing an inlet unstart, the BFSC control law is able to maintain more separation with the constraint boundary than the SMSC controller while also producing less chatter in the control signal. This demonstrates the BFSC controller's capability to enforce state constraints not only when large command signals are applied but also in the presence of disturbances.

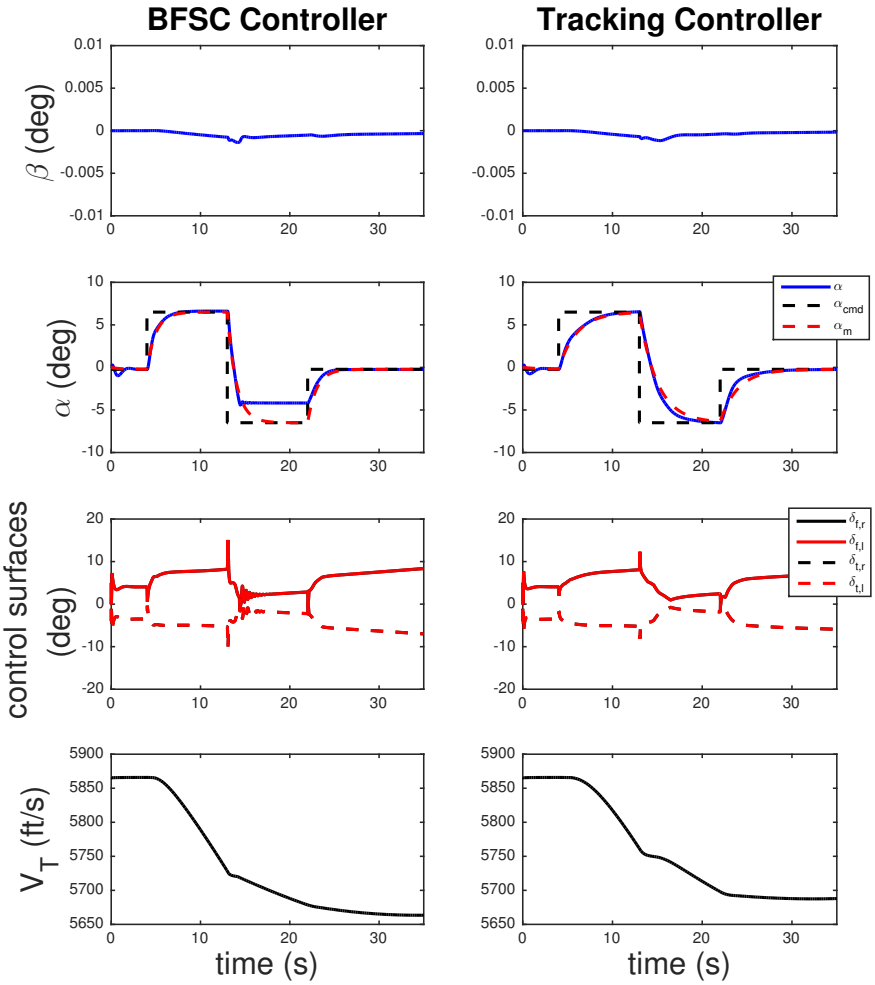

Figure 3.1: Response to 6 degree doublet command in angle-of-attack. Time histories are shown of sideslip angle, angle-of-attack, the control surface deflections and total velocity.

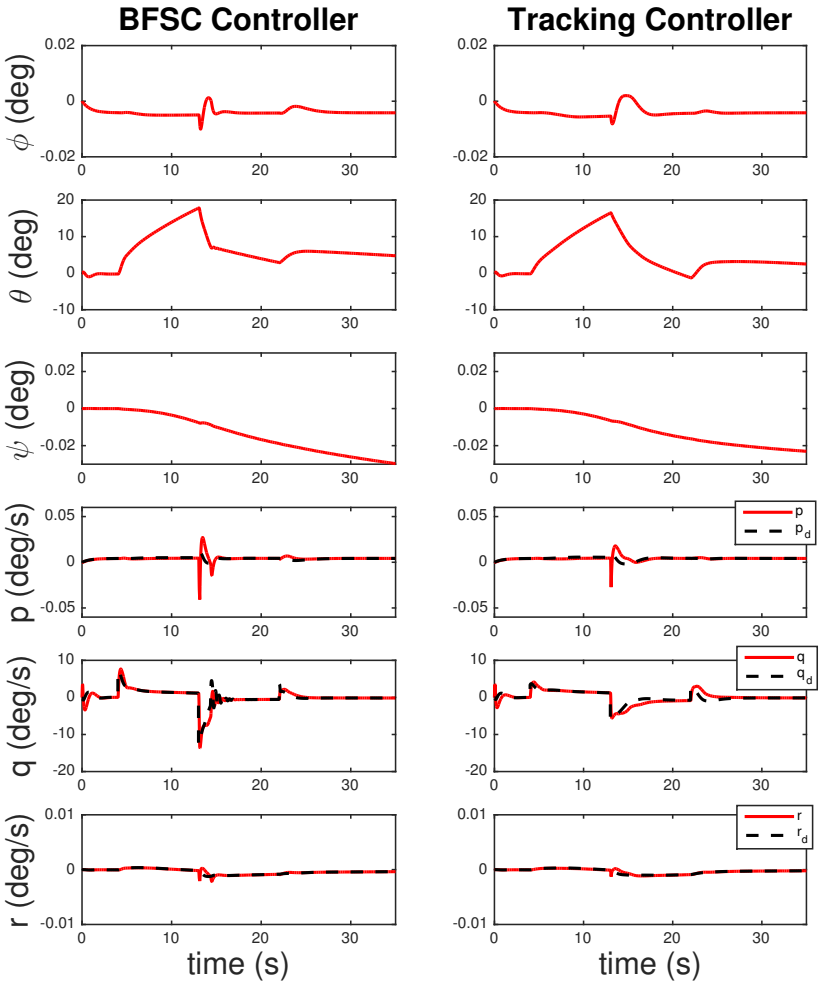

Figure 3.2: Response to 6 degree doublet command in angle-of-attack. Time histories are shown of the vehicle's Euler angles and body-fixed angular rates.

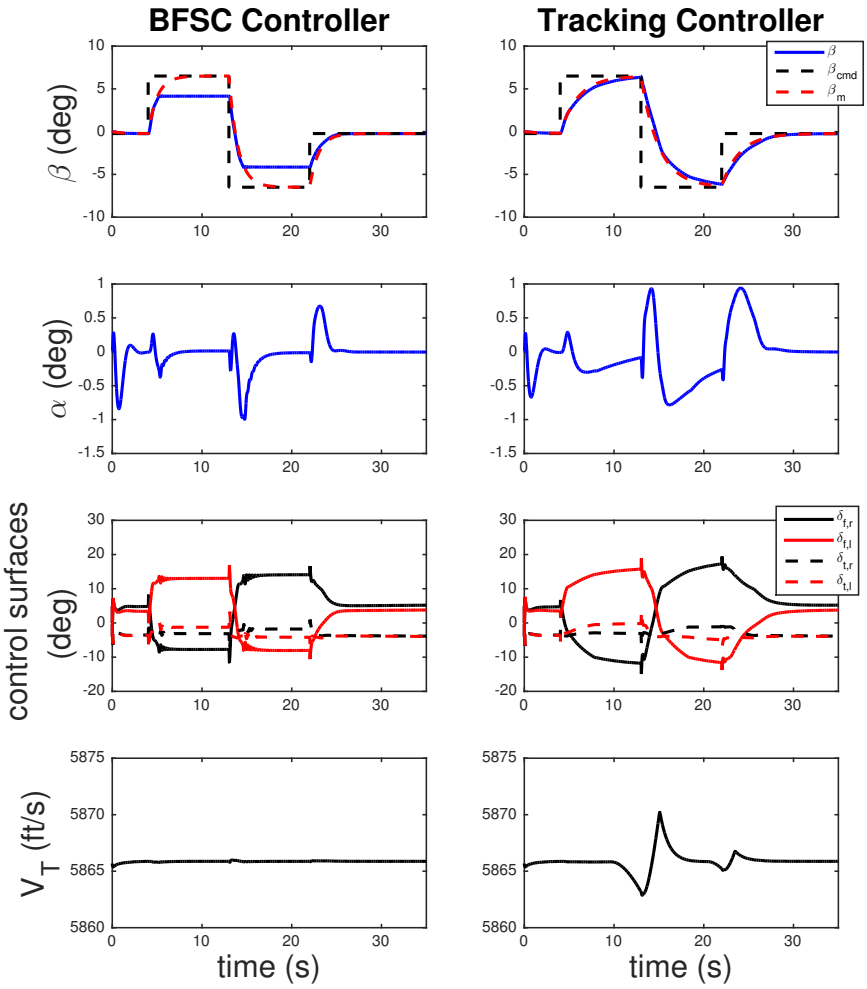

Figure 3.3: Response to 6 degree doublet command in sideslip angle. Time histories are shown of sideslip angle, angle-of-attack, the control surface deflections and total velocity.

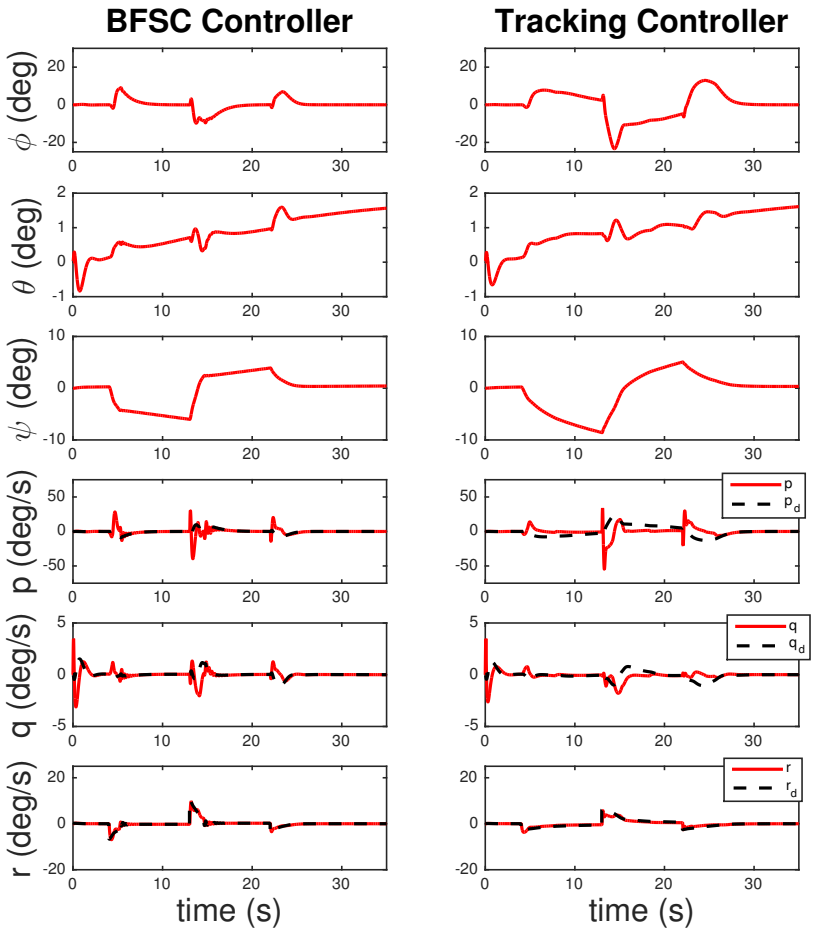

Figure 3.4: Response to 6 degree doublet command in sideslip angle. Time histories are shown of the vehicle's Euler angles and body-fixed angular rates.

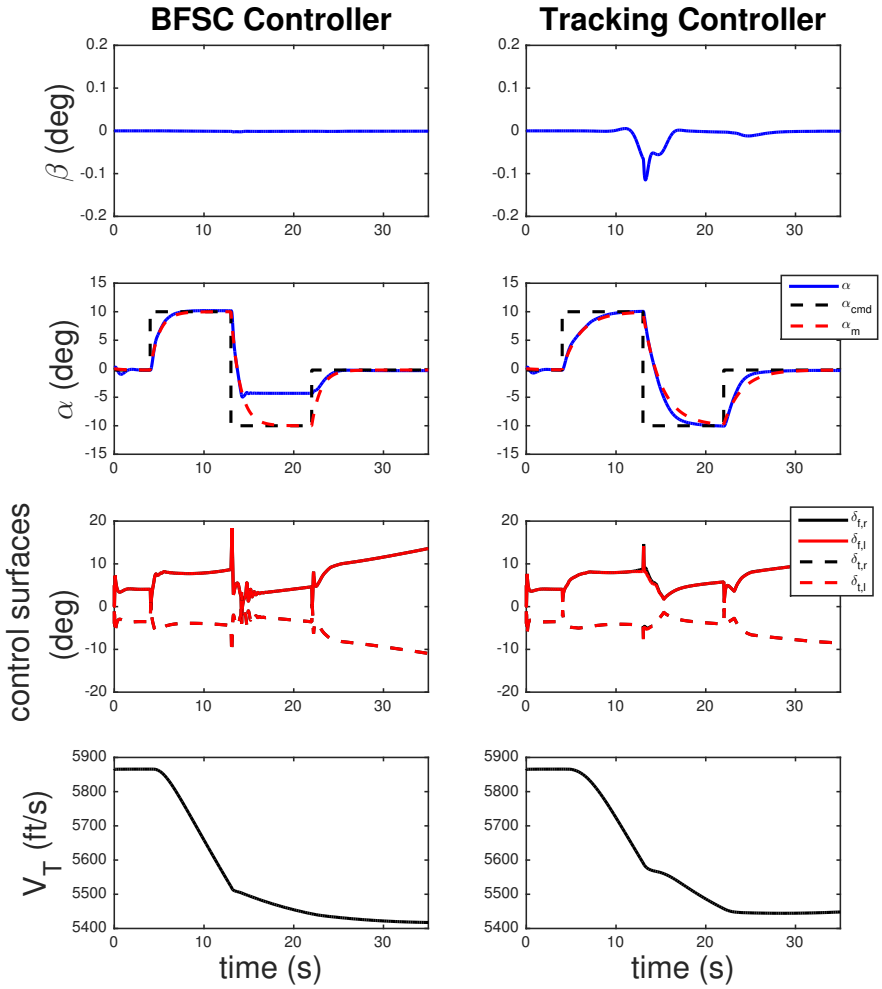

Figure 3.5: Response to 10 degree doublet command in angle-of-attack. Time histories are shown of sideslip angle, angle-of-attack, the control surface deflections and total velocity.

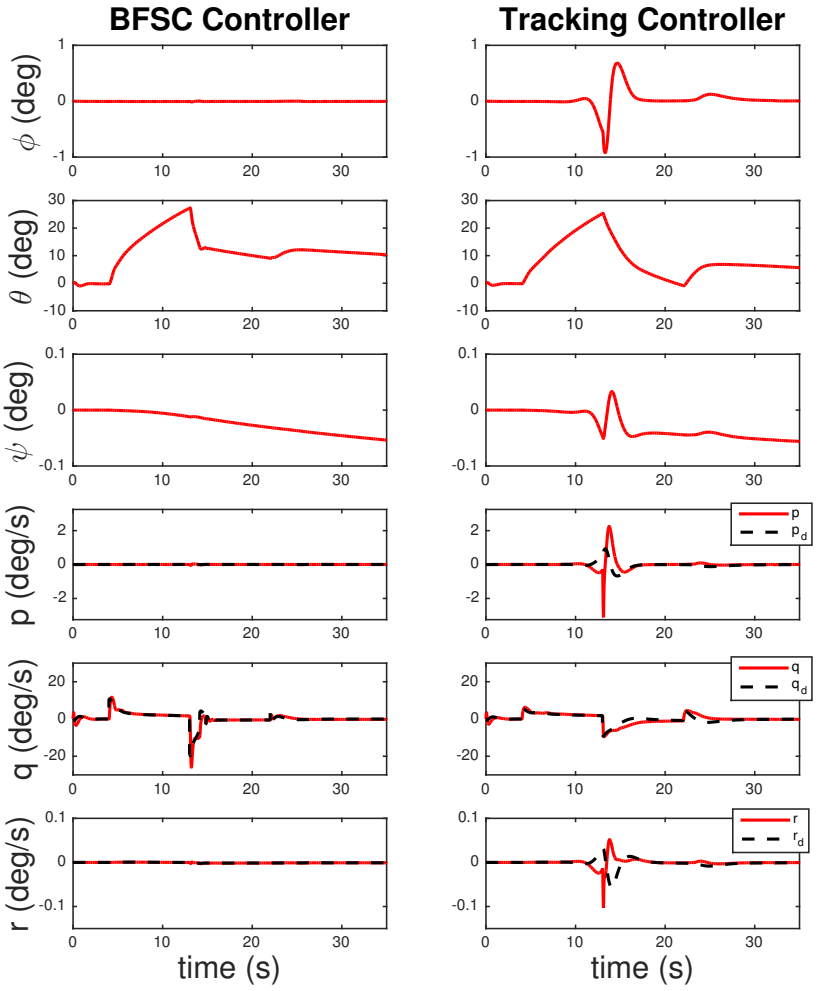

Figure 3.6: Response to 10 degree doublet command in angle-of-attack. Time histories are shown of the vehicle's Euler angles and body-fixed angular rates.

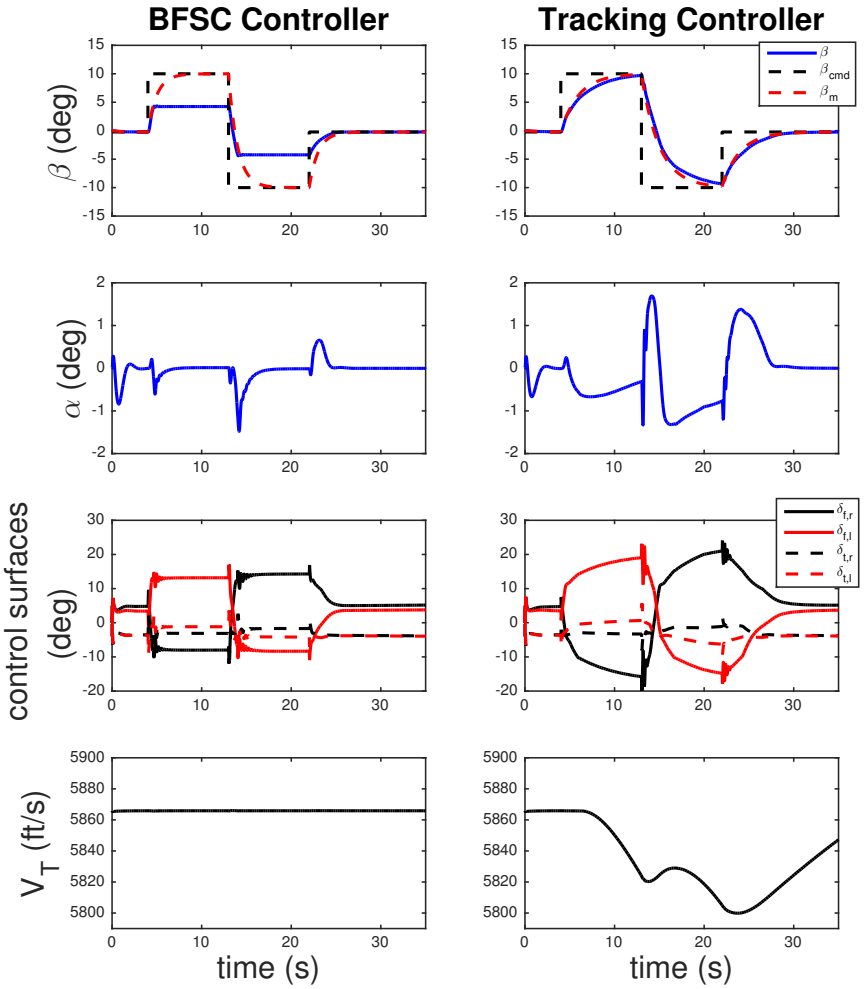

Figure 3.7: Response to 10 degree doublet command in sideslip angle. Time histories are shown of sideslip angle, angle-of-attack, the control surface deflections and total velocity.

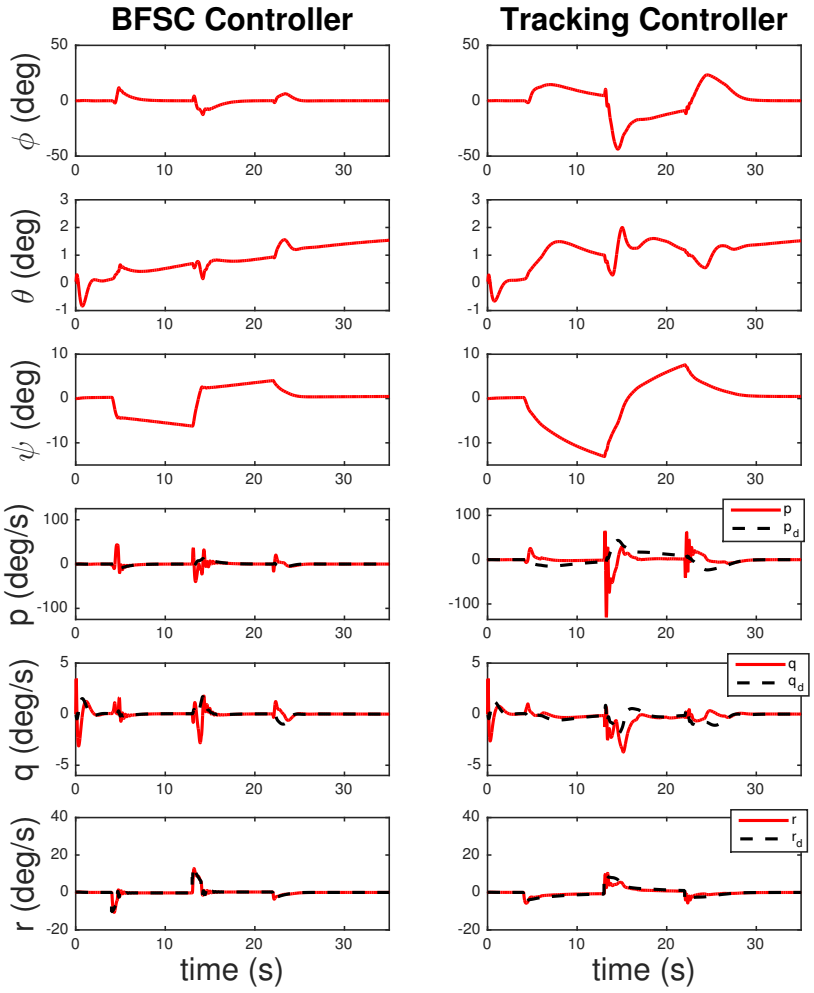

Figure 3.8: Response to 10 degree doublet command in sideslip angle. Time histories are shown of the vehicle's Euler angles and body-fixed angular rates.

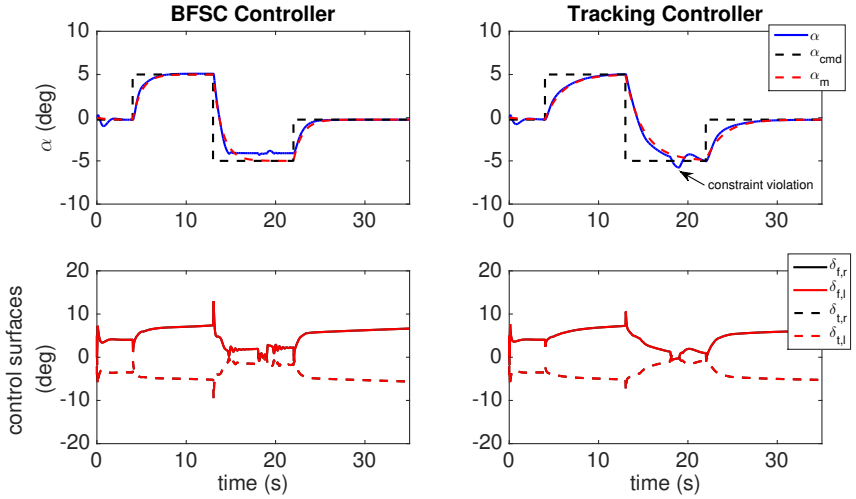

Figure 3.9: Longitudinal Disturbance Rejection Example. Time histories are shown of angle-of-attack and the control surface deflections.

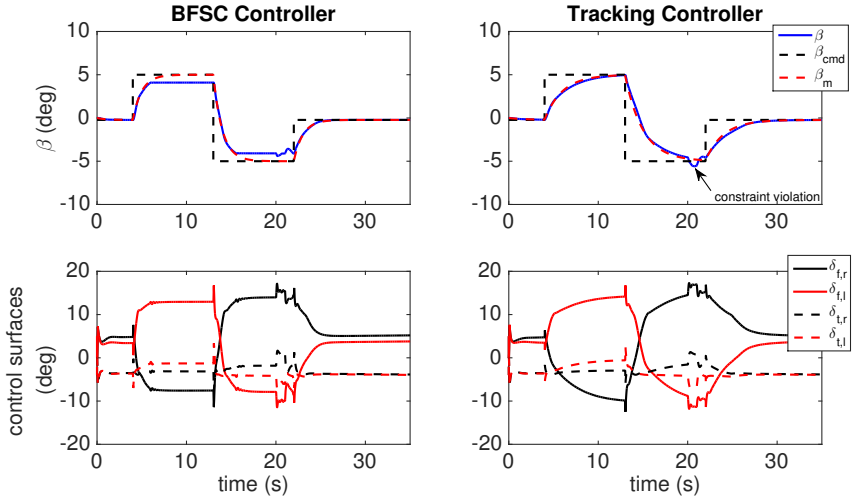

Figure 3.10: Lateral/Directional Disturbance Rejection Example. Time histories are shown of sideslip angle and the control surface deflections.

3.7 Prevention and Recovery from Inlet Unstart: A Simulation Study

A simulation study was designed in order to demonstrate how enforcing state constraints can potentially be used for both prevention of and recovery from an inlet unstart. A complete solution to the inlet unstart problem would, in addition to the vehicle states, focus on the aerodynamic effects on the inlet itself and would likely include some type of throttle constraints or actuation in the inlet. The objective is to prevent the vehicle from leaving the region of the state-space that would trigger an unstart and, in the extreme conditions where the prevention technique fails, to maintain control effectiveness and quickly drive the vehicle into a safer flight envelope so that the engine restarts. The BFSC technique described above can be utilized in both situations. To explain how the BFSC controller can also be used to recover from an inlet unstart, the unstart model used in the simulation is now introduced.

3.7.1 Modeling Inlet Unstart

A simplified inlet unstart model was included in the GHV simulation to test the performance of the BFSC technique in the event of an inlet unstart. The model is hysteresis-based and depends solely on angle-of-attack, sideslip angle and freestream Mach number. Starting in a nominal flight condition, the inlet will unstart if the vehicle leaves the region of the $\alpha\beta$-space marked by the blue outer ellipsoid in Figure 3.11. To regain normal engine function the vehicle must re-enter the region marked by the inner ellipsoid outlined in red. Once restarted, the vehicle is again free to traverse the inter-ellipsoid region with full thrust and nominal performance.

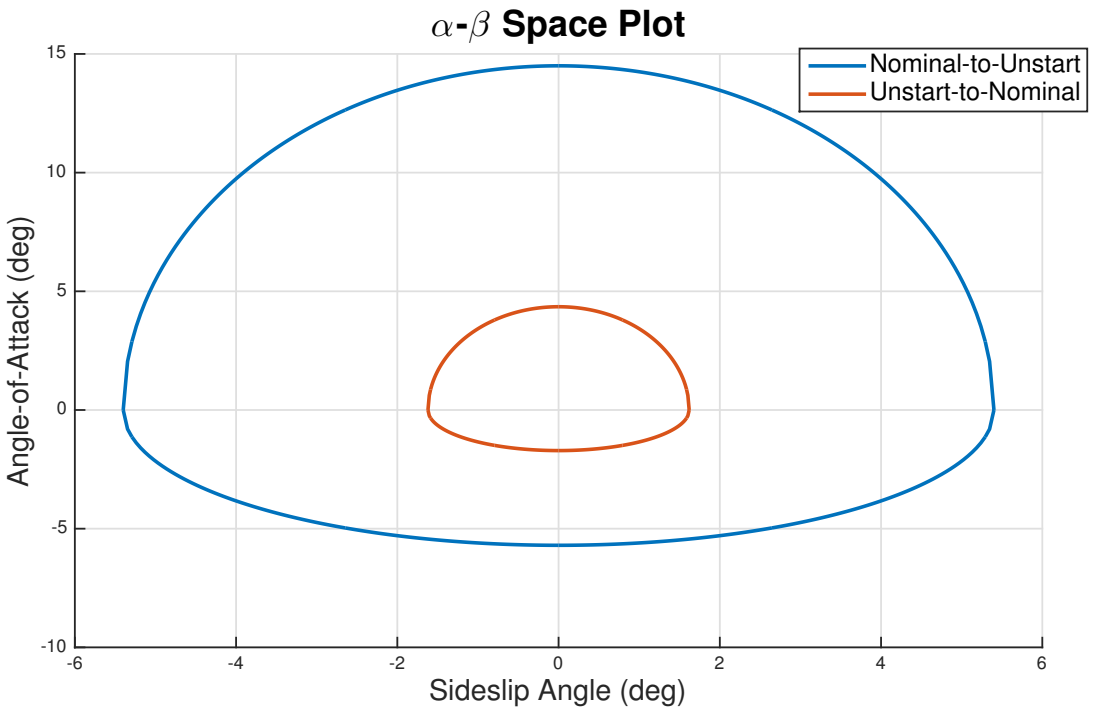

Figure 3.11: Inlet unstart model

In this model, the boundary of the outer ellipsoid is defined based on the constraint set given in [32] and used in Section 3.6. Note that the size parameters of this ellipsoid, and even perhaps its shape, are highly dependent upon specific vehicle geometries. As a result, the susceptibility of any given vehicle to inlet unstart may vary significantly.

Due to the comparative lack of aerodynamic research on modeling inlet restart, the size of the inner ellipsoid is chosen arbitrarily but conservatively. More aerodynamic research on how freestream Mach number affects these unstart parameters is required for a higher fidelity model. Since the inlet can reasonably be expected to perform as intended when the vehicle is straight and level, the inner ellipsoid is chosen to be 70% smaller than the outer ellipsoid. This ellipsoid is limited to 4.35° and -1.71° in angle-of-attack and $\pm 1.62^\circ$ in sideslip angle. It should also be noted that the values above correspond to Mach 6 flight. The model is set up such that the size of the

ellipsoids vary linearly with Mach number, but all simulation cases presented below use an initial flight condition of Mach 6 and the ellipsoid sizes described above. The shape of these ellipsoids is an attempt to capture the unstart characteristics when the reference dynamics are not only a non-zero command in one specific state, but time-varying trajectories in multiple states. That is, although the limits experimentally determined from the HIFiRE experiment were produced by an uncoupled, independent study on the effects of angle-of-attack and sideslip angle, this model allows for the triggering of an inlet unstart as a function of both angles, the values of which may not exceed their respective, individual experimental limits. Although the specific implementation used here is concerned directly with two particular states, similar concepts could easily be extended for higher dimensional models.

The aerodynamic and propulsive consequences of the inlet unstart model should be addressed. First, when an unstart is triggered, the vehicle experiences a complete and instantaneous loss of thrust and an increase in the magnitude of aerodynamic drag. Conversely, when the inlet is restarted, the vehicle experiences a restoration of thrust according to the equivalence ratio (throttle) commanded by the controller. Since the apparent lack of thrust prompts an increase in the commanded equivalence ratio, this command is typically saturated at maximum throttle by the time the vehicle is posed for restart. Due again to insufficient information on the geometry-specific flow characteristics and resulting changes in aerodynamic force and moment coefficients and stability derivatives, significant post-unstart changes in the plant dynamics are not modeled. These changes are difficult to predict and, as a result, are not addressed in the simulation studies presented below. Although a more thorough testing of the state constraint mechanism's performance in the event of an inlet unstart would include these effects, quantifiably substantiated by experiment or computational fluid dynamics, the cases presented below still act as a feasibility study towards solving the recovery problem.

3.7.2 Prevention and Recovery Strategy

Given the inlet unstart model described above, the use of state constraints for the prevention of inlet unstart is very intuitive. If the control law and bounding functions are designed such that the angle-of-attack and sideslip angle of the GHV can never exit the outer ellipsoid of Figure 3.11, then theoretically, inlet unstart will not occur. This prevention approach is based on two assumptions. The first assumption is that there is a known bound on any external disturbances that can affect the system, a common assumption in control theory. This known bound on disturbances can be reflected in the norm-bounds used by the projection operator. The second assumption is perfect knowledge of the inlet unstart model, i.e. perfect knowledge of the sizes and shapes of the ellipsoids of Figure 3.11. This requires extensive wind tunnel testing and modeling of each specific vehicle and inlet. Other aerodynamic causes of inlet unstart add another layer of uncertainty. In this study, it is assumed that the ellipsoids given above are correct and known perfectly, and, as mentioned above, only exiting the outer ellipsoid, i.e. flying at large aerodynamic angles, can cause inlet unstart.

The use of state constraints for recovery from inlet unstart is developed based on an analysis of the BFSC control technique presented in this section when the system is initialized at a point in the state-space that violates a constraint. It is straightforward to show both mathematically and computationally that in these situations the system is very quickly driven within the constraint bounds before any attempt to track the reference model is carried out. If, at the moment an inlet unstart occurs, the bounding functions used in the control law are switched to reflect the inner ellipsoid of Figure 3.11 instead of the outer ellipsoid, this is analogous to initializing the system in violation of a constraint. If the vehicle maintains control effectiveness, the behavior described above, i.e. quickly driving the system inside of the constraint set, will occur and the engine will restart. This concept is demonstrated in Figure 3.12 representing a fictitious one-dimensional system with state x. This figure is not based on actual dynamic simulation but can be looked at as a

diagram demonstrating how this technique is *supposed* to affect the system. For a one-dimensional system, the outer and inner ellipsoids of Figure 3.11 are analogous to the scalars, shown by the blue and red lines in Figure 3.12 and arbitrarily set to 2 and 1, respectively. In Figure 3.12, when the ellipsoid values are represented by a solid line, it indicates that the bounding function is being calculated based on that constraint value. Therefore, until $t = 1\,s$, the upper ellipsoid is used to calculate the bounding function as a preventative measure, and the state tracks its reference model. At $t = 0.95\,s$, a disturbance is introduced, driving the state above its upper limit which corresponds to an unstart at $t = 1\,s$. The bounding function then switches to correspond to the lower ellipsoid value, the state is quickly driven below this new constraint, the inlet restarts, and the state can once again track its reference model.

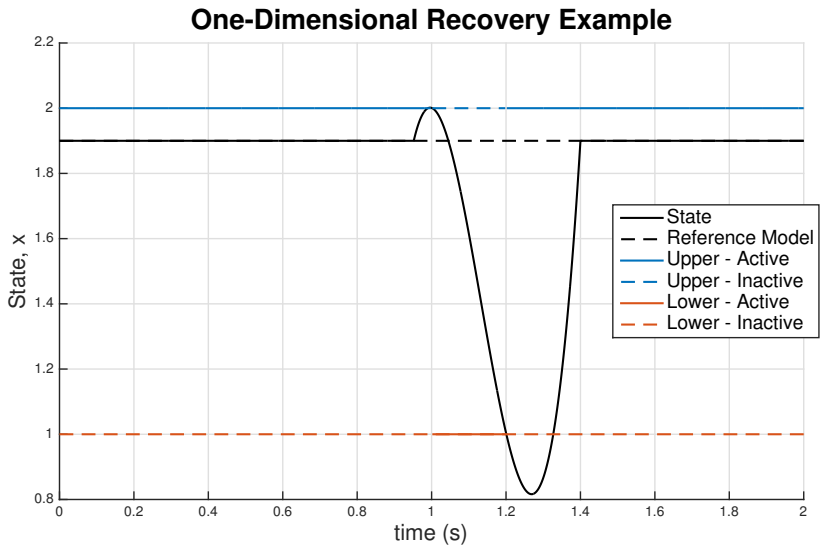

Figure 3.12: One-dimensional example of the inlet unstart recovery technique. The bounding function corresponds to whichever ellipsoid value is represented by a solid line at the current time.

One cause for concern with this recovery technique is if the stability analysis will still hold given the instantaneous change in the bounding functions and, therefore, infinite derivative values.

In general, switching the bounding functions should be done at times when the constraints are not in danger of being exceeded and the bounding function is inactive, i.e. $f_b(y_i^2) = 0$. This will ensure that the bounding function and its derivative are continuous and differentiable at all times. In the presence of an unstart, this approach is implausible, as corrective action must be taken extremely quickly. However, any real-life digital flight controller (even with an extremely fast sampling time as would be expected on a hypersonic vehicle) would calculate the bounding function derivative based on its analytical polynomial or exponential form given in Section 3.3.1 and therefore never produce an unbounded derivative; no actual differentiation would be done on-line. For this reason, it is assumed that switching the bounding functions in this way is valid and does not affect the results of the stability analysis of Section 3.5.

3.7.3 Results: Inlet Unstart Prevention

In this section, results are shown which again display the BFSC controller's capability to reject disturbances, now with an inlet unstart model included in the simulation. A trajectory that commands both angle-of-attack and sideslip angle was generated to purposefully drive the vehicle to a region of the $\alpha\beta$-space that nearly triggers an inlet unstart as seen in Figure 3.13. During the simulation trial, a $500lbf$ disturbance force lasting one second was applied in the positive z (down) direction at $t = 10.8s$. The vehicle response is shown in Figure 3.14. This disturbance was selected with the intention of making angle-of-attack more negative and even closer to the region of state-space in which an unstart will occur. As was demonstrated in the example given in Section 3.6.2, the BFSC controller is again able to take the proper corrective action to reject the disturbance and prevent an unstart from occurring. The control surface deflection, total velocity, and body-axis angular rate trajectories are also given in Figure 3.14.

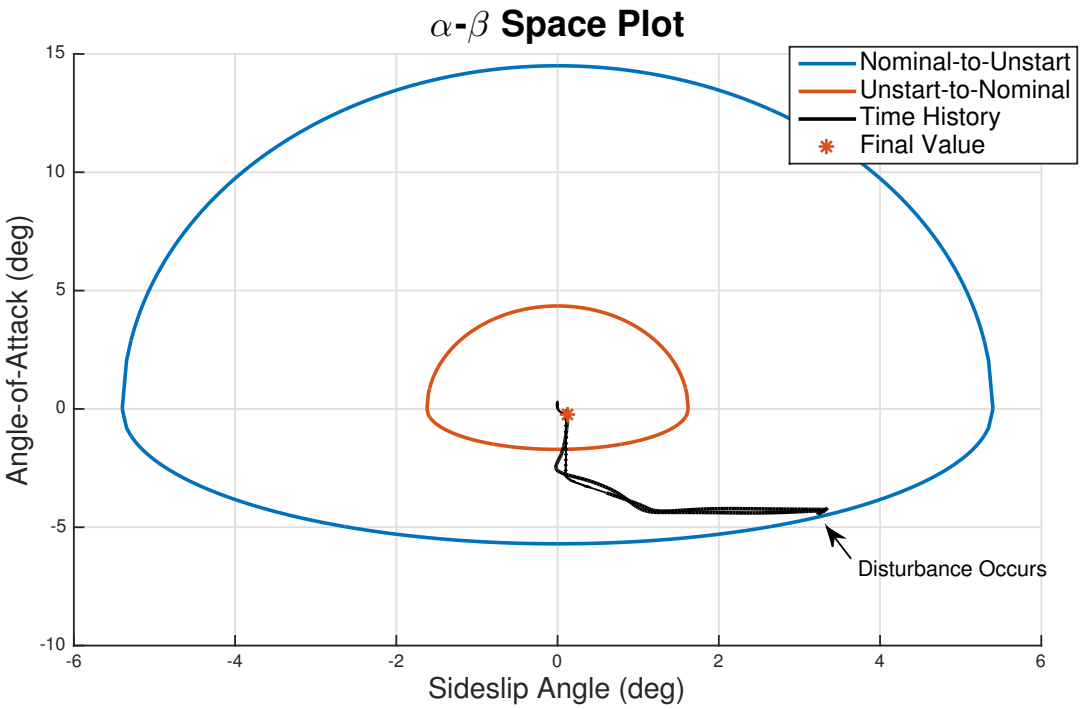

Figure 3.13: $\alpha\beta$-Space plot of inlet unstart prevention example.

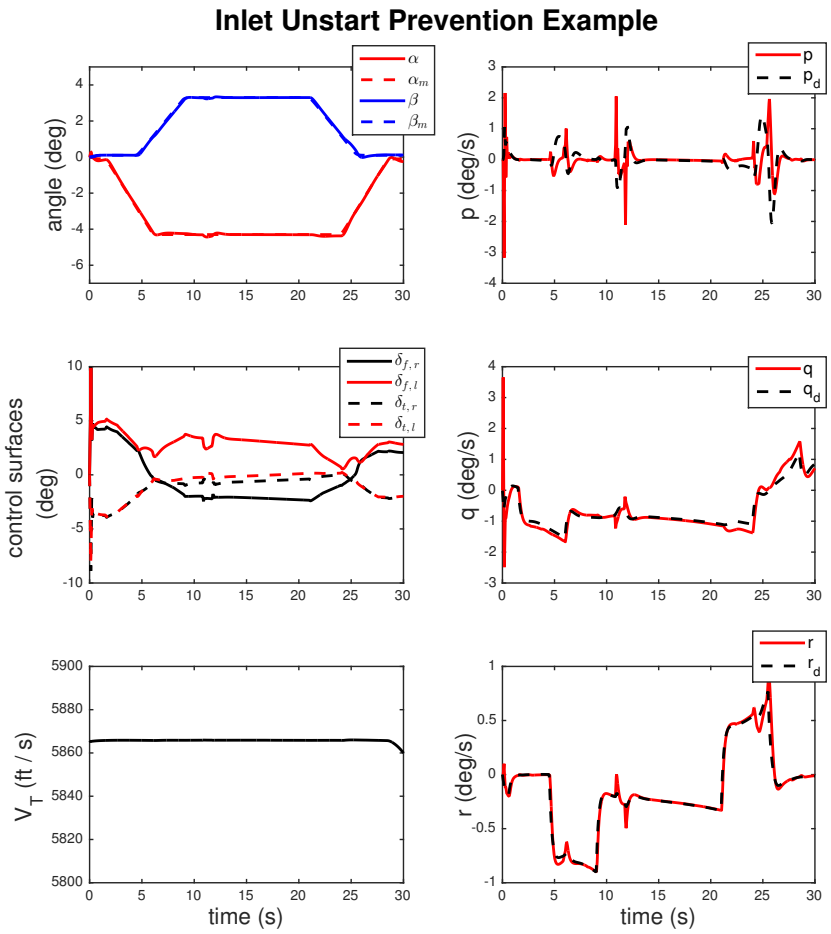

Figure 3.14: Vehicle states during inlet unstart prevention example.

3.7.4 Results: Inlet Unstart Recovery

In this section, results are shown from a simulation example in which the same reference trajectory was commanded, again intentionally driving the vehicle to a region of the state-space where inlet unstart will very nearly be triggered. An excessively large disturbance force is applied to the vehicle for which the preventative bounding functions were not tuned in order to purposefully trigger an unstart and to test out the recovery technique. A $2500lbf$ disturbance force lasting one second was applied in the positive z (down) direction at $t = 10.8s$, triggering an unstart, as seen in

Figure 3.15. The controller was augmented with a second set of bounding functions which were set to activate in the event of an unstart and which corresponds to the inner red ellipse in the inlet unstart model. This second set of recovery bounding functions were constructed using the method presented in Section 3.3.1 with parameters,

$$\begin{bmatrix} \alpha^*_{max} & \alpha^*_{min} & \delta^*_{\alpha} & \beta^*_{max} & \beta^*_{min} & \delta^*_{\beta} \end{bmatrix} = \begin{bmatrix} 3.4 & -1 & 0.5 & 1 & -1 & 0.5 \end{bmatrix} \text{deg} \tag{3.58}$$

$$\begin{bmatrix} \rho^{*,min}_{\alpha} & \rho^{*,max}_{\alpha} \rho^{*,min}_{\beta} & \rho^{*,max}_{\beta} \end{bmatrix} = \begin{bmatrix} 2 & 2 & 2.35 & 2.35 \end{bmatrix} \tag{3.59}$$

where the notation $(\cdot)^*$ is used to differentiate the parameters of the recovery bounding functions from those of the nominal preventative bounding functions.

Following the activation of the new bounding functions, the constrained states are rapidly driven to the inner ellipse of the inlet unstart model as seen in Figure 3.16. The controller is able to drive the vehicle back into a restarted state in $0.83s$, leading to a restoration of thrust and the bounding function parameters to their nominal values. In addition, following the engine restart, both angle-of-attack and sideslip angle successfully track the desired trajectory until the end of the simulation. As might be expected, large fluctuations are seen in the control surface deflections during the unstart event, however saturation limits are not reached. Given the successful recovery demonstration, these results substantiate the need for further testing on higher fidelity inlet unstart models.

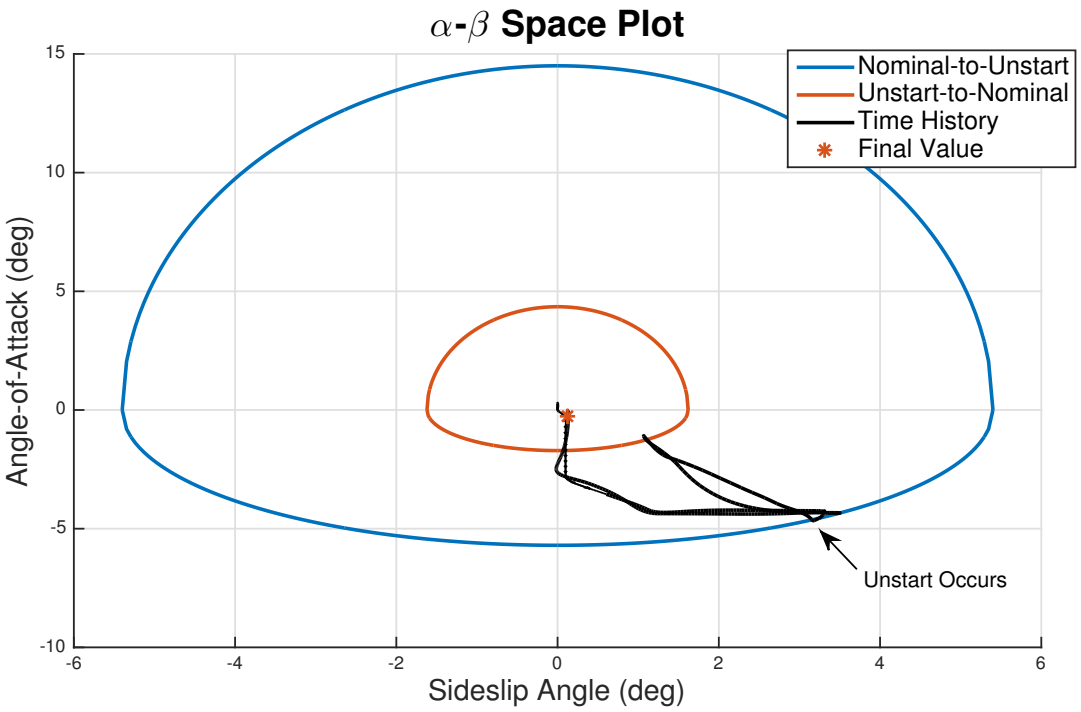

Figure 3.15: $\alpha\beta$-Space plot of inlet unstart recovery example.

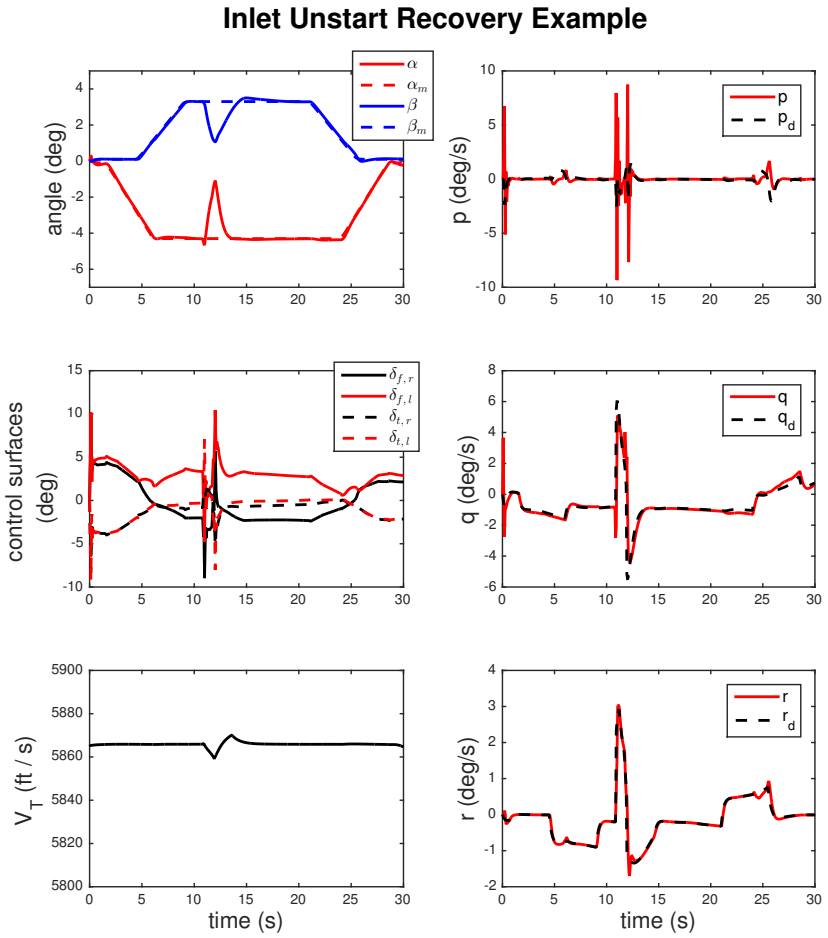

Figure 3.16: Vehicle states during inlet unstart recovery example.

4. OBSERVER-BASED NONLINEAR DYNAMIC INVERSION ADAPTIVE CONTROL: LONGITUDINAL HYPERSONIC VEHICLE MODEL*

4.1 Introduction

This section introduces an observer-based feedback controller that is capable of controlling a nonlinear longitudinal model of a hypersonic air vehicle without measuring angle-of-attack. The control objective is to command and track a desired pitch attitude angle trajectory. Due to the high speed and high operating temperature of these vehicles, external angle-of-attack vanes cannot be used and an estimated value must be used in the control law. This practical concern is often neglected in the literature and full state feedback is assumed.

As was shown in Sections 1-3, NDI controllers are effective because they can cancel out undesirable nonlinear dynamics and replace them, driving the plant to track a stable reference model. Due to the inability to directly measure angle-of-attack however, in this section it is not assumed that the nonlinear control effectiveness matrix can be canceled perfectly by the control law *a priori*.

This section also presents the development of a nonlinear observer, used to produce an estimated angle-of-attack signal. In practice, estimation of the vehicle's aerodynamic angles would likely be done using a nonlinear Kalman filtering technique. Unfortunately, proving stability of the closed-loop system with this type of estimation can be exceedingly difficult. Additionally, angle-of-attack could be directly calculated using know geometric relationships and sensor readings as in [45]. This approach however is heavily dependent on accurate knowledge of the vehicle's control and stability derivatives and so cannot be used in cases with large parametric uncertainty or unfiltered measurement signals. The nonlinear observer developed in this section allows for a rigorous

*Part of this Section is reprinted with permission from "ObserverBased Feedback Adaptive Control for Nonlinear Hypersonic Vehicles" by Douglas Famularo, John Valasek, Jonathan A. Muse and Michael A. Bolender in AIAA Guidance, Navigation and Control Conference (Grapevine, Texas), January 2017.

proof, ensuring that all closed-loop signals are uniformly ultimately bounded through Lyapunov analysis. The estimated angle-of-attack produced by the observer is fed into the inversion based control law and the adaptive laws. This approach was first developed in [46].

Observer-based or output feedback adaptive controllers have been developed for a handful aerospace applications. In [47] an adaptive output feedback controller is developed to control a linear model of a hypersonic vehicle. A procedure was developed for designing gain matrices such that the transfer function of the system is guaranteed to be strictly positive real. A sliding mode adaptive controller and sliding mode observer are developed in [8] for the purpose of controlling the response of a longitudinal model of a hypersonic vehicle, with parametric uncertainty and without full state feedback, to velocity and altitude step changes. In [48] an adaptive output feedback control strategy for linear systems with nonlinear uncertainties is derived. It takes advantage of the asymptotic properties of the algebraic Riccati Equation and proves ultimate boundedness of the system states, observer states, and a designer developed reference model. A linear dynamic inversion adaptive controller is developed in [49] for the application of a linear model of an unmanned air vehicle that is robust with respect to nonlinear uncertainties. Additionally, in [50], a neural network based adaptive control law using output feedback was developed in order to control a class of nonlinear single-input-single-output (SISO) systems.

A variety of nonlinear observers have been studied in the literature as well. Often a technique that can successfully estimate the states for one nonlinear system without complications arising will not work nearly as well for a different system. In [51] the concept a of sliding mode observer was developed for nonlinear systems and was shown to perform well in the presence of modeling errors and measurement noise. An output feedback controller utilizing a high gain observer was developed in [52] in order to control multi-input-multi-output (MIMO) nonlinear uncertain systems. A feedforward neural network compensator was used to account for system uncertainty. In [53] a high gain observer with the gains chosen through an adaptive law to control uniformly observable, nonlinear, SISO systems was developed. The ability to lessen the impact of noise sensitivity in

high gain observers for nonlinear systems was examined through the use of adaptive gains and an extended Kalman Filter in [54].

While they work very well in simulation, nonlinear observers often require high gains which can lead to the practical drawbacks of either high noise amplification or the peaking phenomenon [55], causing a high amplitude peak in the control signal. The choice to use an observer of this type was made with the knowledge that due to the small magnitude of the system nonlinearities, and assuming there are high quality sensors available to be used on hypersonic vehicles, gains would not need to be enormously high and noise amplification would be avoidable. Despite this fact, noisy state measurements were included in the GHV simulation studies and were shown to have minimal effect on the capabilities of the observer to accurately estimate the aerodynamic angles or of the vehicle to track its command signal.

4.2 Longitudinal Generic Hypersonic Vehicle Model

In Section 1, the full six degree-of-freedom model of the Generic Hypersonic vehicle was introduced. For clarity, the simplified longitudinal model that is the focus of this section is now given separately. This model is derived from the model in Section 1 and simplified by assuming,

$$\beta = \phi = \psi = p = r = 0$$

The state vector for the longitudinal axis of the GHV, $x \in \mathbb{R}^4$, and the control vector, $u \in \mathbb{R}^4$, are defined as,

$$x = \begin{bmatrix} V_T & \theta & \alpha & q \end{bmatrix}^T \tag{4.1}$$

$$u = \begin{bmatrix} \delta_{f,r} & \delta_{f,l} & \delta_{t,r} & \delta_{t,l} \end{bmatrix}^T \tag{4.2}$$

The dynamics of the longitudinal model are given by the following first-order differential equations:

$$\dot{V}_T = \frac{F_T}{m}\cos(\alpha) - \frac{D}{m} - g\sin(\gamma) \tag{4.3}$$

$$\dot{\theta} = q \tag{4.4}$$

$$\dot{\alpha} = \frac{1}{mV_T}\left(-L + mg\cos(\gamma) - F_{Tx}\sin(\alpha) + F_{Tz}\cos(\alpha)\right) + q \tag{4.5}$$

$$\dot{q} = \frac{1}{I_y}\left(M_T + \bar{q}S\bar{c}C_m\right) \tag{4.6}$$

where the following decompositions can be formed,

$$L = C_L\bar{q}S \tag{4.7}$$

$$D = C_D\bar{q}S \tag{4.8}$$

$$C_m = C'_m(\alpha) + \frac{\bar{c}}{2V_T}C_{m_q}q + \bar{C}_{m,\delta} + Hu \tag{4.9}$$

The total pitch moment's dependence on angle-of-attack is described by the polynomial $C'_m(\alpha)$. The constant $\bar{C}_{m,\delta}$ represents the effect of the control surface deflections on the total pitch moment at the trim condition and is given by,

$$\bar{C}_{m,\delta} = \frac{\partial C_m}{\partial \delta_{f,r}}(\delta_{f,r} = \bar{\delta}_{f,r}) + \frac{\partial C_m}{\partial \delta_{f,l}}(\delta_{f,l} = \bar{\delta}_{f,l}) + \frac{\partial C_m}{\partial \delta_{t,r}}(\delta_{t,r} = \bar{\delta}_{t,r}) + \frac{\partial C_m}{\partial \delta_{t,l}}(\delta_{t,l} = \bar{\delta}_{t,l}) \tag{4.10}$$

and the control effectiveness term $H \in \mathbb{R}^{1\times 4}$ is given by

$$H = \begin{bmatrix} \frac{\partial C_m}{\partial \delta_{f,r}} & \frac{\partial C_m}{\partial \delta_{f,l}} & \frac{\partial C_m}{\partial \delta_{t,r}} & \frac{\partial C_m}{\partial \delta_{t,l}} \end{bmatrix} \tag{4.11}$$

For the sake of brevity, these longitudinal dynamics are rewritten in vector form as

$$\dot{x} = f(x) + g(x)u \tag{4.12}$$

$$\begin{bmatrix} \dot{V}_T \\ \dot{\theta} \\ \dot{\alpha} \\ \dot{q} \end{bmatrix} = \begin{bmatrix} f_{VT}(x) \\ q \\ f_\alpha(x) + q \\ f_q(x) \end{bmatrix} + \begin{bmatrix} 0 \\ 0 \\ 0 \\ g_q(x) \end{bmatrix} u \tag{4.13}$$

where,

$$g_q(x) = \frac{1}{I_y}(\bar{q}S\bar{c}H) \tag{4.14}$$

Consider the scenario, common to hypersonic flight control, where only V_T, q, and θ are available for measurement while α is not. Before proceeding to the control law development, the following assumptions are made about the vehicle operating conditions and the structure of the parametric uncertainty in the system:

Assumption 4.2.1. *The vehicle is operating within a known thrust profile such that*

$$V_T \in [V_{T,min}, V_{T,max}] \tag{4.15}$$

$$\|F_T\| \leq F_{T,max} \tag{4.16}$$

$$\|M_T\| \leq M_{T,max} \tag{4.17}$$

for known $V_{T,min}$, $V_{T,max}$, $F_{T,max}$, $M_{T,max}$ and where the lift, drag, and pitching moment coefficient

term C'_m can be approximated by

$$C_L = C_{L0} + C_{L1}\alpha \tag{4.18}$$

$$C_D = C_{D0} + C_{D1}\alpha + C_{D2}\alpha^2 \tag{4.19}$$

$$C'_m = C_{m0} + C_{m1}\alpha + C_{m2}\alpha^2 + C_{m3}\alpha^3 \tag{4.20}$$

where C_{Li},C_{Dj}, and C_{mk} are constant $\forall\ i, j, k$ and $C_{L1} > 0$.

Assumption 4.2.2. *There is bounded uncertainty in the system such that for the following parameters*

$$|C_{Li} - \hat{C}_{Li}| \leq \Delta\bar{C}_{Li} \textit{ for } i = 0, 1 \tag{4.21}$$

$$|C_{Dj} - \hat{C}_{Dj}| \leq \Delta\bar{C}_{Dj} \textit{ for } j = 0, 1, 2 \tag{4.22}$$

$$|C_{mk} - \hat{C}_{mk}| \leq \Delta\bar{C}_{mk} \textit{ for } k = 0, 1, 2, 3 \tag{4.23}$$

$$|\bar{C}_{m,\delta} - \hat{\bar{C}}_{m,\delta}| \leq \Delta\bar{C}_{m,\delta} \tag{4.24}$$

$$|C_{mq} - \hat{C}_{mq}| \leq \Delta\bar{C}_{mq} \tag{4.25}$$

$$|I_y - \hat{I}_y| \leq \Delta\bar{I}_y \tag{4.26}$$

where the $(\hat{\cdot})$ notation represents the estimated value of each respective vehicle parameter and where $\Delta\bar{C}_{Li}$, $\Delta\bar{C}_{Dj}$, $\Delta\bar{C}_{mk}$, $\Delta\bar{C}_{mq}$ and $\Delta\bar{I}_y$ are known constants $\forall\ i, j, k$. All other vehicle parameters contained in $f(x)$ of Equation (4.12) are assumed to be known or measured perfectly.

Assumption 4.2.3. *The control effectiveness term $g_q(x)$ is known well enough such that an estimate of this term based on an estimated angle-of-attack and containing parameter uncertainty, $\hat{g}_q(x_c)$, can be formed which obeys the following conditions*

$$0 < \Delta\bar{g}_{qL}\mathbf{1}_2 \leq \begin{bmatrix} 1 & 1 - g_q(\mathbf{x})\hat{g}_q^{-1}(x_c) \\ 1 - (g_q(x)\hat{g}_q^{-1}(x_c))^T & g_q(x)\hat{g}_q^{-1}(x_c) \end{bmatrix} \leq \Delta\bar{g}_{qU}\mathbf{1}_2 \tag{4.27}$$

$$0 < \Delta\bar{g}_{qL} \leq g_q(x)\hat{g}_q^{-1}(x_c) \leq \Delta\bar{g}_{qU} \tag{4.28}$$

where, in order to avoid confusion with the moment of inertia matrix, $\mathbf{1}_M$ *is the* $M \times M$ *identity matrix and* $\hat{g}_q^{-1}(x_c)$ *is the pseudo-inverse of* $\hat{g}_q(x_c)$*. The vector* x_c *is given by*

$$x_c = \begin{bmatrix} V_T & \theta & \hat{\alpha} & q \end{bmatrix}^T \tag{4.29}$$

and represents a combination of the measured states and $\hat{\alpha}$*, the estimation of* α*. The parameters* $0 \leq \Delta\bar{g}_{qL}$ *and* $0 \leq \Delta\bar{g}_{qU}$ *are known constants. For simplicity, define*

$$\Delta\bar{g}_q = \max(|1 - \Delta\bar{g}_{qL}|, |1 - \Delta\bar{g}_{qU}|) \tag{4.30}$$

Assumption 4.2.4. *The initial angle-of-attack estimation error is bounded such that*

$$|\alpha(t = 0) - \hat{\alpha}(t = 0)| \leq \tilde{\alpha}_{0,max} \tag{4.31}$$

where $\tilde{\alpha}_{0,max} > 0$ *is a known constant.*

4.3 Control Law Development

4.3.1 Selecting the Command Signal

Because the control vector u directly influences the velocity level dynamics, achieving the control objective of tracking a pitch attitude angle trajectory must be done indirectly by commanding

pitch rate. In other words, the desired pitch rate trajectory, q_d, should be chosen such that if it is successfully tracked, the vehicle will also successfully track the desired pitch attitude angle trajectory, θ_d^*, which is assumed to be continuous and bounded. It is desired that the vehicle's pitch rate dynamics track a stable linear reference model with dynamics described by

$$\dot{q}_m = a_q q_m + b_q q_d \tag{4.32}$$

where a_q and b_q are designer chosen scalars and $a_q < 0$. In order to prevent the vehicle from exceeding a predefined pitch rate limit $\bar{q}_d > 0$, we differentiate between the designer chosen ideal desired pitch angle trajectory θ_d^* and the actual desired pitch angle trajectory θ_d. In a nominal flight condition where the vehicle pitch rate has a magnitude smaller than $\bar{q}_d$, the two trajectories will be equivalent, i.e. $\theta_d = \theta_d^*$. If the pitch rate limit is in danger of being exceeded, θ_d will be modified accordingly. This allows for the definition of two tracking error terms

$$e_q \triangleq q_m - q \tag{4.33}$$

$$e_\Theta \triangleq \theta_d - \theta \tag{4.34}$$

Since the goal is to design q_d such that θ follows a desired command, the pitch attitude angle error dynamics should be analyzed. Desired pitch rate should be chosen such that these dynamics are stabilizing and drive e_Θ to zero if $e_q = 0$. These dynamics are given by

$$\dot{e}_\theta = \dot{\theta}_d - \dot{\theta} = \dot{\theta}_d - q \tag{4.35}$$

Adding and subtracting the pitch rate reference signal leaves,

$$\dot{e}_\theta = \dot{\theta}_d + (q_m - q) - q_m \tag{4.36}$$

$$\dot{e}_\theta = \dot{\theta}_d + e_q - q_m \tag{4.37}$$

Therefore, if the reference model chosen for q is stable and can perfectly track a reference command signal, q_d, then choosing a desired pitch angle and pitch rate of

$$\dot{\theta}_d = \dot{\theta}_d^* \tag{4.38}$$

$$q_d = \dot{\theta}_d^* + K_\theta e_\theta \tag{4.39}$$

where K_θ is a positive scalar gain leaves,

$$\dot{e}_\theta = -K_\theta e_\theta + e_q \tag{4.40}$$

which implies that $e_\theta \to 0$ as long as $e_q \to 0$. In order to handle the predetermined pitch rate limit $\bar{q}_d$, the desired pitch angle and pitch rate are modified slightly to include saturation limits such that

$$\dot{\theta}_d = \begin{cases} -K_\theta e_\theta & \text{if } \dot{\theta}_d^* + K_\theta e_\theta < -\bar{q}_d \\ \dot{\theta}_d^* & \text{if } -\bar{q}_d \leq \dot{\theta}_d^* + K_\theta e_\theta \leq \bar{q}_d \\ -K_\theta e_\theta & \text{if } \dot{\theta}_d^* + K_\theta e_\theta > \bar{q}_d \end{cases} \tag{4.41}$$

$$q_d = \begin{cases} -\bar{q}_d & \text{if } \dot{\theta}_d^* + K_\theta e_\theta < -\bar{q}_d \\ \dot{\theta}_d^* + K_\theta e_\theta & \text{if } -\bar{q}_d \leq \dot{\theta}_d^* + K_\theta e_\theta \leq \bar{q}_d \\ \bar{q}_d & \text{if } \dot{\theta}_d^* + K_\theta e_\theta > \bar{q}_d \end{cases} \tag{4.42}$$

These saturation limits restrict the magnitude of the desired pitch rate and allow one to claim *a priori* that q_m is both stable and bounded. In practice, $\bar{q}_d$ can be set such that the saturation limits on q_d are never encountered in nominal flight. However, the pitch angle error dynamics still must

be analyzed in the presence of these saturation limits. This leaves,

$$\dot{e}_\theta = \begin{cases} -K_\theta e_\theta + e_q + \bar{q}_d & \text{if } \dot{\theta}_d^* + K_\theta e_\theta < -\bar{q}_d \\ -K_\theta e_\theta + e_q & \text{if } -\bar{q}_d \leq \dot{\theta}_d^* + K_\theta e_\theta \leq \bar{q}_d \\ -K_\theta e_\theta + e_q - \bar{q}_d & \text{if } \dot{\theta}_d^* + K_\theta e_\theta > \bar{q}_d. \end{cases} \tag{4.43}$$

With the appropriate desired pitch rate chosen as in (4.42), the control law can be developed with the new objective of stabilizing the pitch rate tracking error. In doing so, bounded tracking of both pitch rate and pitch angle will be achieved and the control objective will be met.

4.3.2 Control and Adaptive Laws

In order to achieve the modified control objective of tracking a desired pitch rate command, the control law is derived by expanding the pitch rate dynamics

$$\dot{q} = f_q(x) + g_q(x)u \tag{4.44}$$

$$\dot{q} = C_{q0} + \frac{\bar{q}S\bar{c}}{I_y}\left(C_{m1}\alpha + \frac{\bar{c}}{2V_T}C_{mq}q\right) + \frac{\bar{q}S\bar{c}}{I_y}\sum_{k=2}^{3} C_{mk}\alpha^k + g_q(x)u \tag{4.45}$$

where

$$C_{q0} = \frac{1}{I_y}\left(M_T + \bar{q}S\bar{c}C_{m0} + \bar{q}S\bar{c}\bar{C}_{m,\delta}\right) \tag{4.46}$$

If angle-of-attack was measured perfectly and if the model contained no parametric uncertainty,a nonlinear dynamic inversion control law of the form,

$$u_{ideal} = g_q^{-1}(x)\left[-f_q(x) + \dot{q}_m + K_q e_q + e_\theta\right] \tag{4.47}$$

where K_q is a constant positive scalar gain, would drive both e_q and e_θ to zero and achieve the control objective. Because perfect information is not available, the actual control law is based on

(4.47) given the system unknowns

$$u = \hat{g}_q^{-1}(x_c)\left[-\hat{f}_q(x_c) + \dot{q}_m + (K_q + K_{q1}(x_c))e_q + e_\theta + \nu_1 + \nu_2\right] \tag{4.48}$$

where $\hat{f}_q(x_c)$ is an estimate of the pitch rate open-loop dynamics given by

$$\hat{f}_q(x_c) = \hat{C}_{q0} + \frac{\bar{q}S\bar{c}}{\hat{I}_y}\left(\hat{C}_{m1}\hat{\alpha} + \frac{\bar{c}}{2V_T}\hat{C}_{mq}q\right) + \frac{\bar{q}S\bar{c}}{\hat{I}_y}\sum_{k=2}^{3}\hat{C}_{mk}\hat{\alpha}^k \tag{4.49}$$

The adaptive signals, ν_1 and ν_2 are time-varying signals, updated using an adaptive law, that account for parameter uncertainty and $K_{q1}(x_c)$ is a time-varying positive gain term, specified in more detail below.

In order to analyze system stability, the effect of the control law on the pitch rate tracking error dynamics must be examined. A full stability analysis will be completed in Section 4.5 but some initial steps are done here in order to introduce the notation required for defining the adaptive law:

$$\dot{e}_q = \dot{q}_m - \dot{q} \tag{4.50}$$

$$\dot{e}_q = \dot{q}_m - f_q(x) - g_q(x)u \tag{4.51}$$

Substituting the control law (4.48) into (4.51) leaves,

$$\dot{e}_q = \dot{q}_m - f_q(x) - g_q(x)\hat{g}_q^{-1}(x_c)\left[-\hat{f}_q(x_c) + \dot{q}_m + (K_q + K_{q1}(x_c))e_q + e_\theta + \nu_1 + \nu_2\right] \tag{4.52}$$

Equation (4.52) can be rearranged as

$$\begin{aligned}\dot{e}_q = &- f_q(x) + \hat{f}_q(x_c) - e_\theta - \nu_1 - \nu_2 - g_q(x)\hat{g}_q^{-1}(x_c)(K_q + K_{q1}(x_c))e_q \\ &- (g_q(x)\hat{g}_q^{-1}(x_c) - 1)\left[-\hat{f}_q(x_c) + \dot{q}_m + e_\theta + \nu_1 + \nu_2\right]\end{aligned} \tag{4.53}$$

It will be useful to expand and examine the difference $\hat{f}_q(x_c) - f_q(x)$. Given the definition of C_{q0}

in (4.46) and its estimate $\hat{C}_{q0}$, this difference can be represented as

$$\hat{f}_q(x_c) - f_q(x) = \left(\hat{C}_{q0} - C_{q0}\right) + \left(\frac{\hat{C}_{mq}}{\hat{I}_y} - \frac{C_{mq}}{I_y}\right)\frac{\bar{q}S\bar{c}^2}{2V_T}q + \bar{q}S\bar{c}\left(\sum_{k=1}^{3}\frac{\hat{C}_{mk}}{\hat{I}_y}\hat{\alpha}^k - \frac{C_{mk}}{I_y}\alpha^k\right) \quad (4.54)$$

The following summation,

$$\frac{\bar{q}S\bar{c}}{I_y}\sum_{k=1}^{3}C_{mk}\hat{\alpha}^k$$

is added to and subtracted from the right hand side of Equation (4.54). Note that this summation is a combination of true, unknown parameters and the estimated aerodynamic angles. Its inclusion is useful for analysis however it can not be calculated on-line. This allows for the difference $\hat{f}_q(x_c) - f_q(x)$ to be simplified further as

$$\hat{f}_q(x_c) - f_q(x) = W^T b(x_c) + \frac{\bar{q}S\bar{c}}{I_y}\sum_{k=1}^{3}C_{mk}\left(\hat{\alpha}^k - \alpha^k\right) \quad (4.55)$$

where W is a constant vector made up of unknown weights given by

$$W = \begin{bmatrix} W_1 & W_2 & W_3 & W_{41} & W_{42} & W_{43} \end{bmatrix}^T \quad (4.56)$$

$$W_1 = \frac{1}{\hat{I}_y} - \frac{1}{I_y} \qquad W_2 = \frac{\hat{C}_{m0} + \hat{\bar{C}}_{m,\delta}}{\hat{I}_y} - \frac{C_{mo} + \bar{C}_{m,\delta}}{I_y} \qquad W_3 = \frac{\hat{C}_{mq}}{\hat{I}_y} - \frac{C_{mq}}{I_y} \qquad W_{4i} = \frac{\hat{C}_{mi}}{\hat{I}_y} - \frac{C_{mi}}{I_y}$$

and $b(x_c)$ is a vector of known basis functions given by

$$b(x_c) = \begin{bmatrix} M_T & \bar{q}S\bar{c} & \frac{\bar{q}S\bar{c}^2}{2V_T}q & \bar{q}S\bar{c}\hat{\alpha} & \bar{q}S\bar{c}\hat{\alpha}^2 & \bar{q}S\bar{c}\hat{\alpha}^3 \end{bmatrix}^T \quad (4.57)$$

With this simplified form, the tracking error dynamics, Equation (4.53), can be rewritten as

$$\begin{aligned}\dot{e}_q =& W^T b(x_c) + \frac{\bar{q}S\bar{c}}{I_y}\sum_{k=1}^{3} C_{mk}\left(\hat{\alpha}^k - \alpha^k\right) - e_\theta - \nu_1 - \nu_2 - g_q(x)\hat{g}_q^{-1}(x_c)(K_q + K_{q1}(x_c))e_q \\ &- \left(g_q(x)\hat{g}_q^{-1}(x_c) - 1\right)\left[-\hat{f}_q(x_c) + \dot{q}_m + e_\theta + \nu_1 + \nu_2\right]\end{aligned} \tag{4.58}$$

The adaptive signals ν_1 and ν_2 can be defined as

$$\nu_1 + \nu_2 = \widehat{W}^T b(x_c) \tag{4.59}$$

$$\nu_1 = \widehat{W}_1^T b_1(x_c) \tag{4.60}$$

$$\nu_2 = \widehat{W}_2^T b_2(x_c) \tag{4.61}$$

$$b_1(x_c) = \begin{bmatrix} M_T & \bar{q}S\bar{c} & \frac{\bar{q}S\bar{c}^2}{2V_T}q \end{bmatrix}^T \tag{4.62}$$

$$b_2(x_c) = \begin{bmatrix} \bar{q}S\bar{c}\hat{\alpha} & \bar{q}S\bar{c}\hat{\alpha}^2 & \bar{q}S\bar{c}\hat{\alpha}^3 \end{bmatrix}^T \tag{4.63}$$

where $\widehat{W}$ is an estimate of the unknown weights W and is updated through an adaptive law. The vector $\widehat{W}_1$ is made up of the first three entries of $\widehat{W}$ and $\widehat{W}_2$ is made up of the final three entries of $\widehat{W}$. They are separated for the purpose of analysis and can be implemented as a single signal, $\nu = \nu_1 + \nu_2$. The estimated weights are updated through the adaptive law

$$\dot{\widehat{W}} = \Gamma_W \mathrm{Proj}_M\left(\widehat{W}, b(x_c)\left(e_q + 2(\hat{q} - q)\right)\right) \tag{4.64}$$

where $\hat{q}$ is the observer state for pitch rate which will be defined in more detail below and Γ_W is a positive definite gain matrix.

With the control and adaptive laws defined, a final expression for the pitch rate tracking error dynamics can be established. Substituting (4.59) into (4.58) and defining $\widetilde{W} = \widehat{W} - W$ leaves

$$\begin{aligned}\dot{e}_q = &- \widetilde{W}^T b(x_c) - \frac{\bar{q}S\bar{c}}{\hat{I}_y} C_{m1}(\alpha - \hat{\alpha}) + \eta_q - e_\theta - g_q(x)\hat{g}_q^{-1}(x_c)(K_q + K_{q1}(x_c))e_q \\ &- (g_q(x)\hat{g}_q^{-1}(x_c) - 1)\left[-\hat{C}_{q0} - \frac{\bar{q}S\bar{c}}{2\hat{I}_y V_T}\hat{C}_{mq}q + \dot{q}_m + e_\theta + \nu_1\right]\end{aligned} \tag{4.65}$$

where

$$\eta_q = \frac{\bar{q}S\bar{c}}{I_y}\sum_{k=2}^{3} C_{mk}(\hat{\alpha}^k - \alpha^k) - (g_q(x)\hat{g}_q^{-1}(x_c) - 1)\left(-\frac{\bar{q}S\bar{c}}{\hat{I}_y}\sum_{k=1}^{3}\hat{C}_{mk}\hat{\alpha}^k + \nu_2\right) \tag{4.66}$$

It will be shown that implementing the adaptive law above, Equation (4.64), allows for the closed-loop system to compensate for uncertainty due to modeling errors in the parameters contained in W. Uncertainty due to the inability to measure angle-of-attack will be handled through the use of a nonlinear observer.

4.4 Nonlinear Observer Design

The observer design process requires the definition of two vectors, the output vector, y, and the observer state vector $\hat{x}$:

$$y \triangleq Cx = \begin{bmatrix} V_T & \theta & q \end{bmatrix}^T \tag{4.67}$$

$$\hat{x} \triangleq \begin{bmatrix} \hat{V}_T & \hat{\theta} & \hat{\alpha} & \hat{q} \end{bmatrix}^T \tag{4.68}$$

where the matrix C is given by

$$C = \begin{bmatrix} 1 & 0 & 0 & 0 \\ 0 & 1 & 0 & 0 \\ 0 & 0 & 0 & 1 \end{bmatrix} \tag{4.69}$$

Note that the vector x_c is used in the control law, Equation (4.48), and not the observer state vector $\hat{x}$. Therefore, the sole purpose of the observer states $\hat{V}_T$, $\hat{q}$, and $\hat{\theta}$ is to generate an accurate estimate $\hat{\alpha}$ which can be fed to the control and adaptive laws. These other observer states will not influence the system otherwise. The estimation error vector is defined as

$$\tilde{x} \triangleq \hat{x} - x = \begin{bmatrix} \tilde{V}_T & \tilde{\theta} & \tilde{\alpha} & \tilde{q} \end{bmatrix}^T \tag{4.70}$$

The design process will proceed as follows: the dynamics will be developed for each observer state ($\dot{\hat{V}}_T$, $\dot{\hat{\theta}}$, etc.) by approximating the unknown dynamics and then adding an estimation correction term. An expression for the estimation error dynamics of each state ($\dot{\tilde{V}}_T$, $\dot{\tilde{\theta}}$, etc.) will then be derived. Finally, the entire estimation error dynamics, $\dot{\tilde{x}}$, will be constructed as a vector differential equation.

4.4.1 Total Velocity Observer Design

Recall that the dynamics for total velocity

$$\dot{V}_T = \frac{F_T}{m}\cos(\alpha) - \frac{D}{m} - g\sin(\gamma)$$

The observer state $\hat{V}_T$ is therefore defined by

$$\dot{\hat{V}}_T = \frac{F_T}{m}\cos(\hat{\alpha}) - \frac{\hat{D}(\hat{\alpha})}{m} - g\sin(\hat{\gamma}) + H_{V_T}(y - C\hat{x}) + H_{V_{T1}}\tilde{V}_T \tag{4.71}$$

where H_{V_T} is a row vector of constant observer-gains, $H_{V_{T1}}(x_c)$ is a scalar time-varying observer-gain, and because only the longitudinal dynamics are being addressed it is assumed that

$$\hat{\gamma} = \hat{\theta} - \hat{\alpha}$$

The estimation error for total velocity, $\tilde{V}_T$, has dynamics described by

$$\dot{\tilde{V}}_T = \dot{\hat{V}}_T - \dot{V}_T = -\frac{\bar{q}S}{m}\hat{C}_{D1}\tilde{\alpha} + \eta_{VT} + \delta_V + H_{V_T}(y - C\hat{x}) + H_{V_{T1}}\tilde{V}_T \tag{4.72}$$

where,

$$\delta_V = \left(\frac{F_T}{m}\cos(\hat{\alpha}) - \frac{F_T}{m}\cos(\alpha)\right) + \frac{\bar{q}S}{m}\left(C_{D0} - \hat{C}_{D0}\right) - g\left(\sin(\hat{\gamma}) - \sin(\gamma)\right) \tag{4.73}$$

$$\eta_{VT} = \frac{\bar{q}S}{m}\left(C_{D1} - \hat{C}_{D1}\right)\alpha + \frac{\bar{q}S}{m}C_{D2}\alpha^2 - \frac{\bar{q}S}{m}\hat{C}_{D2}\hat{\alpha}^2 \tag{4.74}$$

Note that given Assumption 4.2.1, made above, the magnitude of the term δ_V can be bounded by

$$|\delta_V| \leq K_{00} \tag{4.75}$$

where $K_{00} > 0$ is a known constant.

4.4.2 Pitch Attitude Angle Observer State

For the pitch attitude angle θ, the observer state dynamics and estimation error dynamics can be derived using the same process as above,

$$\dot{\theta} = q \tag{4.76}$$

$$\dot{\hat{\theta}} = \hat{q} + H_\theta(y - C\hat{x}) \tag{4.77}$$

$$\dot{\tilde{\theta}} = \dot{\hat{\theta}} - \dot{\theta} = \tilde{q} + H_\theta(y - C\hat{x}) \tag{4.78}$$

where H_θ is a row vector containing constant observer-gains.

4.4.3 Angle-of-Attack Observer Design

Recall the angle-of-attack dynamics

$$\dot{\alpha} = \frac{1}{mV_T}\left(-L + mg\cos(\gamma) - F_{Tx}\sin(\alpha) + F_{Tz}\cos(\alpha)\right) + q$$

which can be rewritten as

$$\dot{\alpha} = -\frac{C_{L1}\bar{q}S}{mV_T}\alpha + f'_\alpha(x) + q \tag{4.79}$$

where

$$f'_\alpha(x) = \frac{1}{mV_T}\left(-C_{L0}\bar{q}S + mg\cos(\gamma) - F_{Tx}\sin(\alpha) + F_{Tz}\cos(\alpha)\right) \tag{4.80}$$

The dynamics for the angle-of-attack observer state are therefore defined as ,

$$\dot{\hat{\alpha}} = -\frac{\hat{C}_{L1}\bar{q}S}{mV_T}\hat{\alpha} + \hat{f}'_\alpha(x_c) + \hat{q} + H_\alpha(y - C\hat{x}) \tag{4.81}$$

where H_α is a row vector containing constant observer-gains. The estimation error for angle-of-attack, $\tilde{\alpha}$, has dynamics described by

$$\dot{\tilde{\alpha}} = \dot{\hat{\alpha}} - \dot{\alpha} = -\frac{\hat{C}_{L1}\bar{q}S}{mV_T}\tilde{\alpha} + \tilde{q} + \delta_\alpha + H_\alpha(y - C\hat{x}) \tag{4.82}$$

where

$$\delta_\alpha = \left(C_{L1} - \hat{C}_{L1}\right)\frac{\bar{q}S}{mV_T}\alpha + \hat{f}'_\alpha(x_c) - f'_\alpha(x) \tag{4.83}$$

Note that given Assumptions 4.2.1 and 4.2.2, the magnitude of δ_α can be bounded by

$$|\delta_\alpha| \leq \frac{\bar{q}S}{mV_T}\Delta\bar{C}_{L1}|\alpha| + K_{10} \tag{4.84}$$

where $K_{10} > 0$ is a known constant.

4.4.4 Pitch Rate Observer Design

By taking a derivative with a respect to time of the expression $q = q_m - e_q$ and substituting in the error dynamics (4.65), the dynamics for pitch rate can be expressed as

$$\begin{aligned}\dot{q} =&\dot{q}_m + \widetilde{W}^T b(x_c) + \frac{\bar{q}S\bar{c}}{\hat{I}_y} C_{m1}(\alpha - \hat{\alpha}) - \eta_q + e_\theta + g_q(x)\hat{g}_q^{-1}(x_c)(K_q + K_{q1}(x_c))e_q \\ &+ (g_q(x)\hat{g}_q^{-1}(x_c) - 1)\left[-\hat{C}_{q0} - \frac{\bar{q}S\bar{c}}{2\hat{I}_y V_T}\hat{C}_{mq}q + \dot{q}_m + e_\theta + \nu_1\right]\end{aligned} \tag{4.85}$$

For the observer state, the dynamics are approximated by assuming

$$\tilde{\alpha} = 0 \qquad\qquad g_q(x)\hat{g}_q^{-1}(x_c) = 1 \qquad\qquad \widetilde{W} = 0$$

and again an estimation correction term is added:

$$\dot{\hat{q}} = \dot{q}_m + (K_q + K_{q1}(x_c))e_q + e_\theta + H_q(y - C\hat{x}) + H_{q1}(x_c)\tilde{q} \tag{4.86}$$

where H_q is a row vector of constant observer-gains and $H_{q1}(x_c)$ is a scalar time-varying observer-gain. The estimation error for pitch rate, $\tilde{q}$, has dynamics described by

$$\dot{\tilde{q}} = \dot{\hat{q}} - \dot{q} = -\widetilde{W}^T b(x_c) + \frac{\bar{q}S\bar{c}}{\hat{I}_y} C_{m1}\tilde{\alpha} + \eta_q + (1 - g_q(x)\hat{g}_q^{-1}(x_c))K_{q1}(x_c)e_q + \delta_q + H_q(y - C\hat{x}) + H_{q1}(x_c)\tilde{q} \tag{4.87}$$

where

$$\delta_q = (1 - g_q(x)\hat{g}_q^{-1}(x_c))\left(K_q e_q - \hat{C}_{q0} - \frac{\bar{q}S\bar{c}^2}{2\hat{I}_y V_T}\hat{C}_{mq}q + \dot{q}_m + e_\theta + \nu_1\right) \tag{4.88}$$

Note that given Assumptions 4.2.2 and 4.2.3, the magnitude of δ_q can be bounded by

$$|\delta_q| \leq K_{20} + K_{21}|e_q| + K_{22}|e_\Theta| \tag{4.89}$$

where K_{20}, K_{21}, and K_{22} are known constants.

4.4.5 Final Estimation Error Dynamics

Let each of the constant observer-gain vectors, H_i, be written as $H_i = \begin{bmatrix} h_{1i} & h_{2i} & h_{3i} \end{bmatrix}$ for $i = V_T, \alpha, q, \theta$ such that

$$H_i(y - Cx) = h_{1i}\tilde{V}_T + h_{2i}\tilde{\theta} + h_{3i}\tilde{q}$$

Combining Equations (4.72), (4.82), (4.87) and (4.78) allows for the full observer error dynamics to be expressed in vector matrix form,

$$\begin{bmatrix} \dot{\tilde{V}}_T \\ \dot{\tilde{\theta}} \\ \dot{\tilde{\alpha}} \\ \dot{\tilde{q}} \end{bmatrix} = \begin{bmatrix} -h_{1V_T} & -h_{2V_T} & -\frac{\bar{q}S}{m}\hat{C}_{D1} & -h_{3V_T} \\ -h_{1\theta} & -h_{2\theta} & 0 & 1 - h_{3\theta} \\ -h_{1\alpha} & -h_{2\alpha} & -\frac{\bar{q}S}{mV_T}\hat{C}_{L1} & 1 - h_{3\alpha} \\ -h_{1q} & -h_{2q} & \frac{\bar{q}S\bar{c}}{\hat{I}_y}C_{m1} & -h_{3q} \end{bmatrix} \begin{bmatrix} \tilde{V}_T \\ \tilde{\theta} \\ \tilde{\alpha} \\ \tilde{q} \end{bmatrix} + \begin{bmatrix} 0 \\ 0 \\ 0 \\ -\widetilde{W}^T b(x_c) + (1 - g_q(x)\hat{g}_q^{-1}(x_c))K_{q1}(x_c)e_q \end{bmatrix} + \begin{bmatrix} \delta_V \\ 0 \\ \delta_\alpha \\ \delta_q \end{bmatrix} + \begin{bmatrix} \eta_{VT} + H_{VT1}(x_c)\tilde{V}_T \\ 0 \\ 0 \\ \eta_q + H_{q1}(x_c)\tilde{q} \end{bmatrix} \tag{4.90}$$

or written more compactly as,

$$\dot{\tilde{x}} = H_O\tilde{x} + \left[-\widetilde{W}^T\beta + (1 - g_q(x)\hat{g}_q^{-1}(x_c))K_{q1}(x_c)e_q \right]_4 + \delta + \eta \tag{4.91}$$

By checking the principal minors of the matrix H_O, it can be shown that given Assumption 4.2.1 which assumed $\hat{C}_{L1} > 0$, the observer-gains h_{1VT}, $h_{2\theta}$ and h_{3q} can always be chosen such that

$$H_O + H_O^T < -Q \tag{4.92}$$

for a constant matrix $Q = Q^T > 0$. In addition, note that the norm of the vector δ can be bounded by

$$\|\delta\| \leq \|K_0\| + |K_{21}e_q| + |K_{22}e_\theta| + |K_3\alpha| \tag{4.93}$$

where

$$K_0 = \begin{bmatrix} K_{00} & K_{10} & K_{20} \end{bmatrix}^T \tag{4.94}$$

$$K_3 = \frac{\bar{q}S}{mV_T}\Delta\bar{C}_{L1} \tag{4.95}$$

4.5 Stability Analysis

In this section a Lyapunov stability analysis of the closed-loop system, based on the control algorithm and nonlinear observer discussed above, will be presented. The following lemma is introduced, which establishes a conservative bound on the magnitude of the true angle-of-attack as a function of time.

Lemma 4.5.1. *Consider the angle-of-attack dynamics given in Equation (4.5). Using only known parameters and measured signals, the time-varying signal $a(t)$ can be calculated such that*

$$|\alpha(t)| \leq a(t) \quad \forall t > 0 \tag{4.96}$$

where $a(t)$ evolves according to the differential equation

$$\dot{a} = -\frac{|\hat{C}_{L1} - \Delta\bar{C}_{L1}|\bar{q}(V_{T,min})S}{mV_{T,min}}a + \left(\bar{f}'_\alpha(x) + |q|\right) \tag{4.97}$$

$$a(0) = |\hat{\alpha}(0)| + \tilde{\alpha}_{0,max} \tag{4.98}$$

and where,

$$\bar{f}'_\alpha(x) = \frac{1}{mV_T}\left(|\hat{C}_{L0} + \Delta\bar{C}_{L0}\text{sign}(\hat{C}_{L0})|\bar{q}S + mg + \|F_T\|\right) \tag{4.99}$$

Proof. Recall the expression derived for the angle-of-attack dynamics in (4.79),

$$\dot{\alpha} = -\frac{C_{L1}\bar{q}S}{mV_T}\alpha + f'_\alpha(x) + q$$

Given that this expression is a first-order linear differential equation, an expression for $\alpha(t)$ can be solved for explicitly as

$$\alpha(t) = e^{\int_0^t -\frac{C_{L1}\bar{q}S}{mV_T}d\tau}\alpha(0) + \int_0^t e^{\int_\tau^t -\frac{C_{L1}\bar{q}S}{mV_T}d\tau'}\left(f'_\alpha(x(\tau)) + q(\tau)\right)d\tau \tag{4.100}$$

Equation (4.100) implies that the following inequalities hold,

$$-e^{-\frac{|\hat{C}_{L1}-\Delta\bar{C}_{L1}|\bar{q}(V_{T,min})S}{mV_{T,min}}t}a(0) - \int_0^t e^{-\frac{|\hat{C}_{L1}-\Delta\bar{C}_{L1}|\bar{q}(V_{T,min})S}{mV_{T,min}}(t-\tau)}\left(\bar{f}'_\alpha(x) + |q|\right)d\tau \leq \alpha(t) \tag{4.101}$$

$$\alpha(t) \leq e^{-\frac{|\hat{C}_{L1}-\Delta\bar{C}_{L1}|\bar{q}(V_{T,min})S}{mV_{T,min}}t}a(0) + \int_0^t e^{-\frac{|\hat{C}_{L1}-\Delta\bar{C}_{L1}|\bar{q}(V_{T,min})S}{mV_{T,min}}(t-\tau)}\left(\bar{f}'_\alpha(x) + |q|\right)d\tau \tag{4.102}$$

The inequalities (4.101) and (4.102) are equivalent to

$$-a(t) \leq \alpha(t) \leq a(t) \tag{4.103}$$

which is equivalent to (4.96). □

Remark 4.5.1. Recall Assumption 4.2.1 where it was stated that $C_{L1} > 0$. This implies that the signal $a(t)$ is bounded if and only if $(\bar{f}'_\alpha(x) + |q|)$ is bounded. Since each term in the definition of $\bar{f}'_\alpha(x)$ is bounded, this implies that $a(t)$ is bounded if and only if the pitch rate q is bounded.

Remark 4.5.2. If it can be shown that the signal $a(t)$ is uniformly ultimately bounded (UUB), as will be claimed in Theorem 6, then any signal designed using this set to stabilize the system will

be UUB as well.

Theorem 6. *Consider the nonlinear dynamical GHV system described by (4.13), the desired pitch rate command calculated by (4.42), the control law defined by (4.48), the adaptive law defined by (4.64) and the nonlinear observer designed in Section 4.4. Suppose that the desired pitch attitude angle input signal, θ_d^*, is bounded and continuous. If the following inequality,*

$$\Delta\bar{C}_{L1} < \frac{1}{2}\sqrt{\frac{mV_T}{\bar{q}S}C_{L1}\lambda_{min}(Q)} \tag{4.104}$$

is satisfied for all $t > 0$, then the tracking errors, e_q and e_θ, the estimation error $\tilde{x}$, the weight estimation error $\widetilde{W}$ and the system states, x, are uniformly ultimately bounded.

Proof. In order to analyze the stability of the system and to show that all of the closed-loop signals are UUB the following candidate Lyapunov function is chosen,

$$V = \tilde{x}^T\tilde{x} + \frac{1}{2}\left(e_q^2 + e_\theta^2 + \alpha^2 + \widetilde{W}^T\Gamma_W^{-1}\widetilde{W}\right) \tag{4.105}$$

The derivative of (4.105) is taken with respect to time along system trajectories, resulting in

$$\dot{V} = \tilde{x}^T\dot{\tilde{x}} + \dot{\tilde{x}}^T\tilde{x} + e_q\dot{e}_q + e_\theta\dot{e}_\theta + \alpha\dot{\alpha} + \widetilde{W}^T\Gamma_W^{-1}\dot{\widehat{W}} \tag{4.106}$$

Substituting the pitch rate tracking error dynamics (4.65) and the estimation error dynamics (4.91) into (4.106) and rearranging results in

$$\begin{aligned}\dot{V} =&\tilde{x}^T H_O\tilde{x} + \tilde{x}^T H_O^T\tilde{x} + 2\tilde{x}^T\delta + 2\tilde{q}(1 - g_q(x)\hat{g}_q^{-1}(x_c))K_{q1}(x_c)e_q + 2\tilde{x}^T\eta + e_\theta\dot{e}_\theta \\ &+ \alpha\dot{\alpha} + e_q\Big(-\frac{\bar{q}S\bar{c}}{\hat{I}_y}C_{m1}(\alpha - \hat{\alpha}) + \eta_q - e_\theta - g_q(x)\hat{g}_q^{-1}(x_c)(K_q + K_{q1}(x_c))e_q \\ &- (g_q(x)\hat{g}_q^{-1}(x_c) - 1)\left[-\hat{C}_{q0} - \frac{\bar{q}S\bar{c}}{2\hat{I}_y V_T}\hat{C}_{mq}q + \dot{q}_m + e_\theta + \nu_1\right]\Big) + \widetilde{W}^T\left(\Gamma_W^{-1}\dot{\widehat{W}} - b(x_c)(e_q + 2\tilde{q})\right)\end{aligned} \tag{4.107}$$

Application of the adaptive law given in (4.64) and the Lyapunov condition given in (4.92) leaves

$$\begin{aligned}\dot{V} \leq & -\tilde{x}^T Q\tilde{x} + 2\tilde{x}^T\delta + 2\tilde{q}(1-g_q(x)\hat{g}_q^{-1}(x_c))K_{q1}(x_c)e_q + 2\tilde{x}^T\eta + e_\theta\dot{e}_\theta \\ & + \alpha\dot{\alpha} + e_q\Big(-\frac{\bar{q}S\bar{c}}{\hat{I}_y}C_{m1}(\alpha-\hat{\alpha}) + \eta_q - e_\theta - g_q(x)\hat{g}_q^{-1}(x_c)(K_q + K_{q1}(x_c))e_q \\ & - (g_q(x)\hat{g}_q^{-1}(x_c)-1)\left[-\hat{C}_{q0} - \frac{\bar{q}S\bar{c}}{2\hat{I}_y V_T}\hat{C}_{mq}q + \dot{q}_m + e_\theta + \nu_1\right]\Big)\end{aligned} \tag{4.108}$$

In order to define the time-varying feedback and observer-gains ($K_{q1}(x_c)$, $H_{q1}(x_c)$, and $H_{VT1}(x_c)$) the following terms from (4.108) are examined,

$$\begin{aligned}& 2\tilde{x}^T\eta + 2\tilde{q}(1-g_q(x)\hat{g}_q^{-1}(x_c))K_{q1}(x_c)e_q - g_q(x)\hat{g}_q^{-1}(x_c)K_{q1}(x_c)e_q^2 + e_q\eta_q \\ & \quad = 2\tilde{V}_T\left(\eta_{VT} + H_{VT1}(x_c)\tilde{V}_T\right) + 2\tilde{q}\left(\eta_q + H_{q1}(x_c)\tilde{q}\right) + 2\tilde{q}(1-g_q(x)\hat{g}_q^{-1}(x_c))K_{q1}(x_c)e_q \\ & \quad\quad - g_q(x)\hat{g}_q^{-1}(x_c)K_{q1}(x_c)e_q^2 + e_q\eta_q\end{aligned} \tag{4.109}$$

where η_q and η_{VT} are defined in Equations (4.66) and (4.74) respectively. Using these definitions, the following bounds can be set,

$$\eta_{VT}(t) \leq \bar{\eta}_{VT}(t) \triangleq \frac{\bar{q}S}{m}\left(\Delta\bar{C}_{D1}a(t) + (\hat{C}_{D2} + \Delta\bar{C}_{D2})a^2(t) - \hat{C}_{D2}\hat{\alpha}^2\right) \tag{4.110}$$

$$\eta_q(t) \leq \bar{\eta}_q(t) \triangleq \frac{\bar{q}S\bar{c}}{\hat{I}_y - \Delta\bar{I}_y}\sum_{k=2}^{3}\left(|\hat{C}_{mk} + \Delta\bar{C}_{mk}\text{sign}(\hat{C}_{mk})|)(|\hat{\alpha}^k + a^k(t)|)\right) + \Delta\bar{q}_q\frac{\bar{q}S\bar{c}}{\hat{I}_y}\sum_{k=1}^{3}|\hat{C}_{mk}\hat{\alpha}^k + \nu_2| \tag{4.111}$$

where $a(t)$ is the signal defined in Lemma 4.5.1. Note that all of the terms that make up $\bar{\eta}_{VT}(t)$

and $\bar{\eta}_q(t)$ are known. Equation (4.109) can be rearranged as

$$\begin{aligned}
&2\tilde{x}^T\eta + 2\tilde{q}(1 - g_q(x)\hat{g}_q^{-1}(x_c))K_{q1}(x_c)e_q - g_q(x)\hat{g}_q^{-1}(x_c)K_{q1}(x_c)e_q^2 + e_q\eta_q \\
&\quad = 2\tilde{V}_T\left(\eta_{VT} + H_{VT1}(x_c)\tilde{V}_T\right) + \begin{bmatrix} 2\eta_q & \eta_q \end{bmatrix}\begin{bmatrix} \tilde{q} \\ e_q \end{bmatrix} \\
&\quad + \begin{bmatrix} \tilde{q} & e_q \end{bmatrix}\begin{bmatrix} 2H_{q1}(x_c) & (1 - g_q(x)\hat{g}_q^{-1}(x_c))K_{q1}(x_c) \\ ((1 - g_q(x)\hat{g}_q^{-1}(x_c))K_{q1}(x_c)) & -g_q(x)\hat{g}_q^{-1}(x_c))K_{q1}(x_c) \end{bmatrix}\begin{bmatrix} \tilde{q} \\ e_q \end{bmatrix}
\end{aligned} \tag{4.112}$$

Therefore, if the time-varying gains are defined as

$$H_{VT1}(x_c) = -\gamma\bar{\eta}_{VT}^2(t) \tag{4.113}$$

$$H_{q1}(x_c) = -\frac{5}{2}\gamma\bar{\eta}_q^2(t) \tag{4.114}$$

$$K_{q1}(x_c) = 5\gamma\bar{\eta}_q^2(t) \tag{4.115}$$

where $\gamma > 0$ is a designer chosen constant scalar, then, according to Assumption 4.2.3, the following bound holds

$$\begin{aligned}
&2\tilde{x}^T\eta + 2\tilde{q}(1 - g_q(x)\hat{g}_q^{-1}(x_c))K_{q1}(x_c)e_q - g_q(x)\hat{g}_q^{-1}(x_c)K_{q1}(x_c)e_q^2 + e_q\eta_q \leq \\
&\quad 2\left(\bar{\eta}_{VT}(t)|\tilde{V}_T| - \gamma\bar{\eta}_{VT}^2(t)|\tilde{V}_T|^2\right) + \sqrt{5}\bar{\eta}_q\left\|\begin{matrix} \tilde{q} \\ e_q \end{matrix}\right\| - 5\gamma\Delta\bar{g}_{qL}\bar{\eta}_q^2\left\|\begin{matrix} \tilde{q} \\ e_q \end{matrix}\right\|^2
\end{aligned} \tag{4.116}$$

Noting that for any scalar c and any positive scalar $d > 0$, the inequality $c - dc^2 \leq 1/4d$ holds, it can be concluded that

$$2\tilde{x}^T\eta + 2\tilde{q}(1 - g_q(x)\hat{g}_q^{-1}(x_c))K_{q1}(x_c)e_q - g_q(x)\hat{g}_q^{-1}(x_c)K_{q1}(x_c)e_q^2 + e_q\eta_q \leq \frac{1}{\gamma}\left(\frac{1}{2} + \frac{1}{4\Delta\bar{g}_{3L}}\right) \tag{4.117}$$

Incorporating the inequality (4.117) in the expression for the derivative of the Lyapunov function

and defining γ^* as

$$\gamma^* \triangleq \frac{1}{\gamma}\left(\frac{1}{2} + \frac{1}{4\Delta\bar{g}_{3L}}\right)$$

results in

$$\begin{aligned}\dot{V} \leq & -\tilde{x}^T Q\tilde{x} + 2\tilde{x}^T\delta + \gamma^* + e_\theta\dot{e}_\theta + \alpha\dot{\alpha} + e_q\Big(-\frac{\bar{q}S\bar{c}}{\hat{I}_y}C_{m1}(\alpha-\hat{\alpha}) - e_\theta - g_q(x)\hat{g}_q^{-1}(x_c)K_q e_q \\ & - (g_q(x)\hat{g}_q^{-1}(x_c)-1)\left[-\hat{C}_{q0} - \frac{\bar{q}S\bar{c}}{2\hat{I}_y V_T}\hat{C}_{mq}q + \dot{q}_m + e_\theta + \nu_1\right]\Big)\end{aligned} \tag{4.118}$$

Using the bound established in (4.93), a bound can be placed on the term $2\tilde{x}^T\delta$ in the following manner,

$$2\tilde{x}^T\delta \leq 2\left(\|K_0\| + |K_{21}e_q| + |K_{22}e_\theta| + |K_3\alpha|\right)\|\tilde{x}\| \tag{4.119}$$

The product $(\alpha\dot{\alpha})$ can similarly be bounded in terms of $|\alpha|$ and the error signals of interest:

$$\alpha\dot{\alpha} = \alpha\left(-\frac{C_{L1}\bar{q}S}{mV_T}\alpha + f'_\alpha(x) + q\right) \tag{4.120}$$

$$\alpha\dot{\alpha} \leq -\frac{C_{L1}\bar{q}S}{mV_T}\alpha^2 + |\alpha|\left(|f'_\alpha(x)|_{max} + |e_q| + |q_m|\right) \tag{4.121}$$

where according to Assumptions 4.2.1 and 4.2.2 the constant $|f'_\alpha(x)|_{max}$ is known. Finally a bound in the form of (4.119) and (4.121) can be found for the following terms, which for the sake of brevity will be referred to as $e_q\xi$,

$$\begin{aligned}e_q\xi = & e_q\Big(-\frac{\bar{q}S\bar{c}}{\hat{I}_y}C_{m1}(\alpha-\hat{\alpha}) - e_\theta - g_q(x)\hat{g}_q^{-1}(x_c)K_q e_q \\ & - (g_q(x)\hat{g}_q^{-1}(x_c)-1)\left[-\hat{C}_{q0} - \frac{\bar{q}S\bar{c}}{2\hat{I}_y V_T}\hat{C}_{mq}q + \dot{q}_m + e_\theta + \nu_1\right]\Big)\end{aligned} \tag{4.122}$$

$$
\begin{aligned}
e_q\xi \leq & -\Delta\bar{g}_{qL}K_q e_q^2 + |e_q|\left|\frac{\bar{q}(V_{T,max})S\bar{c}}{I_y}C_{m1}\right|\|\tilde{x}\| + |e_q||e_\theta| \\
& + |e_q|\Delta\bar{g}_q\left(|\hat{C}_{q0}|_{max} + \left|\frac{\bar{q}(V_{T,max})S\bar{c}^2}{2\hat{I}_y V_{T,max}}\hat{C}_{mq}\right|(|e_q| + |q_m|) + |\dot{q}_m| + |e_\theta|\right. \\
& \left. + \widehat{W}_{max}\left(M_{T,max} + \bar{q}(V_{T,max})S\bar{c} + \frac{\bar{q}(V_{T,max})S\bar{c}^2}{2V_{T,max}}(|e_q| + |q_m|)\right)\right)
\end{aligned} \tag{4.123}
$$

where $\widehat{W}_{max}$ is a positive bound set by the projection operator and where, according to Assumption 4.2.1, $|\hat{C}_{q0}|_{max}$ is a known constant. With the above bounds in place, (4.118) can be written compactly as

$$
\dot{V} \leq -\frac{1}{2}\lambda_{min}(Q)\|\tilde{x}\|^2 + \gamma^* - \frac{1}{2}K_\theta e_\theta^2 - \frac{1}{2}\Delta\bar{g}_{qL}K_q e_q^2 - \frac{C_{L1}\bar{q}S}{2mV_T}\alpha^2 + \zeta(\|\tilde{x}\|, |\alpha|, |e_q|, |e_\theta|) \tag{4.124}
$$

where $\zeta(\|\tilde{x}\|, |\alpha|, |e_q|, |e_\theta|)$ is defined by,

$$
\zeta(\|\tilde{x}\|, |\alpha|, |e_q|, |e_\theta|) = \begin{bmatrix} \|\tilde{x}\| \\ |\alpha| \\ |e_q| \\ |e_\theta| \end{bmatrix}^T \begin{bmatrix} m_{11} & m_{12} & m_{13} & m_{14} \\ m_{12} & m_{22} & m_{23} & 0 \\ m_{13} & m_{23} & m_{33} & m_{34} \\ m_{14} & 0 & m_{34} & m_{44} \end{bmatrix} \begin{bmatrix} \|\tilde{x}\| \\ |\alpha| \\ |e_q| \\ |e_\theta| \end{bmatrix} + 2 \begin{bmatrix} \|\tilde{x}\| \\ |\alpha| \\ |e_q| \\ |e_\theta| \end{bmatrix}^T \begin{bmatrix} b_1 \\ b_2 \\ b_3 \\ b_4 \end{bmatrix} \tag{4.125}
$$

$$
\zeta(\|\tilde{x}\|, |\alpha|, |e_q|, |e_\theta|) = v^T M_\zeta v + 2v^T b_\zeta \tag{4.126}
$$

and where $M_\zeta = M_\zeta^T$. The matrix entries m_{ij} and vector entries b_k are given in Appendix C.

Since the vector b_ζ is bounded, the function $\zeta(\|\tilde{x}\|, |\alpha|, |e_q|, |e_\theta|)$ has a unique global maximum if and only if the matrix M_ζ is strictly negative definite, which can be tested for by checking if its four principal minors alternate sign. The first principal minor must be negative. This is equivalent to

$$
M_{\zeta,1} = m_{11} = -\frac{1}{2}\lambda_{min}(Q) < 0 \tag{4.127}
$$

which by definition of Q is always satisfied.

The second principal minor must be positive. This is equivalent to

$$M_{\zeta,2} = m_{11}m_{22} - m_{12}^2 > 0 \tag{4.128}$$

$$\left(-\frac{1}{2}\lambda_{min}(Q)\right)\left(-\frac{C_{L1}\bar{q}S}{2mV_T}\right) - |K_3|^2 = \left(-\frac{1}{2}\lambda_{min}(Q)\right)\left(-\frac{C_{L1}\bar{q}S}{2mV_T}\right) - \frac{\bar{q}^2S^2}{m^2V_T^2}\Delta\bar{C}_{L1}^2 > 0 \tag{4.129}$$

If the condition given by (4.104) holds, the second principal minor will always be positive. From here, it is straightforward to show that the designer chosen gains K_q and K_θ can always be chosen such that the third and fourth principal minors have the appropriate sign as long as (4.104) holds. Therefore, (4.124) can be rewritten as

$$\dot{V} \leq -\frac{1}{2}\lambda_{min}(Q)\|\tilde{x}\|^2 + \gamma^* - \frac{1}{2}K_\theta e_\theta^2 - \frac{1}{2}\Delta\bar{g}_{qL}K_q e_q^2 - \frac{C_{L1}\bar{q}S}{2mV_T}\alpha^2 + |\zeta|_{max} \tag{4.130}$$

where $|\zeta|_{max}$ is the unique global maximum of the function ζ. This implies that $\dot{V} < 0$ outside of the compact set S_{GHV} where

$$\begin{aligned} S_{GHV}(\tilde{x}, \alpha, e_q, e_\theta, \widetilde{W}) = &\left\{(\tilde{x}, \alpha, e_q, e_\theta, \widetilde{W}) : \|\tilde{x}\|^2 \leq \frac{2\left(|\zeta|_{max} + \gamma^*\right)}{\lambda_{min}(Q)}\right\} \\ &\bigcap\left\{(\tilde{x}, \alpha, e_q, e_\theta, \widetilde{W}) : |\alpha|^2 \leq \frac{2mV_T\left(|\zeta|_{max} + \gamma^*\right)}{C_{L1}\bar{q}S}\right\} \\ &\bigcap\left\{(\tilde{x}, \alpha, e_q, e_\theta, \widetilde{W}) : |e_q|^2 \leq \frac{2\left(|\zeta|_{max} + \gamma^*\right)}{\Delta\bar{g}_q K_q}\right\} \\ &\bigcap\left\{(\tilde{x}, \alpha, e_q, e_\theta, \widetilde{W}) : |e_\theta|^2 \leq \frac{2\left(|\zeta|_{max} + \gamma^*\right)}{K_\theta}\right\} \\ &\bigcap\left\{(\tilde{x}, \alpha, e_q, e_\theta, \widetilde{W}) : \|\widetilde{W}\| \leq \|\widetilde{W}\|_{max}\right\} \end{aligned}$$

where $\|\widetilde{W}\|_{max}$ depends on the bound set by the projection operator. The Lyapnuov function V cannot grow outside of this set. This implies that $\tilde{x}$, α, e_q, e_θ, $\widetilde{W}$ are UUB and therefore so is the state vector x. The fact that $\tilde{x}$ and α are bounded implies that $\hat{\alpha}$ is bounded as well. This implies

that the filter signal $a(t)$ and therefore, the time-varying observer and controller gains $K_{q1}(x_c)$, $H_{q1}(x_c)$, and $H_{VT1}(x_c)$ are also bounded. Thus, all closed-loop signals are proven to be UUB. $\square$

4.6 Simulation Setup and Results

The NDI adaptive control architecture and nonlinear observer were implemented in the GHV simulation framework and a numerical example was explored. There were several objectives to the simulation testing. The first goal was to accurately track a desired pitch angle command. The second goal was to accurately estimate angle-of-attack using the nonlinear observer designed in Section 4.4. The third and final goal was to avoid the common problems associated with high gain nonlinear observers: the peaking phenomenon and large noise amplification.

There are two reasons why the nonlinear observer presented here can be effective with relatively low gains and therefore will not lead to peaking or noise amplification. The first reason is due to the specific aerodynamics associated with flying at hypersonic speeds. The nonlinear disturbances represented in this paper by the vector δ, and the scalars η_{VT} and η_q typically have very small magnitudes. It is the "role" of the Hurwitz matrix H_O and the time-varying gains to stabilize the estimation error dynamics in the presence of these disturbances. If the nonlinearities are small, it can play this role effectively without excessively high gains. The second reason is a practical one and only addresses the issue of noise amplification: hypersonic vehicles are extremely expensive to build and operate and because of this, they will be equipped with high quality sensors that are unlikely to produce very noisy measurement signals. Despite this fact, significant measurement noise was included in the presented simulation with the belief that performance should only improve with better sensing capabilities.

Two different desired pitch rate trajectories were examined. The first trajectory commanded called for the vehicle to ramp up to a pitch angle of $8.5\,\mathrm{deg}$, hold that pitch angle for approximately $20s$ and then ramp back down to zero deg. The second trajectory commanded called for the vehicle to track a pitch angle sinusoid with an amplitude of $8.5\,\mathrm{deg}$ and a frequency of approx-

imately $11.5\,\mathrm{deg}/s$. The two velocity level measurement signals needed to drive the nonlinear observer, pitch rate and total velocity, were corrupted by noise. For both trajectories tested a low measurement noise case and a high measurement noise case were examined. The low noise case was associated with zero mean white noise and a standard deviation of $7.07ft/s$ and $0.1\,\mathrm{deg}/s$, for total velocity and pitch rate respectively while the high noise case was associated with zero mean white noise and a standard deviation of $10ft/s$ and $0.5deg/s$, for total velocity and pitch rate respectively. The observer-gains were selected such that the matrix H_O remains Hurwitz for the entire simulation as required. These gain values can be found in Appendix D.

The bounded uncertainties described in Assumption 4.2.2 are given in Table 4.1 and the

Table 4.1: Longitudinal Aerodynamic Parameter Uncertainty Bounds

$\Delta\bar{C}_{L0} = 0.005$	$\Delta\bar{C}_{m0} = 2e-4$
$\Delta\bar{C}_{L1} = 0.22$	$\Delta\bar{C}_{m1} = .005$
$\Delta\bar{C}_{D0} = .002$	$\Delta\bar{C}_{m2} = .005$
$\Delta\bar{C}_{D1} = 0.006$	$\Delta\bar{C}_{m3} = .05$
$\Delta\bar{C}_{D2} = 0.015$	$\Delta\bar{C}_{mq} = .018$
$\Delta\bar{I}_y = 10$ lbm ft^2	$\Delta\bar{C}_{m,\delta} = .018$

bounded uncertainties described in Assumption 4.2.3 and Assumption 4.2.4 are given by $\Delta\bar{g}_q = 0.1$ and $\tilde{\alpha}_{0,max} = 1\,\mathrm{deg}$. Except for the moment of inertia bound, each uncertainty value listed is at least 20% of the magnitude of the assumed value of the parameters it is associated with, that is $|\Delta\bar{C}_X| \geq 0.2|\hat{C}_X|\ \forall X$. The pitch rate reference model parameters were set to $a_q = -15$ and $b_q = 15$. The other relevant control parameters were set as follows: the tracking gains were set such that $K_q = 20$ and $K_\theta = 2$ and the adaptive gain Γ_W was set as a diagonal matrix with the vector

$$\begin{bmatrix} 1e-5 & 1e-5 & 1 & 1 & 1e-3 \end{bmatrix}^T$$

along the diagonal. In order to make the simulation more realistic, second-order actuator dynamics with damping ratio $\zeta = 0.7$ and natural frequency $\omega_n = 25Hz$ were included and position and rate limits were placed on the actuators of $30\,\mathrm{deg}$ and $100\,\mathrm{deg}/s$, respectively. In addition, a time delay of $0.01s$ was included in the simulation. The initial flight condition was a velocity of Mach 6 and altitude of $80,000ft$. The initial true angle-of-attack was $0\,\mathrm{deg}$ however the observer was initialized such that $\hat{\alpha}(0) = 0.5\,\mathrm{deg}$.

For comparison purposes, the same litany of simulation tests were run using an ensemble Kalman filter (EnKF) to estimate angle-of-attack instead of the nonlinear observer derived in this paper. This filtering technique is a popular alternative to the extended Kalman filter (EKF) used for the estimation of nonlinear systems. The EnKF has been referred to as a sequential Monte Carlo method and has two major benefits when compared to the EKF: it does not require the propagation of a state covariance matrix which can be computationally expensive for high order systems and it also does not require a linearized model of the system [56]. For the results shown in this section, the ensemble size was set to $N = 100$ members and the process noise covariance matrix used, defined by $Q_f = E[w_k w_k^T]$ where w_k represents a vector of zero-mean white process noise is given by

$$Q_f = \begin{bmatrix} E[w_{VT,k}^2] & 0 & 0 & 0 \\ 0 & E[w_{\theta,k}^2] & 0 & 0 \\ 0 & 0 & E[w_{\alpha,k}^2] & 0 \\ 0 & 0 & 0 & E[w_{q,k}^2] \end{bmatrix} = \begin{bmatrix} 50 & 0 & 0 & 0 \\ 0 & 1e-5 & 0 & 0 \\ 0 & 0 & 0.01 & 0 \\ 0 & 0 & 0 & 4 \end{bmatrix} \tag{4.131}$$

The measurement noise covariance matrix is defined as $R_f = E[v_k v_k^T]$ where v_k represents a vector of zero-mean white measurement noise. The EnKF update procedure requires that R_f be non-singular. Therefore, despite assuming perfect measurement of the vehicle's pitch angle, the

measurement noise covariance matrix was set as

$$R_f = \begin{bmatrix} E[v_{VT,k}^2] & 0 & 0 \\ 0 & E[v_{\theta,k}^2] & 0 \\ 0 & 0 & E[v_{q,k}^2] \end{bmatrix} = \begin{bmatrix} E[v_{VT,k}^2] & 0 & 0 \\ 0 & 1e-6 & 0 \\ 0 & 0 & E[v_{q,k}^2] \end{bmatrix} \tag{4.132}$$

where $E[v_{VT,k}^2]$ and $E[v_{q,k}^2]$ varied based on whether a low noise case or high noise case was being examined. For completeness, a brief mathematical description of the comparative EnKF used in this study is now given.

Consider a general nonlinear systems with dynamics described by the differential equation (4.12). The EnKF is initialized by randomly sampling the state many times. This is the initial "ensemble" of members. Letting the i^{th} member of the ensemble at the $(k-1)^{th}$ time step be defined as $\hat{x}_{k-1}^i$, then at any time step the estimated mean and covariance can be approximated by

$$\hat{x}_{k-1} = \frac{1}{N}\sum_{i=1}^{N} \hat{x}_{k-1}^i \tag{4.133}$$

$$P_{k-1} = \frac{1}{N-1}\sum_{i=1}^{N} (\hat{x}_{k-1}^i - \hat{x}_{k-1})(\hat{x}_{k-1}^i - \hat{x}_{k-1})^T \tag{4.134}$$

Each of the ensemble members is predicted forward in time according to

$$\hat{x}_k^{i-} = f(\hat{x}_{k-1}^i) + g(\hat{x}_{k-1}^i)(u_{k-1} + w_{k-1}) \tag{4.135}$$

where w_k represents a vector of zero-mean white process noise with covariance defined by $E[w_k w_k^T] = Q_f$. Note that the EnKF requires no covariance prediction step.

After a measurement is taken, noise is added to the measurement vector such that an ensemble of measurements is created of the same size as the ensemble of state estimates, that is

$$y^i = y + v_k \tag{4.136}$$

where v_k represents a vector of zero-mean white measurement noise with covariance defined by $E[v_k v_k^T] = R_f$. Following the creation of the measurement ensemble, each state ensemble member is updated according to

$$\hat{x}_k^i = \hat{x}_k^{i-} + P_{k-1}^- C^T (C P_{k-1}^- C^T + R_f)^{-1} (y^i - C\hat{x}_{k-1}^{i-}) \tag{4.137}$$

and a single state estimate vector is calculated according to (4.133).

Test Case 1: The first case tested was based on the ramp pitch angle trajectory described above. Figure 4.1 shows the time histories of the state vector and the control surface deflections for the low noise case and Figure 4.2 shows the results pertaining to the high noise case. The top plots in these figures show the estimation performance of both the nonlinear observer and the EnKF. Both estimation techniques are able to produce accurate estimates of angle-of-attack, leading to successful tracking of the pitch rate reference model and therefore the pitch angle desired trajectory. In the high noise case, the control surface deflections that were generated using the nonlinear observer were affected slightly more by measurement noise than those generated using the EnKF, however the difference is minimal and no peaking phenomenon is seen.

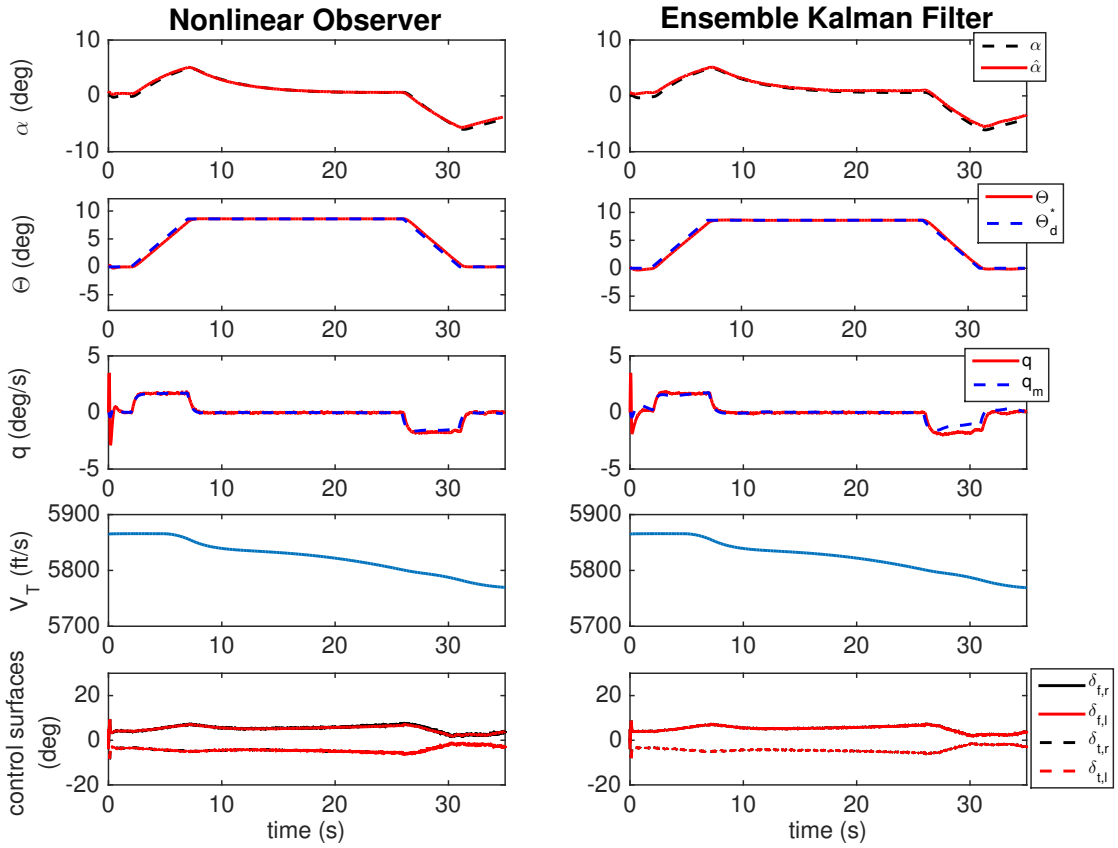

Figure 4.1: Test Case 1. Low Noise Case. True and estimated angle-of-attack trajectories are shown followed by the tracking performance of pitch angle and pitch rate, the vehicle total velocity, and the control surface deflections.

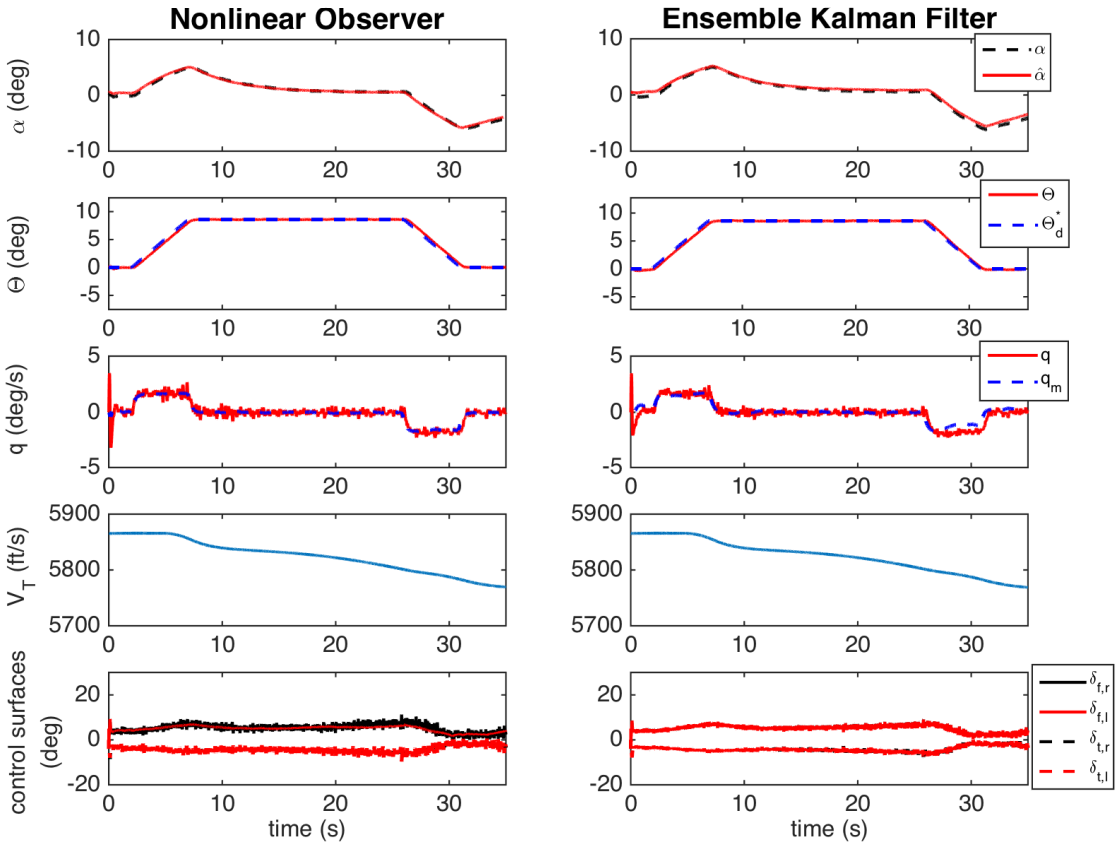

Figure 4.2: Test Case 1. High Noise Case. True and estimated angle-of-attack trajectories are shown followed by the tracking performance of pitch angle and pitch rate, the vehicle total velocity, and the control surface deflections.

Test Case 2: The second case tested was based on the sinusoidal pitch angle trajectory described above. Figure 4.3 shows the time histories of the state vector and the control surface deflections for the low noise case and Figure 4.4 shows the results pertaining to the high noise case. Again it is seen that both nonlinear estimation techniques are able to accurately estimate angle-of-attack and that the control objective is achieved despite parametric uncertainty in the model. The successful implementation of these test cases demonstrates the nonlinear observer's ability to perform comparably to nonlinear Kalman filtering techniques while also being provably stable in the NDI

adaptive control framework.

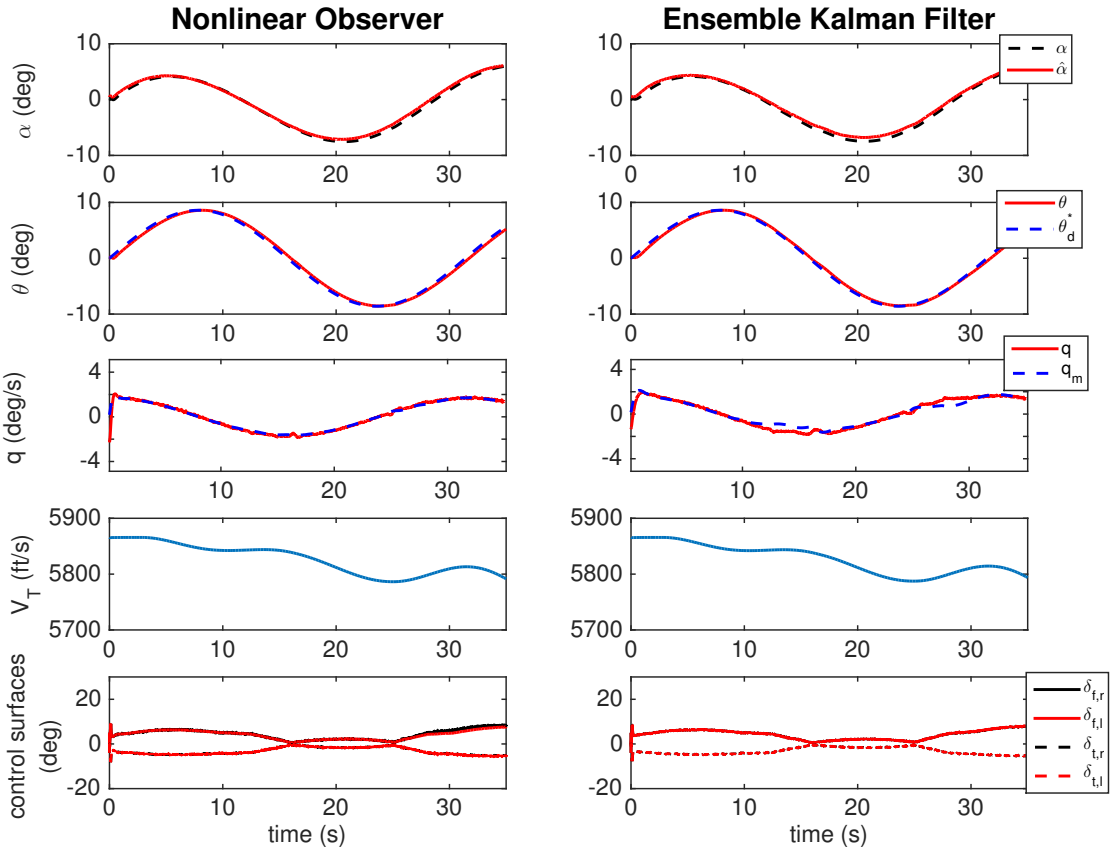

Figure 4.3: Test Case 2. Low Noise Case. True and estimated angle-of-attack trajectories are shown followed by the tracking performance of pitch angle and pitch rate, the vehicle total velocity, and the control surface deflections.

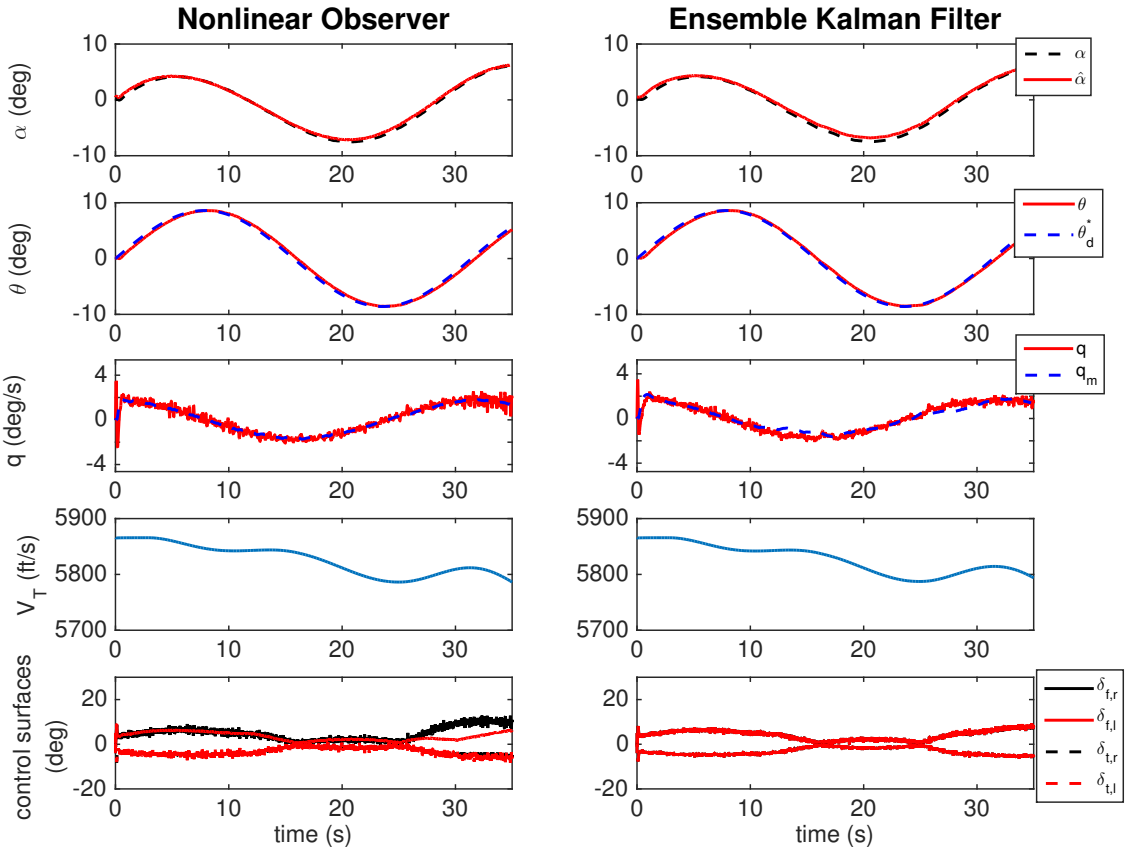

Figure 4.4: Test Case 2. High Noise Case. True and estimated angle-of-attack trajectories are shown followed by the tracking performance of pitch angle and pitch rate, the vehicle total velocity, and the control surface deflections.

4.7 Robustness Analysis

A simulation-based analysis was performed in order to test the robustness of the observer-based NDI adaptive controller with respect to parameter uncertainty. Most nonlinear control techniques lack neat analytical robustness measures. Instead, Monte Carlo approaches, such as the one presented here, must be performed. In this analysis, the assumed values of the aerodynamic coefficients C_{L1} and C_{mq} were systematically varied and the effect on estimation and tracking performance was studied. In each episode of the study, the vehicle was commanded to track a

pitch angle doublet maneuver with a magnitude that was randomly selected between 1 and $6\,\deg$. Each doublet command lasted for a total of $20s$ as seen in Figure 4.5. Similarly, the measurement noise covariances were also varied randomly through out each episode. All measurement noise had zero mean and the covariances were randomly selected values between 50 and $100(ft/s)^2$ for total velocity measurements and between 0.01 and $0.25(\deg/s)^2$ for pitch rate measurements.

For each assumed parameter value set $(\hat{C}_{L1}, \hat{C}_{mq})$ the integrated square error of the angle-of-attack estimation error and the pitch angle and pitch rate tracking errors were averaged across all episodes and charted in Tables 4.2-4.4. Given an arbitrary error signal e_X the integrated square error is defined as

$$ISE_{e_X} = \int_0^{t_f} e_X^2 dt \tag{4.138}$$

The full process used to conduct the robustness analysis is summarized below.

Let N_{ep} be the number of episodes performed for a given assumed parameter set $(\hat{C}_{L1}, \hat{C}_{mq})$ and define $(\hat{C}^0_{L1}, \hat{C}^0_{mq})$ as the best initial estimate of the aerodynamic parameters C_{L1} and C_{mq}.

1. Select Δ_{L1} and Δ_{mq} and define the assumed aerodynamic parameter set as

$$\hat{C}_{L1} = (1 + \Delta_{L1})\hat{C}^0_{L1}$$
$$\hat{C}_{mq} = (1 + \Delta_{mq})\hat{C}^0_{mq}$$

2. for $i = 1, 2, \ldots N_{ep}$

   (a) Randomly select the pitch angle desired doublet maneuver magnitude between $1-6\,\deg$

   (b) Randomly select the total velocity measurement noise covariance between $50-100(ft/s)^2$

   (c) Randomly select the pitch rate measurement noise covariance between $0.01-0.25(\deg/s)^2$

   (d) Run the simulation

(e) Calculate $ISE_{\tilde{\alpha}}(i)$, $ISE_{e_\theta}(i)$ and $ISE_{e_q}(i)$ according to (4.138)

3. Calculate the average integrated square error values $\overline{ISE}_{\tilde{\alpha}}$, $\overline{ISE}_{e_\theta}$ and $\overline{ISE}_{e_q}$ according to

$$\overline{ISE}_{e_X} = \frac{1}{N_{ep}} \sum_{i=1}^{N_{ep}} ISE_{e_X}(i) \tag{4.139}$$

For the results given in Tables 4.2-4.4, N_{ep} was set to 30 and t_f was $40s$. Due to the fact that the size of the robustness metric $\overline{ISE}_{e_X}$ is heavily dependent on the simulation run time t_f, these tables are best interpreted by comparing the relative values of the entries rather than the absolute values. Tables 4.3 and 4.4 indicate that the tracking performance is robust with respect to the parameter variation included in the study. The difference between the best and worst case scenario of $\overline{ISE}_{e_\theta}$ was just $2.2\,\mathrm{deg}^2$ over the $40s$ simulation time. The absolute value of the average integrate square error is large for the pitch rate tracking error compared with that of the pitch angle tracking error due to the higher impact of noisy measurent signals on velocity-level states. However, once again the difference between the best and worst case scenario is small: $5.3\,\mathrm{deg}^2$ over the $40s$ simulation time. The ability of the controller to compensate for such parameter uncertainty is due to the adaptive control mechanism.

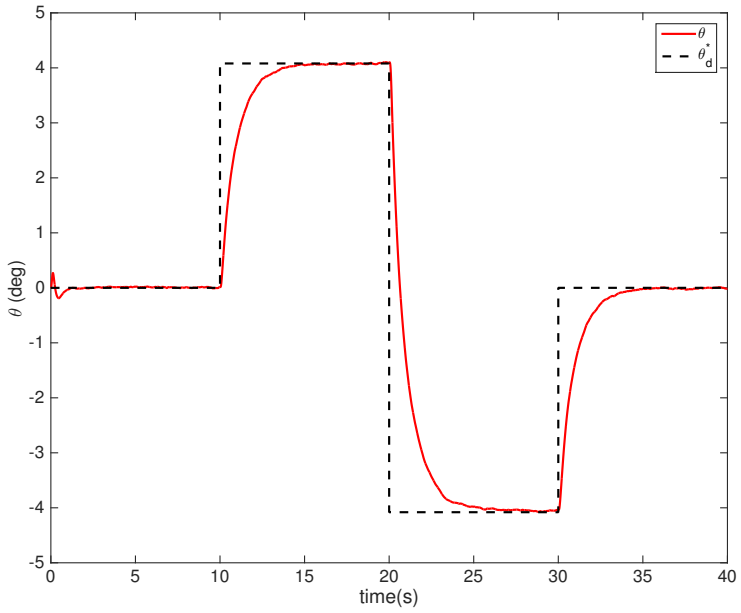

Figure 4.5: Sample pitch angle trajectory used in robustness analysis. The varying doublet magnitudes were selected randomly.

Table 4.2: Longitudinal Controller Robustness Analysis. Average integrated square error of the angle-of-attack estimation error over 40 seconds, $\overline{ISE}_{\tilde{\alpha}}$ $[\text{deg}^2]$

	$\Delta_{L1} = -0.25$	$\Delta_{L1} = -0.125$	$\Delta_{L1} = 0$	$\Delta_{L1} = 0.125$	$\Delta_{L1} = 0.25$
$\Delta_{mq} = -0.25$	15.98	7.29	4.70	3.16	4.71
$\Delta_{mq} = -0.125$	15.92	7.3076	3.68	5.28	3.62
$\Delta_{mq} = 0$	15.80	6.95	4.10	4.49	4.49
$\Delta_{mq} = 0.125$	15.74	7.14	3.45	4.36	4.83
$\Delta_{mq} = 0.25$	16.30	7.31	3.89	3.19	6.91

Table 4.3: Longitudinal Controller Robustness Analysis. Average integrated square error of the pitch angle tracking error over 40 seconds, $\overline{ISE}_{e_\theta}$ $[\deg^2]$

	$\Delta_{L1} = -0.25$	$\Delta_{L1} = -0.125$	$\Delta_{L1} = 0$	$\Delta_{L1} = 0.125$	$\Delta_{L1} = 0.25$
$\Delta_{mq} = -0.25$	1.46	1.53	2.69	1.47	1.53
$\Delta_{mq} = -0.125$	1.49	1.51	1.56	3.35	1.13
$\Delta_{mq} = 0$	1.25	1.21	2.03	2.89	1.41
$\Delta_{mq} = 0.125$	1.22	1.35	1.34	2.48	1.40
$\Delta_{mq} = 0.25$	2.46	1.57	1.67	1.49	2.39

Table 4.4: Longitudinal Controller Robustness Analysis. Average integrated square error of the pitch rate tracking error over 40 seconds, $\overline{ISE}_{e_q}$ $[(\deg/s)^2]$

	$\Delta_{L1} = -0.25$	$\Delta_{L1} = -0.125$	$\Delta_{L1} = 0$	$\Delta_{L1} = 0.125$	$\Delta_{L1} = 0.25$
$\Delta_{mq} = -0.25$	13.18	11.51	14.42	11.76	10.55
$\Delta_{mq} = -0.125$	10.46	9.56	13.77	12.29	9.57
$\Delta_{mq} = 0$	12.09	12.60	13.27	10.93	11.07
$\Delta_{mq} = 0.125$	10.02	10.52	13.14	12.87	12.52
$\Delta_{mq} = 0.25$	14.36	12.23	12.44	12.30	14.86

5. OBSERVER-BASED NONLINEAR DYNAMIC INVERSION ADAPTIVE CONTROL: SIX DEGREE-OF-FREEDOM HYPERSONIC VEHICLE MODEL

5.1 Introduction

In this section, the observer-based NDI adaptive control framework, developed in Section 4, is extended to the full six degree-of-freedom GHV model defined in Section 1. The vehicle's Euler angles, body-axis rates and total velocity are assumed to be measured while both the angle-of-attack and sideslip angle are not. The problem statement is briefly re-summarized: Due to the high speed and high operating temperature of hypersonic vehicles, typical external sensors such as angle-of-attack and sideslip angle vanes cannot be used. As in Section 4, it is not assumed that the nonlinear control effectiveness matrix can be canceled perfectly due to imperfect state knowledge. Additionally, a full-order nonlinear observer is developed similarly to the longitudinal analog. It is shown that using the angle-of-attack and sideslip angle estimates produced by this observer, all closed-loop signals are stable and bounded. This framework is tested in the GHV simulation by commanding a trajectory that excites both the longitudinal and lateral/directional modes of the vehicle and a robustness analysis is performed.

5.2 Operating Condition and Uncertainty Assumptions

The state and control vector for the six degree-of-freedom GHV model are given by

$$x = \begin{bmatrix} V_T & \Phi & x_a & x_r \end{bmatrix}^T$$
$$\Phi = \begin{bmatrix} \phi & \theta & \psi \end{bmatrix}^T$$
$$x_a = \begin{bmatrix} \beta & \alpha \end{bmatrix}^T$$
$$x_r = \begin{bmatrix} p & q & r \end{bmatrix}^T$$
$$u = \begin{bmatrix} \delta_{f,r} & \delta_{f,l} & \delta_{t,r} & \delta_{t,l} \end{bmatrix}^T$$

and the dynamics are described in Equations (1.30)-(1.45). The following assumptions are made about the vehicle operating conditions and the total uncertainty in the system:

Assumption 5.2.1. *The vehicle is operating within a known thrust profile such that*

$$V_T \in [V_{T,min}, V_{T,max}] \tag{5.1}$$
$$\|F_T\| \leq F_{T,max} \tag{5.2}$$
$$\|M_T\| \leq M_{T,max} \tag{5.3}$$

for known $V_{T,min}$, $V_{T,max}$, $F_{T,max}$, $M_{T,max}$ and where the lift, drag, sideforce and aerodynamic

moment coefficients terms (C'_ℓ, C'_m and C'_n) can be approximated by

$$C_L = C_{L0} + C_{L1}\alpha + \epsilon_L(\beta) \tag{5.4}$$

$$C_D = C_{D0} + C_{D1}\alpha + C_{D2}\alpha^2 + \epsilon_D(\beta) \tag{5.5}$$

$$C_Y = C_{Y0} + C_{Y1}\beta + \epsilon_Y(\alpha) \tag{5.6}$$

$$C'_\ell = \sum_{k=0}^{3} C_{\ell k}\beta^k + \epsilon_\ell(\alpha) \tag{5.7}$$

$$C'_m = \sum_{k=0}^{3} C_{mk}\alpha^k + \epsilon_m(\beta) \tag{5.8}$$

$$C'_n = \sum_{k=0}^{3} C_{nk}\beta^k + \epsilon_n(\alpha) \tag{5.9}$$

where

$$\epsilon_i(\cdot) < \bar{\epsilon}_i \tag{5.10}$$

for all i and $\bar{\epsilon}_i$ represent known constants. The coefficients C_{Li},C_{Di}, C_{Yi}, $C_{\ell i}$, C_{mi}, and C_{ni} are constant $\forall$ i and $C_{L1} > 0 > C_{Y1}$.

Assumption 5.2.2. *There is bounded uncertainty in the system such that for the following parameters*

$$|C_{ij} - \hat{C}_{ij}| \leq \Delta\bar{C}_{ij} \quad \textit{for } i = L, Y \;\; j = 0, 1 \tag{5.11}$$

$$|C_{Dj} - \hat{C}_{Dj}| \leq \Delta\bar{C}_{Dj} \textit{ for } j = 0, 1, 2 \tag{5.12}$$

$$|C_{ij} - \hat{C}_{ij}| \leq \Delta\bar{C}_{ij} \textit{ for } i = \ell, m, n \;\; j = 0, 1, 2, 3 \tag{5.13}$$

$$|\bar{C}_{m,\delta} - \hat{\bar{C}}_{m,\delta}| \leq \Delta\bar{C}_{m,\delta} \tag{5.14}$$

$$|C_i - \hat{C}_i| \leq \Delta\bar{C}_i \textit{ for } i = \ell_p, m_q, n_r \tag{5.15}$$

$$|I_i - \hat{I}_i| \leq \Delta\bar{I}_i \textit{ for } i = x, y, z, xz \tag{5.16}$$

where the $(\hat{\cdot})$ notation represents the estimated value of each respective vehicle parameter and where $\Delta\bar{C}_X$ and $\Delta\bar{I}_X$ are known constants $\forall\ X$. All other vehicle parameters contained in $f(x)$ of Equation (1.43) are assumed to be known or measured perfectly.

Assumption 5.2.3. *The control effectiveness term $g_r(x)$ has full row rank and is known well enough such that an estimate of this term based on estimated aerodynamic angles ($\hat{\alpha}$, $\hat{\beta}$) and containing parameter uncertainty, $\hat{g}_r(x_c)$, can be formed which obeys the following conditions*

$$0 < \Delta\bar{g}_{rL}\mathbf{1}_6 \leq \begin{bmatrix} \mathbf{1}_3 & \mathbf{1}_3 - g_r(x)\hat{g}_r^{-1}(x_c) \\ \mathbf{1}_3 - (g_r(x)\hat{g}_r^{-1}(x_c))^T & g_r(x)\hat{g}_r^{-1}(x_c) \end{bmatrix} \leq \Delta\bar{g}_{rU}\mathbf{1}_6 \tag{5.17}$$

$$0 < \Delta\bar{g}_{rL}\mathbf{1}_3 \leq g_r(x)\hat{g}_r^{-1}(x_c) \leq \Delta\bar{g}_{rU}\mathbf{1}_3 \tag{5.18}$$

where, in order to avoid confusion with the moment of inertia matrix, $\mathbf{1}_M$ is the $M \times M$ identity matrix and $\hat{g}_r^{-1}(x_c)$ is the pseudo-inverse of $\hat{g}_r(x_c)$. The vector x_c is given by

$$x_c = \begin{bmatrix} V_T & \Phi & \hat{x}_a & x_r \end{bmatrix}^T \tag{5.19}$$

and represents a combination of the measured states and $\hat{x}_a$, the estimate of x_a. The parameters $0 \leq \Delta\bar{g}_{rL}$ and $0 \leq \Delta\bar{g}_{rU}$ are known constants. For simplicity, define

$$\Delta\bar{g}_r = \max(|1 - \Delta\bar{g}_{rL}|, |1 - \Delta\bar{g}_{rU}|) \tag{5.20}$$

Assumption 5.2.4. *The vehicle does not pass through any kinematic or dynamic singularities, i.e.*

$$|\theta(t)|, |\beta(t)| < \frac{\pi}{2}\ \ \forall t > 0 \tag{5.21}$$

Furthermore, there exist known constants d_i such that

$$1 \leq \frac{1}{\cos(i)} < d_i \quad \textit{for } i = \theta, \beta \tag{5.22}$$

Assumption 5.2.5. *The initial aerodynamic angle estimation error is bounded such that*

$$|x_a(0) - \hat{x}_a(0)| \leq \tilde{x}_{a,max} \tag{5.23}$$

where for any vector $v \in \mathbb{R}^p$, the absolute value $|v|$ signifies $\begin{bmatrix} |v_1| & |v_2| & \dots & |v_p| \end{bmatrix}^T$ and $\tilde{x}_{a,max}$ is a known constant vector with entries greater than or equal to zero.

5.3 Control Law Development

5.3.1 Selecting the Command Signal

Because the control vector directly influences the velocity level dynamics, achieving the control objective of commanding an attitude angle trajectory must be done indirectly by commanding the body-axis angular rates. In other words, an expression must be found for the desired rate trajectory, $x_{r,d}$, which forces the vehicle to achieve the desired attitude angle trajectory, Φ_d^*, which is assumed to be continuous and bounded. It is desired that the vehicle's angular rate dynamics follow a stable linear reference model described by

$$\dot{x}_{r,m} = A_m x_{r,m} + B_m x_{r,d} \tag{5.24}$$

where (A_m, B_m) are a controllable pair, $A_m \in \mathbb{R}^{3\times3}$ is Hurwitz, and $B_m \in \mathbb{R}^{3\times3}$. Next, two tracking error terms are defined

$$e_r \triangleq x_{r,m} - x_r \tag{5.25}$$

$$e_\Phi \triangleq \Phi_d - \Phi \tag{5.26}$$

Since the goal is to design $x_{r,d}$ such that Φ follows a desired command, the attitude angle error dynamics should be analyzed. The desired rates should be chosen such that the attitude angle dynamics are stabilizing and drive e_Φ to zero if $e_r = 0$. These dynamics are given by

$$\dot{e}_\Phi = \dot{\Phi}_d - \dot{\Phi} = \dot{\Phi}_d - f_\Phi(x) \tag{5.27}$$

Let $f_\Phi(x) = A_\Phi x_r$. Adding and subtracting $A_\Phi x_{r,m}$ leaves,

$$\dot{e}_\Phi = \dot{\Phi}_d + A_\Phi(x_{r,m} - x_r) - A_\Phi x_{r,m} \tag{5.28}$$

$$\dot{e}_\Phi = \dot{\Phi}_d + A_\Phi e_r - A_\Phi x_{r,m} \tag{5.29}$$

Therefore, if the reference model chosen for x_r is stable and can perfectly track a reference command signal, choosing desired attitude angle and angular rate trajectories of

$$\dot{\Phi}_d = \dot{\Phi}_d^* \tag{5.30}$$

$$x_{r,d} = A_\Phi^{-1}\left(\dot{\Phi}_d^* + K_\Phi e_\Phi\right) \tag{5.31}$$

where $K_\Phi > 0$ is a diagonal matrix, leaves

$$\dot{e}_\Phi = -K_\Phi e_\Phi + A_\Phi e_r \tag{5.32}$$

which implies that $e_\Phi \to 0$ as long as $e_r \to 0$ as desired. Due to Assumption 5.2.4, the matrix A_Φ is always invertible. The desired trajectories are modified slightly to include saturation limits such

that

$$\dot{\Phi}_d(i) = \begin{cases} -K_\Phi(i,i)e_\Phi(i) & \text{if } \left(A_\Phi^{-1}(\dot{\Phi}_d^* + K_\Phi e_\Phi)\right)(i) < -\bar{x}_{r,d}(i) \\ \dot{\Phi}_d^*(i) & \text{if } -\bar{x}_{r,d}(i) \leq \left(A_\Phi^{-1}(\dot{\Phi}_d^* + K_\Phi e_\Phi)\right)(i) \leq \bar{x}_{r,d}(i) \\ -K_\Phi(i,i)e_\Phi(i) & \text{if } \left(A_\Phi^{-1}(\dot{\Phi}_d^* + K_\Phi e_\Phi)\right)(i) > \bar{x}_{r,d}(i) \end{cases} \tag{5.33}$$

$$x_{r,d}(i) = \begin{cases} -\bar{x}_{r,d}(i) & \text{if } \left(A_\Phi^{-1}(\dot{\Phi}_d^* + K_\Phi e_\Phi)\right)(i) < -\bar{x}_{r,d}(i) \\ \left(A_\Phi^{-1}(\dot{\Phi}_d^* + K_\Phi e_\Phi)\right)(i) & \text{if } -\bar{x}_{r,d}(i) \leq \left(A_\Phi^{-1}(\dot{\Phi}_d^* + K_\Phi e_\Phi)\right)(i) \leq \bar{x}_{r,d}(i) \\ \bar{x}_{r,d}(i) & \text{if } \left(A_\Phi^{-1}(\dot{\Phi}_d^* + K_\Phi e_\Phi)\right)(i) > \bar{x}_{r,d}(i) \end{cases} \tag{5.34}$$

where $v(i)$ is the i^{th} element of an arbitrary vector v and $\bar{x}_{r,d}(i) > 0 \, \forall i$ are predetermined saturation limits for p, q and r. These saturation limits restrict the magnitude of the desired angular rates and allow one to claim *a priori* that $x_{r,m}$ is both stable and bounded. In practice, $\bar{x}_{r,d}$ can be set such that the saturation limits on $x_{r,d}$ are never encountered in nominal flight. Nevertheless, the attitude angle error dynamics still must be analyzed in the presence of these saturation limits,

$$\dot{e}_\Phi(i) = \begin{cases} -K_\Phi(i,i)e_\Phi(i) + A_\Phi^i e_r + A_\Phi^i \bar{x}_{r,d} & \text{if } \left(A_\Phi^{-1}(\dot{\Phi}_d^* + K_\Phi e_\Phi)\right)(i) < -\bar{x}_{r,d}(i) \\ -K_\Phi(i,i)e_\Phi(i) + A_\Phi^i e_r & \text{if } -\bar{x}_{r,d}(i) \leq \left(A_\Phi^{-1}(\dot{\Phi}_d^* + K_\Phi e_\Phi)\right)(i) \leq \bar{x}_{r,d}(i) \\ -K_\Phi(i,i)e_\Phi(i) + A_\Phi^i e_r - A_\Phi^i \bar{x}_{r,d} & \text{if } \left(A_\Phi^{-1}(\dot{\Phi}_d^* + K_\Phi e_\Phi)\right)(i) > \bar{x}_{r,d}(i) \end{cases} \tag{5.35}$$

where A_Φ^i represents the i^{th} row of A_Φ. With the appropriate desired angular rates given by (5.34), the control law can be developed with the new goal in mind of bounding the angular rate tracking error. In doing so, bounded tracking of both the angular rates and the Euler angles will be realized and the control objective will be met.

5.3.2 Control and Adaptive Laws

The control law development begins by examining the angular rate dynamics

$$\dot{x}_r = f_r(x) + g_r(x)u \tag{5.36}$$

$$\dot{x}_r = I^{-1}\left(I_M f_{rr}(x_r) + M_T + \bar{q}SG\right) + g_r(x)u \tag{5.37}$$

where I is the moment of inertia matrix, defined in full in (1.33), and

$$I_M = \begin{bmatrix} \frac{-I_{xz}(I_x - I_y + I_z)}{I_{xz}^2 - I_x I_z} & \frac{I_{xz}^2 + I_z^2 - I_y I_z}{I_{xz}^2 - I_x I_z} & 0 & 0 \\ 0 & 0 & \frac{I_z - I_y}{I_y} & \frac{-I_{xz}}{I_y} \\ \frac{-(I_x^2 - I_x I_y + I_{xz}^2)}{I_{xz}^2 - I_x I_z} & \frac{I_{xz}(I_x - I_y + I_z)}{I_{xz}^2 - I_x I_z} & 0 & 0 \end{bmatrix} \tag{5.38}$$

$$f_{rr}(x_r) = \begin{bmatrix} pq \\ qr \\ pr \\ p^2 - r^2 \end{bmatrix} \tag{5.39}$$

If the aerodynamic angles were measured perfectly and all of the vehicle parameters were known perfectly as well, a dynamic inversion control law of the form,

$$u_{ideal} = g_r^{-1}(x)\left[-f_r(x) + \dot{x}_{r,m} + K_r e_r + e_\Phi\right] \tag{5.40}$$

where $K_r > 0$ is a constant feedback gain matrix, would drive both e_r and e_Φ to zero and achieve the desired control objective. Because perfect information is not available, the actual control law will be based on (5.40) given the system unknowns

$$u = \hat{g}_r^{-1}(x_c)\left[-\hat{f}_r(x_c) + \dot{x}_{r,m} + (K_r + K_{r1}(x_c))e_r + e_\Phi + \nu_1 + \nu_2\right] \tag{5.41}$$

where $\hat{f}_r(x_c)$ is given by

$$\hat{f}_r(x_c) = \hat{I}^{-1}\left(\hat{I}_M f_{rr}(x_r) + M_T + \bar{q}S\hat{G}\right) \tag{5.42}$$

$$\hat{G} = \begin{bmatrix} b(\sum_{i=0}^{3}\hat{C}_{\ell i}\hat{\beta}^i + \frac{b}{2V_T}\hat{C}_{\ell p}p) \\ \bar{c}(\sum_{i=0}^{3}\hat{C}_{mi}\hat{\alpha}^i + \frac{\bar{c}}{2V_T}\hat{C}_{mq}q) \\ b(\sum_{i=0}^{3}\hat{C}_{ni}\hat{\beta}^i + \frac{b}{2V_T}\hat{C}_{nr}r) \end{bmatrix} \tag{5.43}$$

The adaptive signals ν_1 and ν_2 are time-varying signals, updated using an adaptive law, that account for parameter uncertainty and $K_{r1}(x_c)$ is a time-varying positive gain term, specified in more detail below.

In order to analyze system stability, the effect of the control law on the angular rate tracking error dynamics must be examined. This analysis will be completed in Section 5.5 but some initial steps can be done here in order to introduce the notation required for defining the adaptive law:

$$\dot{e}_r = \dot{x}_{r,m} - \dot{x}_r \tag{5.44}$$

$$\dot{e}_r = \dot{x}_{r,m} - f_r(x) - g_r(x)u \tag{5.45}$$

Substituting the control law (5.41) into (5.45) leaves,

$$\dot{e}_r = \dot{x}_{r,m} - f_r(x) - g_r(x)\hat{g}_r^{-1}(x_c)\left[-\hat{f}_r(x_c) + \dot{x}_{r,m} + (K_r + K_{r1}(x_c))e_r + e_\Phi + \nu_1 + \nu_2\right] \tag{5.46}$$

Adding and subtracting everything contained in the bracket of (5.46) except for $(K_r + K_{r1}(x_c))e_r$ results in

$$\begin{aligned} \dot{e}_r = -f_r(x) + \hat{f}_r(x_c) - e_\Phi - \nu_1 - \nu_2 - g_r(x)\hat{g}_r^{-1}(x_c)(K_r + K_{r1}(x_c))e_r \\ - (g_r(x)\hat{g}_r^{-1}(x_c) - \mathbf{1}_3)\left[-\hat{f}_r(x_c) + \dot{x}_{r,m} + e_\Phi + \nu_1 + \nu_2\right] \end{aligned} \tag{5.47}$$

It will be useful to expand and examine the difference $\hat{f}_r(x_c) - f_r(x)$. By defining the term f_{r0} as,

$$f_{r0} = I^{-1}\left(M_T + \bar{q}S\begin{bmatrix} bC_{\ell 0} \\ \bar{c}(C_{m0} + \bar{C}_{m\delta}) \\ bC_{n0} \end{bmatrix}\right) \tag{5.48}$$

and its estimate $\hat{f}_{r0}$, the difference can be written as

$$\begin{aligned}\hat{f}_r(x_c) - f_r(x) =& (\hat{f}_{r0} - f_{r0}) + (\hat{I}^{-1}\hat{I}_M - I^{-1}I_M)f_{rr}(x_r) + \frac{\bar{q}S}{2V_T}\begin{bmatrix} \left(\hat{I}^{-1}\hat{C}_{\ell p} - I^{-1}C_{\ell p}\right)b^2 p \\ \left(\hat{I}^{-1}\hat{C}_{mq} - I^{-1}C_{mq}\right)\bar{c}^2 q \\ \left(\hat{I}^{-1}\hat{C}_{nr} - I^{-1}C_{nr}\right)b^2 r \end{bmatrix} \\ &+ \hat{I}^{-1}\bar{q}S\begin{bmatrix} b\sum_{i=1}^{3}\hat{C}_{\ell i}\hat{\beta}^i \\ \bar{c}\sum_{i=1}^{3}\hat{C}_{mi}\hat{\alpha}^i \\ b\sum_{i=1}^{3}\hat{C}_{ni}\hat{\beta}^i \end{bmatrix} - I^{-1}\bar{q}S\begin{bmatrix} b\left(\sum_{i=1}^{3}C_{\ell i}\beta^i + \epsilon_\ell(\alpha)\right) \\ \bar{c}\left(\sum_{i=1}^{3}C_{mi}\alpha^i + \epsilon_m(\beta)\right) \\ b\left(\sum_{i=1}^{3}C_{ni}\beta^i + \epsilon_n(\alpha)\right) \end{bmatrix}\end{aligned} \tag{5.49}$$

The following vector

$$I^{-1}\bar{q}S\begin{bmatrix} b\sum_{i=1}^{3}C_{\ell i}\hat{\beta}^i \\ \bar{c}\sum_{i=1}^{3}C_{mi}\hat{\alpha}^i \\ b\sum_{i=1}^{3}C_{ni}\hat{\beta}^i \end{bmatrix}$$

is added to and subtracted from the right hand side of equation (5.49). Note that this vector is a combination of true, unknown parameters and the estimated aerodynamic angles. Its inclusion is useful for analysis however it can not be calculated on-line. This allows for the difference

$\hat{f}_r(x_c) - f_r(x)$ to be simplified further as

$$\hat{f}_r(x_c) - f_r(x) = W^T b(x_c) + I^{-1}\bar{q}S \begin{bmatrix} b\left(\sum_{i=1}^{3} C_{\ell i}(\hat{\beta}^i - \beta^i) - \epsilon_\ell(\beta)\right) \\ \bar{c}\left(\sum_{i=1}^{3} C_{mi}(\hat{\alpha}^i - \alpha^i) - \epsilon_m(\beta)\right) \\ b\left(\sum_{i=1}^{3} C_{ni}(\hat{\beta}^i - \beta^i) - \epsilon_n(\alpha)\right) \end{bmatrix} \tag{5.50}$$

where W is a constant matrix made up of unknown weights given by

$$W = \begin{bmatrix} W_1 & W_2 & W_3 & W_4 & W_{51} & W_{52} & W_{53} \end{bmatrix} \tag{5.51}$$

$$W_1 = \hat{I}^{-1} - I^{-1} \tag{5.52}$$

$$W_2 = \hat{I}^{-1} \begin{bmatrix} b\hat{C}_{\ell 0} \\ \bar{c}(\hat{C}_{m0} + \hat{\bar{C}}_{m\delta}) \\ b\hat{C}_{n0} \end{bmatrix} - I^{-1} \begin{bmatrix} bC_{\ell 0} \\ \bar{c}(C_{m0} + \bar{C}_{m\delta}) \\ bC_{n0} \end{bmatrix} \tag{5.53}$$

$$W_3 = \hat{I}^{-1} \begin{bmatrix} b^2\hat{C}_{\ell p} & 0 & 0 \\ 0 & \bar{c}^2\hat{C}_{mq} & 0 \\ 0 & 0 & b^2\hat{C}_{nr} \end{bmatrix} - I^{-1} \begin{bmatrix} b^2C_{\ell p} & 0 & 0 \\ 0 & \bar{c}^2C_{mq} & 0 \\ 0 & 0 & b^2C_{nr} \end{bmatrix} \tag{5.54}$$

$$W_4 = \hat{I}^{-1}\hat{I}_M - I^{-1}I_M \tag{5.55}$$

$$W_{5i} = \hat{I}^{-1} \begin{bmatrix} b\hat{C}_{\ell i} & 0 \\ 0 & \bar{c}\hat{C}_{mi} \\ b\hat{C}_{ni} & 0 \end{bmatrix} - I^{-1} \begin{bmatrix} bC_{\ell i} & 0 \\ 0 & \bar{c}C_{mi} \\ bC_{ni} & 0 \end{bmatrix} \tag{5.56}$$

and $b(x_c)$ is a vector of known basis functions given by

$$b(x_c) = \begin{bmatrix} M_T^T & \bar{q}S & \frac{\bar{q}S}{2V_T}x_r^T & f_{rr}^T(x_r) & \bar{q}S\hat{x}_a^{(1)T} & \bar{q}S\hat{x}_a^{(2)T} & \bar{q}S\hat{x}_a^{(3)T} \end{bmatrix}^T \tag{5.57}$$

where

$$\hat{x}_a^{(i)} = \begin{bmatrix} \hat{\beta}^i \\ \hat{\alpha}^i \end{bmatrix} \tag{5.58}$$

With this simplified form, the tracking error dynamics, Equation (5.47), can be rewritten as

$$\begin{aligned} \dot{e}_r =& W^T b(x_c) + I^{-1}\bar{q}S \begin{bmatrix} b\left(\sum_{i=1}^{3} C_{\ell i}(\hat{\beta}^i - \beta^i) - \epsilon_\ell(\alpha)\right) \\ \bar{c}\left(\sum_{i=1}^{3} C_{mi}(\hat{\alpha}^i - \alpha^i) - \epsilon_m(\beta)\right) \\ b\left(\sum_{i=1}^{3} C_{ni}(\hat{\beta}^i - \beta^i) - \epsilon_n(\alpha)\right) \end{bmatrix} - e_\Phi - \nu_1 - \nu_2 \\ & - g_r(x)\hat{g}_r^{-1}(x_c)(K_r + K_{r1}(x_c))e_r - (g_r(x)\hat{g}_r^{-1}(x_c) - \mathbf{1}_3)\left[-\hat{f}_r(x_c) + \dot{x}_{r,m} + e_\Phi + \nu_1 + \nu_2\right] \end{aligned} \tag{5.59}$$

The adaptive signals ν_1 and ν_2 can be defined as

$$\nu_1 + \nu_2 = \widehat{W}^T b(x_c) \tag{5.60}$$

$$\nu_1 = \widehat{W}_1^T b_1(x_c) \tag{5.61}$$

$$\nu_2 = \widehat{W}_2^T b_2(x_c) \tag{5.62}$$

$$b_1(x_c) = \begin{bmatrix} M_T^T & \bar{q}S & \frac{\bar{q}S}{2V_T} x_r^T \end{bmatrix}^T \tag{5.63}$$

$$b_2(x_c) = \begin{bmatrix} f_{rr}^T(x_r) & \bar{q}\hat{x}_a^{(1)T} & \bar{q}\hat{x}_a^{(2)T} & \bar{q}\hat{x}_a^{(3)T} \end{bmatrix}^T \tag{5.64}$$

where $\widehat{W}$ is the best estimate of the unknown weights W. The estimated weights are updated through the adaptive law

$$\dot{\widehat{W}} = \Gamma_W \mathrm{Proj}_M\left(\widehat{W}, b(x_c)\left(e_r + 2(\hat{x}_r - x_r)\right)^T\right) \tag{5.65}$$

where $\hat{x}_r$ is the observer state vector for the angular rates and Γ_W is a positive definite gain matrix. Substituting (5.60) into (5.59) and defining $\widetilde{W} = \widehat{W} - W$ leaves

$$\dot{e}_r = -\widetilde{W}^T b(x_c) + I^{-1}\bar{q}S \begin{bmatrix} b\left(C_{\ell 1}(\hat{\beta}-\beta) - \epsilon_\ell(\alpha)\right) \\ \bar{c}\left(C_{m1}(\hat{\alpha}-\alpha) - \epsilon_m(\beta)\right) \\ b\left(C_{n1}(\hat{\beta}-\beta) - \epsilon_n(\alpha)\right) \end{bmatrix} + \eta_r - e_\Phi - g_r(x)\hat{g}_r^{-1}(x_c)(K_r + K_{r1}(x_c))e_r$$
$$- \left(g_r(x)\hat{g}_r^{-1}(x_c) - \mathbf{1}_3\right)\left(-\hat{f}_{r0} - \hat{I}^{-1}\bar{q}S \begin{bmatrix} \frac{b^2}{2V_T}\hat{C}_{\ell p}p \\ \frac{\bar{c}^2}{2V_T}\hat{C}_{mq}q \\ \frac{b^2}{2V_T}\hat{C}_{nr}r \end{bmatrix} + \dot{x}_{r,m} + e_\Phi + \nu_1\right) \tag{5.66}$$

where

$$\eta_r = I^{-1}\bar{q}S \begin{bmatrix} b\sum_{i=2}^{3} C_{\ell i}(\hat{\beta}^i - \beta^i) \\ \bar{c}\sum_{i=2}^{3} C_{mi}(\hat{\alpha}^i - \alpha^i) \\ b\sum_{i=2}^{3} C_{ni}(\hat{\beta}^i - \beta^i) \end{bmatrix}$$
$$- \left(g_r(x)\hat{g}_r^{-1}(x_c) - \mathbf{1}_3\right)\left(-\hat{I}^{-1}\hat{I}_M f_{rr}(x_r) - \hat{I}^{-1}\bar{q}S \begin{bmatrix} \sum_{i=1}^{3} b\hat{C}_{\ell i}\hat{\beta}^i \\ \sum_{i=1}^{3} \bar{c}\hat{C}_{mi}\hat{\alpha}^i \\ \sum_{i=1}^{3} b\hat{C}_{ni}\hat{\beta}^i \end{bmatrix} + \nu_2\right) \tag{5.67}$$

It will be shown that implementing the adaptive law (5.65), allows for the closed-loop system to compensate for uncertainty due to modeling errors in the parameters contained in W. Uncertainty due to the inability to directly measure the aerodynamic angles will be handled through the use of a nonlinear observer.

5.4 Nonlinear Observer Design

The observer design process requires the definition of two vectors: the output vector, y, and the observer state vector $\hat{x}$:

$$y \triangleq Cx = \begin{bmatrix} V_T & \Phi^T & x_r^T \end{bmatrix}^T \tag{5.68}$$

$$\hat{x} \triangleq \begin{bmatrix} \hat{V}_T & \hat{\Phi} & \hat{x}_a & \hat{x}_r \end{bmatrix}^T \tag{5.69}$$

where the matrix C is given by

$$C = \begin{bmatrix} 1 & 0 & 0 & 0 \\ 0 & \mathbf{1}_3 & 0 & 0 \\ 0 & 0 & 0 & \mathbf{1}_3 \end{bmatrix} \tag{5.70}$$

The estimation error vector is defined as

$$\tilde{x} \triangleq \hat{x} - x = \begin{bmatrix} \tilde{V}_T & \tilde{\Phi} & \tilde{x}_a & \tilde{x}_r \end{bmatrix}^T \tag{5.71}$$

The design process will proceed as follows: the dynamics will be developed for each observer state ($\dot{\hat{V}}_T$, $\dot{\hat{\Phi}}$, etc.) by approximating the unknown dynamics and then adding an estimation correction term. An expression for the estimation error dynamics of each state ($\dot{\tilde{V}}_T$, $\dot{\tilde{\Phi}}$, etc.) will then be derived. Finally, the entire estimation error dynamics, $\dot{\tilde{x}}$, will be constructed as a vector differential equation.

5.4.1 Total Velocity Observer Design

Recall that the dynamics for total velocity were given by

$$\dot{V}_T = \frac{F_T}{m}\cos(\alpha)\cos(\beta) - \frac{D}{m} + g_1$$

The observer state $\hat{V}_T$ is therefore defined by

$$\dot{\hat{V}}_T = \frac{F_T}{m}\cos(\hat{\alpha})\cos(\hat{\beta}) - \frac{\hat{D}(\hat{\alpha},\hat{\beta})}{m} + \hat{g}_1(\hat{\alpha},\hat{\beta}) + H_{V_T}(y - C\hat{x}) + H_{V_{T1}}(x_c)\tilde{V}_T \tag{5.72}$$

where H_{V_T} is a matrix of constant observer-gains for this state, $H_{V_{T1}}$ is a scalar time-varying observer-gain and

$$\hat{g}_1(\hat{\alpha},\hat{\beta}) = g\left(-\cos(\hat{\alpha})\cos(\hat{\beta})\sin(\hat{\theta}) + \sin(\hat{\beta})sin(\hat{\phi})\cos(\hat{\theta}) + \sin(\hat{\alpha})\cos(\hat{\beta})\cos(\hat{\phi})\cos(\hat{\theta})\right) \tag{5.73}$$

The estimation error for total velocity, $\tilde{V}_T$, has dynamics described by

$$\dot{\tilde{V}}_T = \dot{\hat{V}}_T - \dot{V}_T = -\frac{\bar{q}S}{m}\hat{C}_{D1}\tilde{\alpha} + \eta_{VT} + \delta_V + H_{V_T}(y - C\hat{x}) + H_{V_{T1}}(x_c)\tilde{V}_T \tag{5.74}$$

where,

$$\delta_V = \left(\frac{F_T}{m}\cos(\hat{\alpha})\cos(\hat{\beta}) - \frac{F_T}{m}\cos(\alpha)\cos(\beta)\right) + \frac{\bar{q}S}{m}\left(C_{D0} - \hat{C}_{D0} + \epsilon_D(\beta)\right) + (\hat{g}_1 - g_1) \tag{5.75}$$

$$\eta_{VT} = \frac{\bar{q}S}{m}\left(C_{D1} - \hat{C}_{D1}\right)\alpha + \frac{\bar{q}S}{m}C_{D2}\alpha^2 - \frac{\bar{q}S}{m}\hat{C}_{D2}\hat{\alpha}^2 \tag{5.76}$$

Note that given Assumption 5.2.1, made above, the magnitude of the term δ_V can be bounded by

$$|\delta_V| \leq K_{00} \tag{5.77}$$

where K_{00} is a known constant.

5.4.2 Euler Angle Observer Design

For the Euler angle vector Φ, derivation of the observer dynamics is straightforward,

$$\dot{\Phi} = A_\Phi x_r$$

$$\dot{\hat{\Phi}} = A_\Phi \hat{x}_r + H_\Phi(y - C\hat{x}) \tag{5.78}$$

$$\dot{\tilde{\Phi}} = \dot{\hat{\Phi}} - \dot{\Phi} = A_\Phi \tilde{x}_r + H_\Phi(y - C\hat{x}) \tag{5.79}$$

where H_Φ is a constant observer-gain matrix.

5.4.3 Aerodynamic Angle Observer Design

Recall the aerodynamic angle dynamics

$$\dot{x}_a = \begin{bmatrix} \frac{1}{mV_T}((Y + F_{T_y})\cos\beta + mg_2 - (F_{T_x}\cos\alpha - F_{T_z}\sin\alpha)\sin\beta) \\ \frac{1}{mV_T\cos\beta}(-L + mg_3 - F_{T_x}\sin\alpha + F_{T_z}\cos\alpha) \end{bmatrix} + \begin{bmatrix} \sin\alpha & 0 & -\cos\alpha \\ -\tan\beta\cos\alpha & 1 & -\tan\beta\sin\alpha \end{bmatrix} x_r$$

which can be rewritten as

$$\dot{x}_a = \bar{q}S \begin{bmatrix} \frac{C_{Y1}\cos\beta}{mV_T} & 0 \\ 0 & \frac{-C_{L1}}{mV_T\cos\beta} \end{bmatrix} x_a + f'_a(x) + \begin{bmatrix} \sin\alpha & 0 & -\cos\alpha \\ -\tan\beta\cos\alpha & 1 & -\tan\beta\sin\alpha \end{bmatrix} x_r \quad (5.80)$$

where

$$f'_a(x) = \begin{bmatrix} \frac{1}{mV_T}(((C_{Y0} + \epsilon_Y(\alpha))\bar{q}S + F_{T_y})\cos\beta + mg_2 - (F_{T_x}\cos\alpha - F_{T_z}\sin\alpha)\sin\beta) \\ \frac{1}{mV_T\cos\beta}(-(C_{L0} + \epsilon_L(\beta))\bar{q}S + mg_3 - F_{T_x}\sin\alpha + F_{T_z}\cos\alpha) \end{bmatrix} \quad (5.81)$$

The dynamics of the aerodynamic angle observer are given by

$$\dot{\hat{x}}_a = \bar{q}S \begin{bmatrix} \frac{\hat{C}_{Y1}\cos\hat{\beta}}{mV_T} & 0 \\ 0 & \frac{-\hat{C}_{L1}}{mV_T\cos\hat{\beta}} \end{bmatrix} \hat{x}_a + \hat{f}'_a(x_c) + \begin{bmatrix} \sin\hat{\alpha} & 0 & -\cos\hat{\alpha} \\ -\tan\hat{\beta}\cos\hat{\alpha} & 1 & -\tan\hat{\beta}\sin\hat{\alpha} \end{bmatrix} \hat{x}_r + H_a(y - C\hat{x}) \quad (5.82)$$

where H_a is a constant observer-gain matrix. The estimation error for the aerodynamic angles, $\tilde{x}_a$, has dynamics described by

$$\dot{\tilde{x}}_a = \dot{\hat{x}}_a - \dot{x}_a = \bar{q}S \begin{bmatrix} \frac{\hat{C}_{Y1}\cos\hat{\beta}}{mV_T} & 0 \\ 0 & \frac{-\hat{C}_{L1}}{mV_T\cos\hat{\beta}} \end{bmatrix} \tilde{x}_a + \begin{bmatrix} \sin\hat{\alpha} & 0 & -\cos\hat{\alpha} \\ -\tan\hat{\beta}\cos\hat{\alpha} & 1 & -\tan\hat{\beta}\sin\hat{\alpha} \end{bmatrix} \tilde{x}_r + \delta_a + H_a(y - C\hat{x}) \tag{5.83}$$

where

$$\begin{aligned} \delta_a = \hat{f}'_a(x_c) - f'_a(x) + & \begin{bmatrix} \frac{\hat{C}_{Y1}\cos\hat{\beta} - C_{Y1}\cos\beta}{mV_T}\bar{q}S & 0 \\ 0 & \frac{1}{mV_T}\left(\frac{-\hat{C}_{L1}}{\cos\hat{\beta}} + \frac{C_{L1}}{\cos\beta}\right)\bar{q}S \end{bmatrix} x_a \\ & + \begin{bmatrix} \sin\hat{\alpha} - \sin\alpha & 0 & -\cos\hat{\alpha} + \cos\alpha \\ -\tan\hat{\beta}\cos\hat{\alpha} + \tan\beta\cos\alpha & 0 & -\tan\hat{\beta}\sin\hat{\alpha} + \tan\beta\sin\alpha \end{bmatrix} x_r \end{aligned} \tag{5.84}$$

Note that given Assumptions 5.2.1, 5.2.2 and 5.2.4, the magnitude of the vector δ_a can be bounded by

$$\|\delta_a\| \leq K_{20} + \frac{\bar{q}S}{mV_T}\sqrt{\left(|(d_\beta - 1)C_{L1}| + \Delta\bar{C}_{L1}\right)^2 + \left(|(1 - \frac{1}{d_\beta})C_{Y1}| + \frac{1}{d_\beta}\Delta\bar{C}_{Y1}\right)^2}\|x_a\| + K_{23}\|e_r\| \tag{5.85}$$

where K_{20} and K_{23} are known constants.

5.4.4 Angular Rate Observer Design

By taking a derivative with a respect to time of the expression $x_r = x_{r,m} - e_r$ and substituting in the error dynamics (5.66), the dynamics for the vehicle's angular rates can be expressed as

$$\begin{aligned}\dot{x}_r =& \dot{x}_{r,m} + \widetilde{W}^T b(x_c) - I^{-1}\bar{q}S \begin{bmatrix} b\left(C_{\ell 1}(\hat{\beta}-\beta) - \epsilon_\ell(\alpha)\right) \\ \bar{c}\left(C_{m1}(\hat{\alpha}-\alpha) - \epsilon_m(\beta)\right) \\ b\left(C_{n1}(\hat{\beta}-\beta) - \epsilon_n(\alpha)\right) \end{bmatrix} - \eta_r + e_\Phi + g_r(x)\hat{g}_r^{-1}(x_c)(K_r + K_{r1}(x_c))e_r \\ &+ \left(g_r(x)\hat{g}_r^{-1}(x_c) - \mathbf{1}_3\right)\left(\begin{bmatrix} \frac{b^2}{2V_T}\hat{C}_{\ell p}p \\ \frac{\bar{c}^2}{2V_T}\hat{C}_{mq}q \\ \frac{b^2}{2V_T}\hat{C}_{nr}r \end{bmatrix} - \hat{f}_{r0} - \hat{I}^{-1}\bar{q}S + \dot{x}_{r,m} + e_\Phi + \nu_1 \right)\end{aligned} \tag{5.86}$$

For the observer, the dynamics are approximated by assuming

$$\tilde{x}_a = 0 \qquad g_r(x)\hat{g}_r^{-1}(x_c) = \mathbf{1}_3 \qquad \widetilde{W} = 0$$

and again an estimation correction term is added:

$$\dot{\hat{x}}_r = \dot{x}_{r,m} + (K_r + K_{r1}(x_c))e_r + e_\Phi + H_r(y - C\hat{x}) + H_{r1}(x_c)\tilde{x}_r \tag{5.87}$$

where H_r is a constant observer-gain matrix and $H_{r1}(x_c)$ is a time-varying observer-gain matrix. The estimation error for angular rates, $\tilde{x}_r$, has dynamics described by

$$\begin{aligned}\dot{\tilde{x}}_r = \dot{\hat{x}}_r - \dot{x}_r =& -\widetilde{W}^T b(x_c) + I^{-1}\bar{q}S \begin{bmatrix} bC_{\ell 1} & 0 \\ 0 & \bar{c}C_{m1} \\ bC_{n1} & 0 \end{bmatrix} \tilde{x}_a + \eta_r \\ &+ (\mathbf{1}_3 - g_r(x)\hat{g}_r^{-1}(x_c))K_{r1}(x_c)e_r + \delta_r + H_r(y - C\hat{x}) + H_{r1}(x_c)\tilde{x}_r\end{aligned} \tag{5.88}$$

where

$$\delta_r = I^{-1}\bar{q}S \begin{bmatrix} b\epsilon_\ell(\alpha) \\ \bar{c}\epsilon_m(\beta) \\ b\epsilon_n(\alpha) \end{bmatrix} - \left(g_r(x)\hat{g}_r^{-1}(x_c) - \mathbf{1}_3\right) \left(K_r e_r - \hat{f}_{r0} - \hat{I}^{-1}\bar{q}S \begin{bmatrix} \frac{b^2}{2V_T}\hat{C}_{\ell p}p \\ \frac{\bar{c}^2}{2V_T}\hat{C}_{mq}q \\ \frac{b^2}{2V_T}\hat{C}_{nr}r \end{bmatrix} + \dot{x}_{r,m} + e_\Phi + \nu_1 \right) \tag{5.89}$$

Note that given the Assumptions 5.2.2 and 5.2.3, the norm of the vector δ_r can be bounded by

$$\|\delta_r\| \leq K_{30} + K_{31}\|e_\Phi| + K_{33}\|e_r\| \tag{5.90}$$

where K_{30}, K_{31}, and K_{33} are known constants.

5.4.5 Final Estimation Error Dynamics

Let each of the constant observer-gain matrices, H_i, be written as $H_i = \begin{bmatrix} h_{1i} & h_{2i} & h_{3i} \end{bmatrix}$ for $i = V_T, \Phi, a, r$ such that

$$H_i(y - Cx) = h_{1i}\tilde{V}_T + h_{2i}\tilde{\Phi} + h_{3i}\tilde{x}_r \tag{5.91}$$

Combining Equations (5.74), (5.79),(5.83), and (5.88) allows for the full observer error dynamics to be expressed in vector matrix form,

$$\begin{bmatrix} \dot{\tilde{V}}_T \\ \dot{\tilde{\Phi}} \\ \dot{\tilde{x}}_a \\ \dot{\tilde{x}}_r \end{bmatrix} = \begin{bmatrix} -h_{1V_T} & -h_{2V_T} & H_O(1,3) & -h_{3V_T} \\ -h_{1\Phi} & -h_{2\Phi} & 0 & A_\Phi - h_{3\Phi} \\ -h_{1a} & -h_{2a} & H_O(3,3) & H_O(3,4) - h_{3a} \\ -h_{1r} & -h_{2r} & H_O(4,3) & -h_{3r} \end{bmatrix} \begin{bmatrix} \tilde{V}_T \\ \tilde{\Phi} \\ \tilde{x}_a \\ \tilde{x}_r \end{bmatrix}$$
$$+ \begin{bmatrix} 0 \\ 0 \\ 0 \\ -\widetilde{W}^T b(x_c) + (\mathbf{1}_3 - g_r(x)\hat{g}_r^{-1}(x_c))K_{r1}(x_c)e_r \end{bmatrix} + \begin{bmatrix} \delta_V \\ 0 \\ \delta_a \\ \delta_r \end{bmatrix} + \begin{bmatrix} \eta_{VT} + H_{V_{T1}}(x_c)\tilde{V}_T \\ 0 \\ 0 \\ \eta_r + H_{r1}(x_c)\tilde{x}_r \end{bmatrix} \tag{5.92}$$

where

$$H_O(1,3) = \frac{\bar{q}S}{m}\begin{bmatrix} 0 & -\hat{C}_{D1} \end{bmatrix} \qquad H_O(3,3) = \frac{\bar{q}S}{mV_T}\begin{bmatrix} \hat{C}_{Y1}\cos\hat{\beta} & 0 \\ 0 & \frac{-\hat{C}_{L1}}{\cos\hat{\beta}} \end{bmatrix}$$

$$H_O(3,4) = \begin{bmatrix} \sin\hat{\alpha} & 0 & -\cos\hat{\alpha} \\ -\tan\hat{\beta}\cos\hat{\alpha} & 1 & -\tan\hat{\beta}\sin\hat{\alpha} \end{bmatrix} \qquad H_O(4,3) = I^{-1}\bar{q}S\begin{bmatrix} bC_{\ell 1} & 0 \\ 0 & \bar{c}C_{m1} \\ bC_{n1} & 0 \end{bmatrix}$$

Equation (5.92) can be written more compactly as,

$$\dot{\tilde{x}} = H_O\tilde{x} + \left[-\widetilde{W}^T b(x_c) + (\mathbf{1}_3 - g_r(x)\hat{g}_r^{-1}(x_c))K_{r1}(x_c)e_r\right]_4 + \delta + \eta \tag{5.93}$$

By checking the principal minors of the matrix H_O, it can be shown that given Assumption 5.2.1 the constant observer-gain matrices can always be chosen such that

$$H_O + H_O^T < -Q \tag{5.94}$$

for some constant matrix $Q = Q^T > 0$. In addition, note that the norm of the vector δ can be bounded by

$$\|\delta\| \leq \|K_0\| + K_{31}\|e_\Phi\| + K_2\|x_a\| + \|K_3\|\|e_r\| \tag{5.95}$$

where

$$K_0 = \begin{bmatrix} K_{00} & K_{01} & K_{02} \end{bmatrix}^T \tag{5.96}$$

$$K_2 = \frac{\bar{q}S}{mV_T}\sqrt{\left(|(d_\beta - 1)C_{L1}| + \Delta\bar{C}_{L1}\right)^2 + \left(|(1 - \frac{1}{d_\beta})C_{Y1}| + \frac{1}{d_\beta}\Delta\bar{C}_{Y1}\right)^2} \tag{5.97}$$

$$K_3 = \begin{bmatrix} K_{23} & K_{33} \end{bmatrix}^T \tag{5.98}$$

5.5 Stability Analysis

In this section a stability analysis of the closed-loop system, using the control algorithm and observer discussed in the previous sections, will be presented.

Lemma 5.5.1. *Consider the aerodynamic angle dynamics given in Equation (1.32). Using only known parameters and measured signals, the time-varying set $\Omega_a(t)$ can be calculated such that*

$$x_a(t) \in \Omega_a(t) \quad \forall t > 0 \tag{5.99}$$

where

$$\Omega_a(t) \triangleq [-\mathbb{X}_a(t), \mathbb{X}_a(t)] \tag{5.100}$$

and where $\mathbb{X}_a$ evolves according to

$$\dot{\mathbb{X}}_a = A_{a,max}\mathbb{X}_a(t) + v_{a,max}(t) \tag{5.101}$$

$$\mathbb{X}_a(0) = |\hat{x}_a(0)| + \tilde{x}_{a,max} \tag{5.102}$$

The constant matrix $A_{a,max}$ and the time-varying vector $v_{a,max}(t)$ are defined as

$$A_{a,max} = \frac{\bar{q}(V_{T,min})S}{mV_{T,min}} \begin{bmatrix} -\frac{1}{d_\beta}|\hat{C}_{Y1} + \Delta\bar{C}_{Y1}| & 0 \\ 0 & -|\hat{C}_{L1} - \Delta\bar{C}_{L1}| \end{bmatrix} \tag{5.103}$$

$$v_{a,max}(t) = \bar{f}'_a(x) + \begin{bmatrix} 1 & 0 & 1 \\ \sqrt{d_\beta^2 - 1} & 1 & \sqrt{d_\beta^2 - 1} \end{bmatrix} |x_r| \tag{5.104}$$

$$\bar{f}'_a(x) = \begin{bmatrix} \frac{1}{mV_T}\left(\bar{q}S|\hat{C}_{Y0} + \Delta\bar{C}_{Y0}\text{sign}(\hat{C}_{Y0}) + \bar{\epsilon}_Y| + mg + \|F_T\|\right) \\ \frac{d_\beta}{mV_T}\left(\bar{q}S|\hat{C}_{L0} + \Delta\bar{C}_{L0}\text{sign}(\hat{C}_{L0}) + \bar{\epsilon}_L| + mg + \|F_T\|\right) \end{bmatrix} \tag{5.105}$$

Proof. Recall Equation (5.80) which can be rewritten as

$$\dot{x}_a = A_a(t)x_a(t) + v_a(t) \tag{5.106}$$

where

$$A_a(t) = \frac{\bar{q}S}{mV_T} \begin{bmatrix} C_{Y1}\cos\beta & 0 \\ 0 & -\frac{C_{L1}}{\cos\beta} \end{bmatrix} \tag{5.107}$$

$$v_a(t) = f'_a(x) + \begin{bmatrix} \sin\alpha & 0 & -\cos\alpha \\ -\tan\beta\cos\alpha & 1 & -\tan\beta\sin\alpha \end{bmatrix} x_r \tag{5.108}$$

Given that Equation (5.106) is a first-order linear differential equation, an expression for $x_a(t)$ can be solved for explicitly as

$$x_a(t) = e^{\int_{t_0}^t A_a(\tau)d\tau}x_a(0) + \int_0^t e^{\int_\tau^t A_a(\tau')d\tau'}v_a(\tau)d\tau \tag{5.109}$$

Equation (5.109) implies that the following inequality holds,

$$-e^{A_{a,max}t}\mathbb{X}_a(0) - \int_0^t e^{A_{a,max}(t-\tau)}v_{a,max}(\tau)d\tau \leq x_a(t) \leq e^{A_{a,max}t}\mathbb{X}_a(0) + \int_0^t e^{A_{a,max}(t-\tau)}v_{a,max}(\tau)d\tau \quad (5.110)$$

where for two vectors $a, b \in \mathbb{R}^p$, the expression $a \leq b$ signifies $a_1 < b_1$, $a_2 < b_2 ... a_p < b_p$. The previous inequality is equivalent to

$$-\mathbb{X}_a \leq x_a(t) \leq \mathbb{X}_a \quad (5.111)$$

□

Remark 5.5.1. If Assumption 5.2.1 holds, the constant matrix $A_{a,max}$ is Hurwitz. Therefore, Equation (5.101) implies that $\mathbb{X}_a$ is bounded if and only if $v_{a,max}$ is bounded. Since each element of $f'_a(x)$ is bounded, the definition of $v_{a,max}$, Equation (5.104), implies that $v_{a,max}$ is bounded if and only if x_r is bounded.

Remark 5.5.2. If it can be shown that the set $\Omega_a(t)$ is uniformly ultimately bounded, as will be done in Theorem 7, then any signal designed using this set to stabilize the system will be UUB as well.

Theorem 7. *Consider the nonlinear dynamical GHV system described by (1.43), the desired angular rate command calculated by (5.34), the control law defined by (5.41), the adaptive law defined by (5.65) and the nonlinear observer designed in Section 5.4. Suppose that the desired attitude angle trajectory, Φ_d^*, is bounded and continuous. If the following inequalities,*

$$\Delta\bar{C}_{L1} < C_* \sqrt{\left(\frac{\lambda_{min}(Q)}{8}\right)\left(\frac{mV_T}{\bar{q}S}\right)} - |(d_\beta - 1)C_{L1}| \quad (5.112)$$

$$\Delta\bar{C}_{Y1} < d_\beta C_* \sqrt{\left(\frac{\lambda_{min}(Q)}{8}\right)\left(\frac{mV_T}{\bar{q}S}\right)} - |(d_\beta - 1)C_{Y1}| \tag{5.113}$$

$$C_* = \sqrt{\min(|\frac{C_{Y1}}{d_\beta}|, |C_{L1}|)} \tag{5.114}$$

are satisfied for all $t > 0$, then the tracking errors, e_r and e_Φ, the estimation error $\tilde{x}$, the weight estimation error $\widetilde{W}$ and the system states, x, are UUB.

Proof. In order to analyze the stability of the system and to show that all of the closed-loop signals are UUB the following candidate Lyapunov function is chosen,

$$V = \tilde{x}^T\tilde{x} + \frac{1}{2}\left(e_r^T e_r + e_\Phi^T e_\Phi + x_a^T x_a + tr(\widetilde{W}^T\Gamma_W^{-1}\widetilde{W})\right) \tag{5.115}$$

Taking the derivative with respect to time along system trajectories leaves,

$$\dot{V} = \tilde{x}^T\dot{\tilde{x}} + \dot{\tilde{x}}^T\tilde{x} + e_r^T\dot{e}_r + e_\Phi^T\dot{e}_\Phi + x_a^T\dot{x}_a + tr(\widetilde{W}^T\Gamma_W^{-1}\dot{\widehat{W}}) \tag{5.116}$$

Substituting (5.66) and (5.93) into (5.116) and applying the trace identity $a^Tb = tr(ba^T)$ results in

$$\begin{aligned}
\dot{V} =& \tilde{x}^T H_O\tilde{x} + \tilde{x}^T H_O^T\tilde{x} + 2\tilde{x}^T\delta + 2\tilde{x}_r^T\left((\mathbf{1}_3 - g_r(x)\hat{g}_r^{-1}(x_c))K_{r1}(x_c)e_r\right) + 2\tilde{x}^T\eta + e_\Phi^T\dot{e}_\Phi \\
&+ x_a^T\dot{x}_a + e_r^T\Bigg(I^{-1}\bar{q}S\begin{bmatrix} bC_{\ell 1}(\hat{\beta}-\beta) \\ \bar{c}C_{m1}(\hat{\alpha}-\alpha) \\ bC_{n1}(\hat{\beta}-\beta)\end{bmatrix} + \eta_r - e_\Phi - g_r(x)\hat{g}_r^{-1}(x_c)(K_r + K_{r1}(x_c))e_r \\
&- \left(g_r(x)\hat{g}_r^{-1}(x_c) - \mathbf{1}_3\right)\left(-\hat{f}_{r0} - \hat{I}^{-1}\bar{q}S\begin{bmatrix} \frac{b^2}{2V_T}\hat{C}_{\ell p}p \\ \frac{\bar{c}^2}{2V_T}\hat{C}_{mq}q \\ \frac{b^2}{2V_T}\hat{C}_{nr}r\end{bmatrix} + \dot{x}_{r,m} + e_\Phi + \nu_1\right)\Bigg) \\
&+ tr\left(\widetilde{W}^T\left(\Gamma_W^{-1}\dot{\widehat{W}} - b(x_c)(e_r^T + 2\tilde{x}_r^T)\right)\right)
\end{aligned} \tag{5.117}$$

Next, application of the adaptive law given in (5.65) and the Lyapunov condition given in (5.94) leaves

$$\begin{aligned}\dot{V} \leq & -\tilde{x}^T Q\tilde{x} + 2\tilde{x}^T\delta + 2\tilde{x}_r^T\left((\mathbf{1}_3 - g_r(x)\hat{g}_r^{-1}(x_c))K_{r1}(x_c)e_r\right) + 2\tilde{x}^T\eta + e_\Phi^T\dot{e}_\Phi \\ & + x_a^T\dot{x}_a + e_r^T\Bigg(I^{-1}\bar{q}S\begin{bmatrix} bC_{\ell 1}(\hat{\beta}-\beta) \\ \bar{c}C_{m1}(\hat{\alpha}-\alpha) \\ bC_{n1}(\hat{\beta}-\beta)\end{bmatrix} + \eta_r - e_\Phi - g_r(x)\hat{g}_r^{-1}(x_c)(K_r + K_{r1}(x_c))e_r \\ & - \left(g_r(x)\hat{g}_r^{-1}(x_c) - \mathbf{1}_3\right)\left(-\hat{f}_{r0} - \hat{I}^{-1}\bar{q}S\begin{bmatrix} \frac{b^2}{2V_T}\hat{C}_{\ell p}p \\ \frac{\bar{c}^2}{2V_T}\hat{C}_{mq}q \\ \frac{b^2}{2V_T}\hat{C}_{nr}r\end{bmatrix} + \dot{x}_{r,m} + e_\Phi + \nu_1\right)\Bigg)\end{aligned} \tag{5.118}$$

In order to define the time-varying observer and feedback gains, the following terms are examined,

$$\begin{aligned}& 2\tilde{x}^T\eta + 2\tilde{x}_r^T(\mathbf{1}_3 - g_r(x)\hat{g}_r^{-1}(x_c))K_{r1}(x_c)e_r - e_r^T g_r(x)\hat{g}_r^{-1}(x_c)K_{r1}(x_c)e_r + e_r^T\eta_r = \\ & 2\tilde{V}_T\left(\eta_{VT} + H_{VT1}(x_c)\tilde{V}_T\right) + 2\tilde{x}_r^T\left(\eta_r + H_{r1}(x_c)\tilde{x}_r\right) + 2\tilde{x}_r^T(\mathbf{1}_3 - g_r(x)\hat{g}_r^{-1}(x_c))K_{r1}(x_c)e_r \\ & - e_r^T g_r(x)\hat{g}_r^{-1}(x_c)K_{r1}(x_c)e_r + e_r^T\eta_r\end{aligned} \tag{5.119}$$

where η_r and η_{VT} are defined in Equations (5.67) and (5.76) respectively. Using these definitions, the following inequalities can be set,

$$\eta_{VT}(t) \leq \bar{\eta}_{VT}(t) \triangleq \frac{\bar{q}S}{m}\left(\Delta\bar{C}_{D1}\mathbb{X}_a(2) + (\hat{C}_{D2} + \Delta\bar{C}_{D2})\mathbb{X}_a^2(2) - \hat{C}_{D2}\hat{\alpha}^2\right) \tag{5.120}$$

$$\eta_r(t) \leq \bar{\eta}_r(t) \triangleq (\hat{I} - \Delta\bar{I})^{-1}\bar{q}S \begin{bmatrix} \sum_{i=2}^{3} b(|\hat{C}_{\ell i} + \Delta\bar{C}_{\ell i}\text{sign}(\hat{C}_{\ell i})|)(|\hat{\beta}^i + \mathbb{X}_a(1)^i|) \\ \sum_{i=2}^{3} \bar{c}(|\hat{C}_{mi} + \Delta\bar{C}_{mi}\text{sign}(\hat{C}_{mi})|)(|\hat{\alpha}^i + \mathbb{X}_a(2)^i|) \\ \sum_{i=2}^{3} b(|\hat{C}_{ni} + \Delta\bar{C}_{ni}\text{sign}(\hat{C}_{ni})|)(|\hat{\beta}^i + \mathbb{X}_a(1)^i|) \end{bmatrix}$$
$$+ \Delta\bar{g}_r \left| -\hat{I}\hat{I}_M f_{rr}(x_r) - \hat{I}^{-1}\bar{q}S \begin{bmatrix} \sum_{i=1}^{3} b\hat{C}_{\ell i}\hat{\beta}^i \\ \sum_{i=1}^{3} \bar{c}\hat{C}_{mi}\hat{\alpha}^i \\ \sum_{i=1}^{3} b\hat{C}_{ni}\hat{\beta}^i \end{bmatrix} + \nu_2 \right| \quad (5.121)$$

where $\mathbb{X}_a(j)$ is the j^{th} element of $\mathbb{X}_a$ and where $\Delta\bar{I}$ is given by

$$\Delta\bar{I} = \begin{bmatrix} \Delta\bar{I}_x & 0 & \Delta\bar{I}_{xz} \\ 0 & \Delta\bar{I}_y & 0 \\ \Delta\bar{I}_{xz} & 0 & \Delta\bar{I}_z \end{bmatrix}$$

Note that all of the terms that make up $\bar{\eta}_{VT}(t)$ and $\bar{\eta}_r(t)$ are known. Equation (5.119) can be rearranged as

$$\begin{aligned} &2\tilde{x}^T\eta + 2\tilde{x}_r^T(\mathbf{1}_3 - g_r(x)\hat{g}_r^{-1}(x_c))K_{r1}(x_c)e_r - e_r^T g_r(x)\hat{g}_r^{-1}(x_c)K_{r1}(x_c)e_r + e_r^T\eta_r = \\ &2\tilde{V}_T\left(\eta_{VT} + H_{VT1}(x_c)\tilde{V}_T\right) + \begin{bmatrix} 2\eta_r^T & \eta_r^T \end{bmatrix}\begin{bmatrix} \tilde{x}_r \\ e_r \end{bmatrix} \\ &+ \begin{bmatrix} \tilde{x}_r^T & e_r^T \end{bmatrix}\begin{bmatrix} 2H_{r1}(x_c) & (\mathbf{1}_3 - g_r(x)\hat{g}_r^{-1}(x_c))K_{r1}(x_c) \\ ((\mathbf{1}_3 - g_r(x)\hat{g}_r^{-1}(x_c))K_{r1}(x_c))^T & -g_r(x)\hat{g}_r^{-1}(x_c))K_{r1}(x_c) \end{bmatrix}\begin{bmatrix} \tilde{x}_r \\ e_r \end{bmatrix} \end{aligned} \quad (5.122)$$

If the time-varying gains are defined as

$$H_{VT1}(x_c) = -\gamma \bar{\eta}_{VT}^2(t) \tag{5.123}$$

$$H_{r1}(x_c) = -\frac{5}{2}\gamma \bar{\eta}_r^T(t)\bar{\eta}_r(t)\mathbf{1}_3 \tag{5.124}$$

$$K_{r1}(x_c) = 5\gamma \bar{\eta}_r^T(t)\bar{\eta}_r(t)\mathbf{1}_3 \tag{5.125}$$

where $\gamma > 0$ is a designer chosen constant scalar, then, according to Assumption 5.2.3, the following bound holds,

$$\begin{aligned} 2\tilde{x}^T\eta + 2\tilde{x}_r^T(\mathbf{1}_3 - g_r(x)\hat{g}_r^{-1}(x_c))K_{r1}(x_c)e_r - e_r^T g_r(x)\hat{g}_r^{-1}(x_c)K_{r1}(x_c)e_r + e_r^T\eta_r \leq \\ 2\left(\bar{\eta}_{VT}(t)|\tilde{V}_T| - \gamma\bar{\eta}_{VT}^2(t)|\tilde{V}_T|^2\right) + \sqrt{5}\|\bar{\eta}_r\|\left\|\begin{matrix}\tilde{x}_r \\ e_r\end{matrix}\right\| - 5\gamma\Delta\bar{g}_{rL}\|\bar{\eta}_r\|^2\left\|\begin{matrix}\tilde{x}_r \\ e_r\end{matrix}\right\|^2 \end{aligned} \tag{5.126}$$

Noting that for any scalar c and any positive scalar $d > 0$, the inequality $c - dc^2 \leq 1/4d$ holds, it can be concluded that

$$2\tilde{x}^T\eta + 2\tilde{x}_r^T(\mathbf{1}_3 - g_r(x)\hat{g}_r^{-1}(x_c))K_{r1}(x_c)e_r - e_r^T g_r(x)\hat{g}_r^{-1}(x_c)K_{r1}(x_c)e_r + e_r^T\eta_r \leq \frac{1}{\gamma}\left(\frac{1}{2} + \frac{1}{4\Delta\bar{g}_{rL}}\right) \tag{5.127}$$

Incorporating the inequality (5.127) and defining γ^* as

$$\gamma^* \triangleq \frac{1}{\gamma}\left(\frac{1}{2} + \frac{1}{4\Delta\bar{g}_{rL}}\right)$$

results in

$$\dot{V} \leq -\tilde{x}^T Q\tilde{x} + 2\tilde{x}^T\delta + \gamma^* + e_\Phi^T\dot{e}_\Phi + x_a^T\dot{x}_a + e_r^T\Big(I^{-1}\bar{q}S\begin{bmatrix} bC_{\ell 1}(\hat{\beta}-\beta) \\ \bar{c}C_{m1}(\hat{\alpha}-\alpha) \\ bC_{n1}(\hat{\beta}-\beta)\end{bmatrix} - e_\Phi - g_r(x)\hat{g}_r^{-1}(x_c)K_r e_r$$
$$- \left(g_r(x)\hat{g}_r^{-1}(x_c) - \mathbf{1}_3\right)\left(-\hat{f}_{r0} - \hat{I}^{-1}\bar{q}S\begin{bmatrix} \frac{b^2}{2V_T}\hat{C}_{\ell p}p \\ \frac{\bar{c}^2}{2V_T}\hat{C}_{mq}q \\ \frac{b^2}{2V_T}\hat{C}_{nr}r\end{bmatrix} + \dot{x}_{r,m} + e_\Phi + \nu_1\right)\Big) \tag{5.128}$$

Using the bound established in (5.95), a bound can be placed on the term $2\tilde{x}^T\delta$ in the following manner,

$$2\tilde{x}^T\delta \leq 2\left(\|K_0\| + K_{31}\|e_\Phi\| + K_2\|x_a\| + \|K_3\|\|e_r\|\right)\|\tilde{x}\| \tag{5.129}$$

The term $x_a^T\dot{x}_a$ can similarly be bounded in terms of $\|x_a\|$ and the error signals of interest,

$$x_a^T\dot{x}_a = x_a^T A_a x_a + x_a^T f_a'(x) + x_a^T\begin{bmatrix} \sin\alpha & 0 & -\cos\alpha \\ -\tan\beta\cos\alpha & 1 & -\tan\beta\sin\alpha\end{bmatrix}x_r \tag{5.130}$$

$$x_a^T\dot{x}_a \leq \lambda_{max}(A_a)\|x_a\|^2 + \|x_a\|\left(\|f_a'(x)\|_{max} + \sqrt{2+2d_\beta^2}\|e_r\| + \sqrt{2+2d_\beta^2}\|x_{r,m}\|\right) \tag{5.131}$$

where according to Assumptions 5.2.1, 5.2.2, and 5.2.4 the constant $\|f_a'(x)\|_{max}$ is known. Finally a bound in the form of (5.129) and (5.131) can be found for the following terms, which for the sake

of brevity will be referred to as $e_r^T\xi$,

$$\begin{aligned} e_r^T\xi =& e_r^T\Bigg(I^{-1}\bar{q}S\begin{bmatrix} bC_{\ell 1}(\hat{\beta}-\beta) \\ \bar{c}C_{m1}(\hat{\alpha}-\alpha) \\ bC_{n1}(\hat{\beta}-\beta) \end{bmatrix} - e_\Phi - g_r(x)\hat{g}_r^{-1}(x_c)K_re_r \\ &- \left(g_r(x)\hat{g}_r^{-1}(x_c)-\mathbf{1}_3\right)\left(-\hat{f}_{r0}-\hat{I}^{-1}\bar{q}S\begin{bmatrix} \frac{b^2}{2V_T}\hat{C}_{\ell p}p \\ \frac{\bar{c}^2}{2V_T}\hat{C}_{mq}q \\ \frac{b^2}{2V_T}\hat{C}_{nr}r \end{bmatrix} + \dot{x}_{r,m} + e_\Phi + \nu_1\right)\Bigg) \end{aligned} \tag{5.132}$$

If K_r is structured in the form $K_r = k_r\mathbf{1}_3$ where $k_r > 0$ is a scalar, then the following bound holds

$$\begin{aligned} e_r^T\xi \leq& -k_r\Delta\bar{g}_{rL}\|e_r\|^2 + \|e_r\|\left(I^{-1}\bar{q}(V_{T,max})S\left\|\begin{matrix} bC_{\ell 1} \\ \bar{c}C_{m1} \\ bC_{n1}\end{matrix}\right\|\|\tilde{x}\|\right) + \|e_r\|\|e_\Phi\| \\ &+ \sqrt{3}\Delta\bar{g}_r\|e_r\|\Bigg(\|\hat{f}_{r0}\|_{max} + \frac{\bar{q}(V_{T,max})S}{2V_{T,max}}\hat{I}^{-1}\left\|\begin{matrix} b^2\hat{C}_{\ell p} \\ \bar{c}^2\hat{C}_{mq} \\ b^2\hat{C}_{nr}\end{matrix}\right\|(\|e_r\| + \|x_{r,m}\|) \\ &+ \|\dot{x}_{r,m}\| + \|e_\Phi\| + \widehat{W}_{max}\left(M_{T,max} + \bar{q}(V_{T,max})S + \frac{\bar{q}(V_{T,max})S}{2V_{T,max}}(\|e_r\| + \|x_{r,m}\|)\right)\Bigg) \end{aligned} \tag{5.133}$$

where $\widehat{W}_{max}$ is a positive bound determined by the projection operator and where, according to Assumption 5.2.1, $\|\hat{f}_{r0}\|_{max}$ is a known constant. With the above bounds in place, (5.128) can be

rewritten compactly as

$$\begin{aligned}\dot{V} \leq & -\frac{1}{2}\lambda_{min}(Q)\|\tilde{x}\|^2 + \gamma^* - \frac{1}{2}\lambda_{min}(K_\Phi)\|e_\Phi\|^2 - \frac{1}{2}k_r\Delta\bar{g}_{rL}\|e_r\|^2 \\ & + \frac{1}{2}\lambda_{max}(A_a)\|x_a\|^2 + \zeta(\|\tilde{x}\|, \|x_a\|, \|e_r\|, \|e_\Phi\|)\end{aligned} \tag{5.134}$$

where $\zeta(\|\tilde{x}\|, \|x_a\|, \|e_r\|, \|e_\Phi\|)$ is defined by,

$$\zeta(\|\tilde{x}\|, \|x_a\|, \|e_r\|, \|e_\Phi\|) = \begin{bmatrix}\|\tilde{x}\| \\ \|x_a\| \\ \|e_r\| \\ \|e_\Phi\|\end{bmatrix}^T \begin{bmatrix} m_{11} & m_{12} & m_{13} & m_{14} \\ m_{12} & m_{22} & m_{23} & 0 \\ m_{13} & m_{23} & m_{33} & m_{34} \\ m_{14} & 0 & m_{34} & m_{44}\end{bmatrix} \begin{bmatrix}\|\tilde{x}\| \\ \|x_a\| \\ \|e_r\| \\ \|e_\Phi\|\end{bmatrix} + 2\begin{bmatrix}\|\tilde{x}\| \\ \|x_a\| \\ \|e_r\| \\ \|e_\Phi\|\end{bmatrix}^T \begin{bmatrix} b_1 \\ b_2 \\ b_3 \\ b_4\end{bmatrix} \tag{5.135}$$

$$\zeta(\|\tilde{x}\|, \|x_a\|, \|e_r\|, \|e_\Phi\|) = v^T M_\zeta v + 2v^T b_\zeta \tag{5.136}$$

and where $M_\zeta = M_\zeta^T$. The matrix entries m_{ij} and vector entries b_k are given in Appendix C.

Since the vector b_ζ is bounded, the function $\zeta(\|\tilde{x}\|, \|x_a\|, \|e_r\|, \|e_\Phi\|)$ has a unique global maximum if and only if the matrix M_ζ is strictly negative definite, which can be tested for by checking if its four principal minors alternate sign. The first principal minor must be negative. This is equivalent to

$$M_{\zeta,1} = m_{11} = -\frac{1}{2}\lambda_{min}(Q) < 0 \tag{5.137}$$

which by definition of Q is always satisfied.

The second principal minor must be positive. This is equivalent to

$$M_{\zeta,2} = m_{11}m_{22} - m_{12}^2 > 0 \tag{5.138}$$

$$\left(-\frac{1}{2}\lambda_{min}(Q)\right)\left(\frac{1}{2}\lambda_{max}(A_a)\right) - K_2^2 > 0 \tag{5.139}$$

If the conditions given by (5.112) and (5.113) hold, the second principal minor will always be positive. Note that these conditions are conservative, i.e. there exist larger values of $\Delta\bar{C}_{L1}$ and $\Delta\bar{C}_{Y1}$ (which lack a neat analytical form) for which (5.112) and (5.113) will be satisfied. From here, it is straightforward to show that the designer chosen gains k_r and K_Φ can always be chosen such that the third and fourth principal minors have the appropriate sign as long as (5.112) and (5.113) hold. Therefore, (5.134) can be rewritten as

$$\begin{aligned}\dot{V} \leq & -\frac{1}{2}\lambda_{min}(Q)\|\tilde{x}\|^2 + \gamma^* - \frac{1}{2}\lambda_{min}(K_\Phi)\|e_\Phi\|^2 - \frac{1}{2}k_r\Delta\bar{g}_{rL}\|e_r\|^2 \\ & + \frac{1}{2}\lambda_{max}(A_a)\|x_a\|^2 + |\zeta|_{max}\end{aligned} \tag{5.140}$$

where $|\zeta|_{max}$ is the unique global maximum of the function ζ. This implies that $\dot{V} < 0$ outside of the compact set S_{GHV} where

$$\begin{aligned}S_{GHV}(\tilde{x}, x_a, e_r, e_\Phi, \widetilde{W}) = & \left\{(\tilde{x}, x_a, e_r, e_\Phi, \widetilde{W}) : \|\tilde{x}\|^2 \leq \frac{2\left(|\zeta|_{max} + \gamma^*\right)}{\lambda_{min}(Q)}\right\} \\ & \bigcap \left\{(\tilde{x}, x_a, e_r, e_\Phi, \widetilde{W}) : \|x_a\|^2 \leq \frac{2\left(|\zeta|_{max} + \gamma^*\right)}{\lambda_{max}(A_a)}\right\} \\ & \bigcap \left\{(\tilde{x}, x_a, e_r, e_\Phi, \widetilde{W}) : \|e_r\|^2 \leq \frac{2\left(|\zeta|_{max} + \gamma^*\right)}{\Delta\bar{g}_r k_r}\right\} \\ & \bigcap \left\{(\tilde{x}, x_a, e_r, e_\Phi, \widetilde{W}) : \|e_\Phi\|^2 \leq \frac{2\left(|\zeta|_{max} + \gamma^*\right)}{\lambda_{min}(K_\Phi)}\right\} \\ & \bigcap \left\{(\tilde{x}, x_a, e_r, e_\Phi, \widetilde{W}) : \|\widetilde{W}\| \leq \|\widetilde{W}\|_{max}\right\}\end{aligned}$$

where $\|\widetilde{W}\|_{max}$ depends on the bound set by the projection operator. The Lyapnuov function V cannot grow outside of this set. This implies that $\tilde{x}, x_a, e_r, e_\Phi, \widetilde{W}$ are UUB and therefore so is the state vector x. The fact that $\tilde{x}$ and x_a are bounded implies that $\hat{x}_a$ is bounded as well. This implies that the set $\Omega_a(t)$ and therefore, the time-varying observer and controller gains H_{VT1}, H_{r1}, and K_{r1} are also bounded. Thus, all closed-loop signals are proven to be UUB. □

5.6 Simulation Setup and Results

The NDI adaptive control architecture and nonlinear observer were implemented in the GHV simulation and two example trajectories were explored. There were several objectives to the simulation testing. The first goal was to track a commanded Euler angle trajectory, Φ_d^*. The second goal was to accurately estimate angle-of-attack and sideslip angle using the nonlinear observer designed in Section 5.4. The third and final goal was to avoid the common problems associated with high gain observers: the peaking phenomenon and large noise amplification.

The first trajectory tested was a $15\,\mathrm{deg}$ roll angle ramp command and hold, followed by a return to level flight, followed by a $5\,\mathrm{deg}$ pitch angle ramp command and hold, followed finally by a return to level flight. The second trajectory tested was a more aggressive roll angle command: a $60\,\mathrm{deg}$ ramp command and hold followed by a return to level flight. All of the velocity level measurement signals needed to drive the nonlinear observer (the body-axis angular rate and total velocity measurements) were corrupted by noise. For both trajectories tested a low measurement noise case and a high measurement noise case were examined. The low noise case was associated with zero mean white noise and a standard deviation of $7.07 ft/s$ and $0.1\,\mathrm{deg}/s$, for total velocity and the body-axis angular rates respectively while the high noise case was associated with zero mean white noise and a standard deviation of $10 ft/s$ and $0.5\,\mathrm{deg}/s$, for total velocity and the body-axis angular rates respectively.

The observer-gains were selected such that the matrix H_O remains Hurwitz for the entire simulation as required. These gain values can be found in Appendix D. The bounded uncertainties described in Assumption 5.2.2 are given in Table 5.1. Except for the moment of inertia bounds, each uncertainty value listed is at least 20% of the magnitude of the assumed value of the parameters it is associated with, that is $|\Delta\bar{C}_X| \geq 0.2|\hat{C}_X| \; \forall X$. The bounded uncertainties defined in

Table 5.1: Aerodynamic Parameter Uncertainty Bounds

$$\begin{bmatrix}\Delta\bar{C}_{L0} & \Delta\bar{C}_{L1}\end{bmatrix} = \begin{bmatrix}0.005 & 0.22\end{bmatrix}$$

$$\begin{bmatrix}\Delta\bar{C}_{Y0} & \Delta\bar{C}_{Y1}\end{bmatrix} = \begin{bmatrix}0.0001 & 0.06\end{bmatrix}$$

$$\begin{bmatrix}\Delta\bar{C}_{D0} & \Delta\bar{C}_{D1} & \Delta\bar{C}_{D2}\end{bmatrix} = \begin{bmatrix}0.002 & 0.006 & 0.02\end{bmatrix}$$

$$\begin{bmatrix}\Delta\bar{C}_{\ell 0} & \Delta\bar{C}_{m0} & \Delta\bar{C}_{n0}\end{bmatrix} = \begin{bmatrix}1e-6 & 2e-4 & 1e-6\end{bmatrix}$$

$$\begin{bmatrix}\Delta\bar{C}_{\ell 1} & \Delta\bar{C}_{\ell 2} & \Delta\bar{C}_{\ell 3}\end{bmatrix} = \begin{bmatrix}0.004 & 1e-6 & 1e-6\end{bmatrix}$$

$$\begin{bmatrix}\Delta\bar{C}_{m1} & \Delta\bar{C}_{m2} & \Delta\bar{C}_{m3}\end{bmatrix} = \begin{bmatrix}0.005 & 0.005 & 0.05\end{bmatrix}$$

$$\begin{bmatrix}\Delta\bar{C}_{n1} & \Delta\bar{C}_{n2} & \Delta\bar{C}_{n3}\end{bmatrix} = \begin{bmatrix}0.01 & 1e-6 & 1e-6\end{bmatrix}$$

$$\begin{bmatrix}\Delta\bar{C}_{\ell_p} & \Delta\bar{C}_{m_q} & \Delta\bar{C}_{n_r}\end{bmatrix} = \begin{bmatrix}0.018 & 0.018 & 0.096\end{bmatrix}$$

$$\begin{bmatrix}\Delta\bar{I}_x & \Delta\bar{I}_y & \Delta\bar{I}_z & \Delta\bar{I}_{xz}\end{bmatrix} = \begin{bmatrix}5 & 20 & 20 & 10\end{bmatrix} \text{ lbm ft}^2$$

$$\Delta\bar{C}_{m,\delta} = .018$$

Assumption 5.2.3 and Assumption 5.2.4 are

$$\bar{\Delta} g_r = 0.2 \tag{5.141}$$

$$d_\Theta = 1.4 \tag{5.142}$$

$$d_\beta = 1.2 \tag{5.143}$$

The body-axis angular rate reference model parameters were set to $A_m = -15\mathbf{1}_3$ and $B_m = 15\mathbf{1}_3$. The other relevant control parameters were set as follows: the tracking gains were set such that $K_r = 15\mathbf{1}_3$ and $K_\Phi = 5\mathbf{1}_3$. The adaptive gain matrix Γ_W was set as a diagonal matrix with the

following vector along the diagonal

$$\begin{bmatrix} 1e-5(4) & 1(7) & 1e-3(6) \end{bmatrix}^T \tag{5.144}$$

where each entry $A(B)$ signifies the row vector

$$A(B) = \begin{bmatrix} A & A & \dots & A \end{bmatrix} \in \mathbb{R}^{1\times B}$$

In order to make the simulation more realistic, second-order actuator dynamics with damping ratio $\zeta = 0.7$ and natural frequency $\omega_n = 25Hz$ were included and position and rate limits were placed on the actuators of $30\,\mathrm{deg}$ and $100\,\mathrm{deg}/s$, respectively. In addition, a time delay of $0.01s$ was included in the simulation. The initial flight condition was a velocity of Mach 6 and altitude of $80,000ft$. The initial true angle-of-attack and sideslip angle were both $0\,\mathrm{deg}$ however the nonlinear observer was initialized such that $\hat{\beta}(0) = 0.1\,\mathrm{deg}$ and $\hat{\alpha}(0) = 0.5\,\mathrm{deg}$. The maximum assumed estimation error, defined in Assumption 5.2.5, was set to

$$\tilde{x}_a(t_0)_{max} = \begin{bmatrix} \tilde{\beta}(t_0)_{max} & \tilde{\alpha}(t_0)_{max} \end{bmatrix}^T = \begin{bmatrix} 0.5 & 1 \end{bmatrix}^T \mathrm{deg}$$

For comparison purposes, the set of simulation tests were also run using an ensemble Kalman filter to estimate the vehicle's aerodynamic angles instead of the nonlinear observer derived in this paper. For the results shown in this section, the ensemble size was set to $N = 100$ members and the process noise covariance matrix used, defined by $Q_f = E[w_k w_k^T]$ where w_k represents a vector

of zero-mean white process noise is given by

$$Q_f = \begin{bmatrix} E[w_{VT,k}^2] & 0 & 0 & 0 \\ 0 & E[w_{\Phi,k}^2] & 0 & 0 \\ 0 & 0 & E[w_{a,k}^2] & 0 \\ 0 & 0 & 0 & E[w_{r,k}^2] \end{bmatrix} \tag{5.145}$$

$$E[w_{VT,k}^2] = 1 \qquad E[w_{\Phi,k}^2] = \begin{bmatrix} 0.01 & 0 & 0 \\ 0 & 0.1 & 0 \\ 0 & 0 & 0.01 \end{bmatrix}$$

$$E[w_{a,k}^2] = \begin{bmatrix} 1e-4 & 0 \\ 0 & 1e-3 \end{bmatrix} \qquad E[w_{r,k}^2] = 4\mathbf{1}_3$$

The measurement noise covariance matrix is defined as $R_f = E[v_k v_k^T]$ where v_k represents a vector of zero-mean white measurement noise. The EnKF update procedure requires that R_f be non-singular. Therefore, despite assuming perfect measurement of the vehicle's Euler angles, the measurement noise covariance matrix was set as

$$R = \begin{bmatrix} E[v_{VT,k}^2] & 0 & 0 \\ 0 & E[v_{\Phi,k}^2] & 0 \\ 0 & 0 & E[v_{r,k}^2] \end{bmatrix} = \begin{bmatrix} E[v_{VT,k}^2] & 0 & 0 \\ 0 & 1e-6\mathbf{1}_3 & 0 \\ 0 & 0 & E[v_{r,k}^2] \end{bmatrix} \tag{5.146}$$

where $E[v_{VT,k}^2]$ and $E[v_{r,k}^2]$ varied based on whether a low noise case or high noise case was being examined. A brief mathematical description of the comparative EnKF used in this study was given in Section 4.

Test Case 1: The first test case corresponds to the roll angle ramp followed by pitch angle ramp maneuver described above. Figures 5.1 and 5.2 show the time histories of the state and control vec-

tors for the low noise case while Figures 5.3 and 5.4 show the results pertaining to the high noise case. The upper two plots in Figures 5.1 and 5.3 show the estimation performance of both the nonlinear observer and the EnKF. Both estimation techniques are able to produce accurate estimates of the aerodynamic angles, leading to successful tracking of the desired Euler angle trajectory shown in Figures 5.2 and 5.4. Both estimation techniques led to very similar control surface responses and no peaking phenomenon is seen. In the high noise case, the sideslip angle estimate generated using the nonlinear observer was affected slightly more by measurement noise than the estimate generated using the EnKF, however there is no noticeable effect on tracking performance.

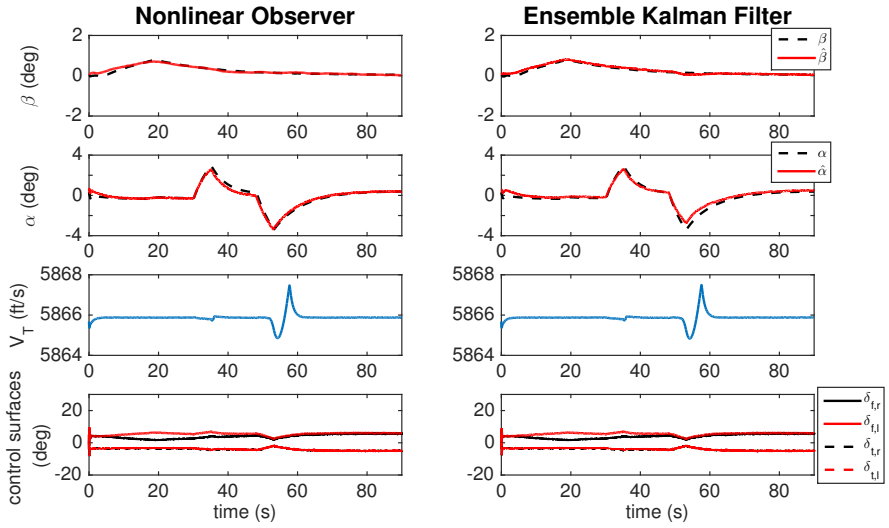

Figure 5.1: Test Case 1. Low Noise Case. True and estimated aerodynamic angle trajectories are shown followed by the vehicle total velocity, and the control surface deflections.

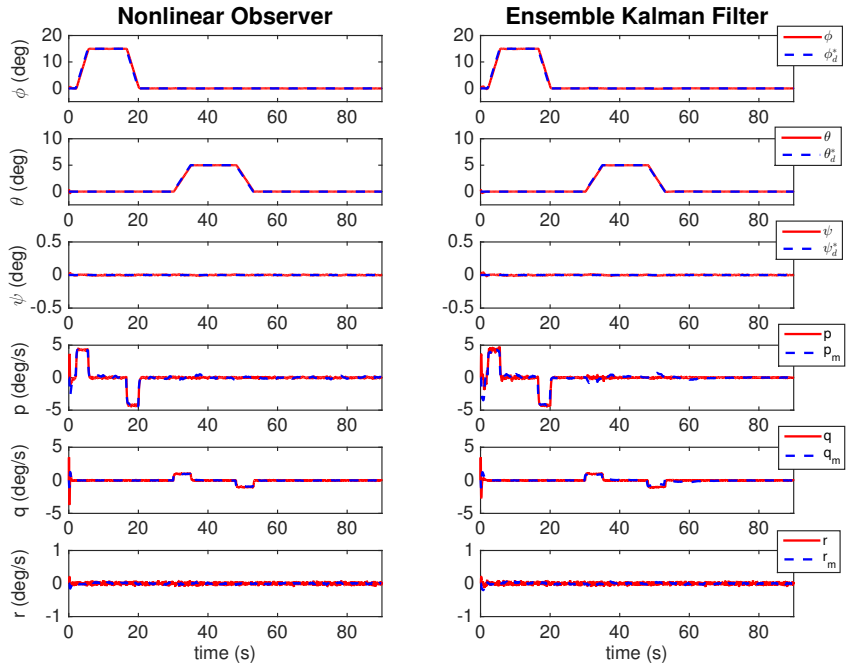

Figure 5.2: Test Case 1. Low Noise Case. Tracking performance of Euler angles and angular rates.

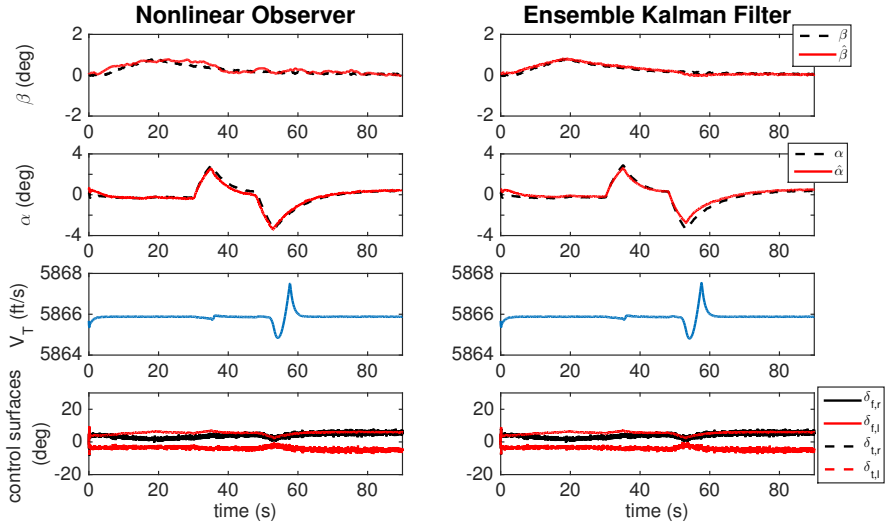

Figure 5.3: Test Case 1. High Noise Case. True and estimated aerodynamic angle trajectories are shown followed by the vehicle total velocity, and the control surface deflections.

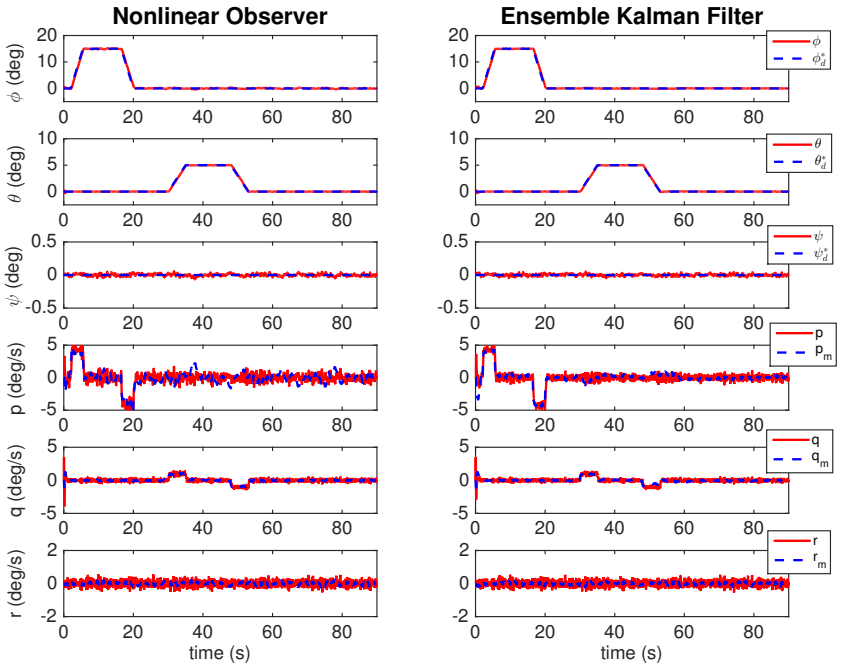

Figure 5.4: Test Case 1. High Noise Case. Tracking performance of Euler angles and angular rates.

Test Case 2: The second test case corresponds to the more aggressive roll maneuver described above. Figures 5.5 and 5.6 show the time histories of the state and control vectors for the low noise case while Figures 5.7 and 5.8 show the results pertaining to the high noise case. Once again, both estimation techniques produce accurate state estimates and the control objective is achieved despite parametric uncertainty in the model and noisy measurement signals. The successful implementation of this control framework in simulation demonstrates the nonlinear observer's ability to perform comparably to well established nonlinear Kalman filtering techniques while also being provably stable in an NDI adaptive control setting.

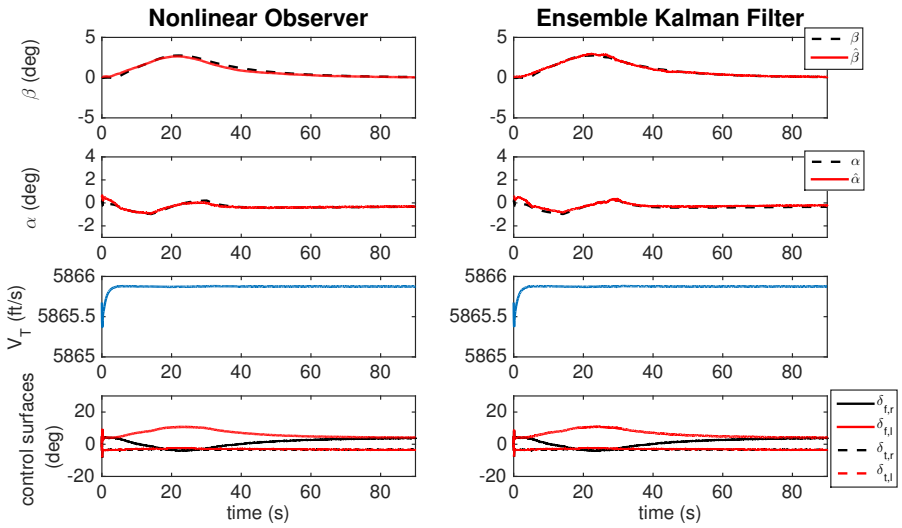

Figure 5.5: Test Case 2. Low Noise Case. True and estimated aerodynamic angle trajectories are shown followed by the vehicle total velocity, and the control surface deflections.

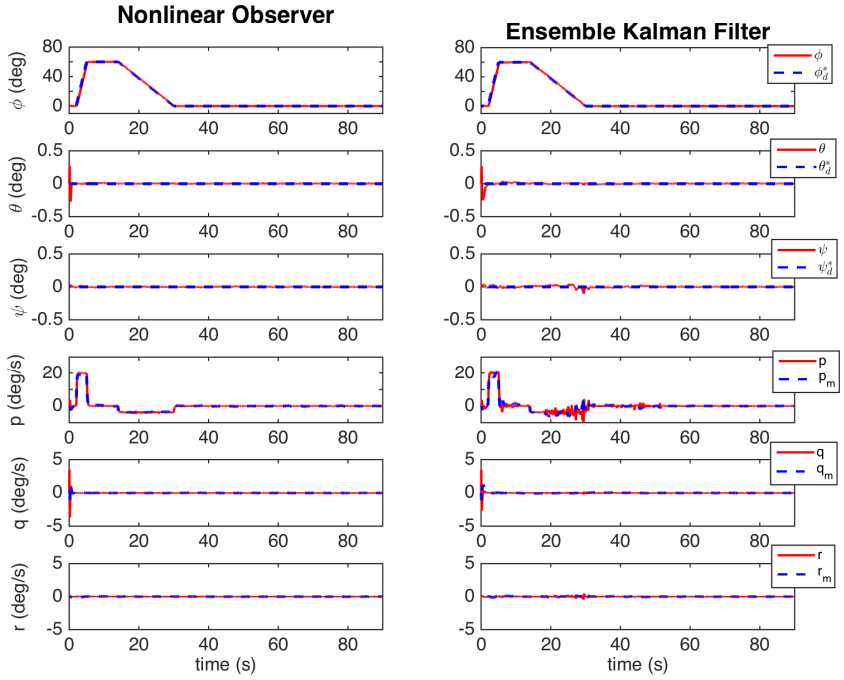

Figure 5.6: Test Case 2. Low Noise Case. Tracking performance of Euler angles and angular rates.

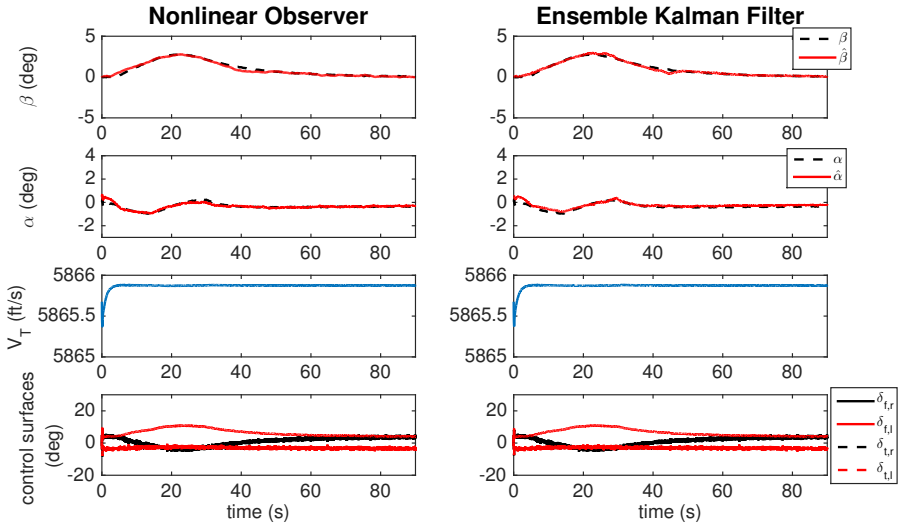

Figure 5.7: Test Case 2. High Noise Case. True and estimated aerodynamic angle trajectories are shown followed by the vehicle total velocity, and the control surface deflections.

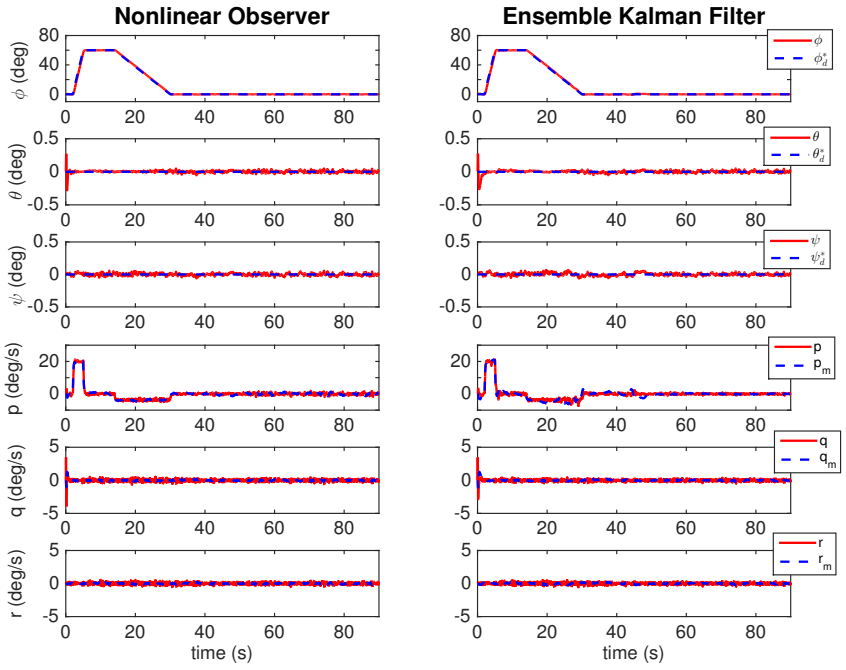

Figure 5.8: Test Case 2. High Noise Case. Tracking performance of Euler angles and angular rates.

5.7 Robustness Analysis

As in Section 4.7, a simulation-based analysis was performed in order to test the robustness of the observer-based NDI adaptive controller with respect to parameter uncertainty. In analyzing the six degree-of-freedom system, the assumed values of the aerodynamic coefficients C_{L1} and C_{Y1} were systematically varied and the effect on estimation and tracking performance was studied. As in Section 4.7, the assumed parameter set was selected according to

$$\hat{C}_{L1} = (1 + \Delta_{L1})\hat{C}^0_{L1}$$

$$\hat{C}_{Y1} = (1 + \Delta_{Y1})\hat{C}^0_{Y1}$$

Using the process described here, analyses varying more than two parameters at a time could also be achieved. These two specific parameters were chosen due to their importance in generating accurate aerodynamic angle estimates.

In each episode of the study, the vehicle was commanded to track a roll angle, pitch angle or yaw angle doublet maneuver command of a randomly chosen magnitude. The Euler angle doublet magnitudes varied between 1 and $6\,\mathrm{deg}$ for bank and pitch angle and between 1 and $3\,\mathrm{deg}$ for heading angle. Each doublet command lasted for a total of 20 seconds as shown in the three sample trajectories of Figure 5.9. As in the analysis of Section 4.7, all measurement noise had zero mean and the covariances were randomly selected values between 50 and $100(ft/s)^2$ for total velocity measurements and between 0.01 and $0.25(\mathrm{deg}/s)^2$ for all angular rate measurements.

For this analysis, the number of episodes N_{ep} was set to 60 (an even distribution of 20 each for pitch angle, roll angle, and yaw angle commands) and t_f was $40s$. The average integrated square error values of the aerodynamic angle estimation errors, Euler angle tracking errors, and angular rate tracking errors were calculated according to (4.138) and (4.139) and the results are given in Tables 5.2-5.9. As in Section 4.7, it is seen that the adaptive control mechanism leads to robustness with respect to tracking performance in both the position-level and velocity-level states.

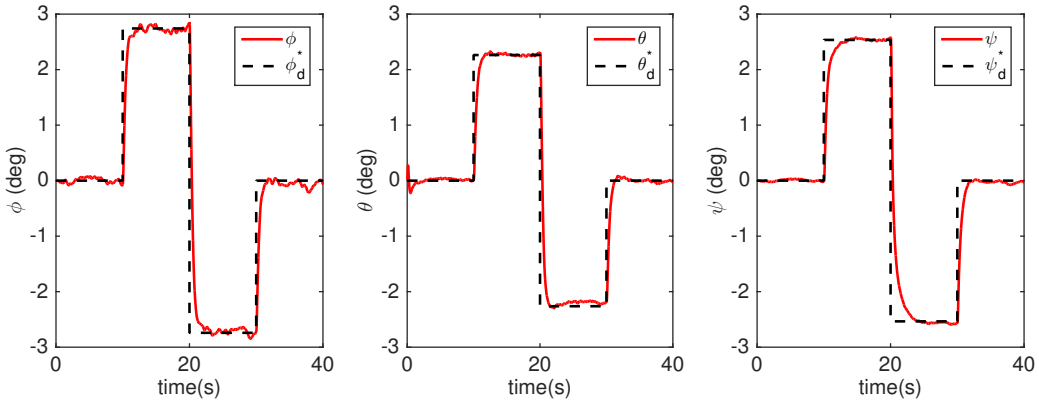

Figure 5.9: Sample Euler angle trajectory used in robustness analysis. The varying doublet magnitudes were selected randomly.

Table 5.2: 6-DOF Controller Robustness Analysis. Average integrated square error of the angle-of-attack estimation error over 40 seconds, $\overline{ISE}_{\tilde{\alpha}}$ $[\deg^2]$

	$\Delta_{L1} = -0.25$	$\Delta_{L1} = -0.125$	$\Delta_{L1} = 0$	$\Delta_{L1} = 0.125$	$\Delta_{L1} = 0.25$
$\Delta_{Y1} = -0.25$	16.11	7.08	2.64	1.03	1.28
$\Delta_{Y1} = -0.125$	15.99	6.89	3.06	1.55	0.91
$\Delta_{Y1} = 0$	15.63	6.76	2.61	0.80	1.42
$\Delta_{Y1} = 0.125$	15.79	6.83	2.55	1.03	0.97
$\Delta_{Y1} = 0.25$	15.64	6.67	2.43	0.84	0.91

Table 5.3: 6-DOF Controller Robustness Analysis. Average integrated square error of the sideslip angle estimation error over 40 seconds, $\overline{ISE}_{\tilde{\beta}}$ $[\deg^2]$

	$\Delta_{L1} = -0.25$	$\Delta_{L1} = -0.125$	$\Delta_{L1} = 0$	$\Delta_{L1} = 0.125$	$\Delta_{L1} = 0.25$
$\Delta_{Y1} = -0.25$	1.06	0.88	0.83	0.98	1.03
$\Delta_{Y1} = -0.125$	0.66	0.77	0.71	0.76	0.81
$\Delta_{Y1} = 0$	0.59	0.70	0.65	0.65	0.81
$\Delta_{Y1} = 0.125$	0.48	0.59	0.65	0.67	0.60
$\Delta_{Y1} = 0.25$	0.55	0.61	0.60	0.76	0.71

Table 5.4: 6-DOF Controller Robustness Analysis. Average integrated square error of the roll angle tracking error over 40 seconds, $\overline{ISE}_{e_\phi}$ $[\deg^2]$

	$\Delta_{L1} = -0.25$	$\Delta_{L1} = -0.125$	$\Delta_{L1} = 0$	$\Delta_{L1} = 0.125$	$\Delta_{L1} = 0.25$
$\Delta_{Y1} = -0.25$	0.41	0.34	0.32	0.38	0.39
$\Delta_{Y1} = -0.125$	0.33	0.34	0.32	0.36	0.38
$\Delta_{Y1} = 0$	0.33	0.36	0.32	0.34	0.41
$\Delta_{Y1} = 0.125$	0.28	0.30	0.33	0.35	0.35
$\Delta_{Y1} = 0.25$	0.27	0.31	0.31	0.36	0.38

Table 5.5: 6-DOF Controller Robustness Analysis. Average integrated square error of the pitch angle tracking error over 40 seconds, $\overline{ISE}_{e_\theta}$ $[\text{deg}^2]$

	$\Delta_{L1} = -0.25$	$\Delta_{L1} = -0.125$	$\Delta_{L1} = 0$	$\Delta_{L1} = 0.125$	$\Delta_{L1} = 0.25$
$\Delta_{Y1} = -0.25$	0.62	0.63	0.45	0.44	0.44
$\Delta_{Y1} = -0.125$	0.49	0.56	0.94	0.90	0.36
$\Delta_{Y1} = 0$	0.35	0.44	0.56	0.33	0.56
$\Delta_{Y1} = 0.125$	0.41	0.56	0.53	0.48	0.40
$\Delta_{Y1} = 0.25$	0.47	0.41	0.38	0.37	0.35

Table 5.6: 6-DOF Controller Robustness Analysis. Average integrated square error of the yaw angle tracking error over 40 seconds, $\overline{ISE}_{e_\psi}$ $[\text{deg}^2]$

	$\Delta_{L1} = -0.25$	$\Delta_{L1} = -0.125$	$\Delta_{L1} = 0$	$\Delta_{L1} = 0.125$	$\Delta_{L1} = 0.25$
$\Delta_{Y1} = -0.25$	0.15	0.12	0.11	0.13	0.14
$\Delta_{Y1} = -0.125$	0.12	0.12	0.11	0.12	0.14
$\Delta_{Y1} = 0$	0.11	0.13	0.11	0.12	0.15
$\Delta_{Y1} = 0.125$	0.10	0.11	0.12	0.12	0.12
$\Delta_{Y1} = 0.25$	0.10	0.11	0.10	0.13	0.13

Table 5.7: 6-DOF Controller Robustness Analysis. Average integrated square error of the roll rate tracking error over 40 seconds, $\overline{ISE}_{e_p}$ $[\text{deg}^2]$

	$\Delta_{L1} = -0.25$	$\Delta_{L1} = -0.125$	$\Delta_{L1} = 0$	$\Delta_{L1} = 0.125$	$\Delta_{L1} = 0.25$
$\Delta_{Y1} = -0.25$	20.62	16.57	15.49	17.86	17.38
$\Delta_{Y1} = -0.125$	16.87	17.37	16	16.55	18.13
$\Delta_{Y1} = 0$	17.32	18.66	16.30	16.85	19.47
$\Delta_{Y1} = 0.125$	14.64	15.43	16.81	16.89	16.79
$\Delta_{Y1} = 0.25$	13.85	16.17	15.15	17.52	17.66

Table 5.8: 6-DOF Controller Robustness Analysis. Average integrated square error of the pitch rate tracking error over 40 seconds, $\overline{ISE}_{e_q}$ $[\text{deg}^2]$

	$\Delta_{L1} = -0.25$	$\Delta_{L1} = -0.125$	$\Delta_{L1} = 0$	$\Delta_{L1} = 0.125$	$\Delta_{L1} = 0.25$
$\Delta_{Y1} = -0.25$	6.01	4.93	4.61	4.70	5.03
$\Delta_{Y1} = -0.125$	5.12	5.44	4.66	4.88	4.27
$\Delta_{Y1} = 0$	4.10	5.15	5.14	4.01	5.05
$\Delta_{Y1} = 0.125$	4.70	4.65	4.94	4.38	3.98
$\Delta_{Y1} = 0.25$	4.51	4.79	4.30	4.54	4.20

Table 5.9: 6-DOF Controller Robustness Analysis. Average integrated square error of the yaw rate tracking error over 40 seconds, $\overline{ISE}_{e_r}$ $[\deg^2]$

	$\Delta_{L1} = -0.25$	$\Delta_{L1} = -0.125$	$\Delta_{L1} = 0$	$\Delta_{L1} = 0.125$	$\Delta_{L1} = 0.25$
$\Delta_{Y1} = -0.25$	0.55	0.47	0.45	0.52	0.50
$\Delta_{Y1} = -0.125$	0.48	0.48	0.49	0.47	0.52
$\Delta_{Y1} = 0$	0.49	0.53	0.48	0.49	0.57
$\Delta_{Y1} = 0.125$	0.43	0.45	0.49	0.50	0.50
$\Delta_{Y1} = 0.25$	0.40	0.48	0.44	0.51	0.51

6. OBSERVER-BASED NONLINEAR DYNAMIC INVERSION ADAPTIVE CONTROL WITH STATE CONSTRAINTS

6.1 Introduction

Based on the discussion of previous sections and the motivational issues presented in Section 1.1, it is evident that in order to successfully prevent inlet unstart, a hypersonic flight control system would need to be able to enforce state constraints without direct measurements of the vehicle's aerodynamic angles. Therefore, in this section a simulation study is presented, within which a state constraining controller is combined with the nonlinear observer developed in Sections 4 and 5. For this study, the BFSC controller developed in Section 3 was chosen as the state constraint mechanism. The nonlinear observer is used to produce estimated aerodynamic angle values and those values are then treated as truth and fed into the state constraining control law. As in Sections 4 and 5 the performance of the nonlinear observer is directly compared with that of an ensemble Kalman filter.

When controlling nonlinear systems, it is exceedingly difficult to prove tracking error stability when attempting to drive an *unmeasured* state to track a reference trajectory. Nonlinear controllers that attempt to do this will be susceptible to steady-state errors as the controller will be based on the estimated tracking error, $\hat{e} = y_m - \hat{y}$, rather than the true tracking error, $e = y_m - y$. Therefore, if $\hat{e} = 0$ but $e \neq 0$ and the system is in steady-state, the controller will have no reason to take corrective action. This is why in Sections 4 and 5 for example, Euler angle trajectories were commanded once it was assumed that the aerodynamic angles were unavailable for measurement. Nevertheless in practice it is not uncommon for systems to be developed that combine well-tested estimation techniques with full state feedback control laws, treating the estimated values as truth. In this section, a similar approach is taken and demonstrated on the GHV simulation.

This section will proceed as follows: First, the combined observer-based state constraining

control laws will be presented. Then, the simulation study results will be given, demonstrating this control framework's ability to track and/or constrain the vehicle's aerodynamic angles despite not measuring them directly.

6.2 Control Law Development

In this section the combined observer-based state constraining controller is introduced. This control law is based on the bounding function state constraint technique derived in Section 3. It is developed in terms of the position-level and velocity-level subsystem breakdown of the GHV used previously,

$$\dot{x}_p = \begin{bmatrix} \dot{\phi} \\ \dot{\theta} \\ \dot{\psi} \\ \dot{\alpha} \\ \dot{\beta} \end{bmatrix} = f_p(x) + g_p(x)\Lambda_p \begin{bmatrix} p_d \\ q_d \\ r_d \end{bmatrix} \tag{6.1}$$

$$y_p = C_p x_p = \begin{bmatrix} \alpha & \beta \end{bmatrix}^T \tag{6.2}$$

$$C_p = \begin{bmatrix} 0 & 0 & 0 & 1 & 0 \\ 0 & 0 & 0 & 0 & 1 \end{bmatrix} \tag{6.3}$$

$$\dot{x}_v = \begin{bmatrix} \dot{p} \\ \dot{q} \\ \dot{r} \end{bmatrix} = f_v(x) + g_v(x) \begin{bmatrix} \delta_{f,r} \\ \delta_{f,l} \\ \delta_{t,r} \\ \delta_{t,l} \end{bmatrix} \tag{6.4}$$

$$y_v = \begin{bmatrix} p & q & r \end{bmatrix}^T \tag{6.5}$$

where it is assumed that $\Lambda_p = \mathbf{1}_3$ is known. In this section, the identity matrix will be signified using the notation of Sections 4 and 5, i.e. $\mathbf{1}_M$ represents the $M \times M$ identity matrix.

Let $y_{p,m} \in \mathbb{R}^2$ be the aerodynamic angle reference model and $y_{v,m} \in \mathbb{R}^3$ be the angular rate reference model such that

$$\dot{y}_{p,m} = A_{p,m} y_{v,m} + B_{p,m} \begin{bmatrix} \alpha_d \\ \beta_d \end{bmatrix} \tag{6.6}$$

$$\dot{y}_{v,m} = A_{v,m} y_{v,m} + B_{v,m} \begin{bmatrix} p_d \\ q_d \\ r_d \end{bmatrix} \tag{6.7}$$

The observer-based BFSC control laws are given by

$$\begin{bmatrix} p_d \\ q_d \\ r_d \end{bmatrix} = [C_p g_p(x_c)]^\dagger \left(\dot{y}_{p,m} - C\hat{f}_p(x_c) + K_p \hat{e}_p + \nu_p - F'_*(\hat{y}_p)[\dot{y}_{p,m} + K_p y_{p,m}] \right) \tag{6.8}$$

$$u = \hat{g}_v^{-1}(x_c) \left(\dot{y}_{v,m} - \hat{f}_v(x_c) + (K_v + K_{v1}(x_c)) e_v + \nu_1 + \nu_2 \right) \tag{6.9}$$

Note that because the aerodynamic angles are not available for measurement, these control laws depend on the vector x_c, defined in Equation (5.19). The position-level tracking error term in

(6.8) is also dependent on the estimated aerodynamic angles,

$$\hat{e}_p = y_{p,m} - \begin{bmatrix} \hat{\alpha} \\ \hat{\beta} \end{bmatrix}$$

The adaptive signal ν_p is defined as

$$\nu_p = \widehat{W}_p^T b_p(x_c) \tag{6.10}$$

$$b_p(x_c) = \begin{bmatrix} \frac{\bar{q}}{V_T \cos\hat{\beta}} & \frac{\bar{q}}{V_T \cos\hat{\beta}}\hat{\alpha} & \frac{\bar{q}}{V_T \cos\hat{\beta}}\hat{\alpha}^2 & \frac{\bar{q}}{V_T} & \frac{\bar{q}}{V_T}\hat{\beta} \end{bmatrix}^T \tag{6.11}$$

where the estimated weight matrix $\widehat{W}_p$ is updated according to the adaptive law

$$\dot{\widehat{W}}_p = \Gamma_{W_p} \mathrm{Proj}_M\Big(\widehat{W}_p, b_p(x_c)\left(\hat{e}_p^T - \hat{y}_p^T F'(\hat{y}_p)\right)\Big) \tag{6.12}$$

The bounding functions are constructed according to equations (3.7) and (3.8) but now depend on the estimated aerodynamic angles. Therefore, the matrices $F'_*(\hat{y}_p)$ and $F'(\hat{y}_p)$ are given by

$$F'_*(\hat{y}_p) = \begin{bmatrix} \frac{f'_{b,1}(\hat{\alpha}^2)}{1+f'_{b,1}(\hat{\alpha}^2)} & 0 \\ 0 & \frac{f'_{b,2}(\hat{\beta}^2)}{1+f'_{b,2}(\hat{\beta}^2)} \end{bmatrix} \tag{6.13}$$

$$F'(\hat{y}_p) = \begin{bmatrix} f'_{b,1}(\hat{\alpha}^2) & 0 \\ 0 & f'_{b,2}(\hat{\beta}^2) \end{bmatrix} \tag{6.14}$$

All other parameters in equations (6.8)-(6.12) retain their meaning from Sections 3 and 5. The feedback gain term K is defined in equation (3.16). The feedback gain K_v is equivalent to the gain K_r defined in (5.41) and the time-varying feedback gain $K_{v1}(x_c)$ is equivalent to the gain $K_{r1}(x_c)$ defined in (5.125). The adaptive parameters ν_1 and ν_2 retain they're definitions from (5.61) and (5.62) respectively.

6.3 Simulation Setup and Results

The combined observer-based, state constraining NDI adaptive control architecture was implemented in the GHV simulation and several example trajectories were explored. The first two trajectories tested were $3\,\mathrm{deg}$ doublet commands, one in angle-of-attack and one in sideslip. These examples do not test the state constraint mechanism but instead demonstrate the controllers ability to track angle-of-attack and sideslip angle commands with bounded error despite not measuring these angles directly. The second set of trajectories tested were $6\,\mathrm{deg}$ doublet commands, again one in angle-of-attack and one in sideslip angle. These commands violate the state constraint values defined in Sections 2 and 3. Therefore, these examples not only test the controllers ability to track unmeasured states but to constrain them as well.

For all trajectories tested, the velocity level measurement signals needed to drive the nonlinear observer (the body-axis angular rate and total velocity measurements) were corrupted by zero mean white noise with a standard deviation of 3.16 ft/s and 0.1 deg/s, for total velocity and the body-axis angular rates respectively. The observer-gains used for the results presented in this section were the same as those used in Section 5 and can be found in Appendix D. Additionally, the bounded uncertainties included in the simulation were identical to those found in Table 5.1 and Equations (5.141)-(5.143).

The aerodynamic angle reference model parameters were set to $A_{p,m} = -\mathbf{1}_2$ and $B_{p,m} = \mathbf{1}_2$ and the body-axis angular rate reference model parameters were set to $A_{v,m} = -10\mathbf{1}_3$ and $B_{v,m} = 10\mathbf{1}_3$. The other relevant control parameters were set as follows: the tracking gains were set such

that

$$K_p = \begin{bmatrix} 1 & 0 \\ 0 & 2 \end{bmatrix} \tag{6.15}$$

$$K_v = \begin{bmatrix} 5 & 0 & 0 \\ 0 & 10 & 0 \\ 0 & 0 & 5 \end{bmatrix} \tag{6.16}$$

The adaptive gain matrix $\Gamma_{W,p}$ was set as $1e-3\mathbf{1}_5$ and the adaptive gain matrix $\Gamma_{W,v}$ was set to the diagonal matrix with the vector given in (5.144) along the diagonal. The process and measurement noise covariance matrices, used in the comparative EnKF, were in the form of Equations (5.145) and (5.146) where,

$$E[w^2_{VT,k}] = 30 \qquad E[w^2_{\Phi,k}] = \begin{bmatrix} 1e-5 & 0 & 0 \\ 0 & 0.1 & 0 \\ 0 & 0 & 1e-5 \end{bmatrix}$$

$$E[w^2_{a,k}] = \begin{bmatrix} 1e-4 & 0 \\ 0 & 1e-2 \end{bmatrix} \qquad E[w^2_{r,k}] = 4\mathbf{1}_3$$

$$E[v^2_{\Phi,k}] = 1e-6\mathbf{1}_3$$

As in previous sections, the simulation included second-order actuator dynamics with damping ratio $\zeta = 0.7$ and natural frequency $\omega_n = 25Hz$ and actuator position and rate limits of 30 deg and $100\,\mathrm{deg}/s$, respectively. In addition, a time delay of $0.01s$ was included in the simulation. The initial flight condition was a velocity of Mach 6 and altitude of $80,000ft$.

Figures 6.1 and 6.3 show the time histories of the aerodynamic angles, using estimated values in the control law, when $3\,\mathrm{deg}$ doublets were commanded. Total velocity and the control surface deflections are shown as well. Results are given comparing the performance when the estimated

values were generated using the nonlinear observer and when they were generated using the ensemble Kalman filter. Successful tracking is achieved for both the angle-of-attack and sideslip angle command cases. In Figure 6.3 it is seen that a small steady-state error occurs in the estimate of angle-of-attack regardless of which estimation technique was used. As was mentioned above, this control framework is susceptible to such steady-state errors. The corresponding Euler angle and angular rate trajectories are shown in Figures 6.2 and 6.4.

Figures 6.5 and 6.7 show the time histories of the aerodynamic angles, using estimated values in the control law, when $6\,\mathrm{deg}$ doublets were commanded. Since these commands exceed the predetermined limits, the state constraint mechanism activates in both of these cases and successful state constraint enforcement is seen. Once again, when sideslip angle was commanded, as seen in Figure 6.7 a steady-state error in angle-of-attack occurred. Nevertheless, no state constraints are exceeded and the control signals remain relatively smooth despite the activation of the bounding functions. The corresponding Euler angle and angular rate trajectories are shown in Figures 6.6 and 6.8.

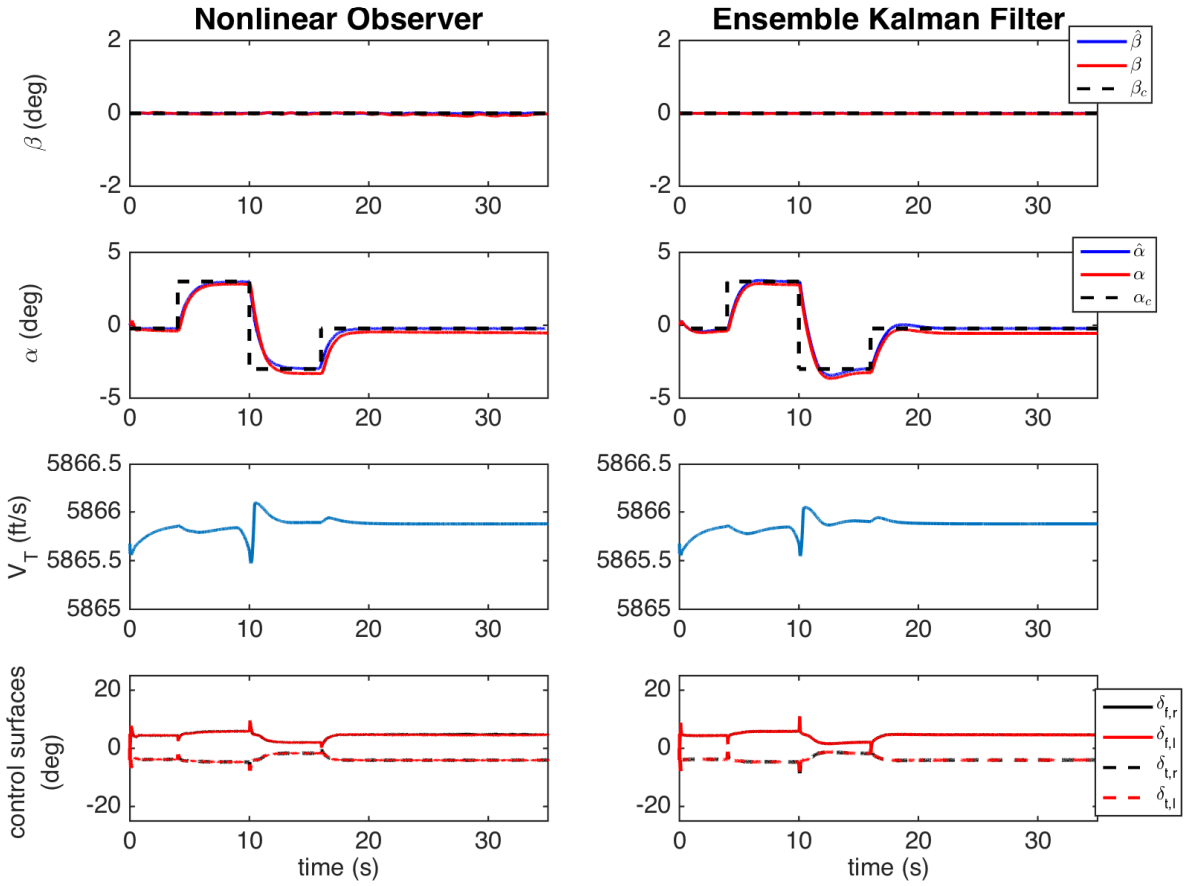

Figure 6.1: Tracking of unmeasured states example. A $3\,\mathrm{deg}$ angle-of-attack doublet trajectory was commanded.

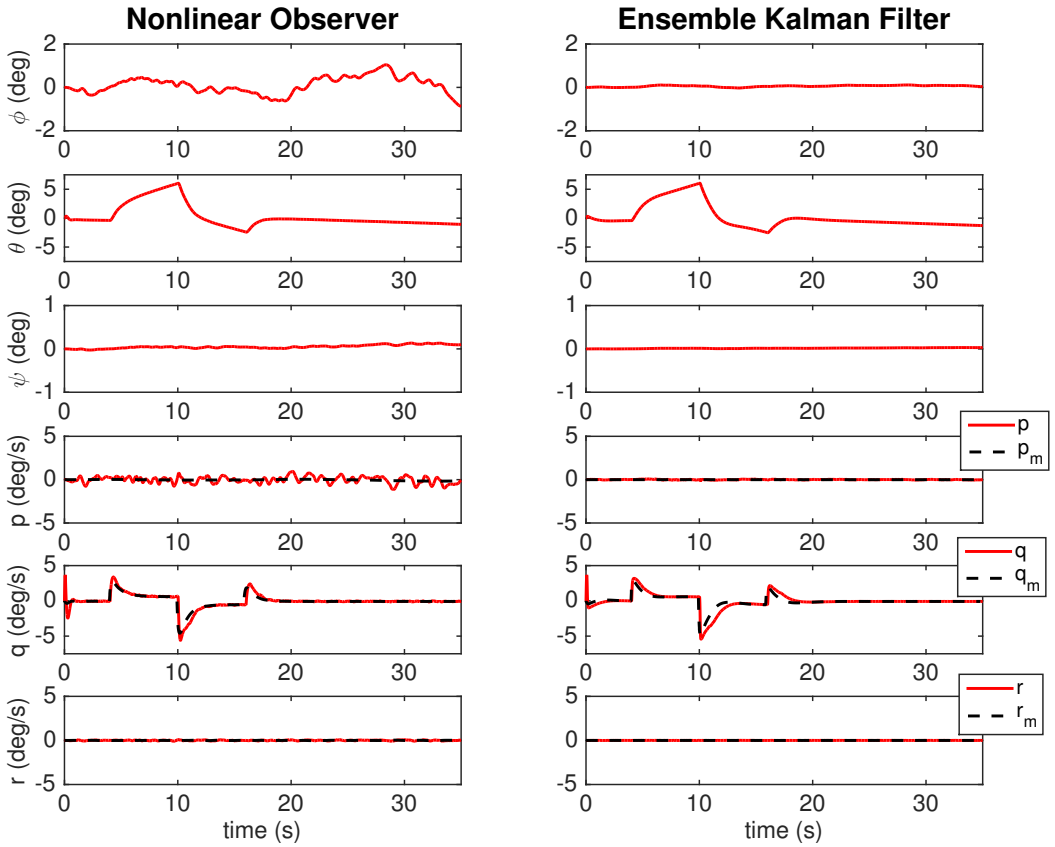

Figure 6.2: Tracking of unmeasured states example. Euler angle and angular rate trajectories are shown for $3\,\mathrm{deg}$ angle-of-attack doublet command.

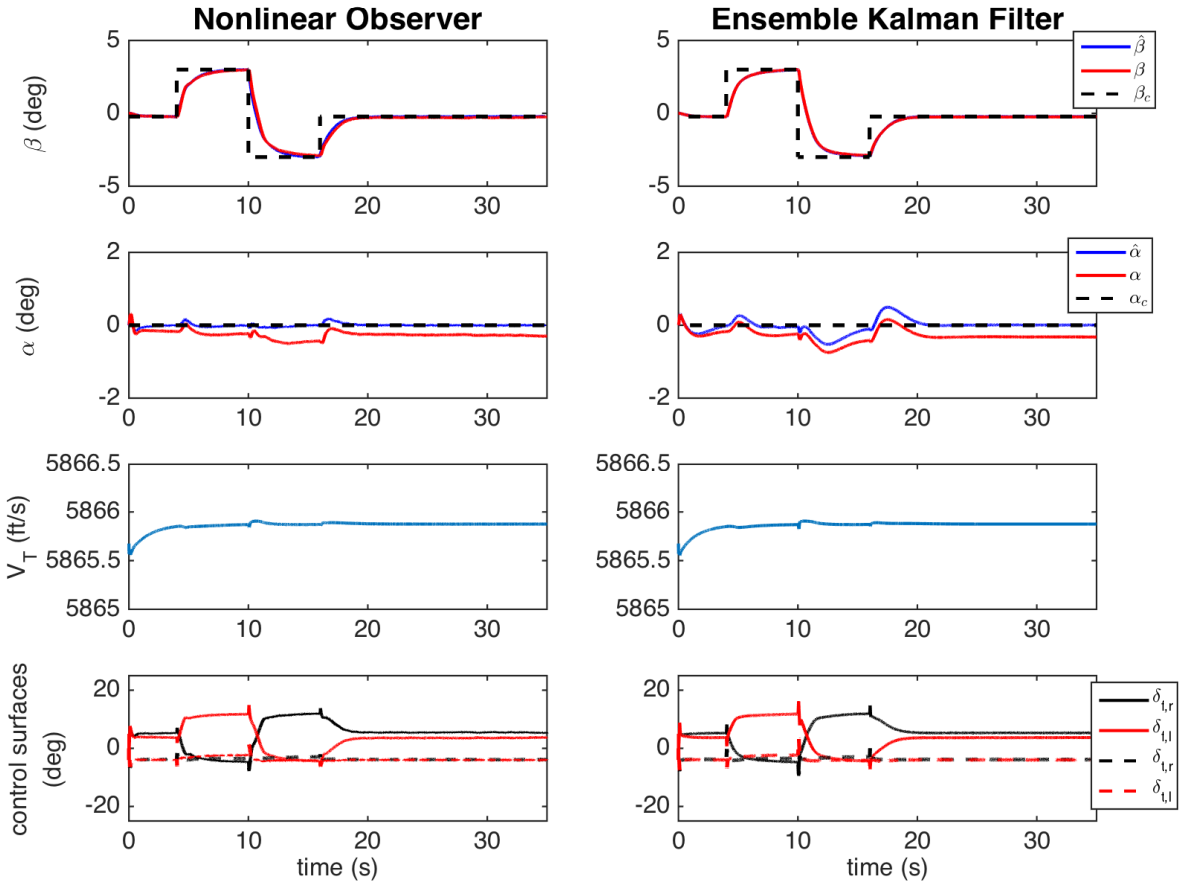

Figure 6.3: Tracking of unmeasured states example. A $3\,\mathrm{deg}$ sideslip angle doublet trajectory was commanded.

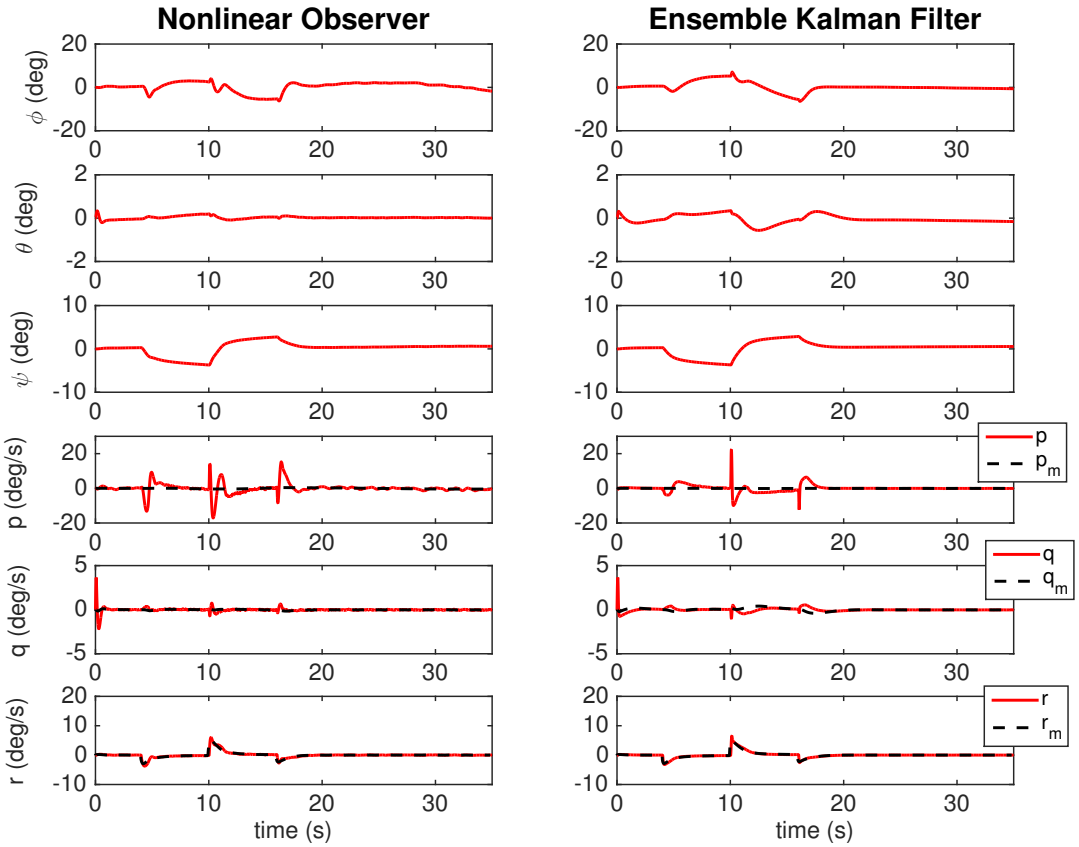

Figure 6.4: Tracking of unmeasured states example. Euler angle and angular rate trajectories are shown for $3\,\mathrm{deg}$ sideslip doublet command.

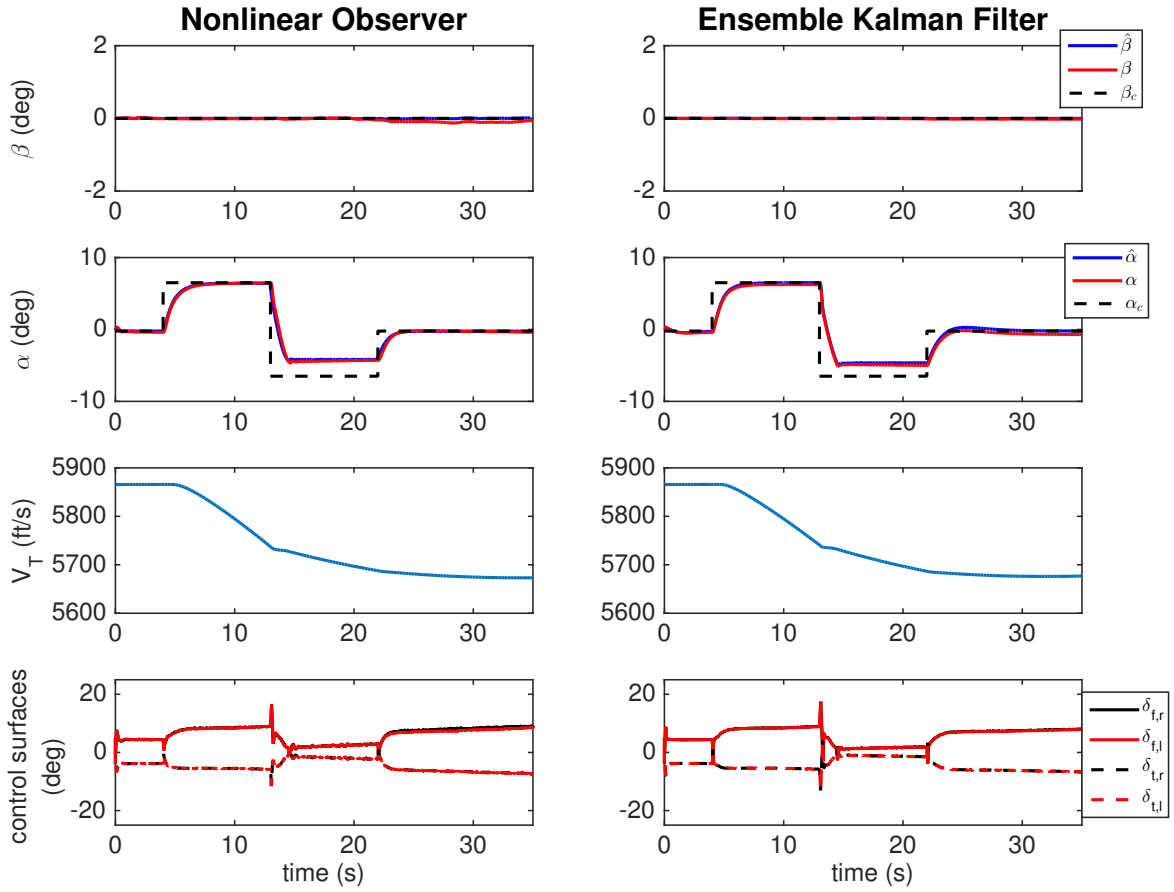

Figure 6.5: Constraining of unmeasured states example. A $6\,\mathrm{deg}$ angle-of-attack doublet trajectory was commanded.

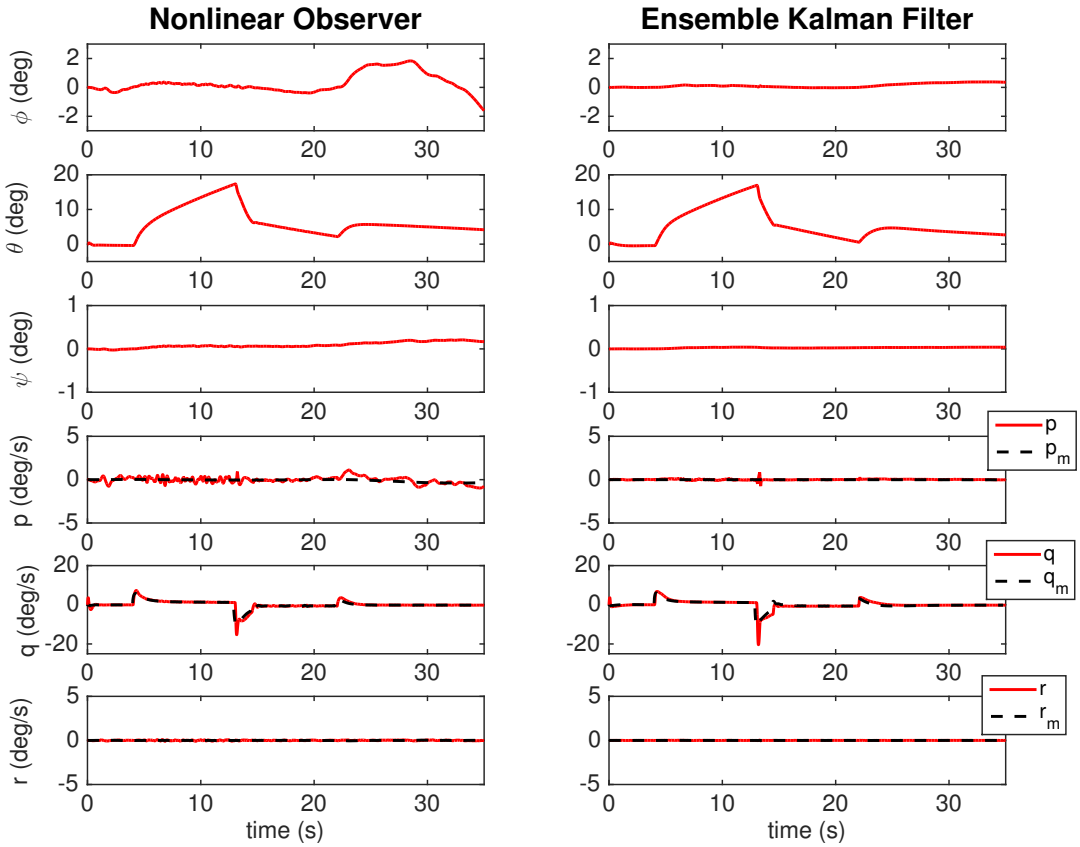

Figure 6.6: Constraining of unmeasured states example. Euler angle and angular rate trajectories are shown for $6\,\mathrm{deg}$ angle-of-attack doublet command.

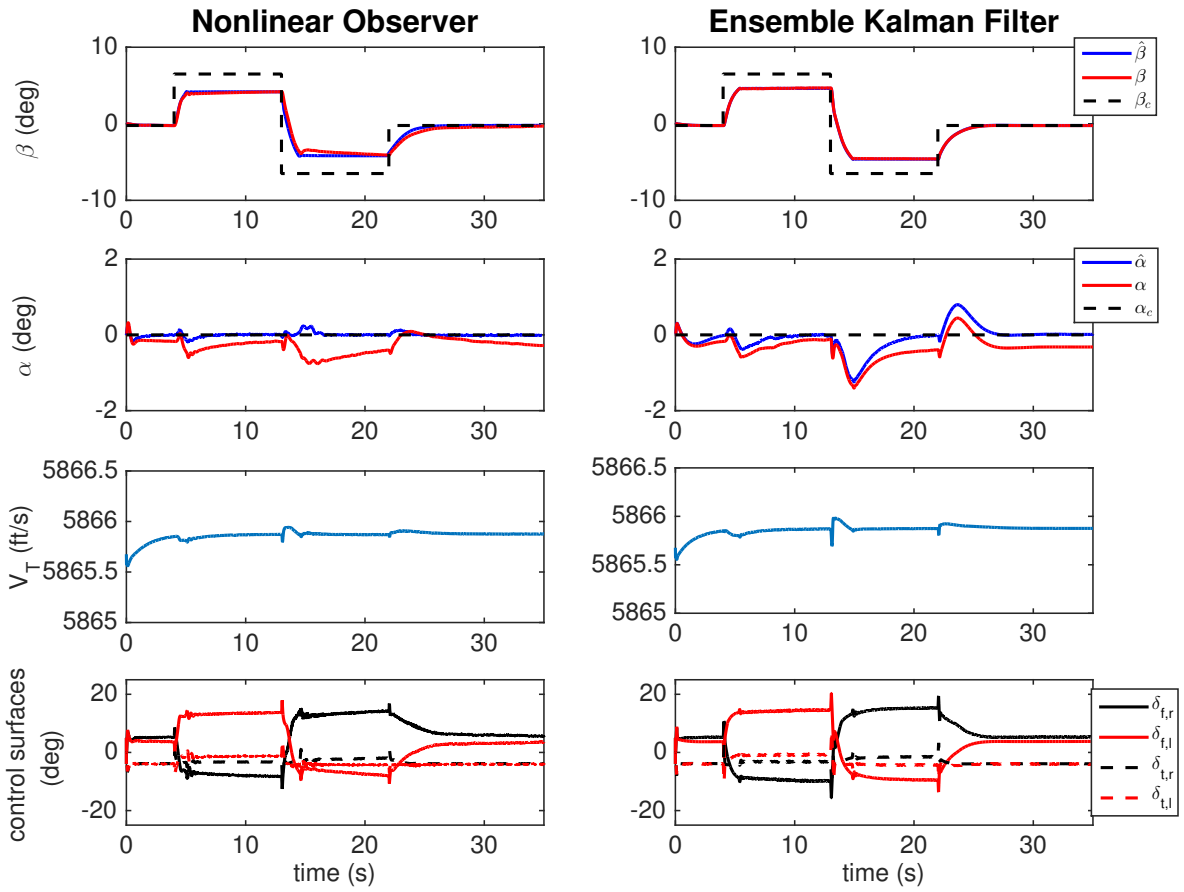

Figure 6.7: Constraining of unmeasured states example. A $6\,\mathrm{deg}$ sideslip angle doublet trajectory was commanded.

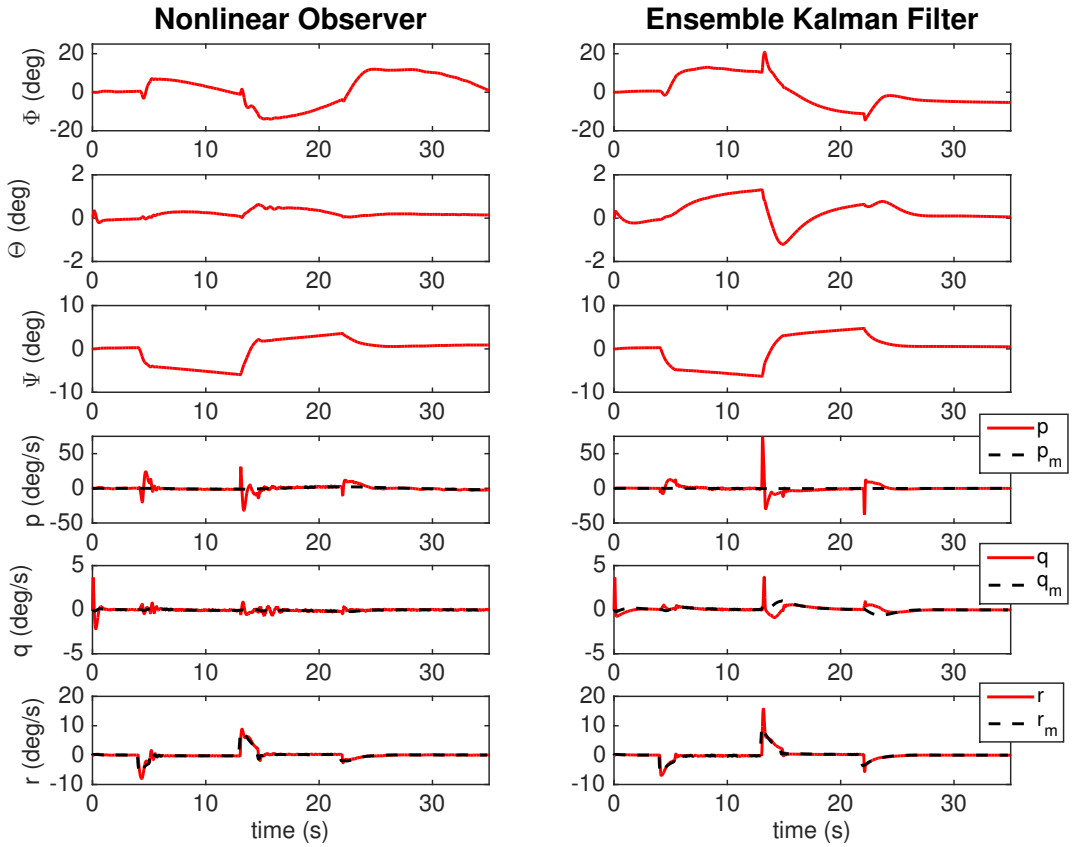

Figure 6.8: Constraining of unmeasured states example. Euler angle and angular rate trajectories are shown for $6\,\mathrm{deg}$ sideslip doublet command.

7. SAMPLED-DATA NONLINEAR DYNAMIC INVERSION ADAPTIVE CONTROL

7.1 Introduction

Control of continuous time nonlinear systems with discrete controls, i.e. sampled-data systems, is a difficult task due in part to the inability to represent a nonlinear system with an exact discrete time representation. Since for linear systems such exact representations can be achieved, sampled-data controllers can be designed that not only stabilize the plant but also take into account the inter-sample motion of the system and guarantee stability bounds between samples. In the literature, there are typically two options for handling nonlinear sampled-data systems: (Approach 1) Develop a continuous time control law that stabilizes the continuous time system and then implement it discretely (Approach 2) Use an approximate discrete time model to represent the nonlinear system and develop a controller based on the approximation. Through Approach 2, important stability results that explain the relationship between an approximate discrete time model and an exact model have been developed for a wide class of nonlinear systems [57, 58] however both approaches have lead to successful results in the past [59]. The study of nonlinear sampled-data control systems has been extended to examining backstepping approaches [60], model predictive control [61], and output feedback control [62].

This section develops a nonlinear sampled-data controller along the lines of Approach 2, described above. A class of nonlinear discretization schemes is utilized which allows for a discrete time NDI control law to be implemented. Analysis of such discretization schemes, commonly found in literature pertaining to numerical analysis or computational fluid dynamics, has be shown to be useful in nonlinear control settings as well [9]. The presented NDI control law transforms the problem of stabilizing the nonlinear discrete time system into a linear, discrete time adaptive control problem for which many solutions have been developed. For stability purposes, this paper focuses on a projection adaptive algorithm based on the methods presented in [63], however other

algorithms such as recursive least squares, multiple models [64], or artificial neural networks [65] could potentially be used as well. Conditions are given such that if the controller sampling time, T, is small enough, the proposed controller is guaranteed to stabilize the true continuous time system.

An important concern when developing sampled-data controllers is the establishment of an explicit bound on the controller sampling time T such that the stability guarantees hold. For nonlinear systems, such a bound is difficult to obtain, once again due to the approximations associated with the discrete time model, and has only been done for a few specific cases [66,67]. Although an explicit bound is not provided for the control framework in this section, considerations for establishing such a bound are discussed and future research directions required for achieving that goal are considered.

In this section, a class of nonlinear discretization schemes that allows for the use of NDI control is presented and application of these schemes to the uncertain nonlinear systems of interest is explained. Next, the NDI control law is presented and it is shown that the nonlinear sampled-data control problem can be transformed into a linear discrete time adaptive control problem. The projection based adaptive algorithm is developed and stability of the algorithm in the context of sampled-data systems is established. Finally, the effectiveness of this control framework is demonstrated on a nonlinear simulation of an F-16 aircraft as well as the GHV. The F-16 simulation is included in order to test out the sampled-data controller on a nonlinear system with slower dynamics than a hypersonic vehicle.

7.2 Nonlinear Discretization Using Linear Multistep Methods

7.2.1 Introduction to Linear Multistep Methods

Many useful techniques have been developed in the fields of numerical methods and computational fluid dynamics for approximating nonlinear differential equations with a discrete time representation. These include well known numerical methods: Runge Kutta, Euler time marching methods, and linear multistep methods (LMMs). Given a nonlinear ordinary differential equation

of the form

$$\frac{dz}{dt} = f(z,t) \tag{7.1}$$

a general form for all linear multistep methods is given by

$$\sum_{k=1-K}^{1} \alpha_k z_{n+k} = h_s \sum_{k=1-K}^{1} \beta_k f_{n+k} \tag{7.2}$$

where h_s is the integration step-size, $f_k = f(z_k, kh_s)$, and α_k, β_k are constant coefficients. These numerical methods are referred to as multistep or K-step methods because in order to progress the method forward one time step, K instances of previous data must be used. When $\beta_1 = 0$, these methods are referred to as explicit LMMs and when $\beta_1 \neq 0$ they are referred to as implicit. For many explicit LMMs, $\alpha_1 = 1$, and this section will focus specifically on this class of methods. It was pointed out in [68] that if the nonlinear differential equation given in (7.1) represents a dynamical system with state x and control input u such that

$$\frac{dx}{dt} = f(x,u,t) \tag{7.3}$$

then explicit LMMs can be used for control design because they allow one to represent a future state based on current and past states and control inputs in a discrete time manner.

The numerical stability and convergence properties of explicit LMMs have been analyzed in great detail [69,70]. For linear ordinary differential equations, analytical tools have been developed which allow for one to calculate an explicit bound on h_s for which a particular method will be numerically stable and convergent. Unfortunately, for nonlinear systems, such analytical tools have not been developed and more approximate methods must be used. One such option is to linearize the nonlinear system of interest and use the linear analytical tools to find an approximate bound on h_s. Nevertheless, LMMs have been shown to accurately approximate the solution of nonlinear ordinary differential equations in practice and with proper analysis given a specific nonlinear

equation, they can be used reliably.

7.2.2 Discretization of a Nonlinear Control System with Parameter Uncertainty

Consider the following nonlinear affine-in-control system with discrete controls

$$\dot{x} = f(x) + \Lambda g(x)u \tag{7.4}$$

$$y = Cx \tag{7.5}$$

where $x \in \mathbb{R}^{n_s}$ is the state vector, $u \in \mathbb{R}^m$ is the control vector with control sampling time T, the vector $f(x) \in \mathbb{R}^{n_s}$ represents the nonlinear open-loop dynamics of the system which are assumed to be bounded for bounded x, and $\Lambda g(x) \in \mathbb{R}^{n_s \times m}$ represents the control effectiveness of the system. It is assumed that $f(x)$ and the constant matrix $\Lambda \in \mathbb{R}^{n_s \times n_s}$ are unknown but that the matrix $g(x) \in \mathbb{R}^{n_s \times m}$ is known. It is also assumed that Λ has full rank. The vector $y \in \mathbb{R}^p$ represents the outputs which are desired to be controlled where $n_s \geq m \geq p$. The matrix $C \in \mathbb{R}^{p \times n_s}$ is constant and assumed to have full rank. In order to simplify the development, the scope of this section is limited to systems with no pure time delays. Past literature on discrete time adaptive control often includes pure time delays (which are assumed to be known exactly) in the systems of interest. However, these papers are typically examining exact discretizations of linear systems if not a truly discrete system. Handling pure time delays in a sampled-data system with an approximate discrete model is a more complicated problem that will be the focus of future research.

The system (7.4) can be approximated by an explicit LMM in the following way,

$$x_{n+1} = -\sum_{k=-K}^{0} \alpha_k x_{n+k} + T \sum_{k=-K}^{0} \beta_k \left(f_{n+k} + \Lambda g_{n+k} u_{n+k} \right) \tag{7.6}$$

It is assumed that full state measurements are available and that the system is equipped with sensors with sampling time T_s such that $\gamma T_s = T$ where $\gamma \geq 1$ is an integer.

Common applications of LMMs such as computational fluid dynamics typically have the following two properties: (P1) Assumed perfect knowledge of the equations of motion and (P2) the inability to take frequent accurate measurements of the system state in real time. Note that in order to initialize the discrete sequence given in (7.6), K previous data points are required. Since often, these data points can't be directly measured, they are usually approximated by a 1-step approximation method or by some other means.

In a controls setting however, the opposite of properties (P1) and (P2) is true. As mentioned above, uncertainty is assumed in $f(x)$ and Λ, and we assume that consistent and accurate sensor readings are available. Therefore the sequence (7.6) can be initialized using actual measurements of the system, and moreover the entire discretization scheme can be redefined to utilize the real-time measurement updates as

$$x_{n+1} = -\sum_{k=-K}^{0} \alpha_k x((n+k)T) + T \sum_{k=-K}^{0} \beta_k \left(f(x((n+k)T)) + \Lambda g(x((n+k)T)) u_{n+k} \right) \quad (7.7)$$

The following lemma shows that if T is small enough such that the sequence given in (7.6) is numerically stable and convergent, the sequence given in (7.7) is numerically stable and convergent as well.

Lemma 7.2.1. *Consider a continuous time system described by (7.4) where K equally spaced, exact measurements of the system state over the last KT seconds have been collected. For notational clarity, let one discrete time model of the system $\{\bar{x}_n\}$ be defined as*

$$\bar{x}_{n+1} = -\sum_{k=-K}^{0} \alpha_k \bar{x}_{n+k} + T \sum_{k=-K}^{0} \beta_k \left(f_{n+k} + \Lambda g_{n+k} u_{n+k} \right)$$

where $f_k = f(\bar{x}_k)$ and $g_k = g(\bar{x}_k)$, and let another discrete time model $\{x_n\}$ be defined by (7.7). If the sequence $\{\bar{x}_n\}$ is numerically stable and convergent, $\{x_n\}$ is also numerically stable and convergent.

Proof. The definition of every element in the sequence $\{x_n\}$ is equivalent to initializing the sequence $\{\bar{x}_n\}$ with K previous exact measurements of the state and progressing forward one time step using the explicit LMM form. In other words, if at any point in time n, initialization of $\{\bar{x}_n\}$ is done by exact measurements of the state, then $\bar{x}_{n+1} = x_{n+1}$. By definition, if $\{\bar{x}_n\}$ is numerically stable and convergent then there exists a constant $\epsilon(T)$ for which

$$|\bar{x}_n - x(nT)| < \epsilon(T) \ \ \forall n \tag{7.8}$$

By the above argument the following also holds,

$$|x_{n+1} - x((n+1)T)| < \epsilon(T) \tag{7.9}$$

Since this line of reasoning can be made regardless of the specific value of n, the condition (7.9) holds for all n, which implies that the sequence $\{x_n\}$ is numerically stable and convergent as intended. □

Since it has been proven that for small enough T, the discrete model given by (7.7) will be numerically stable and convergent, that sequence will be used as the discretization method of choice. Furthermore, the output equation can now be represented discretely as,

$$y_{n+1} = Cx_{n+1} = -C \sum_{k=-K}^{0} \alpha_k x((n+k)T) + CT \sum_{k=-K}^{0} \beta_k \left(f(x((n+k)T)) + \Lambda g(x((n+k)T)) u_{n+k} \right) \tag{7.10}$$

The scope is restricted to systems where the product $Cg(x)$ has full rank for all x. This allows for the development of a discrete time nonlinear dynamic inversion control law.

7.3 Control Law Development

Given the discussion of the previous section, the control objective is to drive the discretized output sequence $\{y_n\}$, defined in (7.10), to track a bounded desired reference trajectory, $\{y_n^*\}$. In other words, it is desired that

$$\lim_{n\to\infty} |y_n - y_n^*| = 0 \tag{7.11}$$

Due to the numerical stability and convergence conditions of LMMs, discussed in Section 7.2, achieving this control objective will guarantee that

$$\lim_{n\to\infty} |y(nT) - y_n^*| < \epsilon(T) \tag{7.12}$$

that is, the continuous time system will track the desired trajectory with bounded error. The non-linear dynamic inversion control law is given by

$$u_n = [Cg(x(nT))]^{-1}\left(-C\hat{f}(x(nT)) + \frac{1}{T\beta_0}(Ge(nT) + v_n)\right) \tag{7.13}$$

where $\hat{f}(x)$ is an assumed model for the open-loop dynamics, $e(nT)$ is the tracking error defined as $e(nT) = y(nT) - y_n^*$, the matrix $G \in \mathbb{R}^{p\times p}$ is a constant feedback gain and $v_n \in \mathbb{R}^p$ is a pseudo-control signal which will be made up of adaptive signals which can account for parameter uncertainty. Because C and Λ are assumed to have full rank and $n_s \geq p$, there exists a full rank, unknown constant matrix $\bar{\Lambda} = C\Lambda C^\dagger \in \mathbb{R}^{p\times p}$ where $C^\dagger$ is a pseudoinverse of C, such that $\bar{\Lambda}C = C\Lambda$. Therefore, substitution of the control law (7.13) into (7.10) results in

$$\begin{aligned} y_{n+1} = &-\sum_{k=-K}^{0} \alpha_k Cx((n+k)T) + T\sum_{k=-K}^{0} \beta_k \left(Cf(x((n+k)T)) - \bar{\Lambda}C\hat{f}(x((n+k)T))\right) \\ &+ \sum_{k=-K}^{0} \frac{\beta_k}{\beta_0}\bar{\Lambda}\left(Ge((n+k)T) + v_{n+k}\right) \end{aligned} \tag{7.14}$$

It is assumed that the following parameterization can be accurately formed,

$$T\left(Cf(x(nT)) - \bar{\Lambda}C\hat{f}(x(nT))\right) = W^T b(x(nT)) \tag{7.15}$$

where $W \in \mathbb{R}^{\ell \times p}$ is a matrix of unknown constant weights and $b(x(nT)) \in \mathbb{R}^{\ell}$ is a vector of known nonlinear basis functions that depend on the system state. Substitution into (7.14) results in

$$y_{n+1} = -\sum_{k=-K}^{0} \alpha_k Cx((n+k)T) + \sum_{k=-K}^{0} \beta_k W^T b(x((n+k)T)) + \frac{\beta_k}{\beta_0}\bar{\Lambda}\left(Ge((n+k)T) + v_{n+k}\right) \tag{7.16}$$

Each element of the output vector $y_{n+1,i}$ can be rewritten as

$$y_{n+1,i} = \phi_{n,i}^T \Theta_i \tag{7.17}$$

where

$$\phi_{n,i} = \left[v_n^T ... v_{n-K}^T \quad y_i(nT) ... y_i((n-K)T) \quad (Ge(nT))^T ... (Ge((n-K)T))^T \quad b^T(x(nT)) ... b^T(x((n-K)T))\right]^T \tag{7.18}$$

$$\Theta_i = \left[\frac{\beta_0}{\beta_0}\bar{\Lambda}_i ... \frac{\beta_{-K}}{\beta_0}\bar{\Lambda}_i \quad \alpha_0 ... \alpha_{-K} \quad \frac{\beta_0}{\beta_0}\bar{\Lambda}_i ... \frac{\beta_{-K}}{\beta_0}\bar{\Lambda}_i \quad \beta_0 W_i^T ... \beta_{-K} W_i^T\right]^T \tag{7.19}$$

The entries $\bar{\Lambda}_i$ and W_i^T represents the i^{th} row of $\bar{\Lambda}$ and W^T respectively. The expression (7.17), where $\phi_{n,i}$ is made up of known entries and Θ_i is made up of unknown entries is a common form used for solving discrete time *linear* adaptive control problems. Thus the nonlinear problem has successfully been transformed into a linear one for which several algorithms have been developed in the past [63, 64, 71]. In the following section one such adaptive algorithm is shown in order to solve for the pseudo-control, v_n, that will achieve the control objective. The presented algorithm

uses a projection adaptive law, which guarantees that the estimate of the unknown parameters, defined as $\hat{\Theta}_{n,i}$ remains bounded for all n.

7.4 Discrete Time Adaptive Control Algorithm

The system described by the discrete time model given by (7.7),(7.10) can be represented in the autoregressive moving average (ARMA) form by

$$\begin{bmatrix} A_1(q_d^{-1}) & \dots & 0 \\ \vdots & \ddots & \vdots \\ 0 & \dots & A_p(q_d^{-1}) \end{bmatrix} y_n = \begin{bmatrix} B_{1,1}(q_d^{-1}) & \dots & B_{1,(2p+\ell)}(q_d^{-1}) \\ \vdots & \ddots & \vdots \\ B_{p,1}(q_d^{-1}) & \dots & B_{p,(2p+\ell)}(q_d^{-1}) \end{bmatrix} \begin{bmatrix} v_n \\ Ge(nT) \\ b(x(nT)) \end{bmatrix} \tag{7.20}$$

where $A_i(q_d^{-1})$ and $B_{ij}(q_d^{-1})$ are scalar polynomials in the unit delay operator, q_d^{-1}. In order to guarantee stability of the closed-loop system, the following assumption must be satisfied

Assumption 7.4.1. *The system given by (7.20) must satisfy the condition that the matrix*

$$\begin{bmatrix} z^{-T}B_{1,1}(z) & \dots & z^{-T}B_{1,p}(z) \\ \vdots & \ddots & \vdots \\ z^{-T}B_{p,1}(z) & \dots & z^{-T}B_{p,p}(z) \end{bmatrix} \tag{7.21}$$

has full rank for $|z| < 1$.

Note that for each output $y_{n,i}$, at least one polynomial $B_{ij}(q_d^{-1})$, with $1 < j < p$, will have a leading coefficient associated with the unit delay operator q_d^{-1} raised to the power T. These are leading coefficients in the sense that for all i, j there are no terms in any of the polynomials $B_{ij}(q_d^{-1})$ of the form, $m_0(q_d^{-1})^{m_1}$ where m_0 is a constant coefficient and $m_1 < T$. Assumption (7.4.1) is equivalent to requiring that the matrix of these leading coefficients has full rank. This assumption is also equivalent to requiring that the transfer function between the output vector and the pseudo-control vector, v_n, be minimum-phase. The assumption is required in order to guarantee that if the

system parameters were known perfectly, any bounded desired output sequence could be achieved by a bounded pseudo-input sequence, $\{v_n\}$.

7.4.1 Mathematical Preliminaries

In order to proceed with the stability analysis, two technical lemmas must be introduced. The first lemma is common in discrete time adaptive control literature.

Lemma 7.4.1. *Given the real scalar sequences $\{s_n\}$, $\{b_{1,n}\}$, $\{b_{2,n}\}$ and the vector sequence $\{\sigma_n\}$ where*

$$\lim_{n\to\infty} \frac{s_n^2}{b_{1,n} + b_{2,n}\sigma_n^T\sigma_n} = 0 \tag{7.22}$$

If the following conditions hold,

$$0 < b_{1,n} < C_0 < \infty, \quad 0 < b_{2,n} < C_0 < \infty \ \ \forall n > 0 \tag{7.23}$$

$$\|\sigma_n\| < C_1 + C_2 \max_{0\le\tau\le n} |s_\tau| \tag{7.24}$$

where C_0, C_1, and C_2 are bounded constants, then

$$\lim_{n\to\infty} s_n = 0 \tag{7.25}$$

and $\{\|\sigma_n\|\}$ is bounded. Condition (7.23) is known as the uniform boundedness condition and condition (7.24) is known as the linear boundedness condition.

For a detailed proof of lemma 7.4.1, readers are directed to [63]. The second technical lemma is also common in the discrete adaptive control literature but is modified from its usual form to account for the nonlinear dynamic inversion controller.

Lemma 7.4.2. *Given the system (7.20) subject to Assumption 7.4.1, if*

$$\max_{\substack{1\leq i\leq p\\ 0\leq \tau\leq n+1}} |y_{\tau,i}| = C_3 \tag{7.26}$$

then there exist constants C_4 and C_5, such that

$$\left\| \begin{matrix} v_{n'} \\ Ge(n'T) \\ b((x(n'T))) \end{matrix} \right\| \leq C_4 + C_3C_5 \quad \forall\ 0 \leq n' \leq n \tag{7.27}$$

Proof. By requiring that the matrix (7.21) has full rank, Assumption 7.4.1 also implies that the matrix

$$\begin{bmatrix} z^{-T}B_{1,1}(z) & \dots & z^{-T}B_{1,(2p+\ell)}(z) \\ \vdots & \ddots & \vdots \\ z^{-T}B_{p,1}(z) & \dots & z^{-T}B_{p,(2p+\ell)}(z) \end{bmatrix} \tag{7.28}$$

has full rank for $|z| < 1$. This implies that (7.28) has a stable pseudoinverse which is all that is required to ensure that the inequality (7.27) holds. □

7.4.2 Adaptive Control Law

Let the discrete model tracking error, $\tilde{e}_n$, be defined as

$$\tilde{e}_n = y_n - y_n^* \tag{7.29}$$

As was shown in equations (7.11), (7.12) if the control objective of driving $\{\tilde{e}_n\} \to 0$ as $n \to \infty$ is achieved it will imply that $e(nT)$ is bounded as $n \to \infty$. Referencing (7.17) it is clear that if the pseudo-control law could be calculated such that

$$y_{n+1,i}^* = \phi_{n,i}^T \Theta_i \tag{7.30}$$

for all i, the control objective would be met. Note that in the output equation given by (7.16), the coefficient of v_n is the full rank matrix $\bar{\Lambda}$. This implies that in the known parameter case, i.e. if Θ_i were known perfectly for all i, a unique solution would always exist for v_n. Since the real Θ_i are not known, the pseudo-control law is instead calculated using the equation

$$y^*_{n+1,i} = \phi^T_{n,i}\hat{\Theta}_{n,i} \tag{7.31}$$

where $\{\hat{\Theta}_{n,i}\}$ is a sequence of estimates of the true parameters Θ_i which is updated through the adaptive law,

$$\hat{\Theta}_{n,i} = \hat{\Theta}_{n-1,i} + \frac{a_n\phi_{n-1,i}}{\Gamma_{\Theta,i} + \phi^T_{n-1,i}\phi_{n-1,i}}\left(y_{n,i} - \phi^T_{n-1,i}\hat{\Theta}_{n-1,i}\right) \tag{7.32}$$

where $0 < \Gamma_{\Theta,i} < \infty$ is a designer chosen bounded gain term. The term a_n is specifically designed to guarantee that the coefficient of v_n in the pseudo-control law (7.31) is nonsingular and therefore a unique solution for v_n will always exist. Given some $\bar{\epsilon}$ such that $0 < \bar{\epsilon} < 1$, the term a_n must satisfy the following two conditions

$$\bar{\epsilon} < a_n < 2 - \bar{\epsilon} \tag{7.33}$$

$$a_n \text{ is not an eigenvalue of } -R^{-1}_{n-1}Q_n \tag{7.34}$$

where

$$S = \begin{bmatrix} I_{p\times p} & 0_{p\times(3K+2)p+(K+1)\ell} \end{bmatrix}$$

$$R_{n-1} = \begin{bmatrix} r_1 & \dots & r_p \end{bmatrix}$$

$$r_i = S\hat{\Theta}_{n-1,i}$$

$$Q_n = \begin{bmatrix} q_1 & \dots & q_p \end{bmatrix}$$

$$q_i = S\frac{\phi_{n-1,i}}{\Gamma_{\Theta,i} + \phi_{n-1,i}^T\phi_{n-1,i}}\left(y_{n,i} - \phi_{n-1,i}^T\hat{\Theta}_{n-1,i}\right)$$

Each r_i is a vector of the coefficients of v_n in $\hat{\Theta}_{n-1,i}$ and each q_i is a vector of the changes to those coefficients each time the adaptive law (7.32) is applied. Setting $a_n = 1$ will almost always allow for a unique solution for v_n and therefore, the proof that (7.33) and (7.34) guarantee a unique solution is omitted. Readers are once again directed to [63]. The adaptive law (7.32) is considered a projection algorithm because through its use, $\{\hat{\Theta}_{n,i}\}$ will never become unbounded. This will be proven in the following section. It will also be shown that through the use of this adaptive law, along with the pseudo-control law (7.31) and the actual NDI control law (7.13) the control objective will be achieved.

7.4.3 Stability Proof

Lemma 7.4.3. *Given the system (7.17), application of the pseudo-control law (7.31) and the adaptive law (7.32) results in*

$$\|\tilde{\Theta}_{n,i}\|^2 - \|\tilde{\Theta}_{n-1,i}\|^2 \leq 0 \tag{7.35}$$

$$\lim_{n\to\infty} \frac{\tilde{e}_{n,i}}{\left(\Gamma_{\Theta,i} + \phi_{n,i}^T\phi_{n,i}\right)^{1/2}} = 0 \tag{7.36}$$

for all i where $\tilde{\Theta}_{n,i} = \hat{\Theta}_{n,i} - \Theta_i$.

Proof. Using the adaptive law (7.32), the vector $\tilde{\Theta}_{n,i}$ can be written as

$$\tilde{\Theta}_{n,i} = \tilde{\Theta}_{n-1,i} - \frac{a_n \phi_{n-1,i}}{\Gamma_{\Theta,i} + \phi_{n-1,i}^T \phi_{n-1,i}} \left(\phi_{n-1,i}^T \tilde{\Theta}_{n-1,i} \right) \tag{7.37}$$

This implies that

$$\|\tilde{\Theta}_{n,i}\|^2 - \|\tilde{\Theta}_{n-1,i}\|^2 = a_n \left(-2 + a_n \frac{\|\phi_{n-1,i}\|^2}{\Gamma_{\Theta,i} + \|\phi_{n-1,i}\|^2} \right) \left(\frac{(\phi_{n-1,i}^T \tilde{\Theta}_{n-1,i})^2}{\Gamma_{\Theta,i} + \|\phi_{n-1,i}\|^2} \right) \tag{7.38}$$

which is less than or equal to zero as long as $a_n < 2$, a condition that is guaranteed by its definition in (7.33). Thus, (7.35) is proven. Moreover, this implies that $\tilde{\Theta}_{n,i}$ is a bounded, non-increasing function and therefore it converges.

Note that the third term on the right hand side of (7.38) can be rewritten as

$$\frac{(\phi_{n-1,i}^T \tilde{\Theta}_{n-1,i})^2}{\Gamma_{\Theta,i} + \|\phi_{n-1,i}\|^2} = \frac{(\phi_{n-1,i}^T \hat{\Theta}_{n-1,i} - \phi_{n-1,i}^T \Theta_i)^2}{\Gamma_{\Theta,i} + \phi_{n-1,i}^T \phi_{n-1,i}} = \frac{(y_{n-1,i} - y_{n-1,i}^*)^2}{\Gamma_{\Theta,i} + \phi_{n-1,i}^T \phi_{n-1,i}} = \frac{\tilde{e}_{n-1,i}^2}{\Gamma_{\Theta,i} + \phi_{n-1,i}^T \phi_{n-1,i}} \tag{7.39}$$

Therefore, since $0 < a_n < 2$, condition (7.35), which has now been proven, implies that

$$\lim_{n \to \infty} \frac{\tilde{e}_{n-1,i}^2}{\Gamma_{\Theta,i} + \phi_{n-1,i}^T \phi_{n-1,i}} = 0 \tag{7.40}$$

which also implies,

$$\lim_{n \to \infty} \frac{\tilde{e}_{n-1,i}}{\left(\Gamma_{\Theta,i} + \phi_{n-1,i}^T \phi_{n-1,i} \right)^{1/2}} = 0 \tag{7.41}$$

Through a unit time shift (7.41) is equivalent to (7.36). □

Theorem 8. *Consider the nonlinear continuous time system with discrete controls described by (7.4) where T is small enough such that the linear multistep method approximation given by (7.6) is numerically stable and convergent. If the nonlinear dynamic inversion control law (7.13) is implemented with the pseudo-control signal v_n being calculated using (7.31) and (7.32) and if*

Assumption 7.4.1 is satisfied, then $\{y_n\}$, $\{u_n\}$ *are bounded and*

$$\lim_{n\to\infty} \tilde{e}_n = 0 \tag{7.42}$$

which ensures that $e(nT)$*, the tracking error for the continuous time system is bounded.*

Proof. Examining (7.36), the second result of Lemma 7.4.3, it can be seen that the uniform boundedness condition is satisfied as

$$0 < b_{1,n} = \Gamma_{\Theta,i} < C_0 < \infty \qquad 0 < b_{2,n} = 1 < C_0 < \infty \ \ \forall n > 0 \tag{7.43}$$

Assumption 7.4.1 and Lemma 7.4.2 imply that

$$\left\| \begin{matrix} v_{n'} \\ Ge(n'T) \\ b((x(n'T))) \end{matrix} \right\| \leq C_4 + C_5 \max_{\substack{1\leq i\leq p \\ 0\leq\tau\leq n+1}} |y_{\tau,i}| \quad \forall \ 0 \leq n' \leq n \tag{7.44}$$

Therefore, using (7.18), the definition of $\phi_{n,i}$, it can be shown that

$$\|\phi_{n,i}\| \leq K \left(C_4 + \max(C_5, 1) \max_{\substack{1\leq i\leq p \\ 0\leq\tau\leq n+1}} |y_{\tau,i}| \right) \tag{7.45}$$

Since it is assumed that the desired trajectory sequence $\{y^*_{n,i}\}$ is bounded, there exists a constant C_6 such that

$$y^*_{n,i} \leq C_6 \quad \forall \ n \tag{7.46}$$

Therefore,

$$|\tilde{e}_{n,i}| \geq |y_{n,i}| - |y^*_{n,i}| \geq |y_{n,i}| - C_6 \tag{7.47}$$

Furthermore, there exists a constant $C_7 \geq 1$ such that

$$\max_{\substack{1\leq i\leq p\\ 0\leq\tau\leq n+1}} |y_{\tau,i}| \leq C_7 \max_{0\leq\tau\leq n+1} |y_{\tau,j}| \quad \forall \ 1 \leq j \leq p. \tag{7.48}$$

The inequalities (7.47) and (7.48) imply that

$$\|\phi_{n,i}\| \leq K \left(C_4 + \max(C_5, 1) C_7 \max_{0\leq\tau\leq n+1} (|\tilde{e}_{\tau,i}| + C_6) \right) \quad \forall \ 0 \leq n' \leq n \tag{7.49}$$

which, after collecting terms and redefining constants, allows one to write

$$\|\phi_{n,i}\| \leq C_1^* + C_2^* \max_{0\leq\tau\leq n+1} |\tilde{e}_{\tau,i}| \tag{7.50}$$

where C_1^* and C_2^* are bounded constants. Therefore, the linear boundedness condition is satisfied as well and Lemma 7.4.1 can be invoked. This implies

$$\lim_{n\to\infty} \tilde{e}_{n,i} = 0 \tag{7.51}$$

and $\{\phi_{n,i}\}$ is bounded. The boundedness of $\{\phi_{n,i}\}$ ensures the boundedness of $\{v_n\}$ and $\{y_{n,i}\}$. Furthermore, since the line of reasoning used in this proof can be made for all i,

$$\lim_{n\to\infty} \tilde{e}_n = 0 \tag{7.52}$$

and $\{\phi_{n,i}\}$, $\{y_{n,i}\}$ are bounded for all i. This implies that $e(nT)$ is bounded. Since it was assumed that $f(x)$ (and therefore $\hat{f}(x)$) is bounded for bounded x and that $Cg(x)$ is invertible for all x, the above implies that $\{u_n\}$ is bounded as well. □

Remark 7.4.1. **Commentary on Bounding the Control Sample Time, T:**

Several conditions must be considered in order to produce and estimate of how large T can get such that the above stability analysis will hold. First and foremost, the region of convergence for the chosen explicit LMM must be analyzed. Linearizing the nonlinear system to establish an approximate bound or Monte Carlo analysis could be used to achieve this. Secondly, Assumption 7.4.1 must hold, which may or may not depend on T.

Another thing to consider that could be affected by the sample time is the violation of actuator position or rate constraints. Assumption 7.4.1 guarantees that a bounded desired output can be achieved by a bounded input, but surely there is some relationship between T and how large of an input is required.

7.5 F-16 Simulation Example

7.5.1 Simulation Setup

The sampled-data nonlinear dynamic inversion adaptive controller was implemented on a nonlinear simulation of an F-16 aircraft developed by Ying Huo at the University of Southern California, based off of the equations of motion and data given in [72, 73]. In order to accurately test the above theory, the simulation was modified such that the aircraft was equipped with discrete controls with a fixed sample time, T. The vehicle's state vector $x \in \mathbb{R}^{13}$ is given by

$$x = \begin{bmatrix} V_T & \alpha & \beta & \phi & \theta & \psi & p & q & r & N_{dis} & E_{dis} & h & P_{eng} \end{bmatrix}^T$$

and the output desired to be controlled was the vehicle's body-fixed angular rates,

$$y = \begin{bmatrix} p & q & r \end{bmatrix}^T$$

The output dynamics used in the simulation are given by the following differential equations,

$$\dot{p} = \frac{I_y - I_z}{I_x} qr + \frac{I_{xz}}{I_x}(\dot{r} + pq) + \frac{\bar{q}Sb}{I_x} C_\ell$$
$$\dot{q} = \frac{I_z - I_x}{I_y} pr + \frac{I_{xz}}{I_y}(r^2 - p^2) + \frac{\bar{q}S\bar{c}}{I_x} C_m - (h_E)r$$
$$\dot{r} = \frac{I_x - I_y}{I_z} pq + \frac{I_{xz}}{I_z}(\dot{p} - qr) + \frac{\bar{q}Sb}{I_z} C_n + (h_E)q$$

where the aerodynamic coefficients C_ℓ, C_m, C_n are modeled in lookup tables based on wind tunnel test data found in [73]. In order to formulate an estimate of the output dynamics ($C\hat{f}(x)$) these coefficients were approximated as constant coefficient polynomials of the form

$$\hat{C}_\ell = \hat{\Theta}_{L1}\beta + \hat{\Theta}_{L2}\tfrac{b}{2V_T}p + \hat{\Theta}_{L3}\tfrac{b}{2V_T} + \hat{\Theta}_{L4}\delta_a + \hat{\Theta}_{L5}\delta_r$$

$$\hat{C}_m = \hat{\Theta}_{M1} + \hat{\Theta}_{M2}\alpha + \hat{\Theta}_{M3}\tfrac{\bar{c}}{2V_T}q + \hat{\Theta}_{M4}\tfrac{\bar{c}}{2V_T}\alpha q + \hat{\Theta}_{M5}\tfrac{\bar{c}}{2V_T}\alpha^2 q + \hat{\Theta}_{M6}\tfrac{\bar{c}}{2V_T}\alpha^3 q + \hat{\Theta}_{M7}\alpha^4 + \hat{\Theta}_{M8}\delta_e$$
$$+\hat{\Theta}_{M9}\alpha^2\delta_e + \hat{\Theta}_{M10}\alpha^3\delta_e$$

$$\hat{C}_n = \hat{\Theta}_{N1}\beta + \hat{\Theta}_{N2}\tfrac{b}{2V_T}p + \hat{\Theta}_{N3}\tfrac{b}{2V_T}r + \hat{\Theta}_{N4}\beta^2 + \hat{\Theta}_{N5}\beta^3 + \hat{\Theta}_{N6}\delta_a + \hat{\Theta}_{N7}\delta_r$$

The methodology for forming these polynomials along with the values used for the constant coefficients, $\hat{\Theta}_i$, can be found in [74]. The nonlinear coefficients associated with the control effectors $\delta_a, \delta_e, \delta_r$ made up the matrix $C\hat{\Lambda}g(x)$ while the remaining terms were included in $C\hat{f}(x)$. Additive uncertainty was also included in the estimated moment of inertia values as

$$\hat{I}_x = I_x + 10 \text{ slug-ft}^2$$
$$\hat{I}_y = I_y + 20 \text{ slug-ft}^2$$
$$\hat{I}_z = I_z + 20 \text{ slug-ft}^2$$
$$\hat{I}_{xz} = I_{xz} + 5 \text{ slug-ft}^2$$

For this simulation study, the explicit linear multistep method selected to approximate the nonlinear system with a discrete time model was the second-order Adams-Bashforth method. This method

is characterized by the coefficient set

$$\alpha_1 = 1 \qquad \alpha_0 = -1 \qquad \alpha_k = 0 \ \ \forall k < 0$$
$$\beta_0 = \frac{3}{2} \qquad \beta_{-1} = -\frac{1}{2} \qquad \beta_k = 0 \ \ \forall k < -1$$

such that the discrete time output, Equation (7.10), can be written as

$$y_{n+1} = y(nT) + \frac{3T}{2} C \left(f(x(nT)) + \Lambda g(x(nT)) \begin{bmatrix} \delta_{a,n} \\ \delta_{e,n} \\ \delta_{r,n} \end{bmatrix} \right) - \frac{T}{2} C \left(f(x((n-1)T)) + \Lambda g(x((n-1)T)) \begin{bmatrix} \delta_{a,n-1} \\ \delta_{e,n-1} \\ \delta_{r,n-1} \end{bmatrix} \right)$$

The vehicle is equipped with throttle control which was kept at the trim value throughout the duration of the simulation. Therefore, the control law (7.13) is only applied to vehicle's control surfaces: aileron, elevon and rudder. The basis functions used, which were defined in (7.15) and help to account for the uncertainty in the moment coefficients and the moment of inertia values, were given by the vector

$$b(x(nT)) =$$
$$\left[\begin{array}{cccccccccccccc} \beta & \frac{b}{2V_T}p & \frac{b}{2V_T}r & 1 & \alpha & \frac{\bar{c}}{2V_T}q & \frac{\bar{c}}{2V_T}\alpha q & \frac{\bar{c}}{2V_T}\alpha^2 q & \frac{\bar{c}}{2V_T}\alpha^3 q & \alpha^4 & \beta^2 & \beta^3 & pr & pq \quad qr \quad r^2 - p^2 \end{array} \right]^T$$

The adaptive gain terms $\Gamma_{\Theta,i}$ were set as

$$\begin{bmatrix} \Gamma_{\Theta,p} \\ \Gamma_{\Theta,q} \\ \Gamma_{\Theta,r} \end{bmatrix} = \begin{bmatrix} 0.01 \\ 1 \\ 1 \end{bmatrix} \tag{7.53}$$

and the feedback gain G was set as $10\mathbf{1}_3$. Having specified the Adams-Bashforth second-order method and defining the basis functions, the known vectors $\phi_{n,i}$ given in (7.18) can be defined more specifically as

$$\phi_{n,i} = \begin{bmatrix} v_n^T & v_{n-1}^T & y_i(nT) & (Ge(nT))^T & (Ge((n-1)T))^T & b^T(x(nT)) & b^T(x(n-1)T) \end{bmatrix}^T$$

such that

$$y_{n+1,i} = \phi_{n,i}^T \Theta_i$$

as required by the theory. With $C\hat{f}(x)$, $g(x)$, $b(x(nT))$, and $\phi_{n,i}$ defined, the control law (7.13) can be implemented.

7.5.2 Results

Two test cases were used to evaluate the effectiveness of the presented control framework and to analyze the effect of varying controller sample times. In the first case a sample time of $T = 0.1sec$ $(10Hz)$ was used and in the second case a sample time of $T = 0.4sec$ $(2.5Hz)$ was used. The same desired trajectory, $\{y_n^*\}$, was used for both cases and was designed specifically to excite both the longitudinal and lateral/directional axes of the aircraft.

For comparison purposes, the baseline tracking controller presented in Section 1 was also implemented in the F-16 simulation using a sampler and a zero-order hold. The purpose of this comparison was to demonstrate the fact that provably stable continuous time control laws can lead to instability once sampling is introduced to the system. The values of the control deflections were calculated according to the continuous time control law at each sample time T and kept constant for the remainder of the sampling period.

For each simulation that was analyzed, the vehicle was initialized at a trim condition of $V_T = 750ft/s$, $h = 20,000ft$ and $x_{cg} = 0.25\bar{c}$.

Test Case 1: $T = 0.1s$

The chosen desired trajectory consists of a doublet command for the body-axis roll rate p and a step command and hold for the body-axis pitch rate q followed by a return to commanding $q = 0$. In order to excite both axes of the aircraft the pitch rate step command is given before the roll rate maneuver has been completed. Figure 7.1 shows the trajectory of the system outputs for the first case. The sampled-data control law allows the vehicle to closely track the reference trajectory despite the dynamic coupling and parametric uncertainty. When the continuous time control law is implemented with the sampling time $T = 0.1s$, the vehicle roughly follows the reference trajectory however it is clear that the tracking performance is not as good as the performance generated using the sampled-data law. In Figure 7.2 the control signals, aerodynamic angles (α and β), and Euler angle trajectories are presented. Once again the sampled-data control law is compared with the sampled, continuous time control law.

Test Case 2: $T = 0.4s$

During the second test case, the reference trajectory remained the same but the sampling rate was slowed to $2.5Hz$. Figure 7.3 shows the trajectories for the system outputs for this case. The sampled-data control law was once again able to track the reference trajectory although a clear degradation in performance is seen with the longer sampling period. In particular, the vehicle's roll and yaw rates become slightly oscillatory. On the other hand, the continuous time control law quickly destabilizes the system. Despite extensive tuning, no set of gains was found for which the system did not diverge when the continuous time controller was implemented with a sampling rate of $2.5Hz$. The performance benefits of utilizing a control law specifically designed for a system with discrete controls are clear. Figure 7.4 once again shows the control signal, aerodynamic angle, and Euler angle trajectories.

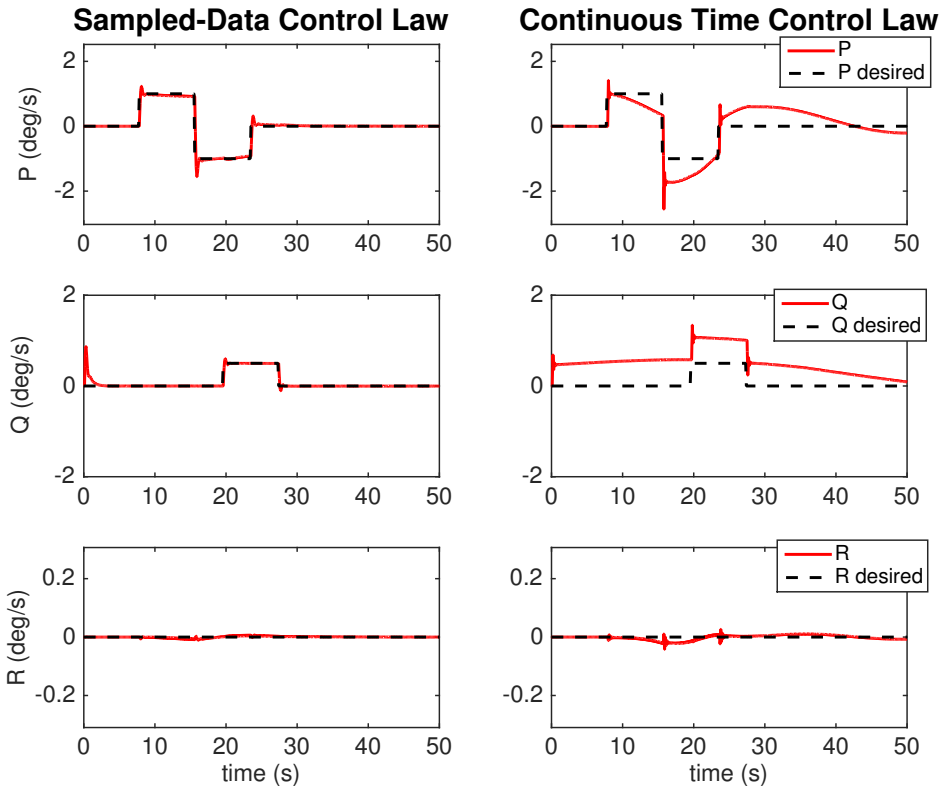

Figure 7.1: Output trajectories for Test Case 1. Results using the sampled-data control law are shown on the left, results using the continuous time control law are shown on the right.

7.6 GHV Simulation Example

The sampled-data NDI adaptive controller was also implemented on the generic hypersonic vehicle simulation. Although hypersonic vehicles are typically equipped with very fast actuators, this simulation study was done in order to test out how the sampled-data control law performs on a system with very fast dynamics. Therefore, the GHV was modified such that a digital control signal with a designer chosen controller sample time could be implemented.

The control objective was to track a desired body-axis angular rate trajectory. In all examples shown the GHV was commanded to track the same trajectory as the F-16 in Section 7.5, once again exciting both the longitudinal and lateral/directional modes simultaneously. The parameter

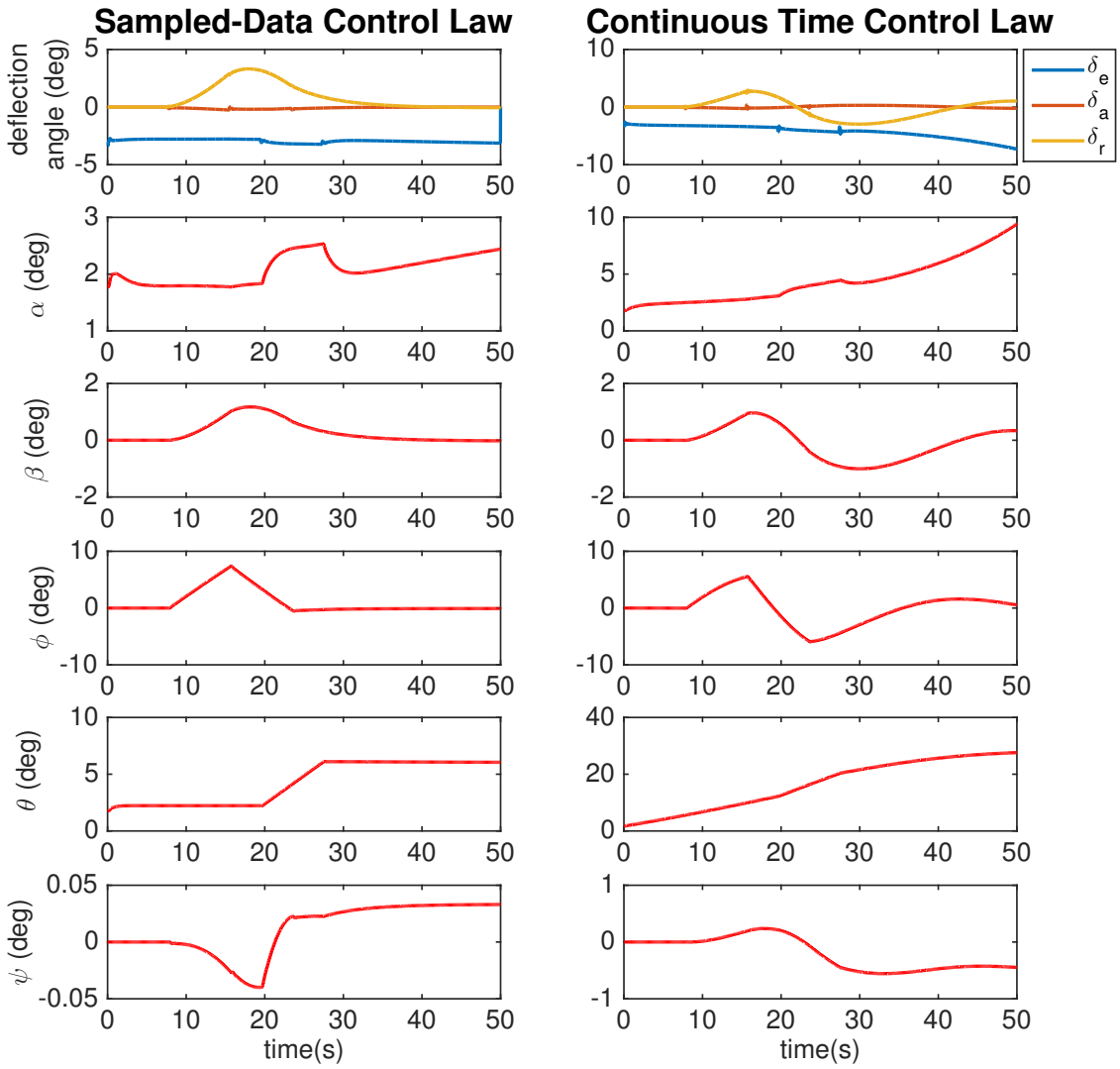

Figure 7.2: Controls, aerodynamic angles, and Euler angles for Test Case 1. Results using the sampled-data control law are shown on the left, results using the continuous time control law are shown on the right.

uncertainty included in the dynamical model had the same bounds as those used in the simulation studies of Sections 2 and 3. The basis functions used in the adaptive law, $b(x(nT))$, are given by

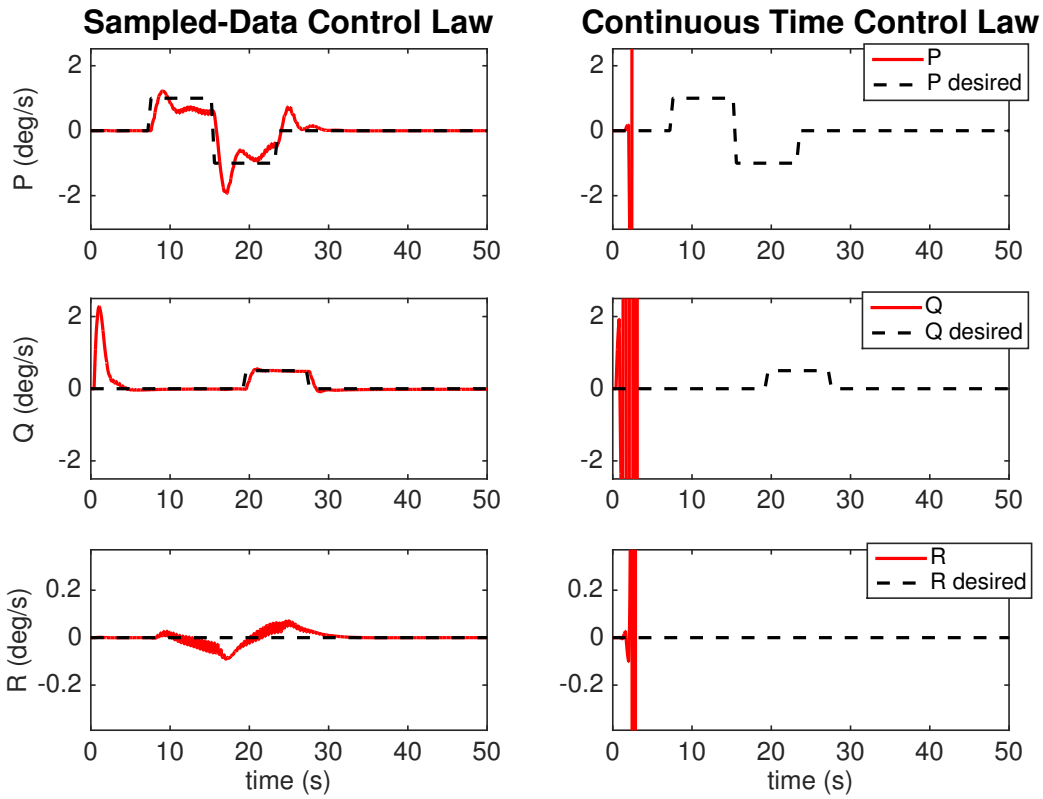

Figure 7.3: Output trajectories for Test Case 2. Results using the sampled-data control law are shown on the left, results using the continuous time control law are shown on the right.

Equation (2.50). The adaptive gain terms $\Gamma_{\Theta,i}$ were set as

$$\begin{bmatrix} \Gamma_{\Theta,p} \\ \Gamma_{\Theta,q} \\ \Gamma_{\Theta,r} \end{bmatrix} = \begin{bmatrix} 1 \\ 1 \\ 1 \end{bmatrix} \tag{7.54}$$

and the feedback gain G was set as $\mathbf{1}_3$. Once again, the explicit LMM used was the second-order Adams-Bashforth method. No time delay was included in the simulation and the initial flight condition was a velocity of Mach 6 and an altitude of $80,000 ft$.

Test Case 1: Comparision with Continuous Time Control Law with Zero-Order Hold

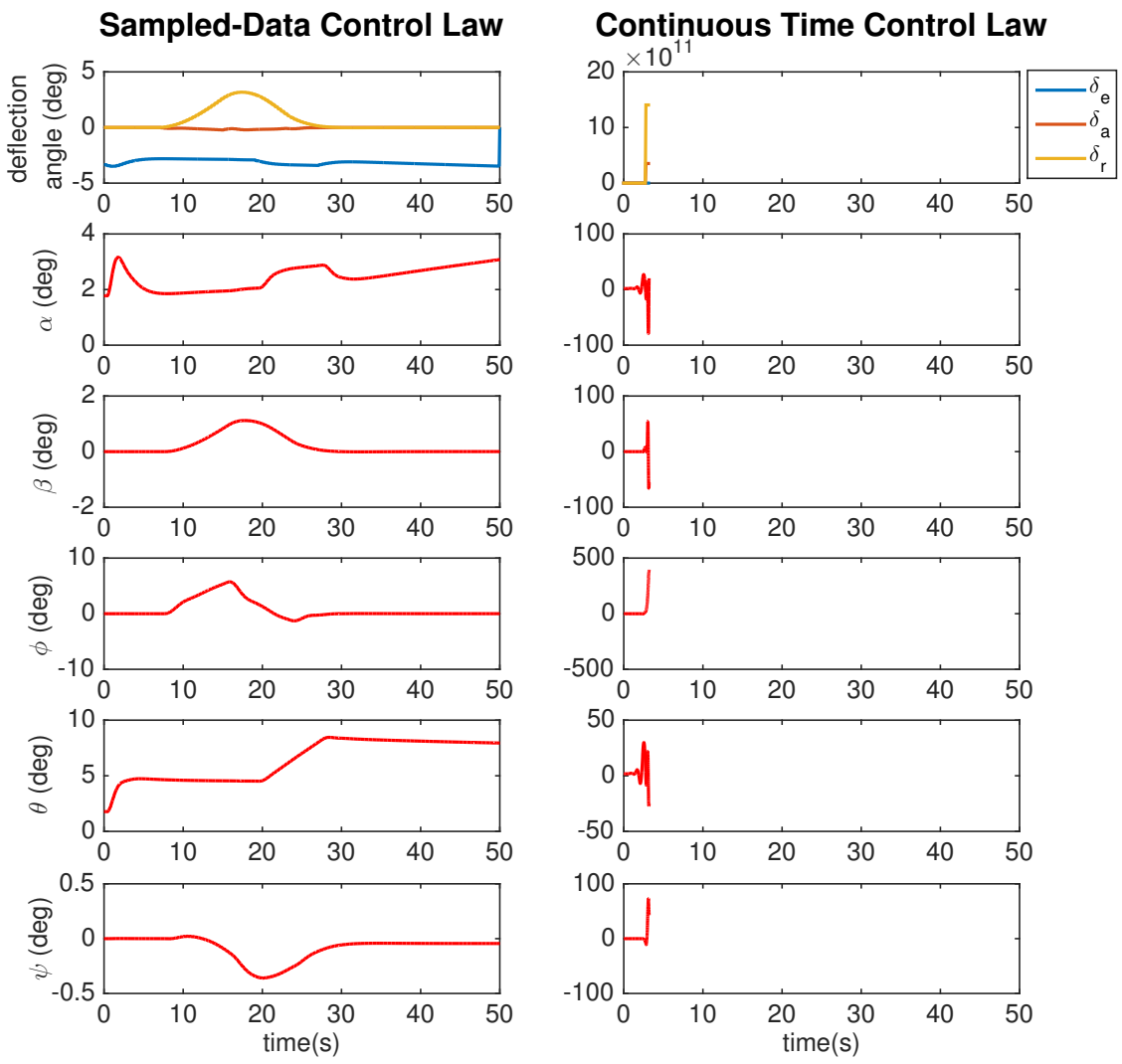

Figure 7.4: Controls, aerodynamic angles, and Euler angles for Test Case 2. Results using the sampled-data control law are shown on the left, results using the continuous time control law are shown on the right.

The sampled-date control law was compared with the baseline tracking NDI controller of Section 1. The continuous time control law was implemented using a sampler and zero-order hold. The controller sample time used in the simulation was $T = 0.01s$. Any sample time larger than this led to an extremely oscillatory response when using the continuous time control law. The sampled-data

control law was able to handle larger control sample times, as will be shown in Test Case 2. Figure 7.5 shows the tracking performance comparison between the two control laws. The response using the continuous time control law is much more oscillatory than the sampled-data controller. Additionally, the sampled-data controller has no problem achieving the control objective despite the extremely fast dynamics. The aerodynamic angles, total velocity, and control surface deflections are shown in Figure 7.6 and the Euler angles are shown in Figure 7.7.

Test Case 2: Controller Sample Time Comparison

In this test case, the controller sample time was varied in order to see how large of a sample time the controller could handle while still producing an acceptable vehicle response. Figure 7.8 shows the response of three different samples times: $T = 0.05s$, $T = 0.1s$ and $T = 0.15s$. As the sample time increases, more oscillation is seen in the response. Nevertheless, this test case demonstrates the ability of the sampled-data NDI control law to successfully track a reference trajectory on a hypersonic vehicle with a controller sampling frequency of $10Hz$ or slower. The aerodynamic angles, total velocity, and control surface deflections are shown in Figure 7.9 and the Euler angles are shown in Figure 7.10.

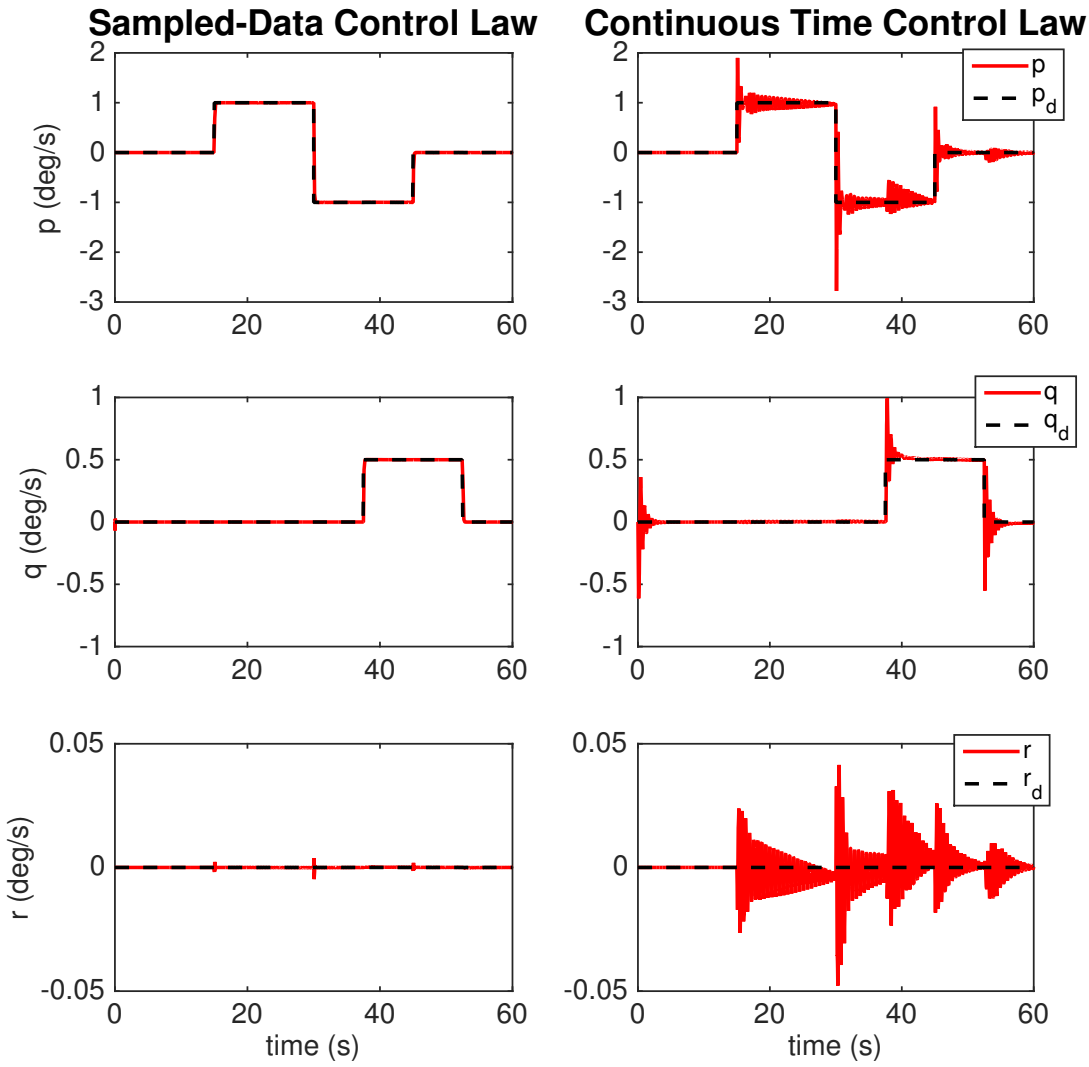

Figure 7.5: GHV comparison of sampled-data control law and continuous time control law with sampler. $T = 0.01s$

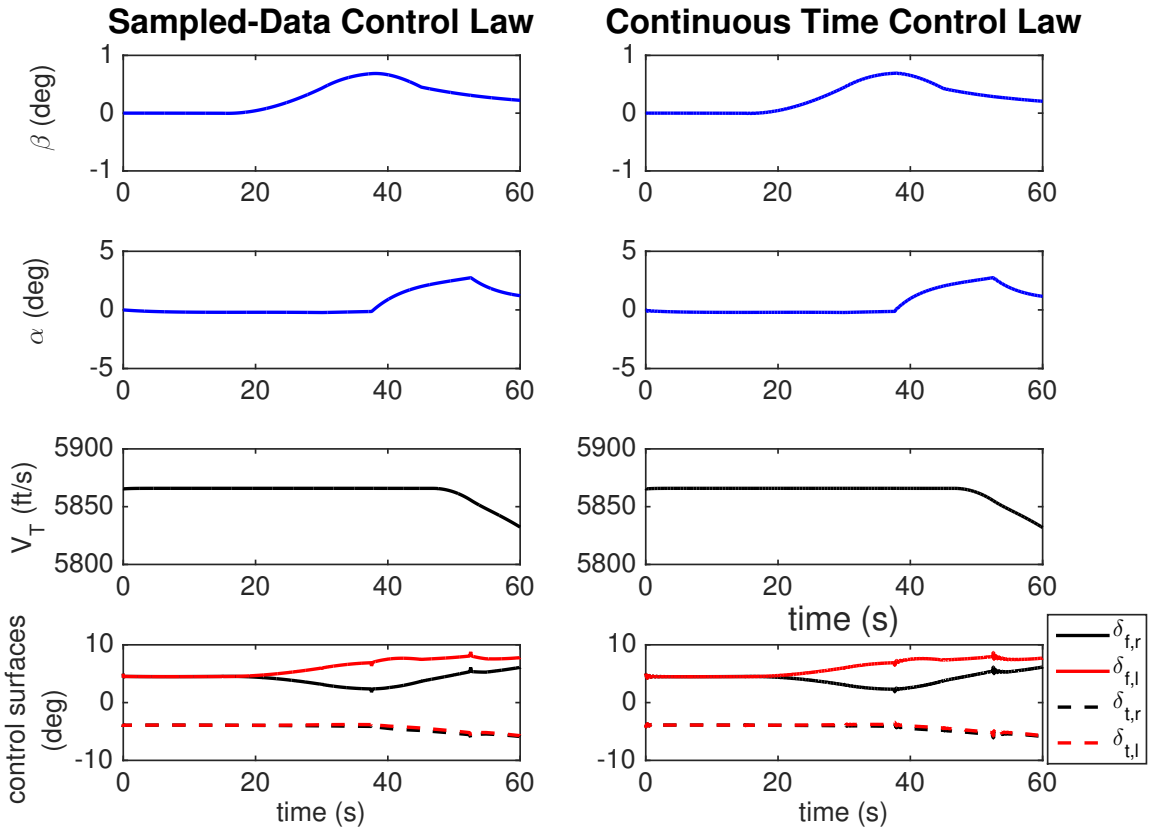

Figure 7.6: GHV comparison of sampled-data control law and continuous time control law with sampler. Aerodynamic angles, total velocity and control surface deflections are shown.

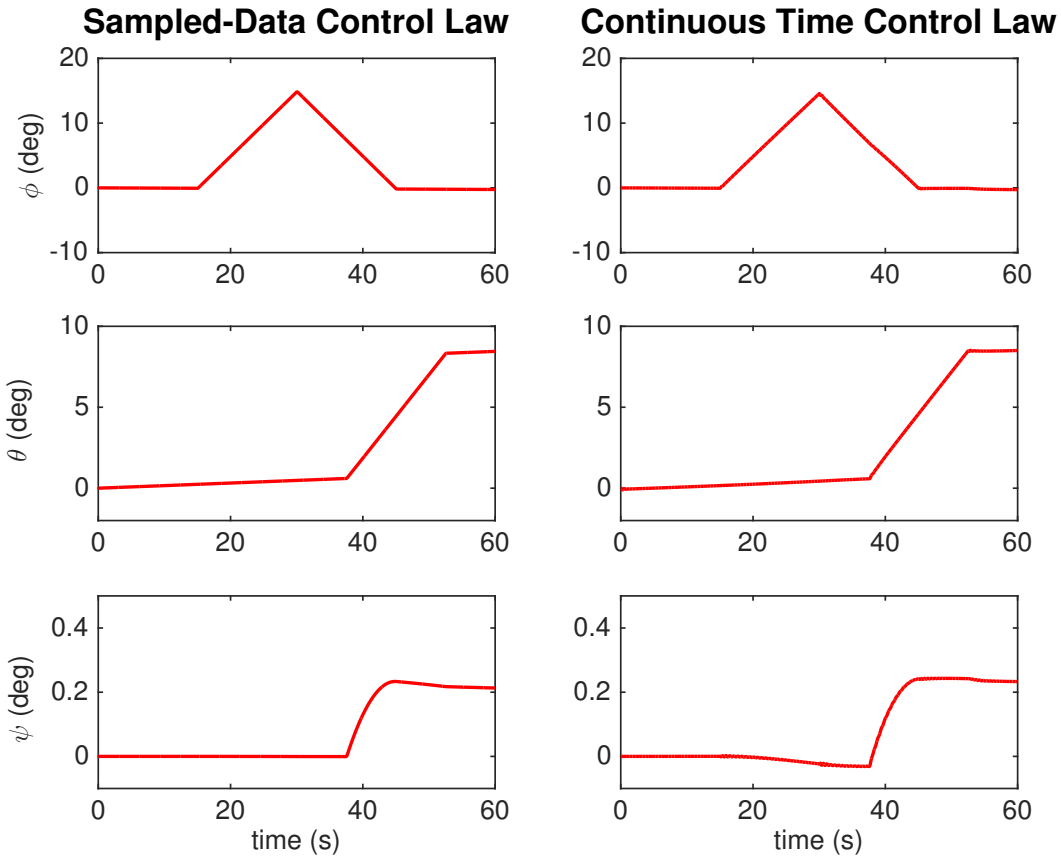

Figure 7.7: GHV comparison of sampled-data control law and continuous time control law with sampler. Euler angles are shown.

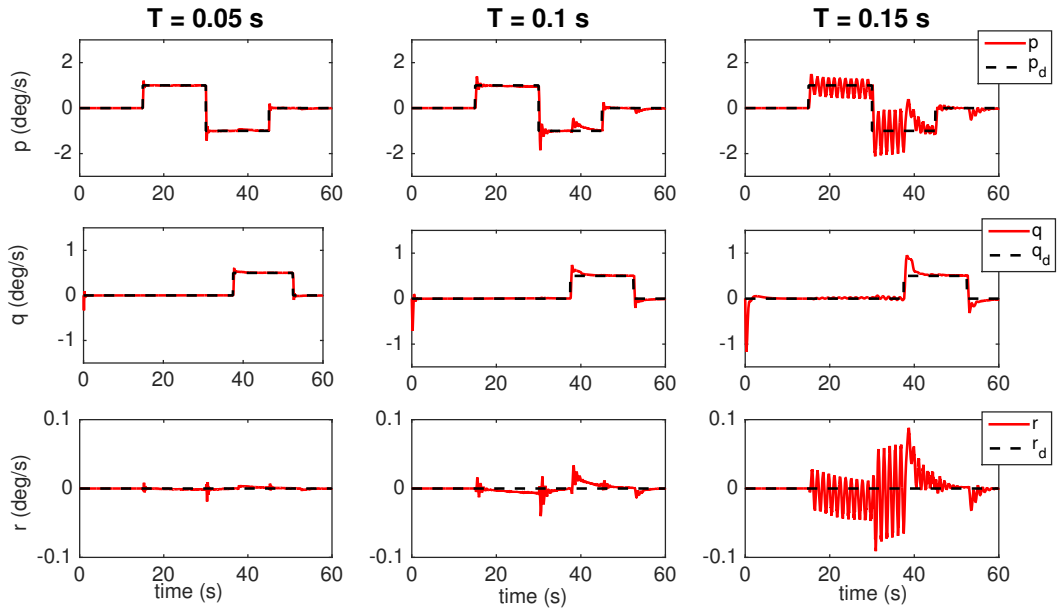

Figure 7.8: GHV comparison of different controller sample times.

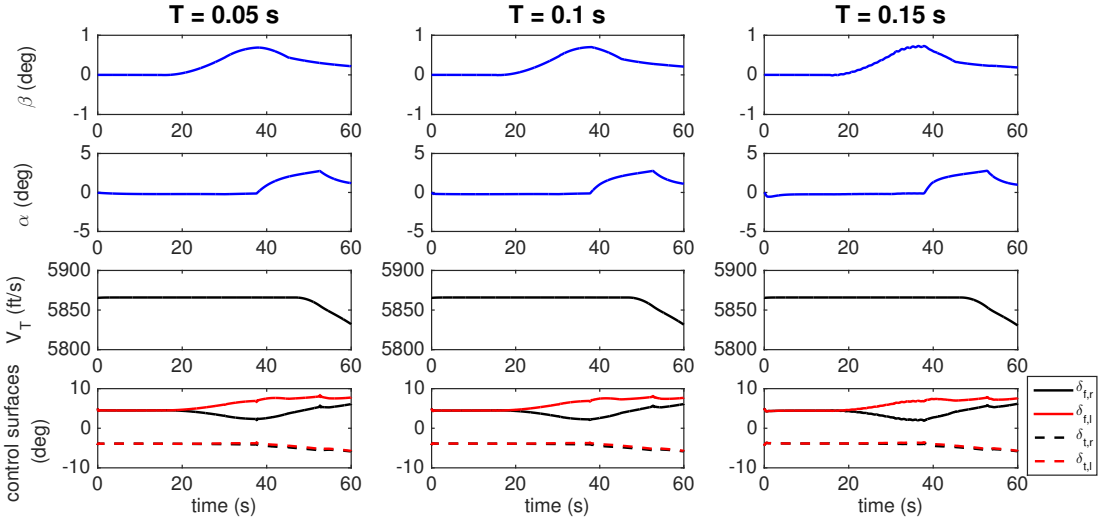

Figure 7.9: GHV comparison of different controller sample times. Aerodynamic angles, total velocity and control surface deflections are shown.

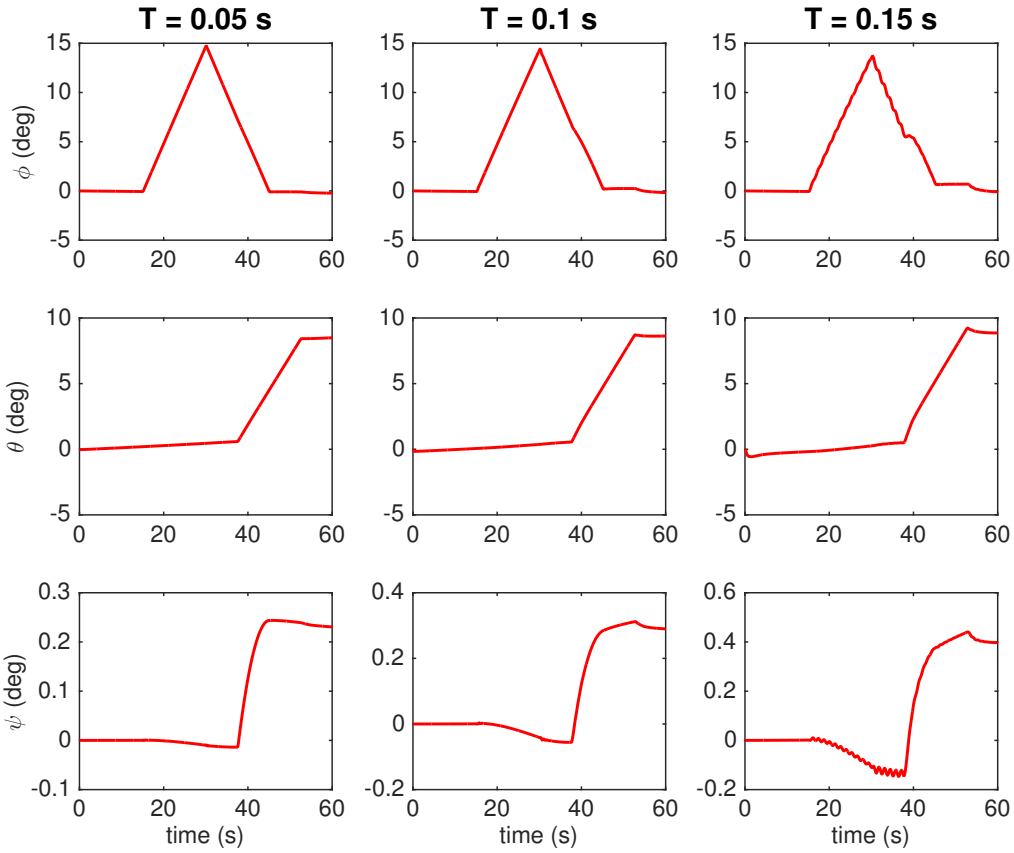

Figure 7.10: GHV comparison of different controller sample times. Euler angles are shown.

8. CONCLUSIONS

This dissertation extended the technique of nonlinear dynamic inversion adaptive control to address several practical problems in control theory: specifically in hypersonic flight control. Novel approaches were developed for each of the research issues presented in Section 1.1. Except when specifically noted and justified, all of the algorithms presented in this dissertation were rigorously proven to produce stable system responses. Furthermore, the controllers developed herein were demonstrated in nonlinear simulation and shown to be potentially useful algorithms for controlling hypersonic vehicles. The following conclusions are drawn:

1. Two state constraining nonlinear dynamic inversion adaptive controllers were developed and rigorously proven to stabilize a nonlinear system containing parametric uncertainty. It was shown that the desired system outputs are bounded to their designer chosen constraint sets. If nothing is forcing the outputs outside of the constraint set, the two developed control laws drive the system to asymptotically track a reference command. It was shown in simulation that both the Sliding Mode State Constraint controller and the Bounding Function State Constraint controller were able to successfully achieve the control objective in the presence of unacceptable trajectory commands or external disturbances.

2. Although both the Sliding Mode State Constraint and Bounding Function State Constraint techniques avoided excessive chattering by the actuators, the Bounding Function State Constraint controller in general produced a smoother control signal. Overall, the Bounding Function State Constraint controller was easier to implement than the Sliding Mode State Constraint controller, primarily due to the flexibility that this technique allows for in defining the constraint set. For this reason, the Bounding Function State Constraint technique was chosen to be combined with the nonlinear observer in Section 6.

3. A nonlinear observer was introduced that allowed for accurate estimation of an air vehi-

cle's angle-of-attack and sideslip angle despite noisy measurement signals. This estimation technique avoided common problems associated with nonlinear observers - the peaking phenomenon and noise amplification. The definition of a time-varying set in which the true angle-of-attack and sideslip angle are contained allowed for the definition of time-varying gains that help to stabilize the closed-loop system. This time-varying set could be replaced by intermittent aerodynamic angle measurements if they became available.

4. Given a class of uncertain nonlinear dynamical systems, an NDI adaptive control algorithm that utilizes estimates of unmeasured system states was presented and rigorously proven to stabilize the system. This control algorithm was demonstrated in simulation, where an Euler angle trajectory was successfully tracked despite no direct measurements of the vehicle's angle-of-attack or sideslip angle.

5. Both state constraint mechanisms were demonstrated on a nonlinear hypersonic vehicle simulation and particular attention was paid to the problem of inlet unstart. The ability to limit the vehicle's angle-of-attack and sideslip angle demonstrated the potential for these controllers to prevent inlet unstart. Furthermore, using a simplified aerodynamic model, a feasibility study was performed, demonstrating the potential for state constraint mechanisms to be used in recovering from unstarts as well.

6. The ability to combine a state constraint technique with the observer-based feedback NDI adaptive control law was demonstrated in simulation. Such a control law would be required to simultaneously address the practical issues of partial state measurement and inlet unstart. Although such a combined control law is susceptible to steady-state error, it was shown that successful tracking and state constraint enforcement can be achieved using this algorithm.

7. Given an accurate nonlinear discretization scheme in the class of explicit linear multistep methods, a sampled-data approach to nonlinear dynamic inversion adaptive control was rig-

orously proven to stabilize uncertain, nonlinear sampled-data systems. The control law allowed for the closed-loop system to be parameterized such that linear, discrete time, adaptive control algorithms could be leveraged. This sampled-data approach was demonstrated on a simulation of an F-16 as well as the Generic Hypersonic Vehicle and in both cases was shown to perform better than a continuous time control law implemented with a sampler and a zero-order hold. Limitations on the controller sample time were discussed and explored in simulation. Despite the extremely fast dynamics of hypersonic flight, bounded tracking was achieved.

9. RECOMMENDATIONS

Based on the results derived in this dissertation, the following reccomendations for future research are made

1. To confidently extend the algorithms developed in this dissertation to systems other than hypersonic vehicles, a comprehensive analysis on the impact of control saturation limits could be performed. Through assumptions regarding the system dynamics, analytical bounds on the size of achievable control magnitudes could be established. Otherwise, Monte Carlo analysis could be performed for the same purpose.

2. Both of the state constraint mechanisms developed in this dissertation allow for a designer to restrict the system outputs. A nonlinear dynamic inversion adaptive controller that can rigorously be proven to enforce constraints on unmeasured or potentially unobservable states would be a powerful technique in hypersonic flight control. Such a technique may allow for the development of a control law that can rigorously be proven to stabilize the closed-loop system while achieving the control objective of Section 6: the ability to constrain a hypersonic vehicle's aerodynamic angles despite not measuring them directly.

3. The presented observer-based NDI adaptive controller relies on assumptions that are valid due to aerospace engineering concepts. A more general assumption set is required to extend this technique to a wider class of nonlinear systems.

4. The sampled-data approach to NDI adaptive control could be formalized such that an explicit bound on the controller sample time is established. This would require extensive development in numerical analysis and the nonlinear discretization scheme selected to represent the true sampled-data system. The effect of actuator saturation limits on acceptable controller sample times could also be explored.

5. Improvements to the hypersonic vehicle simulation model could be made to make the system more realistic. This includes the modeling of elastic vehicle dynamics and the introduction of a higher fidelity inlet unstart model.

REFERENCES

[1] G. Kreisselmeier and K. Narendra, "Stable Model Reference Adaptive Control in the Presence of Bounded Disturbances," *IEEE Transactions on Automatic Control*, vol. 27, December 1982. doi: 10.1109/TAC.1982.1103093.

[2] B. Peterson and K. Narendra, "Bounded Error Adaptive Control," *IEEE Transactions on Automatic Control*, vol. 27, December 1982. doi: 10.1109/TAC.1982.1103112.

[3] J. S. Brinker and K. A. Wise, "Stability and Flying Qualities Robustness of a Dynamic Inversion Aircraft Control Law," *Journal of Guidance, Control, and Dynamics*, vol. 19, November-December 1996. doi: 10.2514/3.21782.

[4] J. Reiner, G. J. Balas, and W. L. Garrard, "Robust Dynamic Inversion for Control of Highly Maneuverable Aircraft," *Journal of Guidance, Control, and Dynamics*, vol. 18, January-February 1995. doi: 10.2514/3.56651.

[5] E. Rollins, *Nonlinear Adaptive Dynamic Inversion Control for Hypersonic Vehicles*. PhD thesis, Aerospace Engineering Department, Texas A & M University, College Station, Texas, 2013.

[6] A. Idris, M. Saad, H. Zare-Behtash, and K. Kontis, "Luminescent Measurement Systems for the Investigation of a Scramjet Inlet-Isolator," *Sensors*, vol. 14, no. 4, 2014. 6606-6632, doi: 10.3390/s140406606.

[7] J. Cang, N. Li, K. Xu, W. Bao, and D. Yu, "Recent Research Progress on Unstart Mechanism, Detection and Control of Hypersonic Inlet," *Progress in Aerospace Sciences*, 2017. 89.10.1016, j.paerosci.2016.12.001.

[8] H. Xu, M. D. Mirmirani, and P. A. Ioannou, "Adaptive Sliding Mode Control Design for a Hypersonic Flight Vehicle," *Journal of Guidance, Control, and Dynamics*, vol. 27, September-

October 2004. doi:10.2514/1.12596.

[9] D. Nesic, A. Teel, and P. Kokotovic, "Sufficient Conditions for Stabilization of Sampled-Data Nonlinear Systems via Discrete-Time Approximations," *Systems & Control Letters*, vol. 38, December 1999. doi:10.1016/S0167-6911(99)00073-0.

[10] R. T. Rysdyk and A. J. Calise, "Adaptive Model Inversion Flight Control for Tilt-Rotor Aircraft," *Journal of Guidance, Control, and Dynamics*, vol. 22, May-June 1999. doi: 10.2514/2.4411.

[11] A. Das, K. Subbarao, and F. Lewis, "Dynamic Inversion with Zero-Dynamics Stabilisation for Quadrotor Control," *IET Control Theory and Applications*, vol. 3, no. 3, 2009. doi: 10.1049/iet-cta:20080002.

[12] M. D. Tandale and J. Valasek, "Fault-Tolerant Structured Adaptive Model Inversion Control," *Journal of Guidance, Control, and Dynamics*, vol. 29, May-June 2006. doi: 10.2514/1.15244.

[13] Q. Wang and R. F. Stengel, "Robust Nonlinear Control of a Hypersonic Aircraft," *Journal of Guidance, Control, and Dynamics*, vol. 23, July-August 2000. doi:10.2514/2.4580.

[14] E. Rollins, J. Valasek, J. A. Muse, and M. A. Bolender, "Nonlinear Adaptive Dynamic Inversion Applied to a Generic Hypersonic Vehicle," in *AIAA Guidance, Navigation and Control Conference*, (Boston,Massachussetts), August 2013. doi:10.2514/6.2013-5234.

[15] M. A. Bolender, "An Overview on Dynamics and Controls Modelling of Hypersonic Vehicles," in *American Control Conference*, (St.Louis, Missouri), June 2009. doi:10.1109/ACC.2009.5159864.

[16] D. O. Sigthorsson, P. Janovsky, A. Serrani, S. Yurkovich, M. A. Bolender, and D. B. Doman, "Robust Linear Output Feedback Control of an Airbreathing Hypersonic Aircraft," *Journal of Guidance, Control, and Dynamics*, vol. 31, July-August 2008. doi:10.2514/1.32300.

[17] E. Johnson, A. Calise, K. Mease, J. Corban, , and M. Curry, "Adaptive Guidance and Control for Autonomous Hypersonic Vehicles," *Journal of Guidance, Control, and Dynamics*, vol. 29, May-June 2006.

[18] J. Yang, S. Li, C. Sun, and L. Guo, "Nonlinear-Disturbance-Observer-Based Robust Flight Control for Airbreathing Hypersonic Vehicles," *IEEE Transactions on Aerospace and Electronic Systems*, vol. 49, April 2013. doi: 10.1109/TAES.2013.6494412.

[19] H. Sun, Z. Yang, and J. Zeng, "New Tracking-Control Strategy for Airbreathing Hypersonic Vehicles," *Journal of Guidance, Control, and Dynamics*, vol. 36, February 2013. doi: 10.2514/1.57739.

[20] A. Serrani and M. A. Bolender, "Nonlinear Adaptive Reconfigurable Controller for a Generic 6-DOF Hypersonic Vehicle Model," in *American Control Conference (ACC)*, (Portland, Oregon), June 2014. doi:10.1109/ACC.2014.6858885.

[21] H. Sun, S. Li, J. Yang, and L. Guo, "Non-Linear Disturbance Observer-Based Back-Stepping Control for Airbreathing Hypersonic Vehicles with Mismatched Disturbances," *IET Control Theory & Applications*, vol. 8, November 2014. doi: 10.1049/iet-cta.2013.0821.

[22] Q. Zong, F. Wang, B. Tian, and S. Rui, "Robust Adaptive Dynamic Surface Control Design for a Flexible Air-Breathing Hypersonic Vehicle with Input Constraints and Uncertainty," *Nonlinear Dynamics*, vol. 78, October 2014. doi: 10.1007/s11071-014-1440-z.

[23] X. Bin, "Robust Adaptive Neural Control of Flexible Hypersonic Flight Vehicle with Dead-Zone Input Nonlinearity," *Nonlinear Dynamics*, vol. 80, May 2015. doi: 10.1007/s11071-015-1958-8.

[24] C. Mu, Z. Ni, C. Sun, and H. He, "Air-Breathing Hypersonic Vehicle Tracking Control Based on Adaptive Dynamic Programming," *IEEE Transactions on Neural Networks and Learning Systems*, vol. 28, February 2016. doi: 10.1109/TNNLS.2016.2516948.

[25] R. Aditya, M. J. Balas, D. B. Doman, and F. J. Franquiz, "Multivariable Direct Adaptive Stability and Command Augmentation of an Air-Breathing Hypersonic Vehicle," in *AIAA Information Systems-AIAA Infotech @ Aerospace, AIAA SciTech Forum*, (Grapevin, TX), January 2017. doi:10.2514/6.2017-1289.

[26] E. Lavretsky, T. E. Gibson, and A. M. Annaswamy, "Projection Operator in Adaptive Systems," *arXiv E-prints*, December 2011.

[27] J.-B. Pomet and L. Praly, "Adaptive Nonlinear Regulation: Estimation from the Lyapunov Equation," *IEEE Transactions on Automatic Control*, vol. 37, June 1992. doi:10.1109/9.256328.

[28] P. A. Ioannou and J. Sun, *Robust Adaptive Control*. Dover Publications, 2012.

[29] K. D. Billamoria and D. K. Schmidt, "Integrated Development of the Equations of Motion for Hypersonic Flight Vehicles," *Journal of Guidance, Control, and Dynamics*, vol. 18, January-February 1995. doi:10.2514/3.56659.

[30] W. Falkena, C. Borst, and J. Mulder, "Investigation of Practical Flight Envelope Protection Systems for Small Aircraft," in *AIAA Guidance, Navigation and Control Conference*, (Toronto,Ontario Canada), August 2010. doi:10.2514/1.53000.

[31] C.-H. Chaung and H. Morimoto, "Periodic Optimal Cruise for a Hypersonic Vehicle with Constraints," *Journal of Spacecraft and Rockets*, vol. 34, March-April 1997. doi:10.2514/2.3205.

[32] E. J. Stephen, S. R. Hoenisch, C. J. Riggs, M. L. Waddel, T. McLaughlin, and M. A. Bolender, "Hifire 6 Unstart Conditions at Off-Design Mach Numbers," in *AIAA SciTech*, (Kissimmee, Florida), January 2015. doi: 10.2514/6.2015-0109.

[33] E. G. Gilbert and K. T. Tan, "Linear Systems with State and Control Constraints: The Theory and Application of Maximal Output Admissible Sets," *IEEE Transactions on Automatic Control*, vol. 36, September 1991. doi:10.1109/9.83532.

[34] R. F. Hartl, S. P. Sethi, and R. G. Vickson, "A Survey of the Maximum Principles for Optimal Control Problems with State Constraints," *SIAM Review*, vol. 37, June 1995. doi:10.1137/1037043.

[35] P. Elbert, S. Ebbesen, and L. Guzella, "Implementation of Dynamic Programming for n-Dimensional Optimal Control Problems with Final State Constraints," *IEEE Transactions on Control Systems Technology*, vol. 21, May 2013. doi:10.1109/TCST.2012.2190935.

[36] T. Kiefer, K. Graichen, and A. Kugi, "Trajectory Tracking of a 3DOF Laboratory Helicopter Under Input and State Constraints," *IEEE Transactions on Control Systems Technology*, vol. 18, July 2010. doi:10.1109/TCST.2009.2028877.

[37] S. Vaddi and P. Sengupta, "Controller Design for Hypersonic Vehicles Accomodating Nonlinear State and Control Constraints," in *AIAA Guidance, Navigation and Control Conference*, (Chicago, Illinois), August 2009. doi:10.2514/6.2009-6286.

[38] R. M. Sanner and J.-J. E. Slotine, "Gaussian Networks for Direct Adaptive Control," *IEEE Transactions on Neural Networks*, vol. 3, November 1992. doi:10.1109/72.165588.

[39] E. Lavretsky and R. Gadient, "Robust Adaptive Design for Aerial Vehicles with State-Limiting Constraints," *Journal of Guidance, Control, and Dynamics*, vol. 33, November-December 2010. doi:10.2514/1.50101.

[40] J. A. Muse, "A Method For Enforcing State Constraints in Adaptive Control," in *AIAA Guidance, Navigation and Control Conference*, (Portland, Oregon), August 2011. doi:10.2514/6.2011-6205.

[41] Y.-J. Liu and S. Tong, "Barrier Lyapunov Functions for Nussbaum Gain Adaptive Control of Full State Constrained Nonlinear Systems," *Automatica*, vol. 76, February 2007. doi:10.1016/j.automatica.2016.10.011.

[42] D. Famularo, J. Valasek, J. A. Muse, and M. A. Bolender, "Enforcing State Constraints on a Model of a Hypersonic Vehicle," in *AIAA Guidance, Navigation and Control Conference*, (San Diego, California), January 2016. doi: 10.2514/6.2016-1865.

[43] K. P. Tee and S. Sam Ge, "Control of Nonlinear Systems with Full State Constraint Using a Barrier Lyapunov Function," in *Joint 48th IEEE Conference on Decision and Control and 28th Chinese Control Conference*, (Shanghai, China), January 2009. doi:10.1109/CDC.2009.5400484.

[44] B. Ren, S. Sam Ge, K. P. Tee, and T. H. Lee, "Adaptive Neural Control for Output Feedback Nonlinear Systems Using a Barrier Lyapunov Function," *IEEE Transactions on Neural Networks*, vol. 21, July 2010. doi:10.1109/TNN.2010.2047115.

[45] J. Valasek, J. Harris, S. Pruchnicki, M. McCrink, J. Gregory, and D. G. Sizoo, "Characterization of Derived Angle-of-Attack and Sideslip Angle Algorithms Using Monte Carlo and Piloted Simulation," in *AIAA Atmospheric Flight Mechanics Conference, AIAA AVIATION Forum*, (Denver, Colorado), June 2017.

[46] D. Famularo, J. Valasek, J. A. Muse, and M. A. Bolender, "Adaptive Control of Hypersonic Vehicles Using Observer-Based Nonlinear Dynamic Inversion," in *AIAA Guidance, Navigation and Control Conference*, (Kississimmee, Florida), January 2018.

[47] D. P. Wiese, A. M. Annaswamy, J. A. Muse, M. A. Bolender, and E. Lavretsky, "Adaptive Output Feedback Based on Closed-Loop Reference Models for Hypersonic Vehicles," *Journal of Guidance, Control, and Dynamics*, 2015. doi:10.2514/1.G001098.

[48] E. Lavretsky, "Adaptive Output Feedback Design Using Asymptotic Properties of LQG/LTR Controllers," *IEEE Transactions on Automatic Control*, vol. 57, June 2012. doi:10.1109/TAC.2011.2174692.

[49] W. MacKunis, Z. Wilcox, M. Kaiser, and W. Dixon, "Global Adaptive Output Feedback Tracking Control of an Unmanned Aerial Vehicle," *IEEE Transaction on Control Systems Technology*, vol. 18, November 2010. doi:10.1109/TCST.2009.2036835.

[50] A. J. Calise, N. Hovakimyan, and M. Idan, "Adaptive Output Feedback Control of Nonlinear Systems Using Neural Networks," *Automatica*, vol. 37, September-October 2001. doi:10.1016/S0005-1098(01)00070-X.

[51] J.-J. Slotine, J. Hedrick, and E. Misawa, "On Sliding Observers for Nonlinear Systems," *Journal of Dynamic Systems, Measurement, and Control*, vol. 109, September 1987. doi:10.1115/1.3143852.

[52] X. Zhang, A. Behal, D. Dawson, and B. Xian, "Output Feedback Control for a Class of Uncertain MIMO Nonlinear Systems with Non-Symmetric Input Gain Matrix," in *Decision and Control, 2005 and 2005 European Control Conference*, (Seville, Spain), January 2005. doi:10.1109/CDC.2005.1583416.

[53] E. Bullinger and F. Allgower, "An Adaptive High-Gain Observer for Nonlinear Systems," in *Conference on Decision and Control*, (San Diego, California), December 1997. doi:10.1109/CDC.1997.649541.

[54] N. Boizot, E. Busvelle, and J.-P. Gauthier, "An Adaptive High-Gain Observer for Nonlinear Systems," *Automatica*, vol. 46, no. 9, 2010. doi:10.1016/j.automatica.2010.06.004.

[55] H. K. Khalil, *Nonlinear Systems*. Prentice Hall, Inc., 1996.

[56] G. Evensen, "The Ensemble Kalman Filter for Combined State and Parameter Estimation," *IEEE Control Systems*, vol. 29, June 2009. doi: 10.1109/MCS.2009.932223.

[57] D. Nesic and A. Teel, "A Framework for Stabilization of Nonlinear Sampled-Data Systems Based on their Approximate Discrete-Time Models," *IEEE Transactions on Automatic Control*, vol. 49, July 2004. doi:10.1109/TAC.2004.831175.

[58] I. M. Mareels, H. Penfold, and R. Evans, "Controlling Nonlinear Time-Varying Systems via Euler Approximations," *Automatica*, vol. 28, July 1992. doi: 10.1016/0005-1098(92)90030-J.

[59] D. Nesic and A. Teel, *Sampled-Data Control of Nonlinear Systems: An Overview of Recent Results*, vol. 268 of *Lecture Notes in Control and Information Sciences*. Springer, London, 2001.

[60] D. Nesic and A. Teel, "Stabilization of Sampled-Data Nonlinear Systems via Backstepping on their Euler Approximate Model," *Automatica*, vol. 42, October 2006. doi:doi.org/10.1016/j.automatica.2006.05.015.

[61] M. Rubagotti, D. M. Raimondo, A. Ferrara, and L. Magni, "Robust Model Predictive Control with Integral Sliding Mode in Continuous-Time Sampled-Data Nonlinear Systems," *IEEE Transactions on Automatic Control*, vol. 56, March 2011. doi:10.1109/TAC.2010.2074590.

[62] W. Lin, W. Wei, and G. Ye, "Global Stabilization of a Class of Nonminimum-Phase Nonlinear Systems by Sampled-Data Output Feedback," *IEEE Transactions on Automatic Control*, vol. 61, October 2016. doi: 10.1109/TAC.2015.2498703.

[63] G. C. Goodwin, P. J. Ramadge, and P. E. Caines, "Discrete Time Multivariable Adaptive Control," *IEEE Transactions on Automatic Control*, vol. 25, no. 3, 1980. 10.1109/TAC.1980.1102363.

[64] K. S. Narendra and C. Xiang, "Adaptive Control of Discrete-Time Systems Using Multiple Models," *IEEE Transactions on Automatic Control*, vol. 45, September 2000. doi:10.1109/9.880617.

[65] F.-C. Chen and H. K. Khalil, "Adaptive Control of a Class of Nonlinear Discrete-Time Systems Using Neural Networks," *IEEE Transactions on Automatic Control*, vol. 40, May 1995. doi: 10.1109/9.384214.

[66] I. Karafyllis and Z.-P. Jiang, "A Small-Gain Theorem for a Wide Class of Feedback Systems with Control Applications," *SIAM J. Control Optim*, vol. 46, September 2007. doi:10.1137/060669310.

[67] D. Nesic, A. Teel, and D. Carnevale, "Explicit Computation of the Sampling Period in Emulation of Controllers for Nonlinear Sampled-Data Systems," *IEEE Transactions on Automatic Control*, vol. 54, March 2009. doi:10.1109/TAC.2008.2009597.

[68] J. Soon Jang, *Nonlinear Control Using Discrete-Time Dynamic Inversion Under Input Saturation: Theory and Experiment on the Stanford Dragonfly UAVs*. PhD thesis, Stanford University, Stanford, California, 2003.

[69] H. Lomax, T. H. Pulliam, and D. W. Zinng, *Fundamentals of Computational Fluid Dynamics*. Springer Verlag, 2000.

[70] J. Butcher, *Numerical Methods for Ordinary Differential Equations, Second Edition*. John Wiley, 2008.

[71] P. Ioannou and B. Fidan, *Adaptive Control Tutorial*. Society for Industrial and Applied Mathematics, 2006.

[72] B. L. Stevens and F. L. Lewis, *Aircraft Control and Simulation*. John Wiley & Sons, Inc., 1992.

[73] L. Nguyen, "Simulator Study of Stall/Post-Stall Characteristics of a Fighter Airplane with Relaxed Longitudinal Static Stability," NASA Technical Paper, NASA, Washington D.C., December 1979.

[74] J. A. Grauer and E. A. Morelli, "A Generic Nonlinear Aerodynamic Model for Aircraft," in *AIAA Atmospheric Flight Mechanics Conference*, (National Harbor, Maryland), 2014.

[75] D. K. Schmidt, *Modern Flight Dynamics*. McGraw Hill, 2012.

[76] J.-J. E. Slotine and W. Li, *Applied Nonlinear Control*. Prentice Hall, Inc., 1991.

APPENDIX A

PROOF OF LEMMAS 1.3.1 AND 1.3.2

In order to prove Lemma 1.3.1 the following Corollary must be introduced.

Corollary A.0.1. *Consider the convex function* $h(\theta) : \mathbb{R}^a \to \mathbb{R}$. *Let* $\theta_i \in \mathbb{R}^a$ *and* $\hat{\theta}_i \in \mathbb{R}^a$ *be vectors where*

$$h(\theta_i) < \delta$$

$$h(\hat{\theta}_i) = \delta$$

for some constant $\delta > 0$. *The following inequality holds,*

$$(\theta_i - \hat{\theta}_i)^T \nabla h(\hat{\theta}_i) \leq 0 \tag{A.1}$$

Proof. Since $h(\theta)$ is convex, the following inequality holds for any $0 \leq \lambda \leq 1$,

$$h(\lambda\theta_i + (1-\lambda)\hat{\theta}_i) \leq \lambda h(\theta_i) + (1-\lambda)h(\hat{\theta}_i) \tag{A.2}$$

By the same property, the following holds

$$h(\hat{\theta}_i + \lambda(\theta_i - \hat{\theta}_i)) \leq h(\hat{\theta}_i) + \lambda h(\theta_i - \hat{\theta}_i) \leq h(\hat{\theta}_i) + \lambda \left(h(\theta_i) - h(\hat{\theta}_i) \right) \tag{A.3}$$

This implies that

$$\frac{h(\hat{\theta}_i + \lambda(\theta_i - \hat{\theta}_i)) - h(\hat{\theta}_i)}{\lambda} \leq h(\theta_i) - h(\hat{\theta}_i) \leq \delta - \delta = 0 \tag{A.4}$$

which in the limit as $\lambda \to 0$ implies (A.1). □

Lemma 1.3.1

Proof. Note that

$$\left(\hat{\theta}_i - \theta_i\right)^T \left(\mathrm{Proj}(\hat{\theta}_i, y) - y\right) = \left(\theta_i - \hat{\theta}_i\right)^T \left(y - \mathrm{Proj}(\hat{\theta}_i, y)\right) \tag{A.5}$$

If $\mathrm{Proj}(\hat{\theta}_i, y) = y$, then (1.18) clearly holds. If instead, $h(\hat{\theta}_i) > 0$ and $y^T \nabla h(\hat{\theta}_i) > 0$ then

$$\left(\theta_i - \hat{\theta}_i\right)^T \left(y - \mathrm{Proj}(\hat{\theta}_i, y)\right) = \left(\theta_i - \hat{\theta}_i\right)^T \left(\frac{\nabla h(\hat{\theta}_i)(\nabla h(\hat{\theta}_i))^T}{\|\nabla h(\hat{\theta}_i)\|^2} y h(\hat{\theta}_i)\right) \tag{A.6}$$

Since $h(\hat{\theta}_i) > 0$, $\nabla h(\hat{\theta}_i)^T y > 0$, and Corollary A.0.1 holds, this implies

$$\left(\theta_i - \hat{\theta}_i\right)^T \left(y - \mathrm{Proj}(\hat{\theta}_i, y)\right) \leq 0 \tag{A.7}$$

which is equivalent to (1.18). □

Lemma 1.3.2

Proof. The derivative of the convex function with respect to time can be written as

$$\dot{h}(\hat{\theta}_i) = (\nabla h(\hat{\theta}_i))^T \dot{\hat{\theta}}_i = (\nabla h(\hat{\theta}_i))^T \mathrm{Proj}(\hat{\theta}_i, y) \tag{A.8}$$

The definition of the vector projection operator (1.17) implies that

$$\dot{h}(\hat{\theta}_i) = \begin{cases} h(\hat{\theta}_i))^T y(1 - h(\hat{\theta}_i)) & \text{if } h(\hat{\theta}_i) > 0 \text{ and } y^T \nabla h(\hat{\theta}_i) > 0 \\ h(\hat{\theta}_i))^T y & \text{otherwise} \end{cases} \tag{A.9}$$

Therefore,

$$\dot{h}(\hat{\theta}_i) \begin{cases} > 0 & \text{if } 0 < h(\hat{\theta}_i) < 1 \text{ and } y^T \nabla h(\hat{\theta}_i) > 0 \\ = 0 & \text{if } h(\hat{\theta}_i) = 1 \text{ and } y^T \nabla h(\hat{\theta}_i) > 0 \\ < 0 & \text{otherwise} \end{cases} \tag{A.10}$$

This implies that if $h(\hat{\theta}_i(t=0)) \leq 1$ then $h(\hat{\theta}_i) \leq 1$ for all $t \geq 0$ which implies that $\hat{\theta}_i \in \Omega_1$ for all $t \geq 0$ as intended. $\square$

APPENDIX B

PROOF OF THE INVERTIBILITY OF $\hat{\Lambda}$

In this Appendix, a lemma is presented which shows that through the use of the projection operator in the adaptive law for the uncertainty in the system control effectiveness, $\delta\hat{\Lambda}$, the total estimate $\hat{\Lambda} = I_m + \delta\hat{\Lambda}$ is guaranteed to be invertible at all times.

Lemma B.0.1. *For all $\delta\hat{\Lambda} \in \mathbb{R}^{m\times m}$, if the 2-norm of each column is less than $1/m$ at all times, which, according to Lemma 1.3.2, can be guaranteed by the projection operator, then $\hat{\Lambda}$ will always be invertible.*

Proof. It can be shown that if λ is an eigenvalue of $\delta\hat{\Lambda}$ then $\lambda + 1$ is an eigenvalue of $\hat{\Lambda}$. Let each element of the matrix $\delta\hat{\Lambda}$ have a magnitude smaller than $1/m$. Suppose that $\hat{\Lambda}$ is not invertible. This implies that $\hat{\Lambda}$ has a zero eigenvalue which implies that $\delta\hat{\Lambda}$ has an eigenvalue equal to -1 and that there exists at least one eigenvector, v, that satisfies

$$\delta\hat{\Lambda}v = -v \tag{B.1}$$

Let v_i correspond to the element of the eigenvector v with the largest magnitude. The i^{th} row of Equation (B.1) can be written as

$$\delta\hat{\Lambda}_{i1}v_1 + \delta\hat{\Lambda}_{i2}v_2 + ... + \delta\hat{\Lambda}_{im}v_m = -v_i$$

This implies that

$$|v_i| = |\delta\hat{\Lambda}_{i1}v_1 + \delta\hat{\Lambda}_{i2}v_2 + ... + \delta\hat{\Lambda}_{im}v_m|$$

$$|v_i| \leq |\delta\hat{\Lambda}_{i1}v_1| + |\delta\hat{\Lambda}_{i2}v_2| + ... + |\delta\hat{\Lambda}_{im}v_m|$$

$$|v_i| \leq |\delta\hat{\Lambda}_{i1}||v_1| + |\delta\hat{\Lambda}_{i2}||v_2| + ... + |\delta\hat{\Lambda}_{im}||v_m|$$

$$|v_i| < (|\delta\hat{\Lambda}_{i1}| + |\delta\hat{\Lambda}_{i2}| + ... + |\delta\hat{\Lambda}_{im}|)|v_i|.$$

Since each element of $\delta\hat{\Lambda}$ has magnitude less than $1/m$, $(|\delta\hat{\Lambda}_{i1}| + |\delta\hat{\Lambda}_{i2}| + ... + |\delta\hat{\Lambda}_{im}|) < 1$. This implies that

$$|v_i| < |v_i|$$

which is a contradiction. Therefore, $\hat{\Lambda}$ must be invertible whenever each element of $\delta\hat{\Lambda}$ is less than $1/m$. If the projection operator is utilized to bound the 2-norm of each column of $\delta\hat{\Lambda}$ to be less than $1/m$ this will ensure that each element is less than $1/m$ as well and guarantees that $\hat{\Lambda}$ is invertible at all times. □

APPENDIX C

COMPONENTS OF M_ζ AND b_ζ

C.1 Longitudinal Hypersonic Vehicle Model

$$m_{11} = -\frac{1}{2}\lambda_{min}(Q) \qquad m_{34} = 1 + \frac{\Delta\bar{g}_q}{2}$$

$$m_{12} = |K_3| \qquad m_{44} = -\frac{1}{2}K_\Theta$$

$$m_{13} = |K_{21}| + \frac{\bar{q}(V_{T,max})S\bar{c}}{2I_y}|C_{m1}| \qquad b_1 = \|K_0\|$$

$$m_{14} = |K_{22}| \qquad b_2 = \frac{1}{2}\left(|f'_\alpha(x)|_{max} + |q_m|\right)$$

$$m_{22} = -\frac{C_{L1}\bar{q}S}{2mV_T} \qquad b_4 = \frac{\bar{q}_d}{2}$$

$$m_{23} = \frac{1}{2}$$

$$m_{33} = -\frac{1}{2}\Delta\bar{g}_{qL}K_q + \Delta\bar{g}_2\left(\frac{\bar{q}(V_{T,max})S\bar{c}^2}{2\hat{I}_y V_{T,max}}\left|\hat{C}_{mq}\right| + \frac{\bar{q}(V_{T,max})S\bar{c}^2}{2V_{T,max}}\widehat{W}_{max}\right)$$

$$b_3 = \frac{\Delta\bar{g}_q}{2}\left(|\hat{C}_{q0}|_{max} + \frac{\bar{q}(V_{T,max})S\bar{c}^2}{2\hat{I}_y V_{t,max}}\left|\hat{C}_{mq}q_m\right| + |\dot{q}_m| + \widehat{W}_{max}\left(M_{T,max} + \bar{q}(V_{T,max})S\bar{c} + \frac{\bar{q}(V_{T,max})S\bar{c}^2}{2V_{T,max}}|q_m|\right)\right)$$

C.2 Six Degree-of-Freedom Hypersonic Vehicle Model

$$m_{11} = -\frac{1}{2}\lambda_{min}(Q)$$

$$m_{12} = K_2$$

$$m_{13} = \|K_3\| + \frac{1}{2}I^{-1}\bar{q}(V_{T,max})S\left\|\begin{matrix} bC_{\ell 1} \\ \bar{c}C_{m1} \\ bC_{n1}\end{matrix}\right\|$$

$$m_{14} = K_{31}$$

$$m_{22} = \frac{1}{2}\lambda_{max}(A_a)$$

$$m_{23} = \sqrt{\frac{1+d_\beta^2}{2}}$$

$$m_{33} = -\frac{1}{2}k_r\Delta\bar{g}_{rL} + \sqrt{3}\Delta\bar{g}_r\left(\frac{\bar{q}(V_{T,max})S}{2V_{T,max}}\hat{I}^{-1}\left\|\begin{matrix} b^2\hat{C}_{\ell p} \\ \bar{c}^2\hat{C}_{mq} \\ b^2\hat{C}_{nr}\end{matrix}\right\| + \frac{\bar{q}(V_{T,max})S}{2V_{T,max}}\widehat{W}_{max}\right)$$

$$m_{34} = \frac{1}{2}\left(1 + \sqrt{3}\Delta\bar{g}_r + \sqrt{3+4d_\Theta^2}\right)$$

$$m_{44} = -\frac{1}{2}\lambda_{min}(K_\Phi)$$

$$b_1 = \|K_0\|$$

$$b_2 = \frac{1}{2}\|f_a'\|_{max} + \sqrt{\frac{1+d_\beta^2}{2}}\|x_{r,m}\|$$

$$b_4 = \frac{1}{2}\sqrt{3+4d_\Theta^2}\bar{x}_{r,d}$$

$$b_3 = \frac{\sqrt{3}}{2}\Delta\bar{g}_r\left(\|\hat{f}_{r0}\|_{max} + \frac{\bar{q}(V_{T,max})S}{2V_{T,max}}\hat{I}^{-1}\left\|\begin{matrix} b^2\hat{C}_{\ell p} \\ \bar{c}^2\hat{C}_{mq} \\ b^2\hat{C}_{nr}\end{matrix}\right\|\|x_{r,m}\| + \|\dot{x}_{r,m}\|\right.$$
$$\left. + \widehat{W}_{max}\left(M_{T,max} + \bar{q}(V_{T,max})S + \frac{\bar{q}(V_{T,max})S}{2V_{T,max}}\|x_{r,m}\|\right)\right)$$

APPENDIX D

CONSTANT OBSERVER-GAINS USED IN GHV SIMULATION

D.1 Longitudinal Hypersonic Vehicle Model

Recall the matrix H_O defined in equation (4.91)

$$H_O = \begin{bmatrix} -h_{1V_T} & -h_{2V_T} & -\frac{\bar{q}S}{m}\hat{C}_{D1} & -h_{3V_T} \\ -h_{1\Theta} & -h_{2\Theta} & 0 & 1-h_{3\Theta} \\ -h_{1\alpha} & -h_{2\alpha} & -\frac{\bar{q}S}{mV_T}\hat{C}_{L1} & 1-h_{3\alpha} \\ -h_{1q} & -h_{2q} & \frac{\bar{q}S\bar{c}}{\hat{I}_y}C_{m1} & -h_{3q} \end{bmatrix}$$

and used in the simulation study of Chapter 4. These constant gain terms were defined as

$$H_O = \begin{bmatrix} -15 & -0.01 & -\frac{\bar{q}S}{m}\hat{C}_{D1} & 0 \\ -1e-4 & -20 & 0 & 0 \\ -0.001 & -0.5 & -\frac{\bar{q}S}{mV_T}\hat{C}_{L1} & 0.25 \\ -5e-5 & -0.1 & \frac{\bar{q}S\bar{c}}{\hat{I}_y}C_{m1} & -10 \end{bmatrix}$$

D.2 Six Degree-of-Freedom Hypersonic Vehicle Model

Recall the matrix H_O defined in equation (5.93)

$$H_O = \begin{bmatrix} -h_{1V_T} & -h_{2V_T} & H_O(1,3) & -h_{3V_T} \\ -h_{1\Phi} & -h_{2\Phi} & 0 & A_\Phi - h_{3\Phi} \\ -h_{1a} & -h_{2a} & H_O(3,3) & H_O(3,4) \\ -h_{1r} & -h_{2r} & H_O(4,3) & -h_{3r} \end{bmatrix}$$

and used in the simulation studies of Chapters 5 and 6. These constant gain terms were defined as

$$h_{1VT} = 15 \qquad h_{2VT} = \begin{bmatrix} 1e-4 & 1e-2 & 1e-4 \end{bmatrix} \qquad h_{3VT} = \begin{bmatrix} 0 & 0 & 0 \end{bmatrix}$$

$$h_{1\Phi} = \begin{bmatrix} 0 & 1e-4 & 0 \end{bmatrix}^T \qquad h_{2\Phi} = \begin{bmatrix} 10 & 0 & 0 \\ 0 & 20 & 0 \\ 0 & 0 & 10 \end{bmatrix} \qquad h_{3\Phi} = \begin{bmatrix} 0 & 0 & 0 \\ 0 & 1 & 0 \\ 0 & 0 & 0 \end{bmatrix}$$

$$h_{1a} = \begin{bmatrix} 0 & 1e-3 \end{bmatrix}^T \qquad h_{2a} = \begin{bmatrix} 0 & 0 & 0.01 \\ 0 & 0.5 & 0 \end{bmatrix} \qquad h_{3a} = \begin{bmatrix} 0 & 0 & 0.01 \\ 0 & 0.75 & 0 \end{bmatrix}$$

$$h_{1r} = \begin{bmatrix} 0 & 5e-5 & 0 \end{bmatrix}^T \qquad h_{2r} = \begin{bmatrix} 0 & 0 & 0 \\ 0 & 0.1 & 0 \\ 0 & 0 & 0 \end{bmatrix} \qquad h_{3r} = \begin{bmatrix} 20 & 0 & 0 \\ 0 & 10 & 0 \\ 0 & 0 & 20 \end{bmatrix}$$